

The Bolivar Roads Surge Barrier

A conceptual design for the environmental section

Peter A.L. de Vries

January 2014



Graduate:

P.A.L. de Vries BSc
Student ID: 1363379
E: *peterdv89@gmail.com*
T: +31 6 15 05 37 38

Bagijnhof 121
2611AN Delft
Netherlands

Educational institution:

Delft University of Technology
Faculty of Civil Engineering and Geosciences
Section Hydraulic Engineering

Stevinweg 1
2628CN Delft
Netherlands

Graduation committee:

Prof. dr. ir. S.N. Jonkman
Ir. A. van der Toorn
Dr. ir. W. Broere
Ir. L.F. Mooyaart
Ir. W.D. van der Wiel

Delft University of Technology
Delft University of Technology
Delft University of Technology
Royal HaskoningDHV
Iv-Infra

Trademarks:

MATLAB R2013a is a registered trademark of The Math Works, Inc.
AutoCAD 2013 is a registered trademark of Autodesk, Inc.
SketchUp and Google Earth are registered trademarks of Google, Inc.
Artlantis is a registered trademark of Abvent R&D

Preface

This is the final report for the thesis titled 'The Bolivar Roads Surge Barrier: A conceptual design for the environmental section'. The thesis is part of the Master's program Hydraulic Engineering, specialization Hydraulic Structures and has been completed at Delft University of Technology. The report describes the design process for the environmental section of a storm surge barrier in Bolivar Roads Pass near Galveston, Texas, United States of America. The study has been performed in collaboration with Royal HaskoningDHV and Iv-Infra. Part of the graduation was a nine week internship at Texas A&M University at Galveston.

I would like to express sincere gratitude to all of the members of my graduation committee. Furthermore I would like to thank all my colleagues at Royal HaskoningDHV, I have always felt very welcome during my graduation at the Rotterdam office. Special thanks go out to Dr. William Merrell, who gave me the best support during my internship in Texas and made sure everything was perfectly arranged. Thanks go out to my fellow students and friends in Texas too, they made sure my stay in Texas was not only very useful from a professional point of view, but also ensured it was an unforgettable experience.

Since this report not only marks the end of my graduation but also my study period I also want to thank all my friends, (ex-)roommates and everyone I know through speed skating for the great time I had. Last I want to thank my family, who always supported me.

Peter de Vries

Delft, January 20, 2014

Abstract

In response to the devastation caused by Hurricane Ike to the Galveston Bay Area, Texas, United States in September 2008, several proposals emerged to protect the region against future storm surges. One of them is a coastal spine called the 'Ike Dike'. A challenge for this 160 km [100 mi] long flood protection is to cross Bolivar Roads, a 2.8 km [1.7 mi] wide channel between Galveston Island and Bolivar Peninsula. A storm surge barrier is required to close the coastal spine and prevent hurricane surges in the Gulf of Mexico from penetrating into the Galveston Bay. This thesis, based on a global-to-detailed approach, presents the design process and a feasible design for a storm surge barrier at this specific site.

The design process starts with drafting a design framework consisting of a program of requirements and boundary conditions. According to the requirements Bolivar Roads is divided in two sections: a navigational section spanning the deeper section of the waterway allowing the passage of vessels and an environmental section which aims to preserve the Galveston Bay ecosystem. The objective of this thesis is to make a conceptual design for a barrier along the environmental section to satisfy two requirements. Firstly to enable sufficient water exchange between the Gulf of Mexico and the Galveston Bay through keeping at least 60% of the original flow area open, and secondly to sufficiently reduce the effect of storm surges with an estimated probability of occurrence of once in ten thousand years.

The first design step considers the barrier as a system. It reveals that the large retention capacity of the Galveston Bay brings an opportunity to construct the barrier more cost-effective: it does not have to be fully retaining. A closed barrier with a continuous retaining height of only 0.1 m [0.3 ft] above mean sea level reduces the storm surge sufficiently. With this retaining height along both the navigational and environmental sections the barrier is vastly overflowed during storms, but the Bay's retention capacity ensures the flood hazard along the Galveston Bay shores to remain acceptable.

Knowing the required retaining height and having a sense of the local conditions, several barrier types for the environmental section are evaluated. A shallow founded caisson barrier meets the drafted design criteria best. During this second design step a preliminary design for a caisson barrier is drafted to find the required main dimensions. The last part of this design step simulates the barrier on its final location through a settlement calculation. This reveals that the subsoil under the caissons is not able to bear the weight at all: the soil settles up to 3.7 m [12.1 ft] in depth, which is unacceptable. An alternative foundation method is therefore required and proposed.

In the third and last design step measures are investigated to improve the soil friction capacity and to deal with the settlements. Four alternatives for a foundation are drafted: 1) a shallow foundation using vertical drainage as soil improvement, 2) a shallow foundation with vacuum preloading as soil improvement, 3) a deep foundation through steel tubular piles and 4) a shallow foundation through replacing the entire weak clay stratum with sand. The sum of foundations costs and caisson construction costs for these alternatives are estimated at \$675, \$800, \$823 and \$897 million respectively. For this caisson barrier design, a shallow foundation with vertical drainage as soil improvement is advised. This third design step provided an important insight: the drafted design criteria in the second design step, on which the choice for a caisson barrier was based, were unbalanced. There should have been more emphasis on the foundation as it is a large portion of the total costs for the environmental barrier ($\pm 40\%$). It subsequently results in a two-fold recommendation. If the decision is to continue the caisson barrier design it is advised to apply vertical drainage. Alternatively, the suggestion is to reassess the barrier types in design step 2 while taking into account that the more expensive deep foundation method is likely more appropriate for Bolivar Roads.

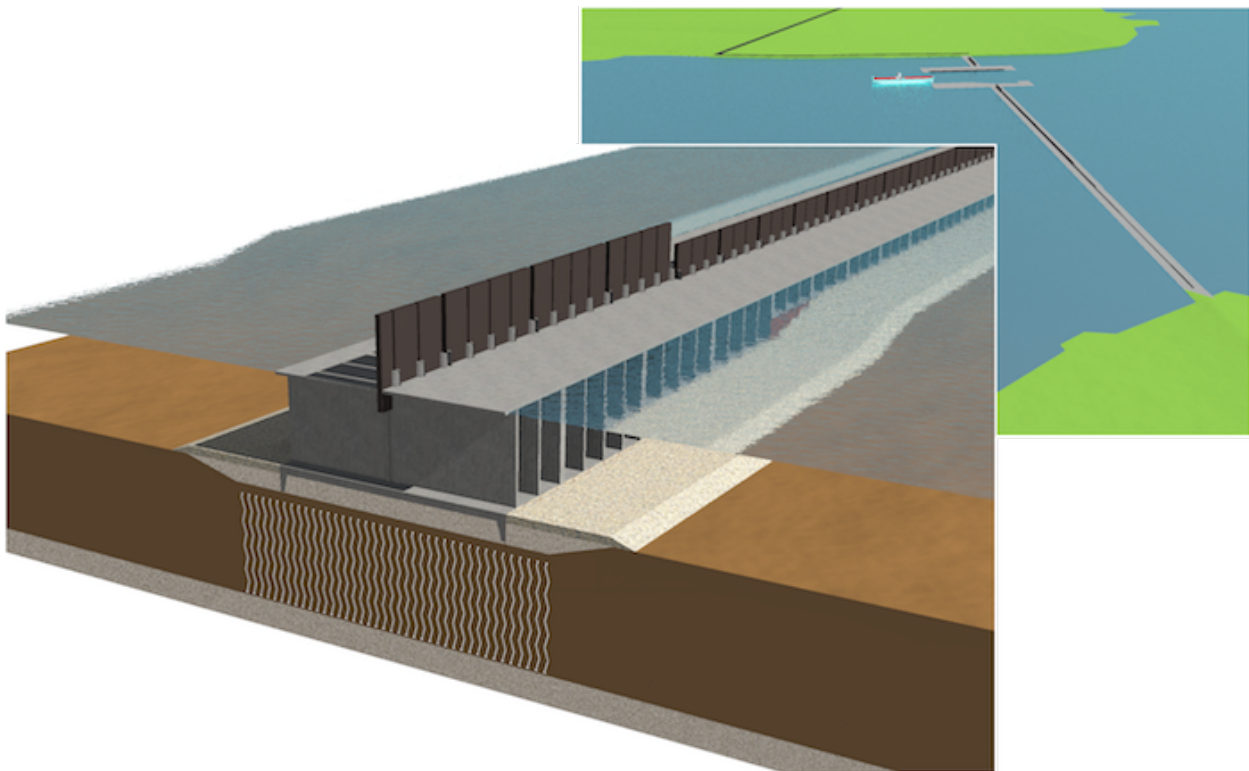
The report proceeds with the construction method for a caisson barrier with vacuum preloading soil improvement. Despite its relatively high costs, further investigating the application of this method is preferred as it has not yet been applied before for a large, shallow founded structure like a storm surge barrier. The construction method shows the consecutive activities up until the completion of the structure, together with a cost estimate. The cost estimate for the complete storm surge barrier in Bolivar Roads ranges from \$2.7 to \$4.0 billion. This includes the navigational section.

In this thesis the focus lies on foundation design. For further design it is recommended to focus on the barrier

doors, the bed protection and the adaptability to uncertain sea level rise. These are, next to the foundation aspects, important cost drivers for the storm surge barrier. For a complete integrated design the construction method should also be fully included in the design process, as for example the construction dock is linked to the optimal barrier type.



Location of the storm surge barrier in the Galveston Bay Area.



Storm surge barrier in Bolivar Roads and cross section of caisson barrier for the environmental section with vacuum preloading soil improvement.

Contents

Preface	i
Abstract	iv
Acronyms	ix
Terminology	x
Symbols	xii
1 Introduction	1
1.1 Background	1
1.2 Previous studies	2
1.3 Main research question	3
1.4 Plan of approach	4
1.5 Report structure	4
2 Galveston Bay Area	7
2.1 Economy	7
2.2 Galveston Bay estuary	7
2.2.1 Rivers debouching in the Bay	9
2.2.2 Inlets	9
2.3 Galveston Island	9
2.4 Galveston Seawall & Ike Dike	11
2.5 Houston Shipping Channel	13
2.6 Gulf Intracoastal Waterway	13
2.7 Hurricane Ike	14
2.8 Galveston Bay ecosystems	14
2.9 Bolivar Roads overview	14
3 Storm surge barriers	17
3.1 Definition	17
3.2 Construction material	18
3.3 Lessons learned	18
3.3.1 Maeslantkering safety system	18
3.3.2 Eastern Scheldt Barrier issues	19
4 Requirements for a Bolivar Roads Surge Barrier design	21
4.1 General requirements	21
4.2 Nautical requirements	21
4.2.1 Navigation channel dimensions	21
4.2.2 Traffic intensity	22
4.2.3 Maximum current velocity in navigation channel	22
4.3 Environmental requirements	22
4.4 Design requirements	22
4.4.1 Safety level	22
4.4.2 Structure lifetime & adaptability	23
4.4.3 Reliability of barrier closure and opening	23
4.4.4 Allowed overflow	23
4.4.5 Retaining character	24
4.5 Operational requirements	24

4.6	Stakeholders	25
4.7	Conclusions & recommendations	25
5	Boundary conditions	27
5.1	Hydrographic and topographic conditions	27
5.2	Hydraulic conditions	27
5.3	Meteorological conditions	29
5.4	Geotechnical conditions	29
5.5	Environmental conditions	29
5.6	Conclusions & recommendations	30
6	Design step 1: barrier system	33
6.1	Cost drivers	33
6.2	Barrier location	33
6.3	Distribution of retaining height	35
6.3.1	Open navigational section and closed environmental section	37
6.3.2	Navigational and environmental sections both limited retaining	38
6.4	Conclusions & recommendations	40
7	Design step 2: environmental barrier	41
7.1	Barrier alternatives assessment	41
7.2	Design input	42
7.3	Caisson barrier: preliminary design	44
7.3.1	Dimensions	45
7.3.2	Inflow area	48
7.4	Simulation: settlements	50
7.5	Key design parameters	52
7.5.1	Overview	52
7.5.2	Parameter influence	54
7.5.3	Conclusion key design parameters	55
7.6	Conclusions & recommendations	56
8	Design step 3: foundation aspects	59
8.1	Optimize caisson dimensions	60
8.2	Foundation design	63
8.2.1	Alternative 1: Shallow foundation using vertical drainage with Prefabricated Vertical Drains	63
8.2.2	Alternative 2: Shallow foundation using vacuum preloading with Capped Prefabricated Vertical Drains	65
8.2.3	Alternative 3: Deep foundation with steel tubular piles	68
8.2.4	Alternative 4: Shallow foundation using complete soil replacement	74
8.2.5	Assessment foundation alternatives	74
8.3	Seepage prevention measures	77
8.4	Conclusions & recommendations	77
9	Construction method and costs	79
9.1	Construction of dry dock	79
9.2	Caisson construction	80
9.3	Preparing final location	82
9.4	Caisson transport and placement	85
9.5	Total project costs	85
9.6	Drawings	87
9.7	Conclusions & recommendations	91
10	Final conclusions & recommendations	93

10.1	Conclusions	93
10.2	Reflection on methodology	94
10.3	Recommendations	94
10.3.1	Design specific recommendations	94
10.3.2	Suggested research topics	95
	References	99
	List of Figures	105
	List of Tables	109
	Appendices	111
A	Conversion factors	A-1
B	Gate and barrier types	B-3
B.1	Mitre gates	B-3
B.2	Radial gates	B-3
B.3	Vertical lifting gates	B-3
B.4	Flap gates	B-4
B.5	Sector gates	B-5
B.6	Visor gate	B-6
B.7	Vertically rotating gate	B-7
B.8	Inflatable rubber dam	B-8
B.9	Parachute barrier	B-8
B.10	Barge gate	B-9
B.11	Reduction barrier	B-9
B.12	Mailbox gate	B-10
B.13	Caisson structure	B-10
C	Requirements	C-1
C.1	Overflow	C-1
C.2	Nautical requirements	C-2
C.2.1	Navigation channel dimensions	C-2
C.2.2	Traffic intensity	C-3
D	Boundary Conditions	D-1
D.1	Bathymetry maps	D-1
D.2	Hydraulic conditions	D-3
D.2.1	Regular hydraulic conditions	D-3
D.2.2	Hurricane conditions	D-4
D.2.3	Surge height and waves	D-4
D.3	Meteorological conditions	D-5
D.3.1	Annual data	D-5
D.3.2	Hurricane data	D-6
D.3.3	Saffir-Simpson Hurricane Wind Scale	D-7
D.4	Geotechnical conditions	D-7
D.4.1	Soil information	D-7
D.4.2	Soil strength	D-8
D.4.3	Boring Logs	D-9
E	Barrier system	E-1
E.1	Overflow distribution	E-1
E.1.1	Open Navigation section	E-1

E.1.2	Both sections limited retaining	E-3
F	Environmental barrier	F-1
F.1	Design input	F-1
F.1.1	General parameters	F-1
F.1.2	Soil properties	F-1
F.1.3	Relevant heights, depths and water levels	F-2
F.1.4	Waves	F-2
F.1.5	Concrete properties	F-3
F.2	Caisson design	F-5
F.2.1	Definition of caisson geometry	F-5
F.2.2	Design checks	F-12
F.2.3	Caisson dimensions and design checks	F-18
F.3	Settlements calculation	F-21
F.3.1	Effective soil stress	F-21
F.3.2	Applied stress due to caisson weight	F-21
F.3.3	Koppejan method	F-22
F.3.4	Bjerrum method	F-24
G	Foundation aspects	G-1
G.1	Modified caisson dimensions	G-1
G.1.1	Weak soil layer replacement	G-1
G.1.2	Caisson skirts	G-1
G.1.3	Revised caisson dimensions	G-3
G.2	Foundation design	G-5
G.2.1	Alternative 1: Soil improvement using vertical drainage with PVDs	G-5
G.2.2	Alternative 2: Soil improvement using vacuum preloading with CPVDs	G-8
G.2.3	Alternative 3: Deep foundation	G-10
G.2.4	Alternative 4: Complete soil replacement	G-17
G.3	Seepage screen design	G-18
H	Construction method and costs	H-1
H.1	Costs per activity	H-1
H.2	Total costs	H-2

Acronyms

ASCE	American Society of Civil Engineers
BESW	Besturingssysteem Waterweg
BOS	Beslis en Ondersteunend Systeem
CPT	Cone Penetration Test
CPVD	Capped Prefabricated Vertical Drain
EIA	Environmental Impact Assessment
FEM	Finite Element Method
FRP	Fiber-Reinforced Plastic
GHMA	Greater Houston Metropolitan Area
GIWW	Gulf Intracoastal Waterway
GLO	General Land Office
HSC	Houston Shipping Channel
IWW	Intracoastal Waterway
mhr	man hour
MOSE	MOdulo Sperimentale Elettromeccanico
MSL	Mean Sea Level
NAP	Normaal Amsterdams Peil
NAVD	North American Vertical Datum of 1988
NHC	National Hurricane Center
NOAA	National Oceanic and Atmospheric Administration
PVD	Prefabricated Vertical Drain
SLR	Sea Level Rise
SLS	Serviceability Limit State
SPT	Standard Penetration Test
SSHWS	Saffir-Simpson Hurricane Wind Scale
SSPEED	Severe Storm Prediction, Education and Evacuation from Disasters
TAMUG	Texas A&M University at Galveston
TPWD	Texas Parks and Wildlife Department
ULS	Ultimate Limit State
USACE	United States Army Corps of Engineers
VTs	Vessel Traffic Service
yr	year

Terminology

Barrier Islands	Barrier islands are long, narrow, offshore deposits of sand or sediments parallel to the coastline. They are typically wave-built features, separated from the main land by a shallow sound, bay or lagoon (Bosboom and Stive, 2012; Freudenrich, 2013).
Bayou	A bayou is a body of water typically found in flat, low-lying area, and can refer either to an extremely slow-moving stream or river or to a marshy lake or wetland. The word was first used by the English in Louisiana and is thought to originate from the Choctaw-Indian word 'bayuk, meaning 'small stream' (National Geographic, 2013).
Caisson	In civil engineering a caisson (French for 'box') could be defined as a retaining watertight case, in order to keep water out during construction, but also for more permanent purposes like breakwater cores and tunnel segments. When referred to in this thesis a <i>flow-through</i> caisson is meant, a concrete structure with a floor plate, top plate and walls. Bulkheads are placed on the short sides during transport to maintain the caisson's floating ability.
Delta Works	The Delta Works is a series of construction projects in the southwest of the Netherlands to shorten the Dutch coastline and protect the hinterland around the Rhine-Meuse-Scheldt delta against storm surges from the North Sea (Nienhuis et al., 1982). The initiative for the construction of the Delta Works was in response to the widespread damage and number of casualties due to the North Sea Flood of 1953. The American Society of Civil Engineers (ASCE) has declared the works to be one of the Seven Wonders of the Modern World (Prasuhn and FitzSimons, 2002).
Dutch Practices	The Dutch Practices is a concept where levees and barriers are combined in order to shorten the coastline perimeter and keep the surge out of the internal waters. It has been applied after the 1953 surge disaster, being the basis for the Dutch Delta Works.
FRP	Fiber-Reinforced Plastic is a polymer matrix, either thermoset or thermoplastic, which is reinforced with a fiber or other reinforcing material with a sufficient aspect ratio (length to thickness) to provide a discernable reinforcing function in one or more directions (FRP & Composite Technology Resource Centre, 2012).
GIWW	The Gulf Intracoastal Waterway is a coastal canal from Brownsville, Texas, to the Okeechobee Waterway at Fort Meyers, Florida, financed and constructed by the United States Army Corps of Engineers (USACE) (Leatherwood, 2013b).
Hydraulic head	The force exerted by a column of water expressed by the height of the liquid above the point at which the pressure is measured. As the force of a water mass is directly proportional to the hydraulic head, it is often used to express pressure on hydraulic structures.
Ike Dike	The 'Ike Dike' is an artificial construction proposed by Prof. Dr. William Merrell (TAMUG) built to protect Galveston Bay in Texas, United States. The barrier extends across Galveston Island and the Bolivar Peninsula to provide a barrier against flooding due to surges from the Gulf of Mexico.
Mean tidal range	The mean tidal range is the difference in height between Mean High Water (MHW) and Mean Low Water (MLW) (NOAA Tides and Currents, 2011).
MHW	Mean High Water is the average of all high water heights with respect to MSL observed over a time period of 19 years (NOAA Tides and Currents, 2011).
MLW	Mean Low Water is the average of all low water heights with respect to MSL observed over a time period of 19 years (NOAA Tides and Currents, 2011).

MSL	Mean Sea Level is a tidal datum commonly used along Galveston beaches. Its elevation is NAVD+0.15 m [NAVD+0.50 ft].
NAP	Normaal Amsterdams Peil: Amsterdam Ordnance Datum. The vertical reference point in use for large parts of Western Europe which was originally established in 1684 for use in the Netherlands.
NAVD	The North American Vertical Datum of 1988 is the vertical control datum established in 1991 by the minimum-constraint adjustment of the Canadian-Mexican-U.S. leveling observations. It held fixed the height of the primary tidal bench mark, referenced to the new International Great Lakes (NOAA-NGS, 2013).
Negative head	The situation where the governing water level and forces on the barrier are directed from the Galveston Bay instead of from the Gulf of Mexico. It is the result of the better known 'backsurge' effect from the Galveston Bay.
New Panamax	The maximum vessel size that is able to sail through the Panama Canal after completion of the new navigation locks in 2015. Dimensions: draft = 15.2 m [50 ft], width = 49 m [161 ft], length = 366 m [1,200 ft] (Benitez, 2009).
Reliability	Reliability is the probability that a structure or part of a structure (existing or to be designed) will perform its prescribed duty without failure for a given time when operated correctly in a specified environment (INC-WG26, 2006). Storm surge barriers deal with three types of reliability: electrical, mechanical and human reliability. Electrical reliability refers for example to the extent to which computer systems fulfil their task. Mechanical reliability refers for example to a barrier that gets stuck. Human reliability regards the consequences due to human failure.
Repetition (factor)	The economic effect of repetition on construction is due to a decrease in operational costs, on the one hand, and to indirect cost savings caused by the reduction of construction time (lower labour oncosts, costs for finance, machinery and equipment etc.), on the other (Economic Commission for Europe, 1965). The repetition factor is the quantification of the achieved repetition on a specific construction activity. The repetition factor for a storm surge barrier can for example be increased by producing as much as possible identical units or the reuse of plywood formwork.
Risk	Risk is the measure of the probability and severity of an adverse effect to life, health, property, or the environment. The scale or significance of risk is described by a combination of probability of failure and consequences of a particular outcome or set of outcomes. The size of a risk is assessed by multiplying probability and consequences (INC-WG26, 2006).
Storm surge	An abnormal rise of water generated by a storm, over and above the predicted astronomical tides (NOAA-NHC, 2012). A wind-driven effect that predominantly occurs in shallow water.
Suezmax	The maximum vessel size that is able to sail through the Suez Canal. Dimensions: draft = 13.7 m [45 ft], width = 50 m [164 ft], length = 275 m [899 ft] (HGNSAC, 2011).
Wind setup	Wind setup within lakes or semi-enclosed bays is the impoundment of water due to wind. The resulting raise of water level in equilibrium state is a function of the wind velocity, fetch and water depth. As the magnitude of wind setup is inversely proportional to water depth the relatively largest setup occurs in shallow water (up to a certain limit).

Symbols

A	[m ²]	Area
B	[m]	Span width
C	[m ^{1/2} /s]	Chezy coefficient
c	[-]	Dimensionless coefficient
c_v	[m ² /s]	Consolidation coefficient (soils)
D	[m]	Draft
D_n	[m]	Stone diameter
d	[m]	depth
E	[N/mm ²]	Young's modulus
e	[m]	Eccentricity of force
e_i	[-]	Void ratio (soils)
F	[kN]	Force
f	[N/mm ²]	Strength
g	[m/s ²]	Gravitational constant (= 10)
H	[m]	(Wave) Height
h	[m]	Water level
Δh	[m]	Level difference
I	[m ⁴]	Mass moment of inertia
i	[-]	Integer
i_c, i_q, i_γ	[-]	Inclination factors (foundation design)
K	[-]	Soil pressure coefficient
k	[m ⁻¹]	Wave number
L	[m]	Length
m_v	[m ² /N]	Coefficient of vertical compressibility (soils)
M	[kNm]	Moment
N_c, N_q, N_γ	[-]	Soil bearing capacity factors
n	[-]	Number
O	[\$]	Costs
o	[\$]	Cost unit rate
P	[kN/m ²]	Pressure
p	[yr ⁻¹]	Return period
Q	[m ³ /s]	Discharge
q	[m ² /s]	Flow velocity per unit area
R	[m]	Hydraulic radius
s	[m]	Distance
s_c, s_q, s_γ	[-]	Foundation shape factors
T	[s]	(Wave) Period
t	[s]	duration
U	[m/s]	Flow velocity
V	[m ³]	Volume
v	[m/s]	Velocity
W	[m]	Width
w	[m]	Thickness
z	[m]	Variable for depth integration
α	[°]	Angle
α_s	[-]	Soil adhesion factor
γ	[-]	Safety factor
θ	[-]	Rotation
λ	[m]	Wave length

ρ	[kN/m ³]	Mass density
σ	[kN/m ²]	Stress
τ	[N/mm ²]	Shear stress
φ	[°]	Angle of internal friction (soil)
ϕ	[m]	Diameter
ζ	[m]	Wave elevation

1 Introduction

This chapter starts with a short description of the Galveston Bay Area and its history of flooding by Hurricanes. Subsequently the key findings of several studies on flooding that have already been conducted in the Galveston Bay Area are presented. This serves as input for the main research question and plan of approach. The structure of the report is presented in the last section.

1.1 Background

The Galveston Bay is a large estuary located in the Greater Houston Metropolitan Area (GHMA), along the upper coast of Texas, United States. The bay has been historically important in Texas' history. The island of Galveston was home to coastal Texas' earliest major settlement. Incorporated in 1839, the city of Galveston quickly became the most active port west of New Orleans and the state's largest city (Galveston.com, 2013b).

In 1900, the Galveston Bay Area got hit by a devastating storm, which is currently known as the 'The Great Storm'. By that time, Galveston had a population of 37,000. One-third of the city was completely destroyed. The estimated damage was more than \$700 million in current dollars and 6,000 – 8,000 lives were lost (Schiller, 2011). After the storm, the inhabitants raised the entire level of the city by 2.4 m [8 ft], jacking up more than 2,000 buildings and filling in underneath them with sand (Casselman, 2009). Also the 5.2 m [17 ft] high Galveston Seawall was built, slanting the ground so water would run off into the bay.

In the next decades the GHMA grew out to the fifth-largest metropolitan area in the U.S. It is among the fastest-growing metropolitan areas in the U.S. with a current population of 6.18 million. The number of inhabitants living within the low-lying areas below the 2-meter [6.7 ft] surge zone is over 900,000. This number is expected to increase at a significant rate (Census, 2012; Schiller, 2011). The combination of strong population growth and high economic activity make the area very vulnerable for coastal flooding from an economic point of view. Therefore the Upper Texas Coast is among the most valuable surge prone areas in the U.S. (Needham and Keim, 2012). This became painfully clear when Hurricane Ike struck the coastal areas of Louisiana and Texas in September 2008. The urban areas around the Galveston Bay were almost completely destroyed by a storm surge of 6.1 m [20 ft] above NAVD⁽¹⁾. Besides 112 casualties it was the costliest hurricane in Texas history. Damages from storm surges caused by Ike in coastal and inland areas are estimated at \$29.5 billion (Berg, 2009).

The resulting damage to Galveston Island and the entire bay area brought the topic of hurricane flood protection to the forefront of local issues. Prof. Dr. William Merrell of Texas A&M University at Galveston (TAMUG) proposed a coastal barrier named the 'Ike Dike'.⁽²⁾ When completed, it will protect a large part of the Galveston Bay Area



Figure 1.1: Location of the proposed Ike Dike, Bolivar Roads Pass and Hurricane Ike's path in the Galveston Bay Area (Merrell, 2010a).

⁽¹⁾The North American Vertical Datum of 1988 is the vertical control datum established in 1991 by the minimum-constraint adjustment of the Canadian-Mexican-U.S. leveling observations. It held fixed the height of the primary tidal bench mark, referenced to the new International Great Lakes (NOAA-NGS, 2013).

⁽²⁾The 'Ike Dike' is an artificial construction proposed by Prof. Dr. William Merrell (TAMUG) built to protect Galveston Bay in Texas, United States. The barrier extends across Galveston Island and the Bolivar Peninsula to provide a barrier against flooding due to surges from the Gulf of Mexico. See also Section 2.4.

against storm surge. The protected areas include the city of Galveston, the Galveston Bay Area, the Bolivar Peninsula, the city of Houston itself and valuable assets along the Houston Shipping Channel (HSC). The project will be a dramatic enhancement of the existing Galveston Seawall. A challenge for this 160 km [100 mi] long flood protection is to cross Bolivar Roads, a 2.8 km [1.7 mi] wide channel (see Figure 1.1). A storm surge barrier is required to close the coastal spine and prevent hurricane surges in the Gulf of Mexico from penetrating into the Galveston Bay. This thesis, based on a global-to-detailed approach, presents a design process and outlines difficulties for a storm surge barrier at this specific site.

1.2 Previous studies

Several studies in the Galveston Bay Area regarding a solution for preventing the area from flooding have been conducted. This section outlines their key findings to serve as an input for the thesis.

The report of the internship entitled 'Applying best practices from the Delta Works and New Orleans to Galveston Bay' carried out by Stoeten (2012) at TAMUG provides a comparison between the Dutch Delta Works, the New Orleans case and the Ike Dike concept. The strategy adopted to protect New Orleans originates from the 'Dutch practices': all systems serve to shorten the coastline perimeter and keep the surge out of the internal waters. Movable barriers in the San Luis Pass and the Bolivar Roads Pass are used to ensure navigation and preserve the ecosystem function of the internal waters. 'The Design of the Bolivar Roads Surge Barrier' is a Capstone Class Project at TAMUG by Davis et al. (2010) under the supervision of Dr. M. Miller. The proposed design is a combination of two barrier types: a combination of vertical lifting gate and sector gates (similar to the Eastern Scheldt Barrier and Maeslantbarrier respectively) is used. The proposed barrier is designed for a 200-year lifetime, once in 10,000 year storm conditions and it is designed for a 20 m [65 ft] deep channel which would be sufficient to accommodate future ship dimensions. Due to the proposed barrier the current velocities through the channel will increase by 14%, which does not hinder ship traffic. Part of the study was also the structural analysis of the sector gates. Finally the environmental impact of the structure is briefly investigated; the study concluded that the impact would be minimal as the moveable barriers still allow flow circulation in the Galveston Bay and no oyster reefs are present nearby. It is concluded that the proposed design would be able to withstand once in 10,000 year storm conditions.

The report by Davis et al. (2010) just starts with the design of sector gate and vertical lifting gate combination. Other design alternatives are only briefly evaluated. A more recent study by Cox et al. (2013) entitled 'Sector Gates in Bolivar Roads' considers other alternatives to a somewhat greater extent. Based on a gate comparison by Dircke et al. (2009) four alternatives are considered. As the span of the Bolivar Roads Surge Barrier will be around 250 m [800 ft] only gates suitable for large spans are considered, namely flap gates and sector gates. The study continues the calculation and verification of the sector gates' structural design using Finite Element Method (FEM) as it was initiated by Davis et al. (2010). Furthermore it contains a design for the foundation concerning a pile foundation because of the soft soil and heavy loads. Their findings regarding the foundation are quite brief since the available data is very limited and high uncertainties were involved in the assumptions.

'The effects of the Ike Dike barriers on the Galveston Bay' is the title of a Master's thesis executed by Ruijs (2011). In this study the impact of a partial closure on the Galveston Bay's hydrodynamics has been examined. The main conclusions concern the fact that a combination of a vertical lifting gate barrier and a sector gate barrier reduces the inflow area with 40% resulting in a 9% decrease in tidal amplitudes and a 9% decrease in discharge. This is solely due to the physical insertion of the barriers. Including energy losses these reductions are 20% and 21%

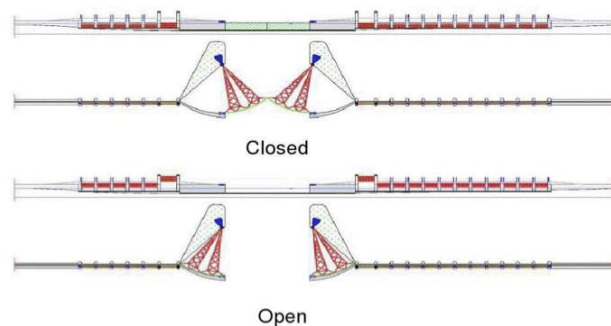


Figure 1.2: Front and top views of the design proposed by Davis et al. (2010). Image based on the design by Arcadis for a Verrezano Narrows Barrier in New York (Dircke et al., 2009).

respectively. Maximum measured current speeds at the Bolivar Roads inlet increase from 1.0 m/s [3.3 ft/s] up to 1.3 m/s [4.3 ft/s] for the 40% closure (Ruijs, 2011). Longitudinal current velocities of more than 1.5 m/s [4.9 ft/s] are considered undesirable for navigation (PIANC-IAPH, 1997). A 40% constriction would therefore not impede navigation.

The Galveston Bay is a relatively large retention basin compared to the size of its inlets. Therefore it is likely to expect that inflow in the Bay results in a relatively small raise of inner water level. This, in turn, influences the wind setup⁽³⁾ in the Bay during storm conditions. Currently this influence of elevated water levels in the Galveston Bay on storm surge height is investigated within a Master's thesis titled 'Hurricane Surge Risk Reduction For Galveston Bay', executed by Stoeten (2012). Supported by the fact that the magnitude of wind setup is inversely related to water depth, the simulations show that a small increase in mean water level due to inflow at Bolivar Roads does not result in significant higher wind setup along the Galveston Bay's shoreline. This raises the question whether a reduction barrier is sufficient in protecting the Galveston Bay against flooding. It is an interesting aspect in the barrier design and could provide opportunities in the barrier design. It will also be treated in this thesis, see Section 4.4.4.

Alternatively to the Bolivar Roads Surge Barrier type solution as investigated in the studies described above, there is also another option for protecting Houston and the HSC against flooding. It is a study performed by the Severe Storm Prediction, Education and Evacuation from Disasters (SSPEED) Center, part of Rice University in Houston. The idea is to construct a storm surge barrier near the Hartman Bridge at the entrance of the HSC: the 'Houston Ship Channel Gate' or 'Centennial Gate'. SSPEED states that constructing a barrier over here is favorable in terms of economics because most of the valuable assets around the Galveston Bay are located along the HSC. In their view constructing a barrier over here fulfills its goal: protect the areas that host industries of economic importance along the flood-prone shoreline of the HSC (Bedient and Penland, 2013). If one also wants to protect other valuable assets along the Galveston Bay dike heightening along the entire Bay will be necessary.



Figure 1.3: Aerial view of the theoretical ship channel gate and levee structure at Hartman Bridge (SSPEED Center, 2011).



Figure 1.4: Location of the HSC Gate in the Galveston Bay. Satellite image: Bing Maps (2013).

⁽³⁾Wind setup within lakes or semi-enclosed bays is the impoundment of water due to wind. The resulting raise of water level in equilibrium state is a function of the wind velocity, fetch and water depth. As the magnitude of wind setup is inversely proportional to water depth the relatively largest setup occurs in shallow water (up to a certain limit).

1.3 Main research question

The main research question of this thesis is:

What is a technically feasible design for a storm surge barrier in Bolivar Roads Pass?

Subquestions concern:

- How can the barrier be constructed in a cost-effective way?
- Is one gate type sufficient for the complete span of Bolivar Roads or should it be divided in different sections?
- What kind of barriers can be applied?
- Should the barrier fully block the surge or is a reduction also sufficient?
- If a reduction barrier appears to be feasible, to what level is the retention area of the Galveston Bay sufficient to apply a reduction barrier? What will be the required magnitude of reduction?
- What are the most important cost drivers and design parameters for the barrier?

1.4 Plan of approach

This thesis focuses on the design of a storm surge barrier located at Bolivar Roads, part of the *Ike Dike* concept. Therefore alternative barrier locations like the location proposed by the SSPEED Center will not be investigated. The studies executed by Davis et al. (2010) and Cox et al. (2013) both present the structural design for the specific case of a sector gate barrier with a vertical lifting gate barrier to close off Bolivar Roads in storm conditions. An extensive evaluation of different barrier types based on functional requirements and boundary conditions is omitted in these studies. Therefore this thesis first takes one step back and focuses on the design from a conceptual level to a detailed level using several design steps. In this way different barrier types can be thoroughly assessed on their applicability to the site.

1.5 Report structure

The goal of this document is to present a continuous, readable report of the design process. In order to do so, extensive calculations are presented in the appendices. For this reason the appendices cannot be seen separately from the main report. The structure of this report is schematically presented in Table 1.1.

First site specific and non-site specific research is executed. This results in an overview of the Galveston Bay Area in chapter 2 and an introduction to storm surge barriers in chapter 3. Appendix B contains an overview of different barriers and gate types.

Subsequently the framework in which the storm surge barrier should be designed is drafted. This consists of the requirements in chapter 4 and the boundary conditions in chapter 5. The combination of the requirements and boundary conditions serves as the input for the design steps. Calculations and more in-depth analysis of requirements and boundary conditions is presented in Appendices C and D.

The design process, based on a global-to-detailed design methodology, starts in chapter 6. This first design step investigates the barrier as a system. The optimal barrier alignment and its required retaining height are determined. Next a preliminary design for the environmental barrier section (a caisson barrier) is presented in chapter 7. This preliminary design aims on giving a feel for required dimensions. During this second step design issues will be faced of which the most important one, the foundations aspects, will be dealt with in the third design step

in chapter 8. Extensive elaborations of the calculations and methodology used in these design steps are presented in Appendices E to G.

An impression of the construction method will be presented in chapter 9 as well as a cost indication. Chapter 10 contains conclusions, design specific recommendations and recommendations for further research.

Table 1.1: Report structure.

	<u>Chapter 1</u> Introduction	
Analysis	<u>Chapter 2</u> Site specific research: Galveston Bay Area	
	<u>Chapter 3</u> Non-site specific research: Storm Surge Barriers	<u>Appendix B</u> Barrier types
Design framework	<u>Chapter 4</u> Requirements	<u>Appendix C</u> Calculations
	<u>Chapter 5</u> Boundary conditions	<u>Appendix D</u> Data & calculations
Design steps	<u>Chapter 6</u> Design step 1: barrier system – Barrier location – Barrier retaining height	<u>Appendix E</u> Calculations Elaborated approach
	<u>Chapter 7</u> Design step 2: environmental barrier – Barrier alternative assessment – Preliminary design caisson barrier – Simulation – Indication decisive design parameters	<u>Appendix F</u> Calculations Elaborated approach
	<u>Chapter 8</u> Design step 3: foundation aspects – Foundation alternative assessment – Foundation design	<u>Appendix G</u> Calculations Elaborated approach
Result of design steps	<u>Chapter 9</u> – Construction method – Cost calculation – Drawings	<u>Appendix H</u> Cost numbers
	<u>Chapter 10</u> – Conclusions – Recommendations	

2 Galveston Bay Area

This chapter contains site specific research into the Galveston Bay Area. It discusses the local economy, the Galveston Bay estuary and ecosystems, and Galveston's history with hurricanes and built flood protection measures. The chapter ends with a satellite overview of the project location: Bolivar Roads Pass.

Currently the Galveston Bay Area is a region that surrounds the Galveston Bay estuary within the Greater Houston Metropolitan Area (GHMA). Residents of Houston and surrounding areas typically refer to it as the 'Bay Area'. Normally the term refers to the mainland communities around the Bay and excludes Galveston as good as best of Houston (Riley, 2006; travelkernel.com, 2013). However, this section presents a short analysis of the Galveston Bay Area, including Galveston and some relevant industrial areas of Houston. It also briefly discusses the Ike Dike, characteristics of the Galveston Bay estuary, and navigational and environmental aspects of the Bay.

2.1 Economy

The Bay area has a diverse economy hosting a pair of one-billion dollar industries. The area's anchor industries are aerospace (NASA's headquarters: the Lyndon B. Johnson Space Center) and petrochemicals/chemical processing. The most widespread economic activities involve around the latter, as the Galveston Bay Area is home to three of the country's largest oil refineries and 40% of its chemical manufacturing capacity. Most of these plants are located on flood-prone locations along the HSC. Other important industries in the Bay Area are high-tech and tourism (Hodgin, 2007).

The Port of Houston, a 40 km [25 mi] long complex, is the largest port located along the Galveston Bay. After the Port of South Louisiana it is the United States' second largest seaport, handling over 237 million tons of cargo annually in 2011. However, up until the year 1900 before the Great Storm (see Section 2.3) struck Galveston Island, the Port of Galveston was the busiest on the Gulf Coast and considered to be second busiest in the U.S. Although the port has recovered since the Great Storm struck, its status was quickly overtaken by the Port of Houston and other deep-water ports. Today the Port of Galveston handles about 14 million tons of cargo annually. The third large port in the Bay Area is the Port of Texas City located at the lower Galveston Bay. Nowadays the annual throughput of this port amounts 58 million tons of cargo, making it the 12th leading port in the U.S. (TAMUG, 2010; USACE, Waterborne Commerce Statistics Center, 2011).

2.2 Galveston Bay estuary

The Galveston Bay estuary is located in southeast Texas, adjacent to the Houston Metropolitan Area. It is the largest estuary on the Texas coast consisting of five sub-bays: West Bay, Galveston Bay (upper and lower), East Bay and Trinity Bay (see Figure 2.1).



Figure 2.1: The Galveston Bay estuary. Satellite image: Bing Maps (2013).

Many smaller bays and lakes are connected to the main system. The Bay has a mud bottom and a total surface area of 1,554 km² [600 sqmi], is on average 48 km [30 mi] long and 27 km [17 mi] wide. The total shoreline length is 372 km [232 mi]. The depth of the bay (excluding the shipping channels) varies between 1 and 4 meter [3-13 ft], with an average of 2.7 meter [9 ft]. The Bay is an inundated drainage system of river and stream valleys which was excavated by fluvial processes when sea level was eustatically lower than present (Philips, 2004; Taylor et al., 2008a).

The Galveston Bay is mainly fed by the Trinity River, San Jacinto River (see Section 2.2.1), and incoming tides from the Gulf of Mexico. The Bay's drainage area is 85,740 km² [33,104 sqmi], of which about 54% is the Trinity River. The San Jacinto River constitutes about 17%, and the remaining 29% is accounted for by various smaller creeks and bayous⁽¹⁾ (Leatherwood, 2013a; Philips, 2004). The fresh water from the rivers mixes with the tidal salt water from the Gulf of Mexico via three inlets, see section 2.2.2. These are two major inlets, Bolivar Roads Pass and San Luis Pass, and one minor cut, the Rollover Pass.

⁽¹⁾A bayou is a body of water typically found in flat, low-lying area, and can refer either to an extremely slow-moving stream or river or to a marshy lake or wetland. The word was first used by the English in Louisiana and is thought to originate from the Choctaw-Indian word 'bayuk', meaning 'small stream' (National Geographic, 2013).

2.2.1 Rivers debouching in the Bay

The San Jacinto River, named after Saint Hyacinth, is formed by the junction of its East and West forks and runs to the Gulf of Mexico through the Galveston Bay. It is a relatively short river, with a total length of 138 km [85 mi]. Accounting for 54% of its drainage area, the Trinity River is the main source of river inflow for the Galveston Bay. According to data from 1989-1996 the total volume that passes Bolivar Roads annually is $1.7 \cdot 10^{10} \text{ m}^3$ [$6.0 \cdot 10^{11} \text{ ft}^3$] (Powell et al., 2005). The average discharge through Bolivar Roads is thus $540 \text{ m}^3/\text{s}$ [$1.9 \cdot 10^4 \text{ ft}^3/\text{s}$]. Data about peak volumes through Bolivar Roads is not available. However, if one assumes a peak discharge four times higher than average, a full closure at Bolivar Roads that lasts for 12 hours the water level in Galveston Bay will only rise 7 cm [2.7 in] due to river inflow.

2.2.2 Inlets

'Bolivar Roads Pass' is the 2.8 km [1.7 mi] wide strip of water enclosed by the North and South jetties between Galveston Island and Bolivar Peninsula, see Figure 2.2a (Handbook of Texas Online, 2013). It provides 80% of the tidal exchange between the Galveston Bay estuary and the Gulf of Mexico. The channel is an important shipping corridor between the Gulf of Mexico and the Galveston Bay. It is part of the HSC and the Gulf Intracoastal Waterway (GIWW), which runs between the Bay and the Gulf (see Section 2.6). In the future it may be possible for vessels with New Panamax size to sail through the Bolivar Roads Pass (see Section 2.5). See Section 2.9 for a complete overview.

The Galveston-Port Bolivar Ferry crosses the Bolivar Roads Pass (see fig. 2.7). It is the bridge between two segments of State Highway 87. Annually, almost 5.8 million passengers and 1.8 million vehicles use the free ferry service between the Galveston Island and Bolivar Peninsula (FindTheData.org, 2013). The ferry service is critical to the residents of the Bolivar Peninsula when a hurricane threatens as the ferries are the primary means of evacuation through Galveston to the mainland (Galveston.com, 2013a).

'San Luis Pass' is a micro-tidal inlet which connects the Gulf of Mexico with the West Bay (see Figure 2.2b). It is approximately 900 m [0.6 mi] wide and on average 2 m [6 ft] deep. It is responsible for 20% of the tidal exchange between the Gulf of Mexico and Galveston Bay. Located at the southwest end of Galveston Island, it separates Galveston Island from Follets and San Luis islands. These islands are connected via the San Luis Pass bridge.

'Rollover pass' is a 60 m [200 ft] wide artificial inlet, connecting East Bay with the Gulf of Mexico at the northeast side of Bolivar Peninsula (see Figure 2.2c). The pass was constructed in 1956 for the purpose of improving fishing in the bay. It is unique, as it is one of the few inlets connecting the upper reach of an estuary with the sea. However, the contribution to the tidal exchange of the Galveston Bay due to the Rollover Pass is zero (Lester and Gonzalez, 2002; Wall, 2008). Because of erosion problems, the Texas General Land Office (GLO) plans to permanently close off the Rollover Pass (Stanton, 2013).

2.3 Galveston Island

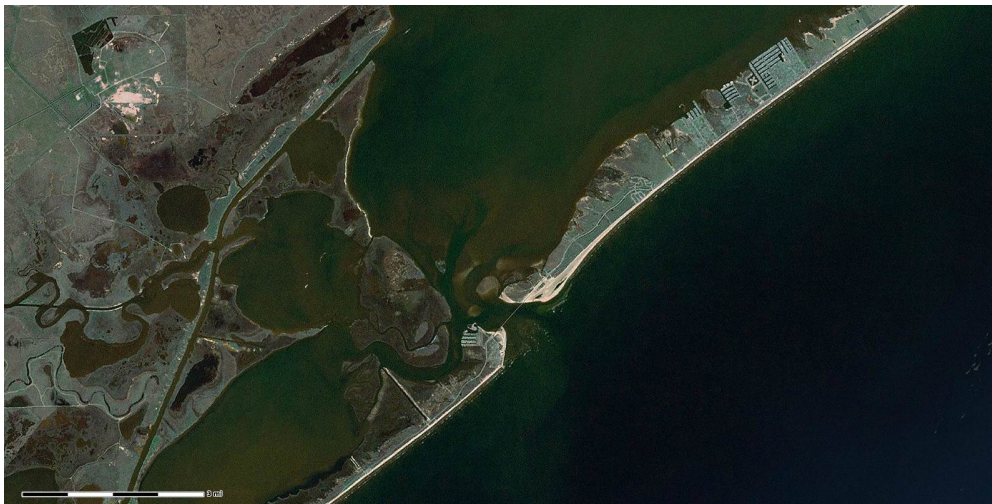
Galveston Island and Bolivar Peninsula are sand barrier islands⁽²⁾ on the Texas Gulf Coast, located approximately 80 km [50 mi] southeast of Houston (see fig. 2.1). They are both narrow strips of land, oriented northeast-southwest, separating the Galveston Bay from the Gulf of Mexico. Galveston Island is 43 km [27 mi] in length and less than 3 mi [4.8 km] wide at its widest point. It runs parallel to the coast approximately 3.2 km [2 mi] out. The Bolivar Roads Pass (see section 2.2.2) separates the two islands by a distance of about 3 km [1.9 mi].

The Galveston Channel separates the island from neighboring Pelican Island, forming a natural harbor for nineteenth-century sailing vessels and small steamers. The island's economy grew on the strength of this port; serving as a

⁽²⁾Barrier islands are long, narrow, offshore deposits of sand or sediments parallel to the coastline. They are typically wave-built features, separated from the main land by a shallow sound, bay or lagoon (Bosboom and Stive, 2012; Freudenrich, 2013).



(a) Bolivar Roads Pass. The dashed line indicates the location of the barrier profile of Figure 5.1.



(b) San Luis Pass



(c) Rollover Pass

Figure 2.2: *Satellite views of the three inlets. Satellite images: Bing Maps (2013).*

transfer point for oceangoing vessels which ran a route to Houston. The link between Galveston and Houston was strengthened through the construction of a railroad between the two towns. The dramatic battle of Galveston, part of the American Civil War (1861-1865), resulted in isolation of the port. Despite of efforts to maintain trade supremacy by improving port facilities and contributing to the construction of railways to the city, Galveston had a population of only 37,000 at the end of the 19th century, ranking back to fourth place in Texas' largest cities. The Great Storm of 1900 destroyed one-third of the city and was responsible for over 6,000 casualties (Galveston.com, 2013b).

2.4 Galveston Seawall & Ike Dike



Figure 2.3: Current Galveston Seawall and shoreline protection.



Figure 2.4: Aerial view of the modern Seawall (Merrell et al., 2011).

In response to The Great Storm, the inhabitants of Galveston raised the entire level of the city by 2.4 m [8 ft], slanting the ground so water would run off into the bay. The 5.2 m [17 ft] high Galveston Seawall was built, designed to withstand a once in 100 year storm event (Adey, 2013). It is a concrete structure founded on timber piles protected from undermining by sheet piling and a layer of riprap; 1.2 m [4 ft] square granite blocks extending over 8 m [27 ft] seawards from the toe. The land-raising and seawall were so successful that when the next heavy hurricane swept down on Galveston in 1915, the city was safe and only eight people were killed (Galveston.com, 2013b). Reporting in the aftermath of the 1983 Hurricane Alicia⁽³⁾, the USACE estimated that \$100 million in damage was avoided because of the seawall (USA Today, 2005).

The curved-face concrete structure is presently 16 km [10 mi] long, 5.2 m [17 ft] high and 4.9 m [16 ft] at its base. It had done its job; prevent catastrophic Gulf overflow, but it does not prevent back surge from the bay (Merrell, 2012; therealgalveston.com, 2013). As stated in chapter 1 a proposal has been put forth to extend the existing seawall and construct a coastal spine⁽⁴⁾, the so-called Ike Dike (see Figure 2.5). It consists of a 100 km [62 mi] massive levee system with gate passages in the San Luis Pass and the Bolivar Roads Pass. The Ike Dike itself will be realized by either constructing land-based revetments along the beaches of Galveston Island and the Bolivar Peninsula or by raising coastal highways, located further away from the beach. A levee or dune system would be constructed stretching 29 km [18 mi] to the San Luis Pass. A 56 km [35 mi] coastal barrier as high as the existing Galveston Seawall (5.2 m [17 ft]) would be constructed along the Bolivar Peninsula (Adey, 2013). An Ike Dike levee with these dimensions will protect the area against a once in 100 year event.

⁽³⁾Hurricane Alicia was a Category 3 hurricane that struck Galveston and Houston directly, being responsible for 21 casualties and \$6 billion in damage (USA Today, 2005).

⁽⁴⁾The coastal spine concept is the approach the Dutch used after their 1953 surge disaster to shorten the coastline (TAMUG, 2010).

The proposed Ike Dike will protect the Galveston Bay and all the important industrial facilities (see sections 2.1 and 2.5) from a future storm. The Ike Dike on Galveston Island only will cost roughly \$3 billion, others estimate this costs higher; around \$7 to \$10 billion. Whatever the final cost may be, there is a high benefit to cost ratio for such a project when financial consideration is given for the structure's potential to prevent future damage (Calkins, 2010).



Figure 2.5: Galveston Seawall and proposed Ike Dike along Galveston Island and Bolivar Peninsula. Satellite image: Bing Maps (2013).

According to Merrell (2012) the Ike Dike should adhere to some important requirements.

- It should shorten the coastline perimeter as much as possible.
- The system may overflow.
- The barrier must not hinder navigation.
- The marine ecosystem function of the bay must be preserved.

2.5 Houston Shipping Channel

The Houston Shipping Channel (HSC) is the conduit for ocean-going vessels between the Port of Houston shipyards and the Gulf of Mexico (see Figure 2.1). It has been used to move goods to the sea since at least 1836. Buffalo Bayou and Galveston Bay were dredged during the late 19th and 20th centuries to accommodate larger ships. By the mid 1900s the Port of Houston had established itself as the leading port in Texas eclipsing the natural harbors at Galveston and Texas City. Over the years, the growth of the Port of Houston has been facilitated by local contributions and federal funds to gradually deepen and widen the HSC. Currently the HSC is a vital economic engine, as it supports more than 150,000 jobs in the Houston area and more than 1 million jobs in Texas (SSPEED Center, 2012).

Channel dimensions Since the opening as an official deep-water channel of 7.6 m [25 ft] in 1914 the channel has been expanded to the current depth of 13.7 m [45 ft] and width of 161.5 m [530 ft], being able to accommodate (not fully loaded) Suezmax⁽⁵⁾ tankers. A larger channel is required in order to accommodate larger ships and maintain a competitive position with respect to other ports.

As the Panama Canal expansion nears its completion, an additional increase in traffic is expected. Statistics from Vessel Traffic Service (VTS) support this expectation, reporting an annual increase of nearly 10% since 2004 (HGNSAC, 2011). In the near future local decision makers may therefore wish to assure the passage of the New Panamax⁽⁶⁾ vessels through the canal. An expansion will also ensure safer and more efficient passage of ships and barges (BUG, 1990).

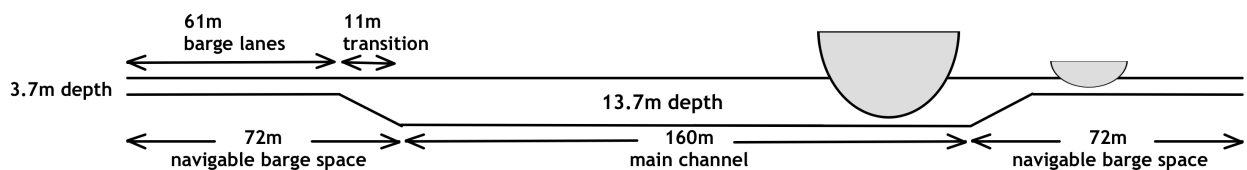


Figure 2.6: Schematic cross section of the HSC showing its current dimensions. Modified from HGNSAC (2011).

Vulnerability Typical flood plain elevations along the HSC range from 4.3-4.6 m [14-15 ft] above sea level. This is significantly lower than what is needed to protect the projected 6.1-7.6 m [20-25 ft] surge tide in a 100 year event (Merrell, 2010b). In the event of a category 5 hurricane⁽⁷⁾ the industries in the ship channel could be shut down for months resulting in a national catastrophe in terms of economic damage.

2.6 Gulf Intracoastal Waterway

The 1700 km [1050 mi] long Gulf Intracoastal Waterway (GIWW) is the part of the Intracoastal Waterway (IWW) located along the Gulf Coast of the United States. It is financed and constructed by the USACE. The IWW runs from Brownsville, Texas, to the Okeechobee waterway at Fort Meyers, Florida. The Texas part stretches over 686 km [426 mi]. Some lengths consist of natural inlets, salt-water rivers, bays and sounds; others are artificial canals. It provides a navigable route along the U.S. coast without many of the hazards of travel on the open sea.

Primarily designed for the transportation of goods, the waterway provides a channel with a controlling depth of 3.7

⁽⁵⁾The maximum vessel size that is able to sail through the Suez Canal. Dimensions: draft = 13.7 m [45 ft], width = 50 m [164 ft], length = 275 m [899 ft] (HGNSAC, 2011).

⁽⁶⁾The maximum vessel size that is able to sail through the Panama Canal after completion of the new navigation locks in 2015. Dimensions: draft = 15.2 m [50 ft], width = 49 m [161 ft], length = 366 m [1,200 ft] (Benitez, 2009).

⁽⁷⁾see Table D.3 for hurricane intensity scale

m [12 ft]. The dimensions limit barges to a total length of 360 m [1,180 ft] and width of 16.8 m [55 ft] (Leatherwood, 2013b). At the location of the Galveston Bay the GIWW extends along the Bolivar Peninsula, crosses the HSC and Pelican Island before it continues in the West Bay (see Figure 2.1).

2.7 Hurricane Ike

Hurricane Ike made landfall over the eastern end of Galveston Island just after 2AM on Saturday September 13, 2008 as a category 2 hurricane on the Saffir-Simpson Hurricane Wind Scale (SSHWS) (for the complete scale: see table D.3). The storm then tracked northward across Galveston Bay. Ike's large wind field contributed to storm surge values well in excess of those normally associated with a category two storm (NWS Weather Forecast Office, 2008b). Surge values along the Gulf Coast were estimated to be 10-13 ft [3.0-4.0 m] along Galveston Island and 13-17 ft [4.0-5.2 m] along the Bolivar Peninsula. Researchers' best estimates of Ike's characteristics reported are (Institute for Business & Home Safety, 2009):

- Maximum 3-second gust wind speeds ranging 177-185 km/h [96-100 kt]
- Maximum surge of 4.6-4.9 m [15-16 ft], with waves that brought highest water levels to 5.8-6.1 m [19-20 ft]
- Maximum rainfall accumulation of 480 mm [18.9 in] just north of Houston along Spring Creek (Berg, 2009)
- Maximum rainfall rate of about 25 mm [1 in] per hour over two periods during the storm

2.8 Galveston Bay ecosystems

The Galveston Bay is a semi-closed estuary and provides multiple different estuary habitats such as marshes, mud and sand flats, sea grass beds, oyster reefs, open bay bottoms and open bay waters. Tidal and other periodical perturbations induce complex mixing of waters from different sources. This gives the Galveston Bay a high variable ecosystem. Only those plants and animals that can tolerate fluctuating salinities and temperatures are found in this environment. Additionally, the small ecosystems formed by bayous, rivers, wetlands and marshes that surround the bay support a variety of flora and fauna. This diversity of habitats and abundance of nutrients provides very high levels of biologic productivity (Lester and Gonzalez, 2002; Ruijs, 2011).

The Galveston Bay is a valuable resource for the state and the nation. Besides recreational opportunities, ecological services and transportation links it also provides natural resources. For example oyster reefs are a primary geologic feature of the Bay, with the largest complex of productive reefs in the middle of the Bay. Large volumes of water can be filtered by a healthy oyster population. The filtering influences subsequently conditions such as water clarity and phytoplankton abundance. Simultaneously, the oysters' tendency to bioaccumulate some pollutants, combined with their lack of mobility, make them an important organic indicator for determining the health of the estuary. Oyster reefs are very sensitive and vulnerable to storm surges. Biologists from the Texas Parks and Wildlife Department concluded that about 60% of the oyster crop have smothered under sediments and debris deposited by the storm surge due to Hurricane Ike (Haby et al., 2009). It is unknown how long it will take for the reefs to recover. This makes the need for the preservation of oyster reefs an important issue. Next to their bioactivity in the Bay the oyster reefs have a small local economic importance as well. The Galveston Bay oyster harvest generates nearly \$10 million per year (Galveston Bay Status and Trends, 2013).

2.9 Bolivar Roads overview

Figure 2.7 summarizes information presented in this chapter highlighting important aspects regarding Bolivar Roads.

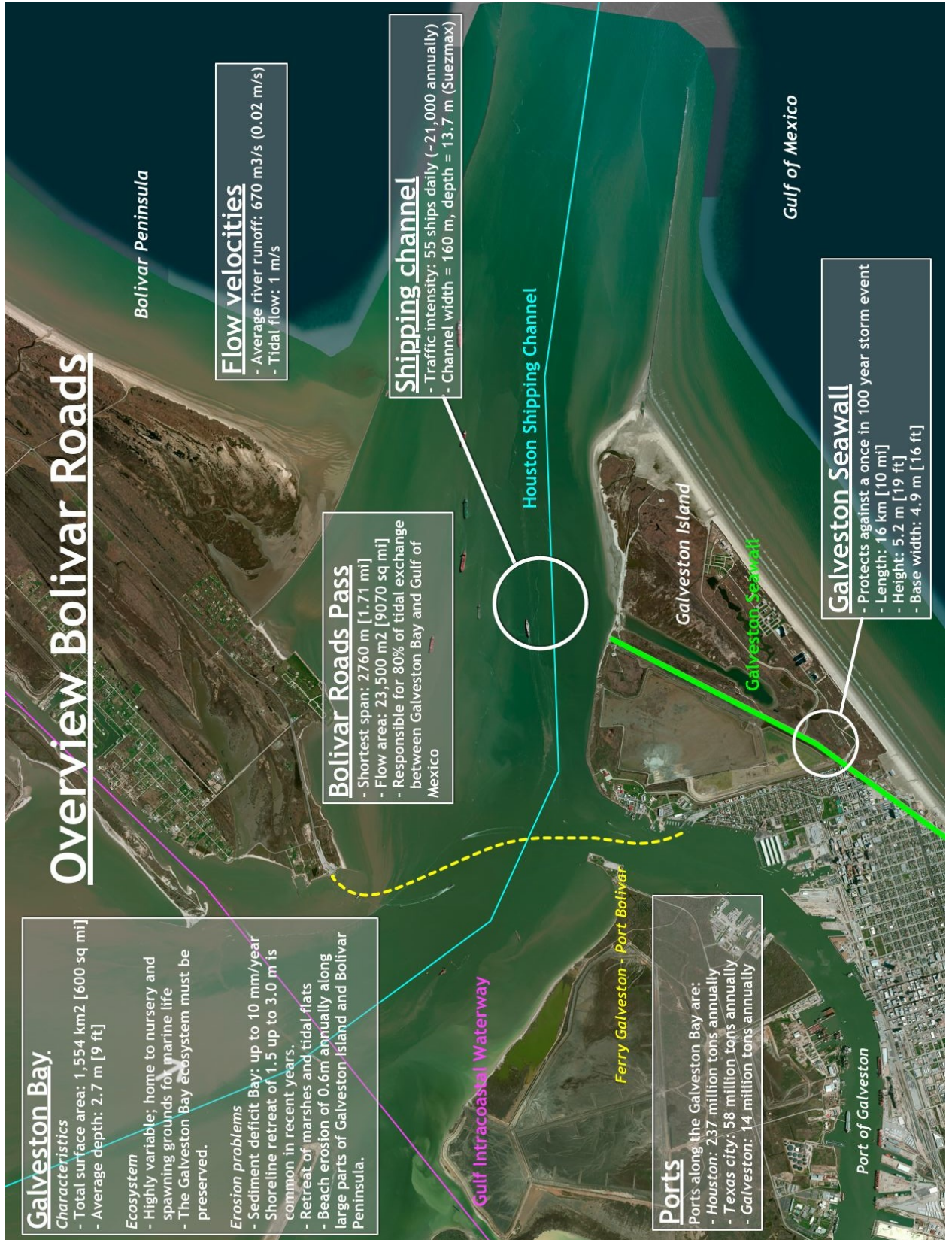


Figure 2.7: Overview of Bolivar Roads highlighting important aspects. Satellite image: Bing Maps (2013).

3 Storm surge barriers

The purpose of this chapter is to introduce the reader to storm surge barriers. First a precise definition of storm surge barriers is presented and a short outline of its key functions is given. Next a short development of applied construction materials is discussed. As reliability is an important property of storm surge barriers attention will be given to this aspect in Section 3.3. For an extensive overview of several gate types refer to Appendix B.

3.1 Definition

Before describing the term 'storm surge barrier' one should define what 'storm surge' is. The U.S. National Hurricane Center (NHC), department of the National Oceanic and Atmospheric Administration (NOAA), defines a storm surge as "an abnormal rise of water generated by a storm, over and above the predicted astronomical tides" (NOAA-NHC, 2012). This onshore rise of water is associated with a low pressure weather system, typically hurricanes. The rise in water level can cause extreme flooding in coastal areas particularly when storm surge coincides with normal high tide. The combined effect of low pressure and persistent wind over a shallow water body is the most common cause of storm surge flooding. Logically, a storm surge barrier (also referred to as 'flood barrier') is a structure that protects people and property from flooding due to storm surges.

Conventionally, most barriers and flood defenses were built as static structures like dikes and closure dams. During the 20th century, society demanded that defenses should not have a major effect on their surroundings anymore. For example migrating fish and sediment transports are heavily influenced when closing off an estuary. This resulted in the development of the moveable barriers (I-Storm, 2013). If one talks about a storm surge barrier nowadays, usually the moveable construction barrier is meant.

Definition: *A storm surge barrier is a partly moveable⁽ⁱ⁾ barrier in an estuary or river branch which can be closed temporarily⁽ⁱⁱ⁾. Its main function during surges is to reduce or prevent the rise of inner water level and thereby sufficiently⁽ⁱⁱⁱ⁾ protecting the hinterlying area against inundation.*

- (i) The ratio of the cross section that is moveable must be large enough to be able to allow sufficient circulation flow in the inner water in normal conditions. This can for example be important for inner water ecosystems.
- (ii) A temporary closure is defined as either (INC-WG26, 2006; van der Toorn and de Gijt, 2012):
 - A closure required to protect against flooding starting from the moment of closing (related to expected high water levels) until the outer water level has dropped sufficiently. Overflow and increased inner water levels are taken into account.
 - A closure required to make the structure available for maintenance or repair.
- (iii) Sufficiently regards the maximum allowable inner water level which, in turn, is influenced by river runoff and is determined by the height and safety standards of the dike ring behind the barrier.

This definition already reveals the primary function of a storm surge barrier. Other functions that may be executed or supported by a storm surge barrier are for example the separation of fresh and salt water, the discharge regulation of fresh (river) water and to give migrating fish free passage. A storm surge barrier is opened under regular circumstances in order to sufficiently discharge river runoff or tidal currents and to enable navigation (van der Toorn and de Gijt, 2012).

3.2 Construction material

In the course of time, people all over the world have designed various types of storm surge barriers. As different boundary conditions require different approaches these barriers vary greatly from each other, also tied to construction date. Wood has been the main construction material for barriers in the past until reinforced concrete and steel were introduced. This allowed people to build larger, stronger, and more durable constructions.

The appliance of other materials is introduced in the last decades, for example rubber fabrics in inflatable rubber dams and the yet-to-be-built parachute barrier (see Appendices B.8 and B.9). However, most storm surge barriers are concrete structures with moving parts made of steel. Unfortunately the conventional steel lifting gates corrode quickly as the gates are exposed to heavy weather influences and mostly placed in aggressive environments. To prevent corrosion they have to be recoated every once in a while, resulting in large maintenance costs. Nowadays the possibilities of applying Fiber-Reinforced Plastics (FRPs)⁽¹⁾ as construction material for gates in barriers and locks are investigated. This material is attractive for gates because it has a high strength to weight ratio, low maintenance costs and is less vulnerable to corrosion than steel (FRP & Composite Technology Resource Centre, 2012). Though not treated in this thesis, the appliance as lifting gates FRPs appear to be very advantageous and technically/economically feasible (Kok, 2013).

3.3 Lessons learned

An important property of storm surge barriers is the reliability⁽²⁾. In general the more complex the structure's system and the closing procedure is, the less reliable it will be. Even though a barrier is designed and constructed very decently, when its reliability is lacking the overall safety level of the barrier can drop significantly. In order to sufficiently perform the barrier's main tasks its reliability should therefore be as high as possible. As various barrier types have different levels of reliability this aspect should be taken into account in the design process. This section presents two examples of storm surge barriers that deal or have dealt with reliability issues. Lessons should be learned from these two examples and where possible included in the design process.

3.3.1 Maeslantkering safety system

The Maeslantkering (see also Appendix B.5), experienced reliability issues when the control systems appeared to malfunction. The computer systems, the Besturingssysteem Waterweg (BESW)⁽³⁾ and the Beslis en Ondersteunend Systeem (BOS)⁽⁴⁾, do the decision and control of all functions of the Maeslantkering. Annual test closures revealed that the barrier was afflicted with problems of a nature that without substantial intervention the barrier would never function as intended (Rijkswaterstaat, 2010). In the context of the Wet op de Waterkering⁽⁵⁾ failure probability requirements had been defined. These induced the maximum failure probability for the Maeslantkering, which is defined as 1 in 100 closures. The test closures revealed that actual failure probability of the barrier was around 1 in 10 closures back in 2003. Main causes for this increase in unreliability were the bad quality of the BESW and to a lesser extent the BOS. It resulted in the introduction of probabilistic management and maintenance⁽⁶⁾: a principle

⁽¹⁾ Fiber-Reinforced Plastic is a polymer matrix, either thermoset or thermoplastic, which is reinforced with a fiber or other reinforcing material with a sufficient aspect ratio (length to thickness) to provide a discernable reinforcing function in one or more directions (FRP & Composite Technology Resource Centre, 2012).

⁽²⁾ Reliability is the probability that a structure or part of a structure (existing or to be designed) will perform its prescribed duty without failure for a given time when operated correctly in a specified environment (INC-WG26, 2006). Storm surge barriers deal with three types of reliability: electrical, mechanical and human reliability. Electrical reliability refers for example to the extent to which computer systems fulfil their task. Mechanical reliability refers for example to a barrier that gets stuck. Human reliability regards the consequences due to human failure.

⁽³⁾ Besturingssysteem Waterweg (BESW): Controlsystem Waterway.

⁽⁴⁾ Beslis en Ondersteunend Systeem (BOS): Decision and Support System. The BOS receives the predicted sea levels on the North Sea, the river discharge and wind data. Using the hydrodynamic model SOBEK the expected water level near the Maeslantkering is calculated (Rijkswaterstaat, 2010)

⁽⁵⁾ A Dutch Law (dated December 21st, 1995) that lays down general rules to ensure the protection by flood defenses against flooding by seawater and control of related matters (Ministerie van Infrastructuur en Milieu, 2009).

⁽⁶⁾ In Dutch: Probabilistisch Beheer en Onderhoud (ProBO)

that links failure probability to the way management and maintenance are executed. Ever since a positive trend deployed finally resulting in a failure probability of 1 in 109; meeting the maximum failure requirements in April 2009, see Figure 3.1 (Rijkswaterstaat, 2010).

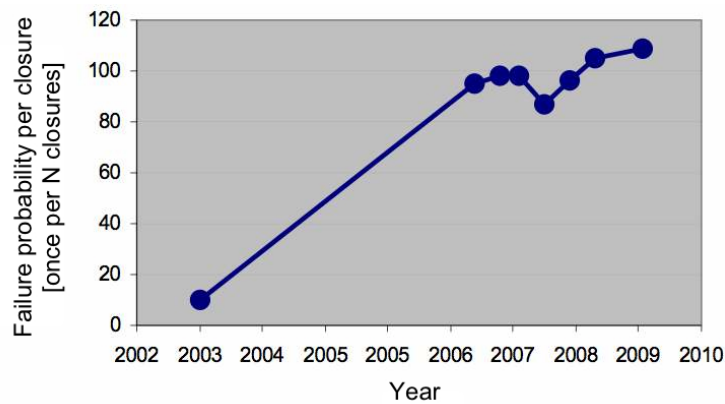


Figure 3.1: Development of the reliability of the Maeslantkering (Rijkswaterstaat, 2010).

3.3.2 Eastern Scheldt Barrier issues

The Eastern Scheldt Barrier (see also Appendix B.3) is a vertical lifting gate structure that encountered some issues during its lifetime. They are listed below.

Scour holes in bed protection. The Eastern Scheldt Barrier (see also Appendix B.3) is a vertical lifting gate structure of which the supporting concrete piers are embedded in several layers of rock. To ensure stability of the structure a bed protection was placed with a width varying of 550 to 650 m [1,800 - 2,130 ft] on either sides of the barrier. This sea-bed protection consists of asphalt mastic and block mats in the outer periphery, and graded filter mattresses under the piers (Van Noortwijk and Klatter, 1999). Despite thorough research unexpected scour holes occurred in the bed protection of the Eastern Scheldt Barrier. Scour-hole initiation and the exact scour-hole development are processes that are still pretty much unclear. The bed protection must be inspected to detect possible scour holes that might endanger the stability of the barrier. Continuous monitoring and resulting maintenance of the bed protection is executed to prevent deterioration of the barrier's reliability. This preventive maintenance measure is similar to the Probabilistic Management and Maintenance principle described above.

Corrosion of the steel doors. A solution for this problem could be found in using FRP as the construction material for the doors (see Section 3.2).

Chloride penetration into concrete inducing reinforcement corrosion. The durability of concrete structures exposed to marine environment highly depends on the the ability of concrete to resist chloride ingress (Costa and Appleton, 1999). It was considered the dominant deterioration mechanism for the Eastern Scheldt Barrier (de Rooij et al., 2003).

The influence on environmental qualities. Originally, the Eastern Scheldt Barrier was designed as a closure dam. Due to resistance from environmental organizations and local fisherman it was decided to make it a partly open barrier, preserving the Eastern Scheldt ecosystem. The constriction is large, the flow area at the inlet decreased to about 20% of its original size (A. van der Toorn, *TU Delft*, personal communication 13-8-2013). Actually one can state that constructing a partial open barrier was already a 'win' for the ecosystem in the Eastern Scheldt compared to the original plan. After all, this loss of 80% flow area had its influence on the ecosystem of the inner water. The freshwater load has decreased to less than 1% of the tidal volume, hence the system has changed from an estuary into a tidal bay (Smaal and Nienhuis, 1992). The tidal range at the innermost point of the Eastern Scheldt near

Yerseke experienced a decrease in tidal range of approximately 30 cm [12 in], see Figure 3.3. Notwithstanding the substantial changes in the environment, the productivity of the system at the primary trophic level has been maintained. The biotic part of the ecosystem has shown a resilient response (Smaal and Nienhuis, 1992). From this example it can be concluded that even a very large constriction at the entrance of a tidal basin does not have to be only disadvantageous for the inner water ecosystem. Ecosystems are resilient and can shift to a new equilibrium which does not per definition have to be a deterioration.

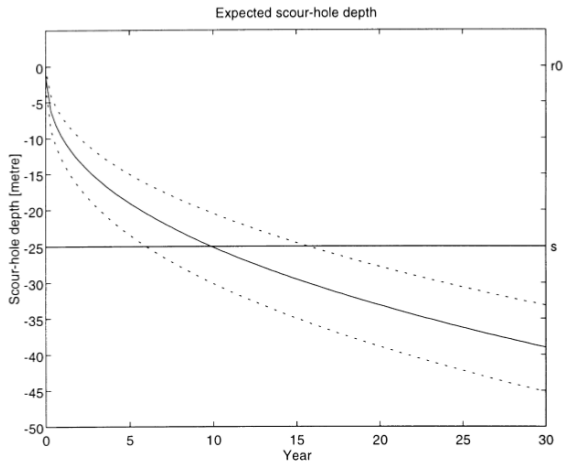


Figure 3.2: Expected scour-hole depth in the Eastern Scheldt block mats, and its 5th and 95th percentile, as a function of time (Van Noortwijk and Klatter, 1999).

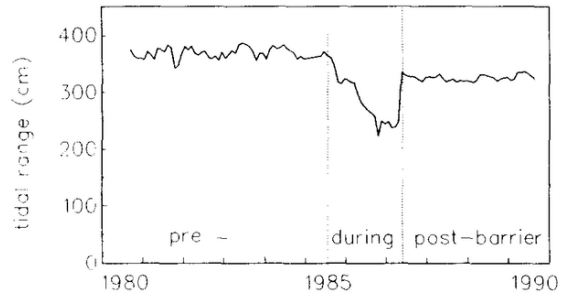


Figure 3.3: Tidal range in the Oosterschelde pre-, during and post-barrier construction at station Yerseke (Smaal and Nienhuis, 1992).

4 Requirements for a Bolivar Roads Surge Barrier design

This chapter lists the requirements for a storm surge barrier in Bolivar Roads. These include general, nautical, environmental, design and operational requirements. The requirements define what the storm surge barrier should be capable of. Furthermore the requirements serve as guidance throughout the design process. Also a brief list of involved stakeholders is presented as their interest and influence may have an impact on the overall progress of the project.

Refer to Appendix C for calculations and detailed derivation of numbers used in this chapter.

4.1 General requirements

Bolivar Roads serves two primary functions. The first is economic of nature: Bolivar Roads is an important shipping corridor connecting three major ports along the Galveston Bay (see Section 2.1) to the Gulf of Mexico. The second is ecological of nature: Bolivar Roads is the largest inlet in the Galveston Bay accounting for 80% of the tidal exchange between the Bay and the Gulf, which is important for the ecosystems in the Bay. Adopted from these main functions the two primary requirements for the storm surge barrier are:

1. In normal conditions a section of the barrier should be open in order to enable navigation between the Galveston Bay and the Gulf of Mexico.
2. When in opened position in normal conditions the barrier must be able to sufficiently exchange water between the Bay and the Gulf of Mexico in order to preserve the Bay's ecosystem.

These general requirements are both further substantiated in the next two sections: the nautical requirements and the environmental requirements.

4.2 Nautical requirements

To maintain the competitive position of the ports in the Galveston Bay with other large ports along the Gulf of Mexico (such as the Port of South Louisiana) Bolivar Roads Pass should have a high standard as it comes to vessels that are able to transit the waterway. Currently Bolivar Roads and the HSC are able to accommodate the Suezmax⁽¹⁾ tanker. In the future, a larger channel is required in order to accommodate larger ships and maintain a competitive position with respect to other ports. An expansion will also ensure safer and more efficient passage of ships and barges (BUG, 1990). As the Panama Canal expansion nears its completion, an additional increase in vessel size is expected. In the near future local decision makers may wish to assure the passage of the New Panamax⁽²⁾ tankers.

Besides the deep-drafted vessels also barges must be able to pass the barrier. Currently their channels are located along the HSC, see Figure 2.6.

⁽¹⁾The maximum vessel size that is able to sail through the Suez Canal. Dimensions: draft = 13.7 m [45 ft], width = 50 m [164 ft], length = 275 m [899 ft] (HGNSAC, 2011).

⁽²⁾The maximum vessel size that is able to sail through the Panama Canal after completion of the new navigation locks in 2015. Dimensions: draft = 15.2 m [50 ft], width = 49 m [161 ft], length = 366 m [1,200 ft] (Benitez, 2009).

4.2.1 Navigation channel dimensions

The minimum depth and width for navigation in Bolivar Roads can be determined using formulas developed by the PIANC group (Ligteringen, 2009). According to these formulas, to accommodate the New Panamax tankers the channel will have to be dredged to a level of MSL-17m [56 ft] and has to be at least 220 m [722 ft] wide (see Appendix C.2).

4.2.2 Traffic intensity

The average day would see 55 ships crossing Bolivar Roads and 21 offshore support vessels. Recreational crafts are not taken into account in these numbers, but should be included (R.W. Welch, *VTS Houston*, personal communication 02-7-2013). As can be seen in Figure 2.6 there are currently two lanes along to the HSC for barges and other smaller vessels that do not need the depth of the HSC. In case a storm surge barrier is constructed navigation must not be limited in the way that vessels have to wait for each other to pass the barrier. All the ships, including the barges and smaller (recreational) vessels have to pass through a navigation section in the storm surge barrier. The calculation in Appendix C.2.2 shows that navigation through just a two-way (deep) channel without additional (shallow) barge lanes does not result in delays for navigation.

4.2.3 Maximum current velocity in navigation channel

For navigation channels a prevailing longitudinal current velocity higher than 1.5 m/s [4.9 ft/s] is classified as strong (PIANC-IAPH, 1997). This is assumed to be the maximum current velocity that may occur in the navigation channel in Bolivar Roads in normal conditions.

4.3 Environmental requirements

The barrier may not adversely affect the Bay's hydrodynamics in regular conditions. A decrease in flow area (constriction) at Bolivar Roads affects the tidal range and tidal prism of the Bay, influencing the water circulation in the bay and thereby the ecosystem. The effects of a decrease in flow opening at Bolivar Roads down to 80% of the original size are relatively small, if the flow opening in Bolivar Roads becomes less than 60% of the original the Bay's ecosystem is adversely affected (Ruijs, 2011). Using this finding the requirement is defined as: the barrier may obstruct the flow opening at Bolivar Roads in such a way that at least 60% of the original flow area is still open⁽³⁾.

Note: for evaluating the influence of a constriction in Bolivar Roads on the Galveston Bay's ecosystem the study by Ruijs (2011) takes energy losses due to in and outflow through a barrier structure in Bolivar Roads into account by modeling the barrier as if it were a spillway with high bottom friction. This gives an estimate of the energy losses, but the actual influence of energy losses will highly depend on the shape of the storm surge barrier. To give a more educated estimate for the implications of a constriction on the Bay's ecosystem it is recommended to include the exact geometry of the barrier in the model.

4.4 Design requirements

The design requirements define what the storm surge barrier should be able to resist in terms of safety level, lifetime and retaining character. Next to these requirements the specific site also offers an opportunity to make the design more cost-effective through the large retention capacity of the Galveston Bay.

⁽³⁾By means of comparison: the Eastern Scheldt Barrier constricts the flow area to the Eastern Scheldt a lot more: only 20% of its original size is still available. See also Section 3.3.2.

4.4.1 Safety level

The storm surge barrier will be designed to protect against surge levels with a return period of $1/10,000 \text{ yr}^{-1}$. According to Stoeten (2013) investing in this protection level gives the highest rate of return. The related surge level and wave heights for this protection are presented in the boundary conditions, see Section 5.2.

4.4.2 Structure lifetime & adaptability

The structure should be designed for a lifetime of 200 years like other large storm surge barrier projects as the Lake Borgne Surge Barrier in New Orleans and Eastern Scheldt Barrier in the Netherlands (see Appendix B.3). This implies that the used construction materials of the barrier must have at least a lifetime of 200 years. The problem with such a long design lifetime is that the exact required retaining height for 200 years from now is hard to determine. This is because the retaining height depends on the amount of Sea Level Rise (SLR) that has to be accounted for. Estimates of SLR are quite accurate for the next 100 years, but beyond a 100 years from now it is rather uncertain. If one would build the structure taking into account for example 200 years of SLR, one pretends that very accurate data is available while in fact that is not true. It will only give a false sense of knowing things and the structure could be overbuilt based on uncertain assumptions (W.J. Merrell, TAMUG, personal communication 27-8-2013).

To take this issue into account the functional lifetime requirement is translated into an adaptability requirement: *The barrier will initially be designed for a 100 year lifetime. After that time period it should be possible to increase the barrier's retaining height to respond flexibly to uncertain future Sea Level Rise up until a lifetime of 200 years (e.g. through constructing a wall on top to gain more retaining height).*

4.4.3 Reliability of barrier closure and opening

If one or more barrier doors fail to close, the barrier must still sufficiently block the surge. The retaining height of the barrier must be increased to compensate for such failure. The exact requirement will be defined later, as it highly depends on the barrier type and its retaining character. See Section 7.2. The same applies to the reliability of reopening the barrier after a closure.

4.4.4 Allowed overflow

As mentioned in Sections 1.2 and 2.4 the Galveston Bay is a relatively large basin compared to the size of its inlets. Therefore it is expected that inflow of water in the Bay results in a relatively small raise of inner water level. It is therefore expected that some overflow over the barrier might be allowed. In that case the barrier does not have to be fully retaining over its entire length, which reduces costs. According Merrell, the proposer of the Ike Dike, the maximum allowed surge level at the governing Northern side of the Bay is 3.4 m [11.0 ft] (TAMUG, personal communication 11-9-2013). Figure 4.1 shows the influence of water elevation in the bay on surge level for the Northern side of the bay. The complete calculation is presented in Appendix C.1.

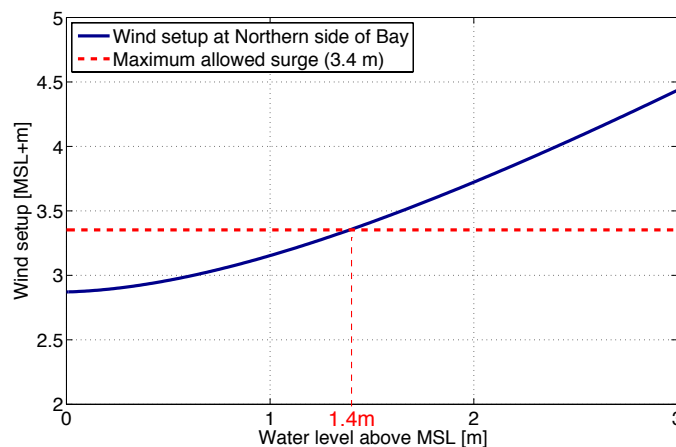


Figure 4.1: Surge due to wind setup related to increase of water level in the Galveston Bay for an average depth of 3 m.

As can be seen from the graph an acceptable surge level of 3.4 m [11 ft] occurs when the water depth in the bay has increased to a level of 1.4 m [4.6 ft] above MSL. This means the average depth has increased to 4.4 m [14.4 ft]. The conclusion is that the volume of water that flows over the barrier may induce at most a 1.4 m [4.6 ft] rise of the average water level inside the Galveston Bay.

Recommendation: as this number of 1.4 m [4.6 ft] determines a lot for the required retaining height of the barrier this calculation must be very accurate. In this thesis it is calculated using assumptions and a very simplified model, it is therefore strongly recommended to model a representative hurricane in a 3-dimensional model to accurately determine the surge levels in the bay due to different water level elevations. Furthermore the economical consideration is also important: the acceptable damage to the buildings and industrial facilities located in the flood prone areas has to be determined and taken into account to determine the maximum allowed surge levels in the Bay. This is outside the scope of this thesis.

4.4.5 Retaining character

The swirling character of a hurricane can induce various surge directions in a basin. Figure D.4 in Appendix D.2.2 is a schematic illustration of the Galveston Bay simplified as a semi-enclosed bay. It shows the influence of landfall location on the surge height for different locations along the shoreline of the Bay. As the hurricane passes by, the surge direction can suddenly flip over. For example the governing surge level for the storm surge barrier initially comes from the open coast. Not so much later as the hurricane passes the surge directions flips over resulting in a negative head⁽⁴⁾ on the barrier. This negative head could very easily damage the barrier structure when not accounted for.

The exact course of the changing surge is highly dependent on the hurricane landfall location and storm character, which are hard to predict a long time in advance. The barrier must therefore be able to cope with this sudden change in surge direction. This could be done in two ways:

- Either enabling the barrier to open and close within a very short period of time (up to fifteen minutes),
- or constructing the barrier in such a way that it is able to deal with negative head.

The first option is not very likely, as the barrier will probably consist of very large structures that are hard to open and close within such a short period of time. It is therefore assumed that the barrier must be able to deal with the negative head: it must be retaining in two directions.

4.5 Operational requirements

Operational requirements of the storm surge barrier are listed as:

- Barrier closure duration. The storm surge barrier will protect the area against high surges, but damage due to wind will still occur. Therefore the whole prone region will still be evacuated in case a major hurricane approaches. Whenever a hurricane approaches the prone region will be evacuated. Already hours/days before a hurricane arrives, most industrial and economic activities around the bay will come to a hold. This results in a negligible amount of ships passing Bolivar Roads (W.J. Merrell, TAMUG, personal communication 18-8-2013). A long lasting barrier closure that impedes navigation is therefore not a big issue. This makes the barrier closure time is not a big issue and may be in the order of a few hours.
- Barrier opening duration. For the same reason opening the barrier again after a hurricane has hit may take a few hours too. However, industries around the bay such as petrochemical industries should start running normally again as quickly as possible after a hurricane. Opening the barrier should therefore not take much

⁽⁴⁾The situation where the governing water level and forces on the barrier are directed from the Galveston Bay instead of from the Gulf of Mexico. It is the result of the better known 'backsurge' effect from the Galveston Bay.

longer than a few hours, as those industries rely heavily on navigation through Bolivar Roads.

- Closure under water flow. The barrier must be able to close under the presence and influence of water flow. The magnitude of the flow velocities must be determined and taken into account in the design.
- The barrier must be accessible for inspection and fit for maintenance.

4.6 Stakeholders

Individuals or groups that affect or are affected by the storm surge barrier (the stakeholders) should be determined, and their interests should be assessed, in order to be able to create the largest added value possible for the project. In the table presented below shows a short list of possible stakeholders and are sorted according to the impact of action on them (interest), and their impact on action (power).

Table 4.1: Stakeholders involved

Stakeholder	Interest/concern	Power
Federal government & State government	Stimulation of the economy, Increase safety of residential areas	++
Environmentalists	Preservation of the Bay's ecosystem	++
Bay Area Houston Economic Partnership	Sustainable stimulation of the country's economy by preserving economic assets	+
Investors	High return rates, low investment risks	+
(Chemical) Industries	Protection against surges	+
Other businesses	Protection against surges	+
Tourism	Preservation of the area's attractions	-
Citizengroups	Protection of personal property	+/-
Contractors	Make profit	-
Operators	Accessible barrier operation	+/-
Maintenance managers	Easy to perform maintenance	+/-

4.7 Conclusions & recommendations

In this chapter the requirements for a storm surge barrier in Bolivar Roads are listed. These concern general, nautical, environmental, design and operational requirements.

In normal conditions a section of the barrier should be open to enable navigation between the Galveston Bay and the Gulf of Mexico. This navigation channel must be dimensioned in such a way, that in the future the New Panamax vessels (the largest expected) are able to pass the barrier. This means the navigation channel must be maintained at a depth of MSL-17 m [56 ft] and has to be at least 220 m [722 ft] wide. Furthermore in normal conditions the barrier must be able to sufficiently exchange water between the Bay and the Gulf of Mexico in order to preserve the Bay's ecosystem. The barrier may obstruct the flow area in such a way, that at least 60% of the original flow opening in Bolivar Roads is still available. A lot depends on this exact value: if a larger obstruction appears to be feasible, the barrier can be built less costly (using for example a partial closure dam). As this number is based on a simplified model further research in this constriction requirement is recommended.

According to Stoeten (2013) the storm surge barrier reaches the highest cost-benefit ratio when designed to protect against surge levels with a return period of $1/10,000 \text{ yr}^{-1}$. As this is based on a flood risk assessment with limited accuracy a more thorough cost benefit analysis should be executed in which wind damage and inundation damage are assessed separately.

The retaining height of the barrier is designed for water levels up to a 100 year lifetime. After that, it should be possible to increase the barrier's retaining height to respond flexibly to uncertain future Sea Level Rise up to a lifetime of 200 years. Furthermore the barrier must be able to cope with surges in opposite direction (negative head; surge directed from the Galveston Bay towards the Gulf of Mexico).

The volume of water that flows over the barrier may induce at most a 1.4 m [4.6 ft] rise of the water level inside the Galveston Bay. This calculation is based on assumptions and the wind setup is calculated using a very simplified model. In order to determine an accurate amount of overflow it is strongly recommended for perform a 3D calculation to investigate the surge levels due to wind setup in the Bay. Besides an economical study into the damage to the buildings and industrial facilities has to be executed to determine the maximum allowed surge levels in the Bay. As this is outside the scope of this thesis just the 1.4 m [4.6 ft] maximum Bay level increase will be used.

Impeded navigation will not a big issue in case of barrier closure, making the open and closure times not so strict. They may both be in the order of a few hours.

Most important stakeholders are the Federal and State government. These parties will eventually be the client and will probably decide what kind of protection for the Galveston Bay Area will be built.

5 Boundary conditions

This chapter lists the boundary conditions for a storm surge barrier in Bolivar Roads. The barrier design must be in compliance with these boundary conditions. This chapter gives an overview of hydrographic/topographic, hydraulic, meteorological, geotechnical and environmental conditions.

Refer to Appendix D for a data and calculation of numbers used in this chapter.

5.1 Hydrographic and topographic conditions

The optimal location of the storm surge barrier is bounded by the orientation of the shipping channel, the positioning of the future *Ike Dike*, the bottom bathymetry, and the alignment between the barrier islands. For bathymetry maps of the Galveston Bay and Bolivar Roads refer to Appendix D.1. Figure 5.1 shows the bottom profile along the shortest span between Galveston Island and Bolivar Peninsula. For the location of this profile in Bolivar Roads see Figure 2.2a.

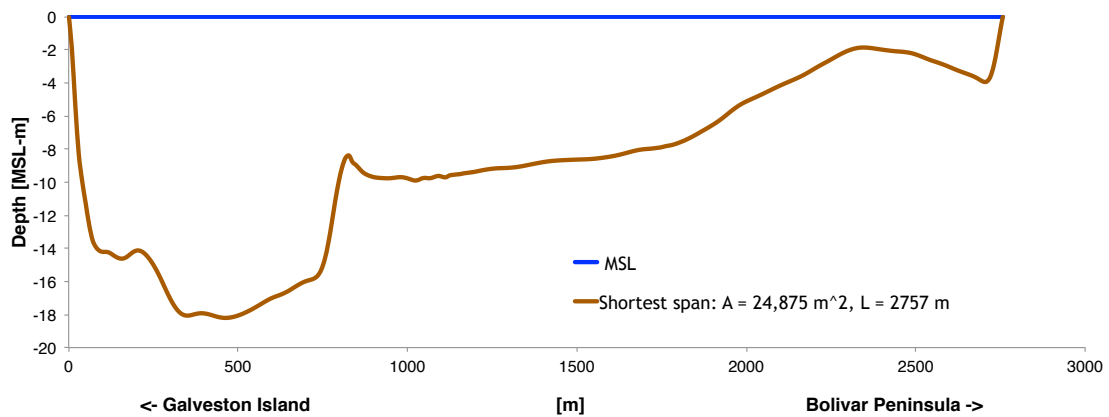


Figure 5.1: Depth profile Bolivar Roads along the shortest span between Galveston Island and Bolivar Peninsula. Based on data by Taylor et al. (2008b).

5.2 Hydraulic conditions

The hydraulic boundary conditions are split up in regular conditions and hurricane conditions. Regular conditions are relevant for the surge barrier's behavior in normal circumstances. Also the magnitude of SLR is mentioned under the regular hydraulic boundary conditions. Hurricane conditions concern especially the $1/10,000$ yr^{-1} surge levels. Table 5.1 gives a summary of all hydraulic conditions. These numbers are substantiated in Appendix D.2.

Note: from here on, unless otherwise stated, when referred to Mean Sea Level (MSL) the level including 100 year Sea Level Rise (1.0 m [3.3 ft]) is meant.

Table 5.1: Hydraulic boundary conditions

Regular conditions		
<u>Tides</u>		
– Tidal difference	0.35 m	1.16 ft
– Tidal prism (low)	$0.85 \cdot 10^8 \text{ m}^3/\text{cycle}$	$3.0 \cdot 10^9 \text{ ft}^3/\text{cycle}$
– Tidal prism (high)	$2.8 \cdot 10^8 \text{ m}^3/\text{cycle}$	$9.9 \cdot 10^9 \text{ ft}^3/\text{cycle}$
<u>Flow</u>		
– Maximum current velocity	1.0 m/s	3.3 ft/s
– Average river discharge	540 m^3/s	$1.9 \cdot 10^4 \text{ ft}^3/\text{s}$
<u>Sea Level Rise</u>		
– For the next 100 years	1.0 m	3.3 ft
Hurricane conditions		
<u>1/10,000 yr⁻¹ surge</u>		
– Maximum surge level h_{surge}	MSL+5.4 m	MSL+17.7 ft
– Maximum wave height H_{max}	5.9 m	19.4 ft
– Significant wave height H_s	3.3 m	10.8 ft
– Peak wave period T_p	7.9 s	

Design storm. By using the computations of Stoeten (2013) the peak surge level of a 1/10,000 yr⁻¹ storm is determined. This storm does not include a forerunner surge, which was in fact a very adverse aspect of Hurricane Ike that increased the surge levels in the Bay. Therefore a forerunner surge is also drafted by extrapolating the forerunner surge of Hurricane Ike. Manually combining it with the absolute peak surge of a 1/10,000 yr⁻¹ storm the design storm for the barrier is drafted, see Figure 5.2.

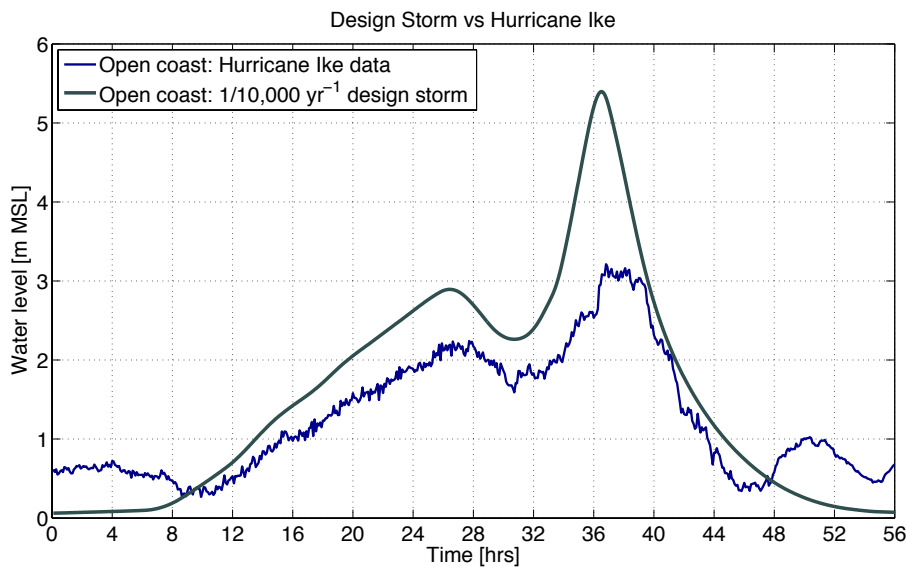


Figure 5.2: Water levels for a 1/10,000 yr⁻¹ design storm compared to the water levels during Hurricane Ike. Hurricane Ike data from NOAA Tides and Currents (2013b).

Note: assuming this combination of forerunner surge and maximum surge height probably results in conservative water levels. A storm generating such water levels might not even be physically possible. Further research is recommended to obtain a more accurate storm with a probability of return of 1/10,000 yr⁻¹.

5.3 Meteorological conditions

Galveston's climate is classified as humid subtropical. This is mainly because prevailing winds from the south and southeast bring both heat from the deserts of Mexico and moisture from the Gulf of Mexico. Annual rainfall in Galveston averages 1104 mm [43.46 in]. Most precipitation falls during the hurricane season which runs from June to November. Peak rainfall occurs during the hurricane season. Rainfall over some parts of the Galveston Bay Area over 48 hours during Hurricane Ike amounts about 200 mm [8 in] (NWS Weather Forecast Office, 2008a). This intense rainfall does not cover the whole surface area of the Bay. The peak rainfall will be spread out over the entire Bay resulting in just a slight increase in water level in the Galveston Bay (W.J. Merrell, TAMUG, personal communication 11-9-2013). So the surge height is expected not to be significantly influenced by rainfall. Furthermore, rainfall over the watersheds takes usually one or more day to flow down the rivers and reach the Galveston Bay. This will also not increase the surge because by that time the hurricane has already passed by (W.J. Merrell, TAMUG, personal communication 11-9-2013).

Refer to Appendix D.3 for the full meteorological data.

5.4 Geotechnical conditions

Table 5.2 presents the soil conditions at the easternmost point of Galveston Island (see Appendix D.4 for exact location). The soil in Bolivar Roads mainly consists of soft and firm clay layers before a strong bearing sand layer starts at MSL-40m [130 ft]. Unfortunately, the available soil data is very limited. The exact properties of the clay layers are unknown. As this is the only data available the storm surge barrier will be designed for these soil properties for the entire span along Bolivar Roads. This generalization is of course not correct, in order to design a foundation in detail data from borings and lab tests on multiple positions along Bolivar Roads is essential, as well as Cone Penetration Test (CPT) (or Standard Penetration Tests (SPTs)) data.

Table 5.2: Soil layer classification and strength properties. Modified from McClelland Engineers (1985).

Layer	Depth		Classification	Relative volumetric density	Undrained shear strength	
	[MSL-m]	[MSL-ft]			[kN/m ²]	[kips/sqft]
1	+1.5 - 0.0	+ 4.9 - 0.0	Very soft clay	50%	12	0.25
	0 - 3	0 - 10	Inter-layered very soft clay		12	0.25
2	3 - 15	10 - 50	Loose to dense recent sands			
3	315 - 20	50 - 66	Soft to firm clay		24	0.50
4	20 - 32	66 - 105	Laminated firm clay and silt		36	0.75
5	32 - 40	105 - 131	Firm to stiff clay		48	1.00
6	40 - 50	131 - 164	Very dense sand	>85%		

5.5 Environmental conditions

Subsidence and wetland loss occurs in the whole Galveston Bay estuarine system. Currently SLR and land subsidence causes a sediment deficit of up to 10 mm/yr [0.4 in/yr] in the Galveston Bay. This causes retreat of the marshes and tidal flats and erosion along the beaches of the barrier islands. Along Galveston Island 57% of the shoreline has experienced erosion rates averaging 0.6 m/yr [2 ft/yr] or more in recent years, while on Bolivar Peninsula this number is 86%. A shoreline retreat of 1.5 up to 3.0 m [5-10 ft] is common in recent years and a loss of marshes to open water of 0.47 km² [0.18 sqmi] has been documented for the Trinity Delta. The increase in erosion and land loss roughly coincides with the impoundment of the Trinity and other Texas rivers. It suggests

the possibility that human modification of both coastal systems and the fluvial systems draining to them may be contributing to erosion and coastal land loss (Philips, 2004).

The decrease of flow area at Bolivar Roads through the construction of a storm surge barrier will enhance these effects. The blocking of the sediment by constructing barriers and the redistribution of the sediment due to the decrease of the tidal prism, tidal range and current velocities might further enhance this problem (Ruijs, 2011).

Tidal and other periodical perturbations induce complex mixing of waters from different sources giving the Galveston Bay a highly variable ecosystem. Only those plants and animals that can tolerate fluctuating salinities and temperatures are found in this environment. Additionally, the small ecosystems formed by bayous, rivers, wetlands and marshes that surround the bay support a variety of flora and fauna. This diversity of habitats and abundance of nutrients provides very high levels of biologic productivity (Lester and Gonzalez, 2002; Ruijs, 2011).

For example oyster reefs are a primary geologic feature of the Bay, with the largest complex of productive reefs in the middle of the Bay. Large volumes of water can be filtered by a healthy oyster population. The filtering influences subsequently conditions such as water clarity and phytoplankton abundance. Simultaneously, the oysters' tendency to bioaccumulate some pollutants, combined with their lack of mobility, make them an important organic indicator for determining the health of the estuary. However, oyster reefs are very sensitive and vulnerable to storm surges. Biologists from the Texas Parks and Wildlife Department (TPWD) concluded that about 60% of the oyster crop have been smothered under sediments and debris deposited by the storm surge due to Hurricane Ike (Haby et al., 2009). It is unknown how long it will take for the reefs to recover. The *Ike Dike* and its surge barriers will assist in the preservation of the oyster fields by blocking the surge. Next to blocking the surge, the surge barriers will also prevent salt intrusion in the bay. Too much salt will wipe the oysters out of the Bay. Reducing the tidal prism at Bolivar Roads will also reduce the salt intrusion into the Bay, which be beneficial for the oysters in the Bay (W.J. Merrell, TAMUG, personal communication 11-9-2013). This shows that a storm surge barrier in Bolivar Roads does not by definition have to be detrimental for the ecosystem at all. In order to investigate the actual effects of a barrier on the ecosystem a thorough Environmental Impact Assessment (EIA) has to be performed.

Next to the effects of a barrier on the ecosystems in Galveston Bay the environment, in turn, can also have an effect on the barrier. Besides the aggressive, salty environment that affect the construction material, one should also think of the growth of acorn barnacles or other sea life growing on the structures. If big amounts of these organisms stick to the gates it can add a significant weight, having for example consequences for the weight of moveable doors. This had been the case at the Brazos River Floodgates project located on the GIWW near Freeport, TX. Due to the oyster growth on the sector gates their weight increased by about 70% over the last 10 years causing alignment issues with the opening/closing equipment (M.S. Peterson, USACE, personal communication 06-11-2013).



Figure 5.3: Oyster growth on sector gates at Brazos River Floodgates Project, Freeport, TX (USACE, 2011).

5.6 Conclusions & recommendations

In this chapter the boundary conditions for a storm surge barrier in Bolivar Roads are listed. These are hydrographic/topographic, hydraulic, meteorological, geotechnical and environmental conditions.

For the barrier a Sea Level Rise of 1.0 m [3.3 ft] for the next 100 years is assumed. This number is based on diverse estimates from different sources. It can be concluded that estimating SLR accurately is hard to do. A rather high uncertainty lies in these estimates, so it is recommended to further investigate future SLR. *From here on, unless otherwise stated, when referred to MSL the level including 1.0 m [3.3 ft] SLR is meant.*

The barrier will be designed for a maximum surge level of MSL+5.4 m [17.7 ft] above the which corresponds to a return period of once in 10,000 years. However, this is determined using a very limited dataset because information of historical storms is only available up to a 160 years ago. This introduces high uncertainties; one hurricane can actually change the entire prediction. Besides the surge levels are determined using simplified models. More advanced modeling and software will have to be used to come up with more reliable predictions.

1/10,000 yr⁻¹ storm character can be differentiated. A compact storm with very short and intense peak surge can have the same return period as a storm with larger diameter with smaller peak surge, but having a large forerunner instead. Hurricane Ike is an example of the latter. A storm generating water levels as presented in Section 5.2 is maybe physically not even possible. Further research in return period of different storm shapes is therefore highly recommended in order to create a representative 1/10,000 yr⁻¹ storm.

From boring logs near Bolivar Roads it becomes clear that the soil is quite weak. The soil in Bolivar Roads consists mainly of soft and firm clay layers before reaching a strong bearing sand layer at MSL-40m [130 ft]. Foundation design could therefore become challenging. Unfortunately, the available soil data is very limited. In order to design a foundation in detail data from borings and lab tests on multiple positions along Bolivar Roads is essential, as well as Cone Penetration Test (CPT) (or Standard Penetration Test (SPT)) data.

The influence of a barrier on the Galveston Bay's ecosystem must be further investigated. Besides, it is presumed that the decrease of flow area at Bolivar Roads enhances the erosion processes inside the bay. It is therefore recommended to perform a thorough Environmental Impact Assessment (EIA) of a storm surge barrier on the Galveston Bay to provide a decisive answer on these issues.

6 Design step 1: barrier system

Now that the design framework is ready the storm surge barrier is designed on system level. The aim is to get a first sense of the required dimensions of the barrier. To do so, first the most important cost drivers are identified. These cost drivers will be used to find critical aspects that lead to a cost-effective barrier.

Refer to Appendix E for calculations and elaborated approaches used in this chapter.

6.1 Cost drivers

First the most important cost drivers (from a constructive point of view) for the storm surge barrier are identified. This is done according to a basic formula drafted by van der Toorn (2012) that relates the total barrier investment costs O_b [\$] to the maximum water level difference over the barrier Δh_b [m], the height of the retaining construction $h_{c,b}$ [m], the barrier span B_b [m] and a certain cost unit rate $\sigma_{U,b}$ [\$/m³]. The latter one, the cost unit rate, is assumed to differentiate for navigable and non-navigable barriers, namely 40,000 and 30,000 \$/m³ respectively (based on estimates by van der Toorn (2012)).

$$O_b = B_b \cdot \Delta h_b \cdot h_{c,b} \cdot \sigma_{U,b} \text{ [\$]} \quad 6.1$$

This formula quickly identifies the important cost drivers for a barrier on a system level. Obviously the barrier's costs go per running meter, so the longer the barrier span, the higher its costs will be. As the soil in Bolivar Roads is weak (see Section 6.2) the foundation costs will probably be an important cost driver. Choosing an optimal location of the barrier across Bolivar Roads is therefore critical. The optimal alignment is further discussed in Section 6.2. Not included in Equation (6.1) is whether or not the barrier will be connected to the higher grounds on Galveston Island and Bolivar Peninsula, but this is also considered in the optimal alignment.

The influence of construction height on costs can be minimized by optimizing the division between the retaining heights for the navigation and the environmental section, as these have their own unit costs. The optimal division is determined in Section 6.3. The magnitude of the maximum water level difference over the barrier is assumed as given.

Note: Equation (6.1) gives just a quick insight in total barrier costs based on a small dataset of only 9 storm surge barriers. It is a basic formula that does not take any details or specific barrier types into account. For the level of accuracy in this design step on system level it does what is needed: just giving an idea of total barrier costs.

6.2 Barrier location

As indicated in the previous section the length of the barrier span is an important cost driver. To find the most optimal barrier span first three possible barrier span alternatives are presented, see Figure 6.1. The shortest span between Galveston Island and Bolivar Peninsula is 2760 m [1.71 mi] and the shortest span between the existing Galveston Seawall and the higher grounds on Bolivar Peninsula is 3050 m [1.90 mi]. The span lying in line with the Galveston Seawall is 3280 m [2.04 mi]. The depth profiles of the different spans are presented in Figure 6.2. These spans will be evaluated in this section and the most optimal span is determined.

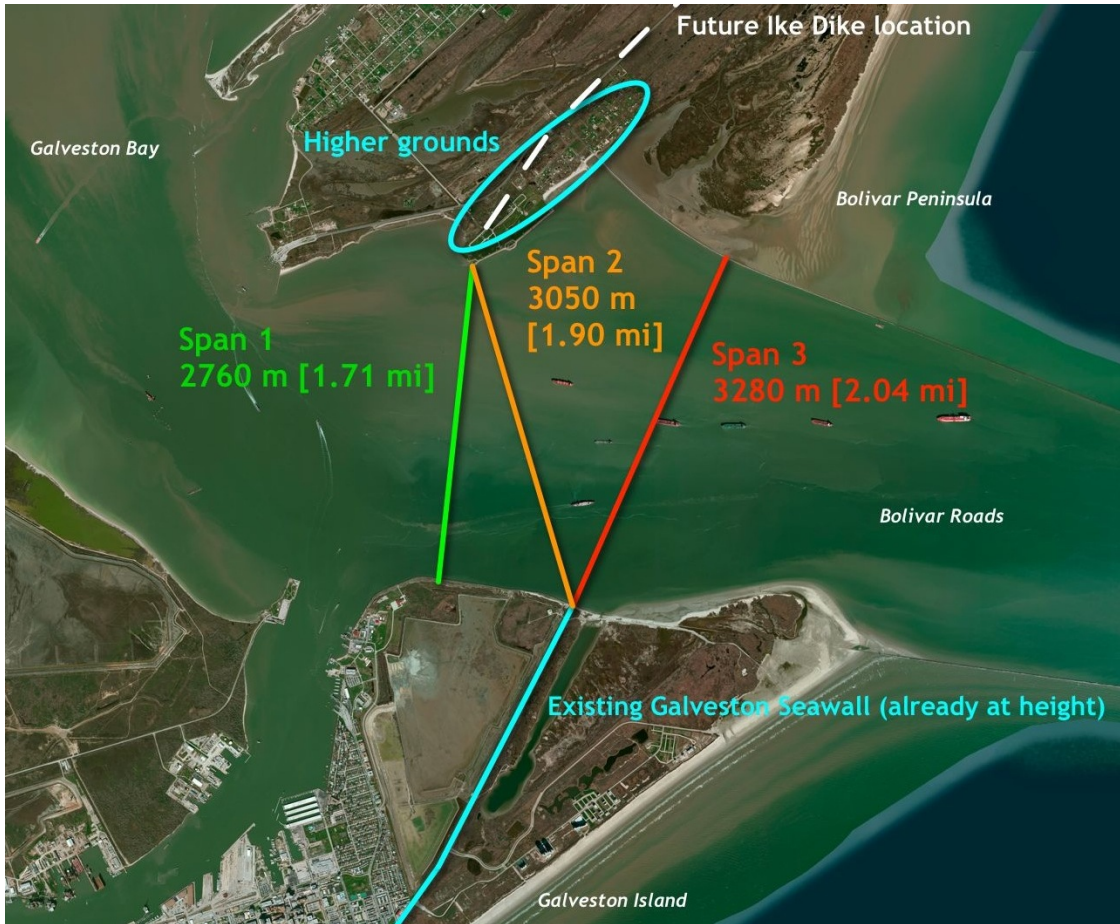


Figure 6.1: Different alignment alternatives in Bolivar Roads. Satellite image: Bing Maps (2013).

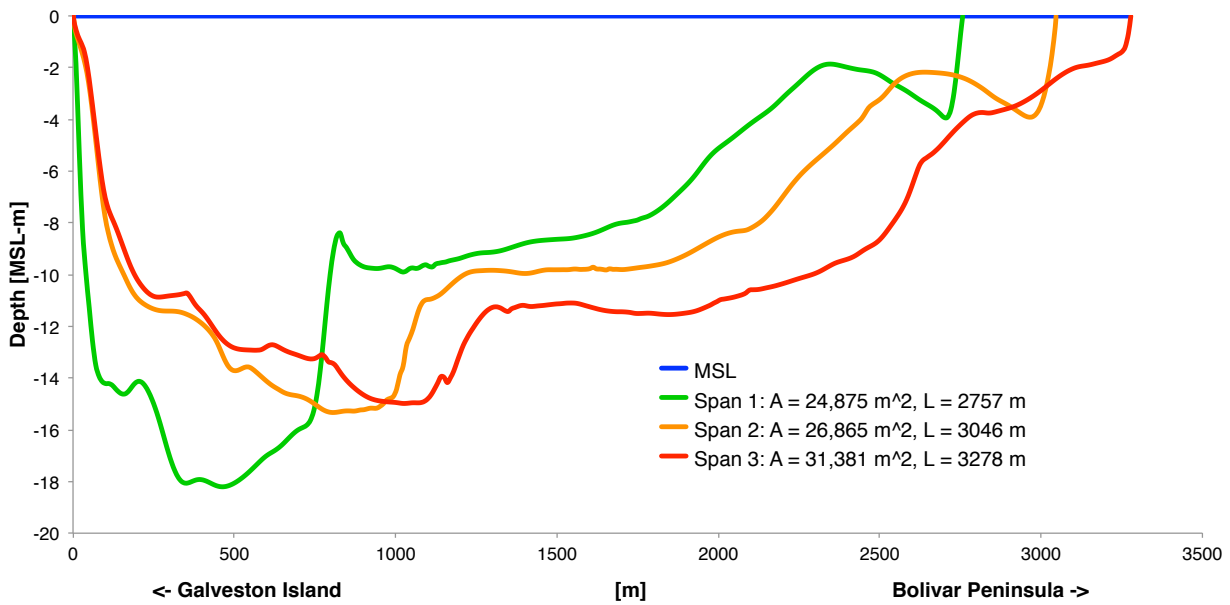


Figure 6.2: Depth profiles barrier spans. Based on data by Taylor et al. (2008b).

These spans have the following (dis)advantages:

Span 1 (green):

- + It is the shortest span between both islands, which limits costs.
- + On Bolivar Peninsula it is connected to area that is already at height
- + It is orientated perpendicular to the shipping channel resulting in minimum obstruction for navigation
- An additional levee of ± 1 km [0.6 mi] has to be constructed on Galveston Island to connect it to the Galveston Seawall

Span 2 (orange):

- + It is connected to the existing Galveston Seawall
- + It is connected to the higher grounds on Bolivar Peninsula.
- It is the middle long span, resulting relatively higher costs
- It is slightly inclined orientated to the navigation channel

Span 3 (red):

- + It is connected to the existing Galveston Seawall
- It is a long span which is disadvantageous in terms of costs.
- It is not connected to the higher grounds on Bolivar Peninsula
- It is slightly inclined orientated to the navigation channel

Conclusion barrier location. The foundation costs are expected to become decisive. Therefore a short span is preferable, which directly rejects the longest alternative: span 3 (red). Span 2 (orange) has the benefit of being directly connected to the higher grounds on both islands but it is a 289 m [948 ft] longer than span 1 (green). The latter one on the other hand has the disadvantage of requiring a 1 km [0.62 mi] levee to connect it to the Galveston Seawall. However, as the costs for 289 m additional storm surge barrier length from span 2 will very likely outnumber the costs for a simple levee of 1 km the first span is favorable.

The conclusion is therefore that the first span (green) is the preferred alignment along Bolivar Roads. For this span a barrier will be designed.

Note: in this assessment the difference in connection between the storm surge barrier and a soft abutment (e.g. a levee) or a hard abutment (like the Galveston Seawall) is not taken into account. Even though the difference in connection will probably not make a difference for which barrier alignment is the best, it is recommended to take this design aspect into account for a more thorough assessment.

6.3 Distribution of retaining height

As stated in Section 4.1 Bolivar Roads Pass serves two main functions which are economic and ecological of nature. It is therefore obvious to divide it in two sections both aiming on serving one of these key functions: a navigational section which spans the Houston Shipping Channel (HSC) and an environmental section, that aims on the preservation of the ecosystem in the Galveston Bay by enabling sufficient water exchange. See figure Figure 6.3.

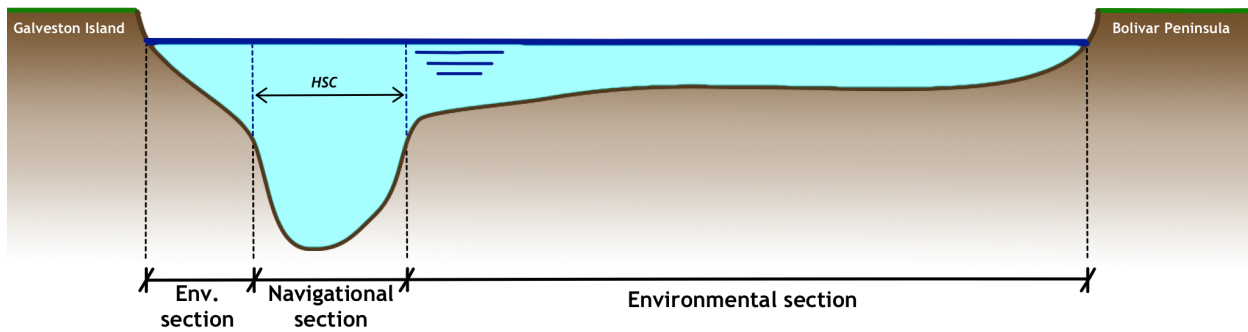


Figure 6.3: Schematic distribution of navigational and environmental barrier sections (not to scale).

The purpose of the storm surge barrier is to *reduce* the surge height in the Galveston Bay. As stated in Section 4.4.4 the volume of water that flows over the barrier may increase the water level in the Galveston Bay by at most 1.4 m [4.6 ft]. It is assumed that whether this volume flows through the navigational or environmental section does not matter for the Bay itself. From this fact there arises a trade-off between the navigational and environmental sections: they do not have to be both fully retaining. If the navigational barrier fully blocks the surge the environmental section may allow more water overflow. Vice versa: if the navigational section is not fully retaining, the environmental section must be able to block a larger part of the surge. From here the following question that arises: What is the most cost-effective and thus optimal distribution in retaining height between the navigational and environmental sections?

In this section different distributions in retaining height are investigated, see Table 6.1. First it is determined whether leaving the navigational section open is a feasible option, this could be very attractive in terms of costs. Next it is determined what the most cost-effective distribution in retaining height is when both sections are partially retaining.

Table 6.1: Overflow configurations

Cross-section	Navigational Environmental	Retaining height	
		Open Closed	Limited Limited

⏟
⏟

First option, treated in Section 6.3.1
Second option, treated in Section 6.3.2

Before this analysis is executed three important assumptions have been made.

- The calculations in this chapter assume that the Ike Dike will be constructed. This means that the barrier islands are heightened and are able to fully block the surge and allow just a little wave overtopping that will not significantly increase the Bay’s water level. In this case, no overflow over the barrier islands is possible so the only way for the surge to enter the Galveston Bay is through Bolivar Roads Pass where the barrier is constructed.
- The duration of the design storm is long enough that any water inflow in Bolivar Roads is able to spread out over the whole Galveston Bay.
- The Sea Level Rise of 1.0 m [3.3 ft] is accounted for by adding this increase in water level *after* computing the design storm.
- The total costs are calculated using the basic costs formula from Equation (6.1).
- The span of the navigational is 220 m [722 ft] (determined in the requirements, Section 4.2.1) and the span of the environmental section 2537 m [8,323 ft] (by subtracting the navigational section from the total span determined in previous paragraph).

6.3.1 Open navigational section and closed environmental section

Just leaving a part of the barrier entirely open sounds attractive in terms of costs, but first it has to be investigated whether the increase in Bay water level due to such an open barrier stays within limits. In order to determine the water levels when applying this barrier the navigational and environmental sections are modeled as follows (for the extensive calculation: refer to Appendix E.1.1).

- The environmental section fully blocks the surge (indicated in grey in Figure 6.4). The water is not able to flow through the environmental section in any conditions and has to flow through the navigational section.
- The navigational section is modeled as a long, narrow channel protected by breakwaters on each side. The bed is protected to increase the bottom roughness and assists in reducing the surge (dashed orange line).

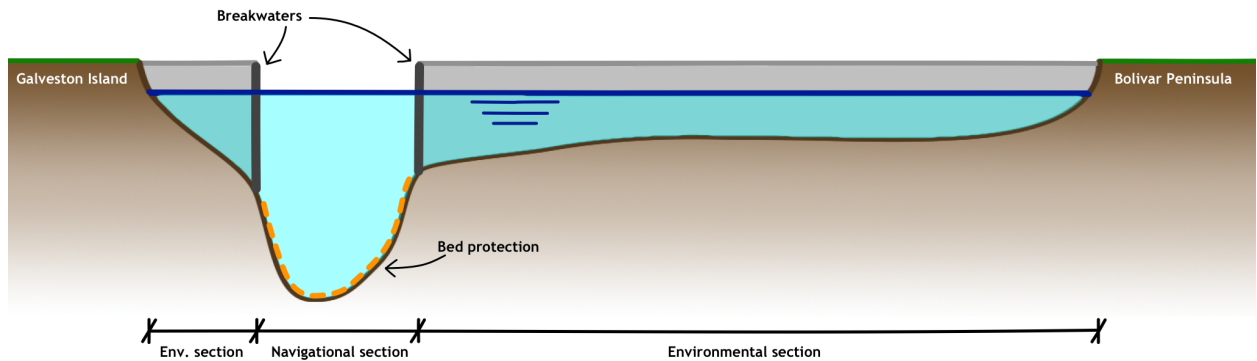


Figure 6.4: Schematic front view of a barrier with open navigational section and fully retaining environmental section (not to scale).

Next the design storm (as defined in Section 5.2) is released on this barrier and using a model based on the 'rigid-column approximation'⁽¹⁾ the resulting water in the Bay is calculated. The results are presented in the graph in Figure 6.5. The grey line represents the design storm (from Section 5.2). The light blue colored line is the water level above MSL inside the Galveston Bay when no barrier is applied (do nothing situation). The dark blue line shows the water level in case a barrier with open navigational section is applied. The red dashed line indicates the maximum allowed increase in bay water level as defined in Section 4.4.4.

Conclusion open navigational section. As can be seen from the graph in Figure 6.5 applying a 1 km [0.62 mi] long channel results in a maximum water level of 2.04 m [6.7 ft] inside the bay. This exceeds the maximum value of 1.4 m [4.6 ft] as it was defined in Section 4.4.4. By increasing the channel length more resistance can be given to the surge. By doing so, it appears when a channel length of at least 7 km [4.35 mi] is applied enough resistance will be given to sufficiently reduce the surge. But such a channel would stretch all the way along Bolivar Roads blocking the Galveston Shipping Channel entrance. The final judgment of applying an open navigation section is that it is *not* feasible.

⁽¹⁾The rigid-column approximation may be applied when the channel length is straight and short ($L_{channel} \ll \lambda_{surge}$) and has a negligible storage compared to the bay ($A_{channel} \ll A_{bay}$) (Labeur, 2007).

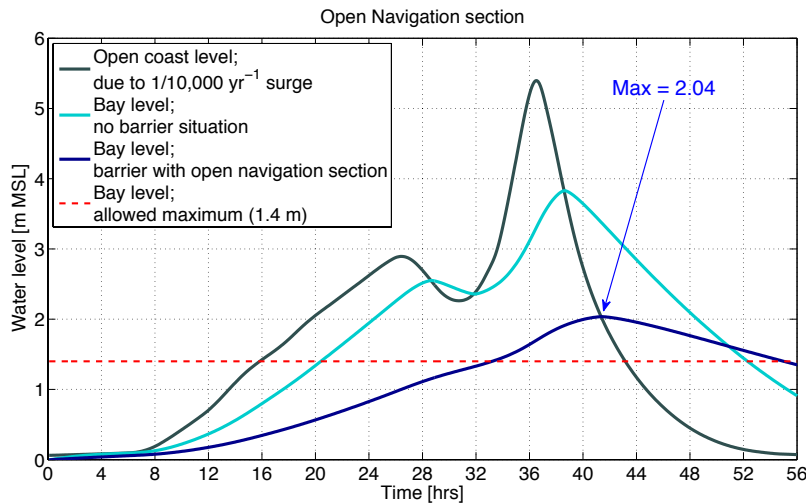


Figure 6.5: Bay water levels due to 1/10,000 yr⁻¹ open coast surge conditions. Current situation compared to applying a storm surge barrier with an open Navigation section.

6.3.2 Navigational and environmental sections both limited retaining

In this subsection it is investigated what the optimal division between retaining heights of the navigational and environmental sections is, see Figure 6.6. This is done using a similar procedure as for the barrier with open navigational section, but now the navigational and environmental sections are both modeled as a (submerged) sharp-crested weir, see Figure E.3.

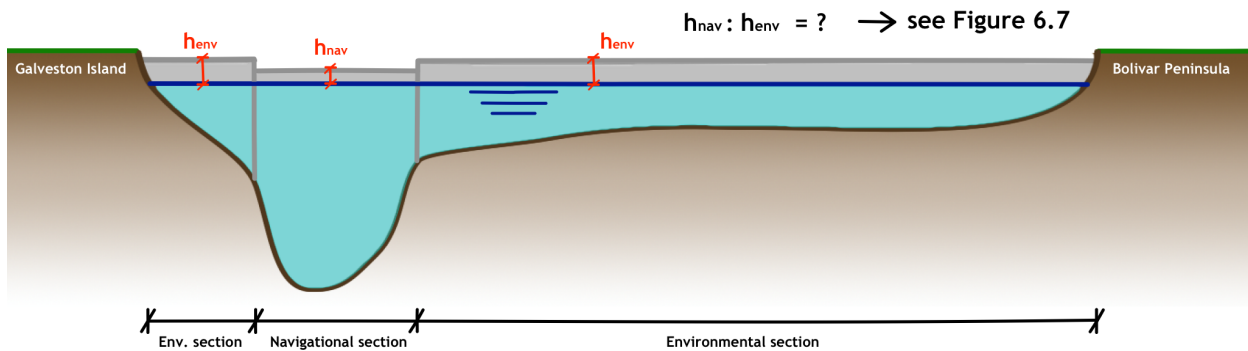


Figure 6.6: Schematic front and top view of barriers with a yet to be determined retaining height (not to scale).

The 1/10,000 yr⁻¹ storm is released on this barrier and using the sharp-crested weir formula the resulting water levels are calculated. The exact calculation procedure is described in Appendix E.1.2. However, the goal was to find the most cost-effective distribution in retaining height for the barrier. For 21 different configurations the total barrier costs are calculated. The calculation procedure is presented in Appendix E.1.2. The results are presented in Figure 6.7. In this figure the distribution in retaining height between the navigational and environmental section is plotted against the total costs. From this figure one can see that an equal retaining height over the full barrier span is the most cost-effective distribution.

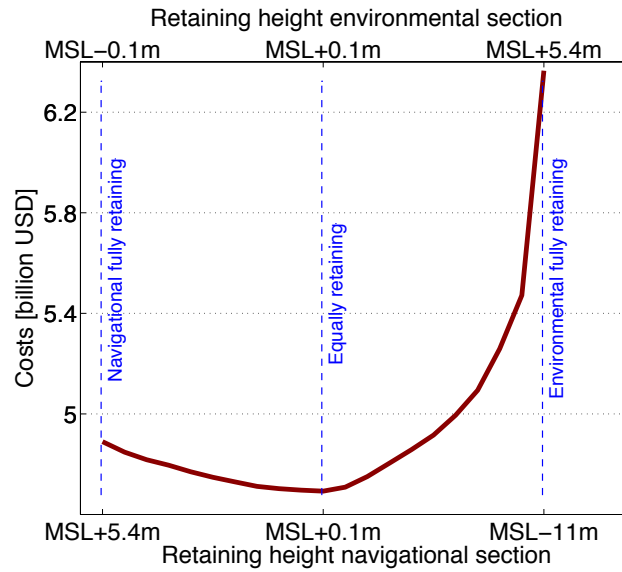


Figure 6.7: Costs for 21 distinct distributions in retaining height that all result in a 1.4 m [4.6 ft] water level rise in the Galveston Bay.

Note: in Figure 6.7 the lower and upper x-axes are both non proportionally scaled (e.g. the upper x-axis runs between MSL-0.1 m and MSL+5.4m). This is done to make the graph more clear. Furthermore the graph is asymmetrical. This is due to the difference in length of the barrier span and the distinct cost unit rates for the navigational and environmental sections.

Conclusion both sections limited retaining. From Figure 6.7 one can see that an equal retaining height over the full length of the storm surge barrier is the least costly. It appears that the barrier will be able to sufficiently block the surge when constructed at a continuous height of MSL+0.1m, see Figure 6.8. The water level inside the Bay (dark blue line) does not exceed the predefined maximum allowed water level increase (red dashed line), so the allowed overflow requirement from Section 4.4.4 is met.

The barrier constructed at a continuous height of MSL+0.1m will cost approximately \$4.7 billion, of which \$3.8 billion for the environmental section and \$0.9 billion for the navigational section.

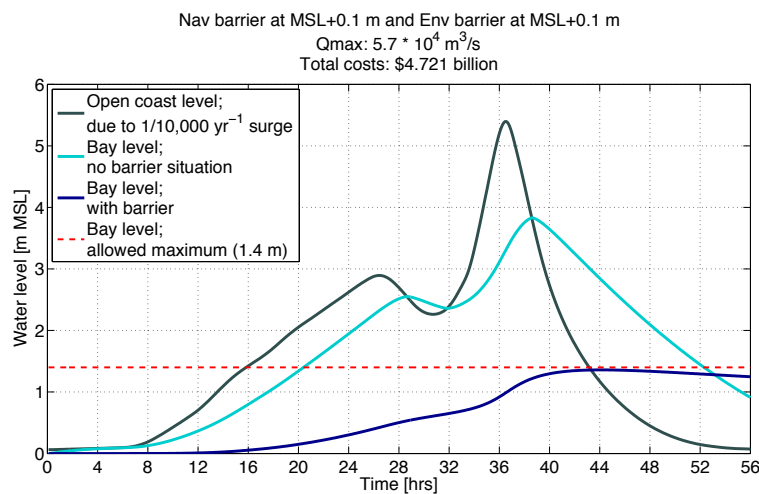


Figure 6.8: Both sections equally retaining (at MSL+0.1m)

6.4 Conclusions & recommendations

In this chapter the storm surge barrier is designed on system level to get a sense of the required dimensions of the barrier.

First the important cost drivers for a barrier design on system level are identified. Obviously these mainly concern the location and the required retaining height of the barrier. It appears that the shortest span between is most beneficial, even though it is not directly connected to the existing Galveston Seawall on Galveston Island.

As Bolivar Roads Pass serves two main functions it is obvious to divide it in two sections both aiming on serving one of these key functions: a navigational section that enables the passing of vessels and an environmental section that aims on the preservation of the ecosystem in the Galveston Bay. As the barrier may be overflowed the question arose what the most cost-effective and thus optimal distribution in retaining height would be. To determine so it is first investigated whether an open navigational section would be feasible, but it appears that the volume of water flowing in the Galveston Bay through this barrier during a $1/10,000 \text{ yr}^{-1}$ storm is too large. Both sections need a barrier. The most cost-effective distribution in retaining height is a continuous barrier height of $\text{MSL}+0.1 \text{ m}$ [$\text{MSL}+0.3 \text{ ft}$] along the whole span of Bolivar Roads.

This barrier costs approximately \$4.7 billion, of which \$3.8 billion for the 2537 m [8,323 ft] wide environmental section and \$0.9 billion for the 220 m [722 ft] wide navigational section. However, this cost calculation is not so accurate as it is drawn according to a very basic cost formula, with only a few design parameters. Furthermore it uses cost unit rates based on a very limited dataset of only 9 storm surge barriers. This limited dataset may draw a different conclusion for the most cost-effective distribution in retaining height. Using a formula that is based on a wider dataset and takes more barrier aspects into account the investment costs can be estimated more accurately. Additional research in storm surge barrier costs is needed to give better cost estimates. Also the door type should be taken into account.

Sea Level Rise (SLR) is accounted for when determining the barrier's optimal retaining height by simply adding 1.0 m [3.3 ft] of water level to the storm surge. This is not correct, SLR should be taken into account *before* modeling the storm surge as it influences the surge height. To determine the optimal retaining height it is recommended to first thoroughly investigate the $1/10,000 \text{ yr}^{-1}$ design storm that also includes SLR and take it into account in the design process.

7 Design step 2: environmental barrier

Because the prescribed workload for a Master's thesis is limited it is decided to focus on the environmental section of the storm surge barrier. In this chapter several barrier alternatives for the environmental section will be considered. First several alternatives will be quickly assessed on their applicability to the site. Thereafter the chosen barrier will be designed in further detail. Refer to Appendix F for calculations and elaborated approaches used in this chapter.

7.1 Barrier alternatives assessment

In this alternative assessment a barrier type is chosen based on four design criteria. These four equally weighed design criteria are drafted under the presumption that they cover the information that is now known from chapters 4, 5 and 6. They obviously do not cover all aspects but it is assumed this set suffices for taking an adequate decision on this level of detail. In this assessment all of these criteria are weighed equally, but for a thorough assessment it is recommended to use more design criteria and distinguish their importance.

The scores on these criteria are indicated by a simple yes (+), medium (\pm), or no (-). The rating scale is composed of three levels because a finer division (e.g. a 1 – 10 scale) gives a false sense of knowing precisely what the effect of the surroundings on the barrier will be and vice versa. However, at this level of detail this is not true, so a more qualitative assessment is executed.

To make a more detailed assessment it would of course be the best strategy to first make a preliminary draft for all alternatives. This is because a well informed decision cannot be made based on just simply comparing barriers on a few, evenly-graded criteria. The specific location of Bolivar Roads can for example enlarge (dis)advantages of a certain barrier type making it more or less preferable compared to another than it would seem at first sight. However, this would be too time consuming, so the barrier assessment is kept briefly and in compliance with the level of detail.

The assessment criteria are presented on the next page. For an extensive description of all barrier types refer to Appendix B.

Table 7.1: Barrier alternatives and their score on different criteria.

	Radial gates	Vertical lifting gates ^(I)	Flap gates	Floating sector gates	Visor gates	Vertical rotating gates	Inflatable rubber dams	Parachute barriers	Barge gates	Mailbox gates	Caisson structures
1) Adaptability of retaining height	-	-	-	-	-	-	\pm	\pm	\pm	-	+
2) Able to deal with (large) negative head	-	+	-	-	-	+	+	+	-	+	+(II)
3) Structure/foundation simplicity	+	+	-	-	+	-	+	\pm	+	-	+
4) Low investment and operational costs	+	+	-	-	\pm	-	+	+	-	+	+

^(I)Vertical lifting gates in between two piers, similar to the Eastern Scheldt Barrier gate type.

^(II)The exact door type that the caisson uses is not yet determined, it is assumed that these are able to be retaining in two directions.

- 1) The possibility to make the barrier adaptable. This means whether or not it is possible to increase the barrier's retaining height in an *easy* way to cope with uncertain future SLR up to 200 years (see Section 4.4.2).
- 2) The barrier's ability to cope with large negative head (see Section 4.4.5).
- 3) The simplicity of the structure. This includes the complexity of the foundation structure and the presence of complex driving mechanisms. Also the extent to which an advantage can be taken from repetition⁽¹⁾ is taken into account.
- 4) As the aim is to find a cost-effective barrier the alternatives are assessed on their estimated investment and operational costs. The simplicity of maintenance is also part of this criterion.

⁽¹⁾The economic effect of repetition on construction is due to a decrease in operational costs, on the one hand, and to indirect cost savings caused by the reduction of construction time (lower labour oncosts, costs for finance, machinery and equipment etc.), on the other (Economic Commission for Europe, 1965). The repetition factor is the quantification of the achieved repetition on a specific construction activity. The repetition factor for a storm surge barrier can for example be increased by producing as much as possible identical units.

Conclusion barrier alternatives assessment. The flap gates, the sector gates, the vertical rotating gates and the barge gate can be rejected based on the fact that their key features (enabling navigation, applicable to large spans) are not of importance for the environmental section. These barriers are unnecessarily expensive. Moreover, relatively smaller spans are preferable for the environmental section because a higher repetition factor can be achieved, which reduces costs. The radial gate and visor gate are structures that are poorly able to deal with a large negative head. These types of structures are mainly used as control weirs in rivers where the water head is directed from one direction only and are less suitable for a storm surge barrier.

The mailbox gate is a new design concept that has not been built yet. Probably a very thick flap is required to give enough pressure to withstand the hydrostatic pressure due to the water head. Also tough issues regarding wave force induces dynamics can be expected. The mailbox gate suits probably better as a weir in continuous flow with a small water head, such as a river or creek. Is also hard to easily increase the retaining height.

The inflatable rubber dam and the parachute barrier both face the same durability issue of the rubber material. It is hard to say how these fabrics barriers will behave in an aggressive environment for a long time. The fabrics might need to be replaced every 25-50 years. This is of course a disadvantageous aspect, but it can also be interpreted as an opportunity to make the barrier's retaining height easily adjustable. After a 100 years the fabrics need to be replaced anyway, so one could place a bigger fabric after this time period to increase the retaining height. Due to this fact both these barriers score a '±' on their adjustability. Fabric replacement also has a side effect as it has to be done quite frequently during the barrier lifetime. This increases costs. Therefore their score on costs (criterion 4) is downgraded from '+' to '±'.

The only structure that scores a '+' on all defined design criteria is a caisson structure, given that that the applied door type is able to retain water head in two directions. It is therefore decided to make a conceptual design for the caisson barrier. The remainder of this chapter will be devoted to the design and simulation of this caisson barrier.

7.2 Design input

Before a design of the caisson barrier can be drafted some important design input is listed. This design input is based on and in addition to Sections 4.7, 5.6 and 6.4.

- The minimum flow area at Bolivar Roads that has to be maintained is 60% of the original flow area (Section 4.3). Currently the flow area in Bolivar Roads is $A_{BR} = 24,875 \text{ m}^2$ (see Figure 6.2). Following the 40% constriction requirement the minimum flow area that has to be maintained is $A_{BR,min} = 0.6 \cdot A_{BR} = 14,925 \text{ m}^2$. The flow area through the navigational section is part of this, so the minimum flow area that has to be main-

tained for the environmental section is $A_{env,eff} = A_{BR,min} - A_{nav,eff} = 14,925 - 17 \cdot 220 = 11,185\text{m}^2$.

- The barrier must be retaining in two directions. The governing water heads and forces are presented in Figures 7.1 and 7.2.
 - The maximum positive head on the barrier Δh_b is 5.92 m. This value is calculated through adding a 1.5 m water level difference⁽¹⁾ (right behind the barrier, due to wind set down) to the maximum water level difference over the barrier in hurricane conditions defined by the design storm (see Figure 5.2).
 - The maximum negative head on the barrier $\Delta h_{b,neg}$ is 3.40 m. This value is adopted from the maximum allowable wind setup in the bay in hurricane conditions (see Figure 4.1).
Note: this negative head applies when the barrier remains in closed position and the surge in the bay is directed in opposite direction of the original storm surge. In reality if this occurs one would have already started opening the gates again, resulting in the water flowing from the Bay back into the Gulf of Mexico and thus relieve the negative head on the barrier. In further detailing it is recommended to take this into account.
- If 10% of the barrier doors fail to close, the barrier must still be able to sufficiently reduce the surge⁽²⁾. The retaining height of the barrier must be increased to compensate for such failure. But as this preliminary design just aims on giving a first estimate of the caisson dimensions this requirement is neglected.
- Horizontal wave loading on the structure according to wave height presented in Table 5.1.
- The reference level MSL is corrected for a 100-year SLR of 1.0 m [3.3 ft].
- According to the system level design the crest of the barrier must be at MSL+0.1m [MSL+0.3 ft] over the entire barrier span (see Section 6.3.2).
- The navigational barrier spans 220 m [722 ft]. On both sides a width of 100 m [330 ft] is reserved for the abutments. The space for these abutments is deducted from the environmental section, which from now on spans 2337 m [7,667 ft].

An overview of the relevant water levels and wave heights for the governing positive head is presented in Table 7.2.

Table 7.2: Relevant levels and depths.

<u>General</u>		
– Barrier crest level	MSL+0.1 m	MSL+0.3 ft
– Maximum wave height H_{max}	5.9 m	19.4 ft
– Wave crest level	MSL+8.4 m	MSL+27.6 ft
– Wave trough level	MSL+3.5 m	MSL+11.5 ft
– Tidal amplitude	MSL+0.18 m	MSL+0.6 ft
<u>Positive head</u>	[MSL+m]	[MSL+ft]
– Maximum surge level h_1	5.4 m	21.0 ft
– Corresponding Galveston Bay level h_2	0.52 m	1.7 ft
<u>Negative head</u>	[MSL+m]	[MSL+ft]
– Maximum surge level h_1	3.4 m	11.1 ft
– Corresponding Gulf of Mexico level h_2	0 m	0 ft

Notes: in this table in the values for Mean Sea Level the 100 year SLR of 1.0 m [3.3 ft] is taken into account. Surcharges for seiches are not taken into account in the design.

⁽¹⁾This value is an assumption. The wind set down depends on the character and pattern of the hurricane and the time of occurrence of the wind set down compared to the maximum surge levels. This modeling is quite complex and is therefore not executed in this thesis. A value of 1.5 m seems like a reasonable assumption when looking at Figure 4.1. In order to accurately determine this wind set down in the bay it is strongly recommended to model a representative hurricane in a 3-dimensional model.

⁽²⁾The door failure requirement for the caisson barrier is adopted from the Eastern Scheldt Barrier design, which is still able to sufficiently block the surge in case 6 of 62 barrier doors ($\approx 10\%$) fail to close in storm conditions (A. van der Toorn, *TU Delft*, personal communication 13-11-2013).

The schemes of forces acting on the barrier for positive and negative head are presented in Figures 7.1 and 7.2. For explanation of variables and assumptions: see Appendix E2.1. The weight of the water that flows over the barrier is not taken into account. This, however, will eventually work out on the safe side as one will see later on that horizontal friction will be governing, and a higher vertical force contributes in resisting this mechanism.

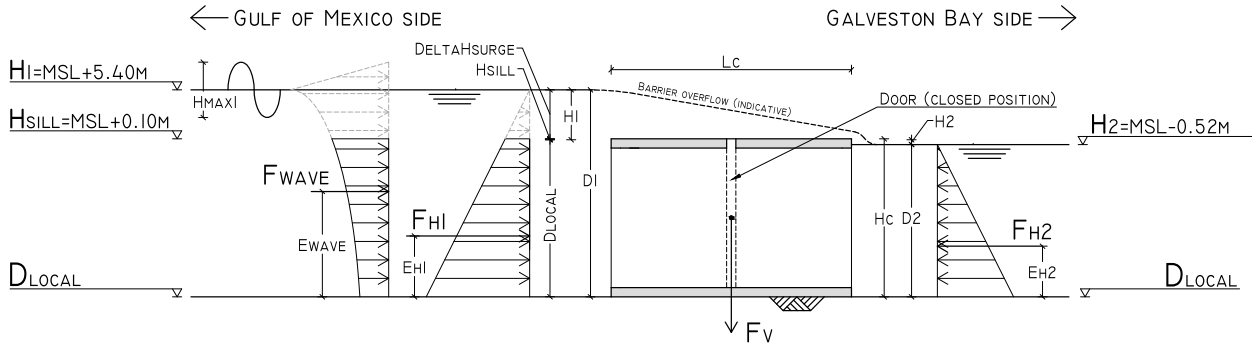


Figure 7.1: Cross-sectional side view of forces due to positive head (surge from the Gulf of Mexico) acting on caissons. Caisson dimensions not to scale. Units: m. MSL includes 100 year SLR.

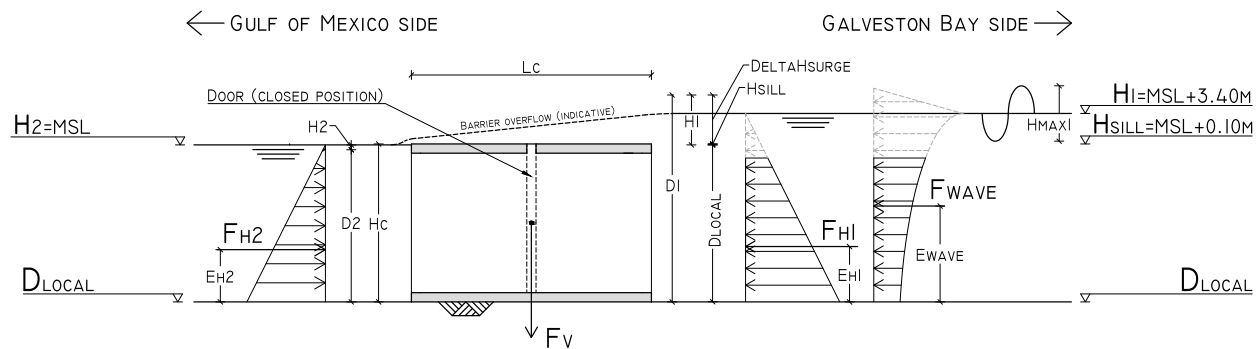


Figure 7.2: Cross-sectional side view of forces due to negative head (backsurge from the Galveston Bay) acting on caissons. Caisson dimensions not to scale. Units: m. MSL includes 100 year SLR.

Figures 7.1 and 7.2 show a simplified scheme of forces acting on the barrier. For example the vertical soil reaction force, the vertical water pressure and the weight of the water overflow are omitted.

7.3 Caisson barrier: preliminary design

For the caisson structure preliminary design is drafted. It intends to give a first sense of the caisson dimensions. The calculation is done with the following starting points and assumptions.

- It is assumed all caissons are founded through a shallow foundation on the soil the way it currently is, so without any soil improvements.
- The caisson barrier is equipped with vertical lifting gates that are able to withstand negative head. In this first draft design the weight of the doors is neglected.
- The calculation is executed in the Serviceability Limit State (SLS). Safety factors for loads are not yet taken into account, only material factors for concrete strength properties.

As this design stage aims on presenting a rough design for a caisson structure some design aspects are not yet taken into account.

- The caisson barrier will not yet be checked on occurring (unequal) settlements. This will take place during the simulation in Section 7.4. The check on settlements is disconnected from the preliminary design because it is expected that fulfilling the settlement criterion would result in considerably longer caissons. This does not need to be necessary, separate measures can be taken to deal with the soil-settling issue.
- Due to differences in water head on either sides of a structure a potential difference occurs. This can result in groundwater flow or 'seepage'⁽³⁾ under the caissons. Measures to prevent the seepage mechanism are seen independent of the first caisson design. In the final design (Section 8.3) will be dealt with this issue.
- High flow velocities around the structure may induce scour holes. These high flow velocities do not only occur during high surge levels, but can also occur in normal conditions due to the constriction of the flow area. The design of scour hole preventive measures are outside the scope of this thesis.

7.3.1 Dimensions

The force scheme as presented in Figures 7.1 and 7.2 and the soil conditions as given Table 5.2 serve as input for obtaining the preliminary caisson dimensions. The calculation (in its entirety presented in Appendix F) is executed in the Serviceability Limit State (SLS).

The environmental section is divided in seven different barrier sections, based on the local depth. For each of these sections the optimal caisson dimensions are determined. The location of these barrier sections are indicated in Figure 7.3 (in this figure a 100-year SLR of 1 m [3.3 ft] is included). This is done by iteratively adjusting the caisson dimensions until they fulfill all of the strength and stability checks listed below.

Checks at final location

- Vertical bearing capacity of soil
- Inclined vertical bearing capacity
- Soil tensile stresses
- Shear capacity of soil
- Overturning moment

Checks during transport

Wall and slab strength

- Shear stress and bending moment capacity floor slab
- Shear stress and bending moment capacity top slab
- Shear stress and bending moment capacity walls

Floating static stability

- Metacentric height

Floating dynamic stability

- Sway
- Natural oscillation

The resulting caisson dimensions are presented in Table 7.3. For the results of the unity checks refer to Table E3, for a list of caisson dimensions in imperial units refer to Table E5.

⁽³⁾ Referred to as 'piping' in the Netherlands.

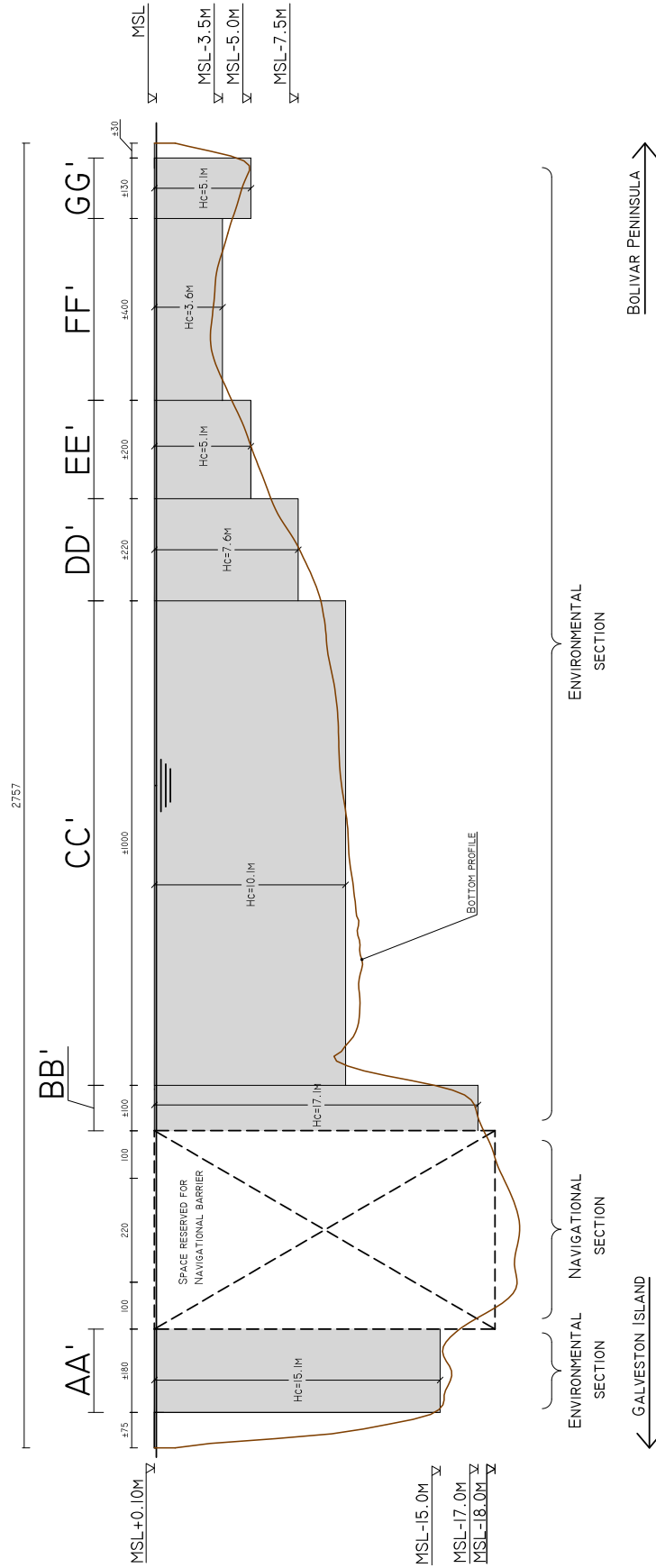


Figure 7.3: Cross sectional front view of Bolivar Roads showing the location of barrier sections AA' - GG' for the environmental barrier. The horizontal scale is compressed 40 times with respect to the vertical scale. Units: m.

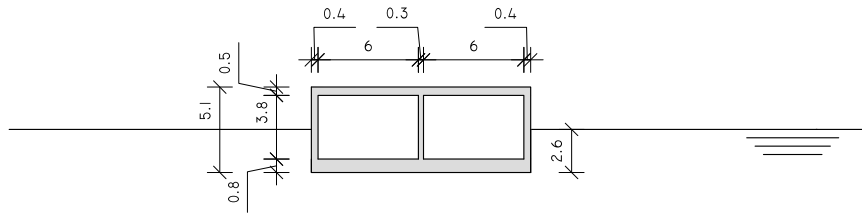
Table 7.3: Caisson dimensions.

Barrier section (see Figure 7.3)		AA'	BB'	CC'	DD'	EE'	FF'	GG'
– Local depth d_{local}	[MSL-m]	15	17	10	7.5	5	3.5	5
Geometry (App. E.2.1)								
<u>Caisson dimensions</u>								
– Height H_c	[m]	15.1	17.1	10.1	7.6	5.1	3.6	5.1
– Width W_c	[m]	20.2	26.9	20.2	13.8	13.3	13.1	13.3
– Length L_c	[m]	70	70	60	55	50	50	50
– Draft D_c	[m]	4.65	5.14	3.87	3.34	2.57	1.91	2.57
– No. compartments n_x	[-]	3	4	3	2	2	2	2
<u>Wall/slab thickness</u>								
– Floor slab w_f	[m]	1.25	1.40	1.25	1.00	0.90	0.60	0.90
– Top slab w_t	[m]	0.50	0.50	0.50	0.50	0.50	0.50	0.50
– Outer wall $w_{w,out}$	[m]	0.70	0.70	0.70	0.70	0.50	0.40	0.50
– Inner wall $w_{w,in}$	[m]	0.40	0.50	0.40	0.40	0.30	0.30	0.30
– Bulkheads w_b	[m]	0.30	0.30	0.30	0.30	0.30	0.30	0.30
Barrier section dimensions								
Number of caissons	[-]	9	4	51	16	16	29	10
Width per section	[m]	181.8	107.6	1030.2	220.8	212.8	379.9	133
Total volume of concrete	[m ³]	40774	26653	164383	27878	18744	24882	11715
Effective flow area	[m ²]	2066	1402	7115	1056	595	661	372

These dimensions are obtained by iteratively adjusting them until the all of the strength and stability checks listed above are met. During this iterative dimensioning process the following regarding the design checks is concluded:

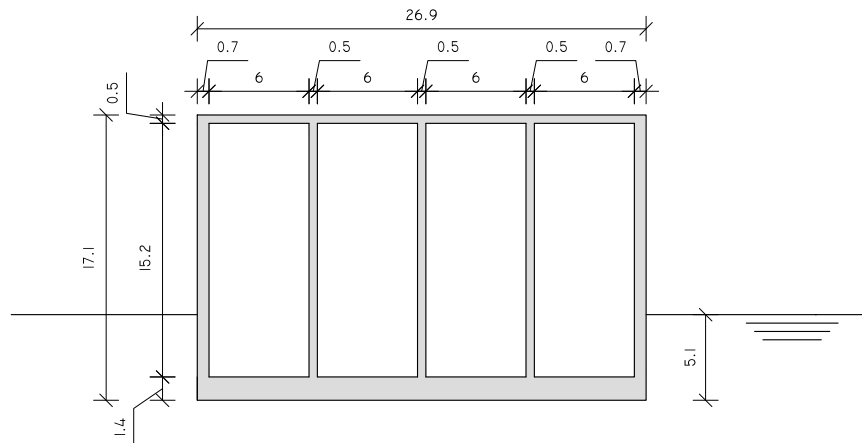
- The shear capacity of the soil is the decisive design check at final location. It determines the required caisson length. In further designing one should certainly pay attention to the consequences of this design check.
- During transport the metacentric height is decisive. This parameter influences the number of caisson compartments. The more compartments needed for a stable caisson the less caisson units are required. One should strive for a large number of caissons to achieve the highest repetition factor.
- For all of the caissons the compartment width is a standard size: 6 m [19.7 ft] (van der Horst, 2011).
- The wall and slab thicknesses are only determined by the shear stress and bending moment capacities in floating conditions. During this stage the highest loads on the walls and slabs occur due to the high acting hydrostatic pressures. The acting forces during construction in a dry dock are assumed to be less than the forces in floating conditions. Other influences that could induce are more adverse loading such as collision during transport/placement are not taken into account.
- Bulkheads will be placed to prevent the water from flowing in during transport. On the final location they will be removed. For simplicity reasons the bulkheads are here designed as reinforced concrete plates

To give an idea of the caisson dimensions, the cross sections of the smallest caisson (barrier section FF') and the largest caisson (barrier section BB') are presented in Figures 7.4 and 7.5.



BARRIER SECTION FF'

Figure 7.4: Cross section of caisson unit without doors in floating condition for barrier section FF'. Units: m.



BARRIER SECTION BB'

Figure 7.5: Cross section of caisson unit without doors in floating condition for barrier section BB'. Units: m.

7.3.2 Inflow area

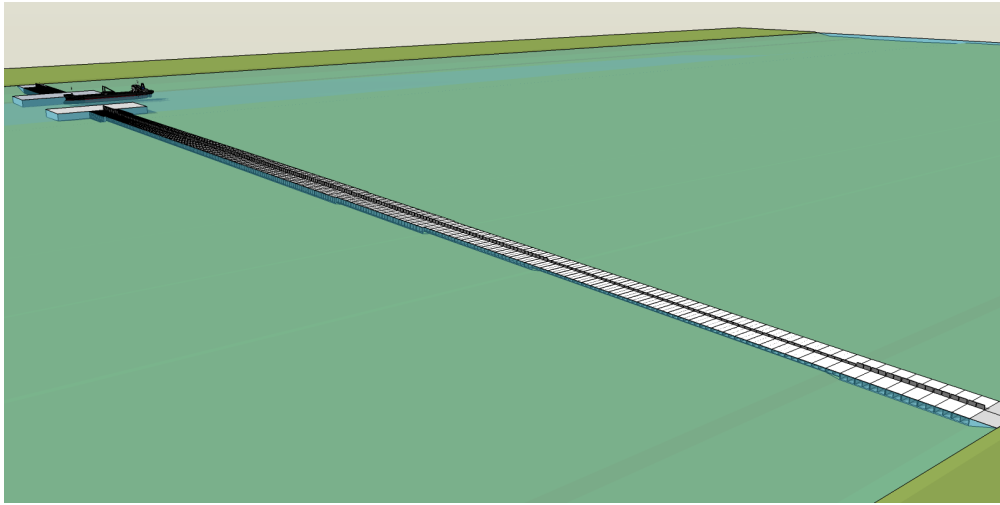
By summing all the effective flow areas for sections AA' to GG' as presented in Table 7.3, the total flow area through the environmental section is $A_{env,eff} = 13,267 \text{ m}^2$. Adding the effective flow area of the navigational section ($A_{nav,eff} = 3,740 \text{ m}^2$, see Section 4.2.1), the total effective flow area through Bolivar Roads is $A_{bar,eff} = 17,007 \text{ m}^2$. This means that the flow opening in Bolivar Roads has reduced to:

$$\frac{A_{BR}}{A_{bar,eff}} = \frac{24,875}{17,007} = 0.68 = 68\% \text{ of its original size.} \quad 7.1$$

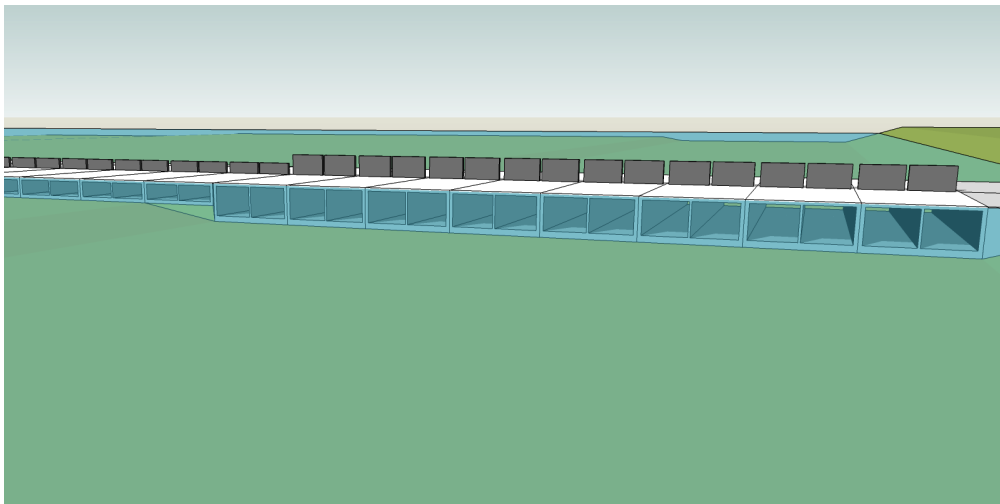
This meets the minimum available flow area requirement, which was set to 60%. But as stated in Section 4.3 one should strive for the largest effective flow area as possible, preferably higher than 80%. In Section 7.5 options to increase the effective flow area will be discussed.

Note: as stated in Section 4.3 the exact geometry of the caisson barrier should be included in the hydrodynamic model to give a more educated estimate of the implications on the tidal amplitude and water circulation in the Galveston Bay.

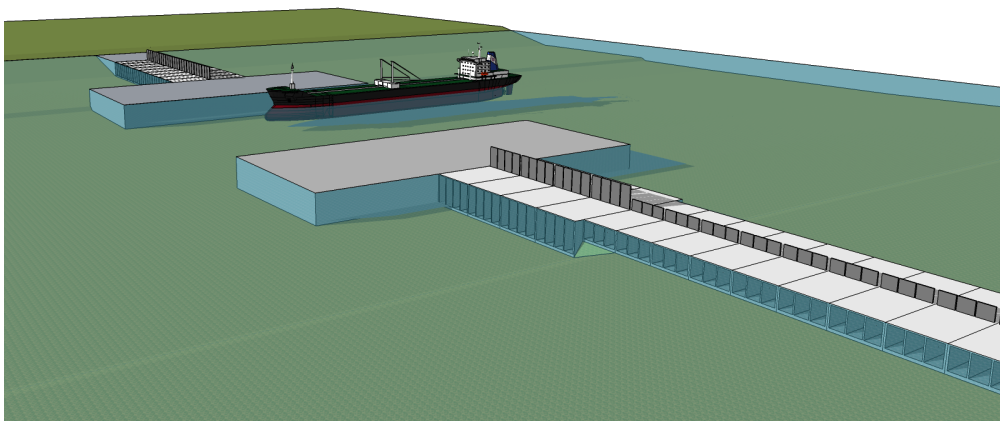
Figure 7.6 give an impression of how a caisson barrier could look like. The 3-D drawings aim on giving a feeling for the dimensions that a caisson solution would be, and are definitely not final. The doors are drawn as vertical lifting gates. One can see that the navigational barrier is omitted, the design of this barrier is outside the scope of this thesis. However, space is reserved for it and the large grey blocks on either sides of the navigation channel represent the barrier's abutments.



(a) Overview barrier with caissons



(b) Close up of caisson barrier near Bolivar Peninsula



(c) Close up of navigational section

Figure 7.6: Preliminary 3-D impressions of caisson barrier alternative.

7.4 Simulation: settlements

In this section a brief simulation of the caisson barrier is executed. The caissons with dimensions as defined in Table 7.3 are checked on occurring settlements. The check on settlements is disconnected from the preliminary design (presented in previous section) because the poor soil conditions raised the expectation that fulfilling the settlement criteria would result in considerably longer, non-economic caissons. For a first design step it would probably have resulted in an overestimation of the caissons dimensions. Therefore the settlements issue is dealt with in this section. Measures to counteract the settlements will be sought. See conclusion below.

The calculation procedure of the settlements per soil layer per barrier section is elaborated in Appendix F.3. The primary and secondary settlements for each soil layer specifically are calculated using two approximation methods: the Koppejan method which is a commonly used in the Netherlands, and Bjerrum method which is more often used in Anglo-Saxon countries. For barrier sections AA' and BB' the results match pretty well, but for barrier section CC' - GG' the results differ quite a lot; especially for secondary compression. This is because in the Bjerrum method the secondary settlements only depend on time whilst in the Koppejan method these are also stress dependent.

The results are presented in Table 7.4. The total compression ratio is expressed as the deformation Δh_{tot} as a percentage of the total soil layer thickness $w_{s,i}$. Figure 7.7 shows the development of the total soil settlements in time for barrier section AA' for both methods.

Table 7.4: Relative deformation under each barrier section.

Barrier section (see Figure 7.3)		AA'	BB'	CC'	DD'	EE'	FF'	GG'
Foundation depth d_{local}		15	17	10	7.5	5	3.5	5
Relative settlement per layer								
Koppejan method								
Total primary settlement	[m]	2.10	2.04	0.69	0.45	0.26	0.18	0.26
Total secondary settlement	[m]	1.64	1.60	0.52	0.33	0.19	0.13	0.19
Total settlement Δh_{tot}	[m]	3.73	3.64	1.21	0.78	0.46	0.30	0.46
Compression ratio $\Delta h_{tot}/w_{s,i}$	[-]	14.9%	15.8%	4.0%	2.4%	1.3%	0.8%	1.3%
Bjerrum method								
Total primary settlement	[m]	2.07	2.66	0.69	0.44	0.26	0.18	0.26
Total secondary settlement	[m]	1.94	1.94	1.94	1.94	1.94	1.94	1.94
Total settlement Δh_{tot}	[m]	4.01	4.60	2.62	2.38	2.20	2.11	2.20
Compression ratio $\Delta h_{tot}/w_{s,i}$	[-]	16.0%	20.0%	8.7%	7.3%	6.3%	5.8%	6.3%

Note: it seems that the Koppejan method gives a more reliable result, but this method is taken for one time compression only. The Bjerrum method is also suitable for soil relaxation after removing a load (swelling) and recompression. As soil swelling and recompression might be relevant in a later design stage the Bjerrum method is also introduced here.

Calculations (in Appendix F.3) show that it takes 18.5 years for the soil to fully consolidate. After this time period the compression for soil layers underneath barrier section AA' has developed to a considerable 14.9% and 16.0% for the Koppejan and Bjerrum methods respectively.

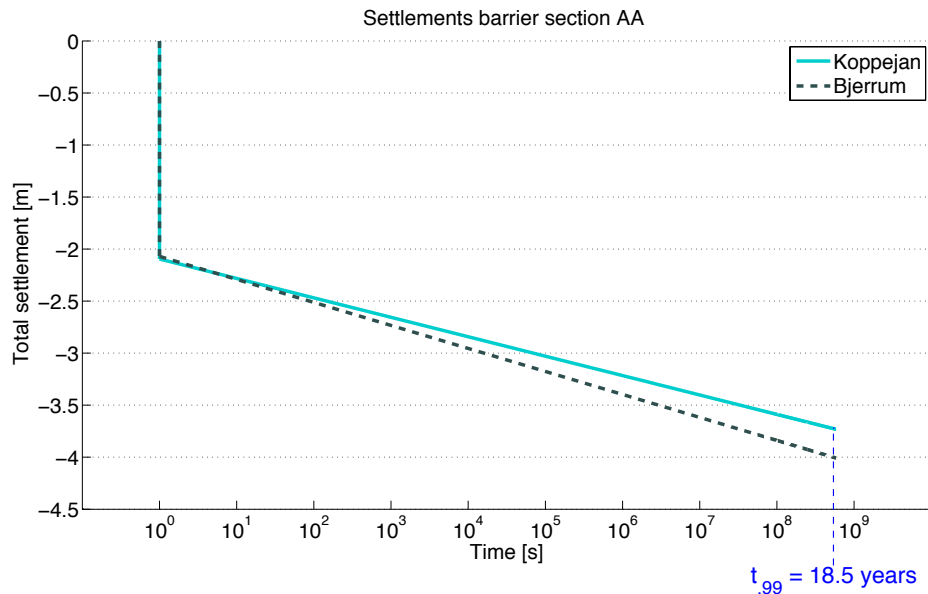


Figure 7.7: Total soil settlement under caisson barrier section AA' (largest occurring) for both methods.

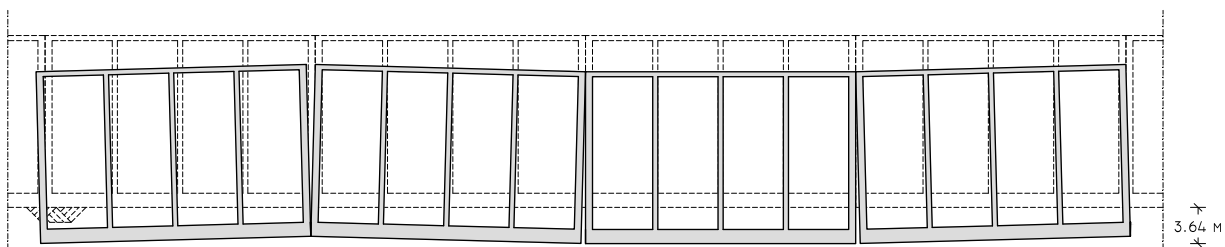


Figure 7.8: Cross section of barrier section BB' showing possible position of caissons after $t_{99\%}=18.5$ years (Koppejan method).

Note: Figure 7.8 shows the position of the caissons due to settlements in barrier section BB'. For this image the tilting (unequal settlement) is drawn such that the difference in caisson settling between both sides is 20% of the total settlement rate. This number is arbitrarily chosen and not evaluated here. The image aims on giving an idea of the settlement magnitude with respect to the caisson dimensions.

Conclusion settlements. From Table 7.4 one can tell that the soil is very weak and the total settlements are high. The rotation due to the unequal settlements are very large for all of the caissons. According to Vrijling et al. (2011) it is required that the unequal settlements may induce at most a rotation of $1/300$ (≈ 0.003), none of the caissons meets this requirement in both directions. In the x-direction (short edge) this problem could be quite easily solved. By increasing the number of compartments the caisson's width is easily enlarged. In the end this will not require more concrete as the barrier span will just be divided in larger sections; the number of caissons just decreases. This is not such a big deal, but it is still disadvantageous as dividing the whole barrier span in larger sections induces a smaller number of caissons. This last fact in turn decreases the repetition factor, which is disadvantageous because a lower repetition factor might result in higher costs.

The y-direction (long edge L_c) is more problematic, to meet the settlement requirement in y-direction the length of all caissons would need to be at least doubled. This requires a lot more concrete, making it very expensive and thus highly unfavorable.

The settlement-induced rotations are of such a magnitude that they could very likely cause alignment issues of the barrier doors, through which they can get stuck. Also damage could occur when the caissons hit each other as a consequence of the settlement-induced rotations. The tilting of the caissons could result in a shifted height between two adjacent caissons as drawn in Figure 7.8. These can be seen from a distance making the barrier less attractive to look at.

7.5 Key design parameters

The preliminary design for a caisson barrier in Bolivar Roads is ready. During the design process and subsequent simulation some design issues came upfront. For further research it is useful to identify and give an overview of these issues to determine the key design parameters. This section outlines the different design parameters that significantly influence three core design aspects of the barrier: cost-effectiveness, reliability and mitigation of the barrier's influence on ecosystems in the Galveston Bay⁽⁴⁾

7.5.1 Overview

As the three core design aspects and their parameters are very interrelated an overview of all of these aspects and parameters is graphically presented in Figure 7.9. It is all about optimizing three core aspects posed in the bottom center of the image, namely the

- preservation of the ecosystems in the Galveston Bay (green) through optimizing the effective flow area of the barrier,
- the minimizing of total costs (red) through optimizing the construction time, construction costs and operational costs,
- and maintaining the reliability of the structure (blue).

Caisson design aspects (purple) and soil/foundation related aspects (orange) are also indicated. The image aims on qualitatively indicating the relation/influence of different design aspects on the three core design aspects.

Note: design variables treated in the system level design are not taken into account. Any variation in these design variables (e.g. barrier alignment along Bolivar Roads and optimal division in retaining height between the navigational and environmental section) are assumed to be determined.

⁽⁴⁾The influence on ecosystems is only considered from a water circulation point of view. Aspects like water contamination during construction are not treated here.

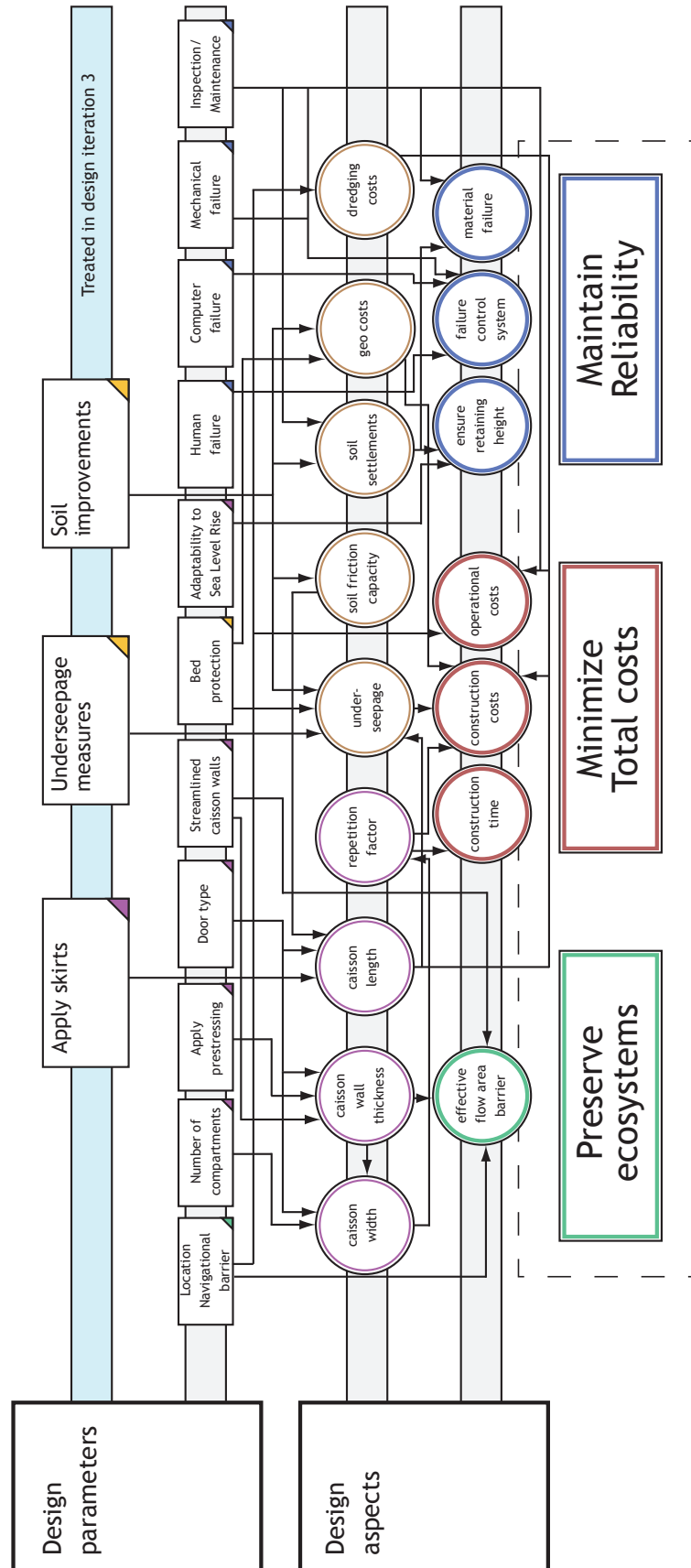


Figure 7.9: Graphical representation of the influence of design parameters on design aspects.

As can be seen from Figure 7.9 many design parameters bring opportunities to optimize the storm surge barrier in terms of costs, reliability and the degree to which the Bay's ecosystem is affected. Their influence is quantified below.

7.5.2 Parameter influence

In Figure 7.9 relevant design parameters and their relation to costs, ecosystem preservation and reliability are qualitatively outlined. Now their degree of influence on these core design aspects is described and rated.

- **Soil improvements.** The soil friction capacity is a governing design criterion for the caissons. Especially for barrier sections AA' and BB' the low friction capacity of the clay soil results in very long caissons and thus high construction costs. The other caissons are founded on a sand layer that has a higher friction capacity (refer to Table 5.2 for soil layer classification), this results in a relatively short caissons for barrier sections CC' - GG'. The issue for sections AA' and BB' could be resolved by excavating the weak clay layer and replace it with sand to increase the horizontal friction capacity. In this way the shorter caissons can be applied which saves construction costs.

After the design steps in Sections 7.3 and 7.4 it appeared that the unequal settlements are of such magnitude that they had to be examined separately. They are a threat to the effective retaining height and the operability of the doors. It is very important for a feasible barrier design that measures to counteract these settlements will be taken.

- **Seepage measures.** Water level differences across the caissons structure can cause groundwater flow or 'seepage' under structures. This seepage can occur at the plane separating the impermeable structure and a loose grain layer. It is the flow of water through a pipe-like channel that has been created by internal erosion. This seepage can cause stability problems for the caissons. When omitted the structure's stability could be easily affected because of this seepage. The seepage measure is not very decisive for the caisson barrier design, furthermore longer caissons contribute in a longer, favorable seepage length.
- **Apply caisson skirts.** By applying skirts at the tips of the caissons additional friction resistance can be obtained. Just like increasing the soil friction capacity this measure will result in shorter caissons.
- **Door type.** The type of applied doors determines the caisson compartment width because certain doors have a limited span. The caisson doors require different door slots. Door slots guide the caisson doors when moving. The effective flow area will decrease as the caisson doors require larger slots, hence the door type influences the effective flow area. For a complete design the barrier doors should be designed in detail, as they are expected to be an important cost driver.
- **Number of compartments.** The width of the caissons depends on the number of compartments. The caisson width and number of compartments, in turn, depend mainly on the static stability of the caissons during transport (the metacentric height). It is interesting to optimize the number of compartments because the lower the number of compartments and thus the caisson width will be, the higher the repetition factor that can be achieved. This is because wider caissons result in a lower number of caissons per barrier section and hence a lower repetition factor. A high repetition factor is preferred because this reduces construction costs and time.
- **Optimize caisson walls.** Currently the caisson inner and outer walls are just quickly dimensioned using rules of thumb. Whether these walls are able to hold all the forces during construction, transport and conditions on its final location is not investigated. This should be done in a next design stage. Furthermore the shape and thickness the caissons walls can be optimized by applying prestressing steel and design streamlined walls. The optimization of the caisson walls is an aspect that is outside the scope of this thesis.

- **Location navigational barrier.** The environmental requirements (Section 4.3) stated that the flow area through the barrier is influenced by the size of the required abutments for the navigational barrier and by the shape and wall thicknesses of the caisson barrier. If one takes a closer look at Figure 7.3 it can be seen that the abutments for the navigational section take a relatively large part of the total barrier span. It could be an idea to move the entire navigational section right next to the shoreline of Galveston Island instead of first a small environmental barrier section. This means that the new navigational section would be aligned more or less on the current position of barrier section AA'. In case of a swinging barge gate the barrier can be placed in just one abutment constructed on Galveston Island. This will save space that can be used to obtain more flow area in Bolivar Roads. Besides it makes the navigational barrier more accessible, which is favorable in terms of inspection and maintenance. The navigational section will have to be deepened, but it will result in a considerable win in flow area as only one abutment will be needed.
- **Adaptable retaining height.** As stated in Section 4.4.2 the barrier will initially be designed for a 100 year lifetime. After that time period it should be possible to increase the barrier's retaining height in a simple way to respond flexibly to uncertain future Sea Level Rise (SLR) up until a lifetime of 200 years. By building the barrier in such a way that it is able to adapt to uncertain future SLR the barrier can fulfill its $1/10,000 \text{ yr}^{-1}$ safety level requirement apart from changing climate. Increasing the retaining height could for example be by means of constructing a wall or small levee on top of the caissons. The additional loads due such a height increment are not taken into account in this design, but it is recommended to do so.
- **Bed protection.** High flow velocities around the structure may induce scour holes. These high flow velocities do not only occur during high surge levels, but can also occur in normal conditions due to the constriction of the flow area. A bed protection could mitigate these scour holes.
- **Human, Computer and Mechanical failure.** The control system that takes care of the opening and closure of the barrier can become less reliable due to human, computer and mechanical failure. For the most reliable barrier design the control system should be optimized.
- **Inspection and maintenance.** Thorough inspection and maintenance can prevent deterioration of the barrier's reliability due to mechanical failure and failure of the control system. Also the monitoring (and anticipation) on occurring settlements can prevent unexpected internal forces inside the caisson structure and eventual loss of strength.

7.5.3 Conclusion key design parameters

From the simulation it appeared that the weak soil conditions are the most important design parameter. By increasing the soil friction capacity and the highly compressible soil determine the caisson dimensions to a high extent. The biggest win in cost-effectiveness lies here. Especially the caisson length can be reduced, which in turn reduces the amount of concrete needed. By applying skirts on either sides of the caissons the horizontal friction between the caisson and the subsoil can be increased which will probably result in shorter caissons.

A win can also be achieved by keeping the number of caissons as low as possible through optimizing the caisson compartment size and quantity, but in comparison with the effect of increased improved soil conditions it is estimated to be a fraction of the possible win in cost-effectiveness. The appliance of prestressing steel and more streamlined caisson walls are design parameters that benefit the barrier's effective flow area, but are of minor importance compared to the problematic soil conditions.

The adaptive retaining height was an important design parameter for the evaluation of different alternatives in Section 7.1 but as the design steps on this design level progressed it also became a requirement of minor importance. In a complete design that also meets the adaptability requirement it can not be omitted. Possibilities for flexibly increasing the caisson's retaining height can be through constructing a wall or small levee on top of the caissons.

The bed protection around the barrier is very important for the stability of the barrier and thus the reliability of the barrier. Measures that benefit the storm surge barrier's overall reliability are more or less disconnected from the other design parameters.

The influence of different design parameters on the three core design aspects is presented in Table 7.5.

Table 7.5: Relative influence of different design parameters.

Design parameter	Total costs	Ecosystem preservation	Overall reliability
Soil improvements	●●●	●	●●
Seepage measures	●	○	●●
Caisson skirts	●	○	●
Door type	●●●	○	●●●
Number of compartments	●●	○	○
Optimize walls	●●●	●●	●
Location navigational barrier	●	●●●	○
Adaptable retaining height	●●	●	●●●
Bed protection	●●●	●	●●●
Human, computer and mechanical failure	●●	○	●●●
Inspection/maintenance	●●	●	●●●

● = low influence, ●● = medium influence, ●●● = high influence, ○ = negligible influence.

For the third and last design step one could decide to design and optimize the barrier doors in deep detail, but the fact will remain that the soil conditions are very problematic to build a storm surge barrier on. Even with highly optimized barrier doors the barrier still has to be founded on the weak soil. Regarding the adaptable retaining height requirement: the soil conditions are already a challenge for a barrier that is just able to withstand the surge conditions for 100 year SLR the soil conditions. For these reasons it makes more sense to focus on the problematic soil conditions rather than door/wall optimization, control system design and adaptive retaining height. Furthermore the design of a bed protection around the barrier is a specialism on its own. It provides enough for an entire thesis, and is not treated too.

Next to dealing with the soft soil conditions the seepage measure and caisson skirt design will also be treated in the third design step. Not because these are key design parameters, but they go more or less hand in hand with foundation design. Usually caissons will already be equipped with skirts and is a seepage measure part of the foundation design.

So the three aspects that will be treated in the third and last design step are the appliance of caisson skirts, soft soil improvements and a seepage measure. These design parameters are also indicated in the upper bar of Figure 7.9.

7.6 Conclusions & recommendations

In this design level focuses on the environmental section of the storm surge barrier. In the alternative assessment a barrier type is chosen based on four design criteria. These four equally weighed design criteria obviously do not cover all aspects but it is assumed this set suffices for taking an adequate decision on this level of detail. For a thorough assessment it is recommended to use more design criteria and distinguish their importance. The rating scale is composed of three levels because a finer division (e.g. a 1 – 10 scale) would give a false sense of knowing precisely what the effects of the surroundings on the barrier will be and vice versa. However, at this level of detail this is not true, so a more qualitative assessment is executed. If one would do this assessment in more detail, the

best strategy would be to first make a preliminary draft for all alternatives and do the assessment afterwards. This is because the specific location of Bolivar Roads can for example enlarge (dis)advantages of a certain barrier type making it more or less preferable compared to another than it would seem at first sight. However, this would be too time consuming, so the barrier assessment is kept briefly and in compliance with the level of detail. In this assessment a caisson barrier appeared to be the best alternative.

Next the design input such as governing water levels and maximum flow area is specified. The loads on the barrier are determined for the entire environmental section. Together with design checks for strength and stability the preliminary caisson dimensions are drafted. A first impression of a caisson barrier is given. It appears that this barrier decreases the flow area at Bolivar Roads down to 68%, which is more than the minimum required flow area of 60%.

During the simulation the caisson barrier is checked on occurring settlements. These appear to be high, after a period of approximately 18.5 years when the soil is fully consolidated the settlements vary between 0.30 m and 3.73 m for the different barrier sections. For barrier section BB' the total compression ratio of the soil is almost 16%. This settlement calculation is based on a generalized soil profile for the entire barrier span with rough assumptions for the compressibility properties. To determine the occurring settlements more precise it is strongly recommended to obtain accurate information about the soil strength and its compressibility properties along the entire span. Instead of hand calculations finite element modeling of the soil is recommended to obtain the most accurate settlement rates.

Now that it appears that settlements are problematic it could be an idea to look back at the barrier alternative assessment in Section 7.1. Apparently the clay soil is decisive for the barrier's applicability. The best strategy could be to reassess other alternatives in the beginning of this chapter taking this knowledge into account and put more emphasis on foundation aspects. However, in this thesis it is decided to continue the caisson barrier design and find measures to cope with the settlements. Different ways to do so are investigated in Section 8.2. In the next chapter a last design step will be executed, on a detailed design level. It will revolve around measures to increase the caisson's horizontal friction capacity, prevent seepage and will contain a design for the caisson barrier foundation.

8 Design step 3: foundation aspects

In this chapter a third design step is executed. It is the last design step in this thesis, but the design process is certainly not finished yet. There are still other aspects (of which some are listed in Section 7.5.2) that still need attention for a complete design.

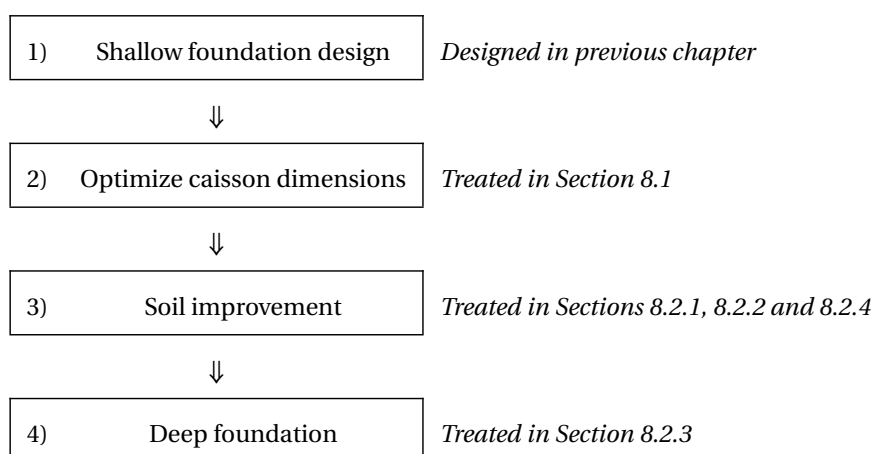
After the environmental barrier design level the soil strength and compressibility properties appeared to be problematic. The occurring unequal settlements are considerable and the weak friction capacity requires long caissons. In this third design step solutions will be sought to deal with the poor soil conditions. To do so, the decision process according to the flowchart in Table 8.1 is carried out. First the caisson's foundation dimensions are optimized through applying skirts. These provide additional horizontal friction capacity. Also the removal of the weak clay layer under barrier sections AA' and BB' is described which will decrease the caisson length for these barrier sections (see Figure 7.3 for barrier section locations). These two measures will result in the optimized caisson dimensions, see Section 8.1.

These optimized dimensions serve as input for steps 3 and 4 of the flowchart in Table 8.1. Usually one will just investigate whether soft ground improvements are possible and economically feasible. If it appears to be feasible to do so, the flowchart tells that the decision process stops and no deep foundation needs to be designed. However, in this chapter the soil improvement and the deep foundation will both be designed. A cost and technical feasibility evaluation will determine whether one of the three soil improvements or the deep foundation is favorable. The evaluation itself is presented in Section 8.2.5.

As the design of an a seepage measure goes more or less hand in hand with foundation design the last part of this third design step will be the quick design of a seepage prevention measure. See Section 8.3.

Refer to Appendix G for calculations and elaborated approaches used in this chapter.

Table 8.1: Flowchart of decision process involved with selection of foundation type. Adopted from Hussin (2006a).



8.1 Optimize caisson dimensions

The optimized caisson dimensions determine the caisson footprint and thus the foundation dimensions. The caisson dimensions are optimized according to two measures: the construction of skirts at the tips of the caisson's floor slab and the replacement of the weak clay layer underneath barrier sections AA' and BB' (see Figure 7.3). Using both these measures it is expected the caisson length can be decreased significantly.

Weak clay layer replacement. Barrier sections CC' - GG' will be founded on a sand layer (see Figure F.1). Barrier sections AA' and BB' do not, if they would be founded on the seabed the way it currently is the friction capacity of clay will be governing. The idea is to remove the clay to a level 1 m below the caisson skirt tips and replace it with sand (which is just soft clay with weak friction capacity, see Table 5.2). In this way the caissons along barrier sections AA' and BB' will experience friction between concrete and sand only, resulting in caissons that are able to bear higher horizontal loads. As stated in Table E.1 the shear stress coefficient of clay is lower (0.35) than that of sand (0.50), so it is expected a big win can be gained for the caisson length for sections AA' and BB'. They can probably be constructed shorter.

It is expected this measure will turn out to be cost-effective. Shorter caissons can be applied while the additional dredging costs for the clay replacement will not result in very high additional costs, as dredging vessels will need to be mobilized anyway to flatten the seabed.

Caisson skirts. Through constructing skirts on either sides of the caissons the horizontal force resistance of the caissons can be increased. Caisson skirts will penetrate into the ground and provide additional resistance against horizontal forces due to passive soil pressure. See Figures 8.1 and 8.2. In Appendix G.1.3 the contribution of skirts to the horizontal resistance is determined. The force scheme due to negative head is presented in Figure G.2.

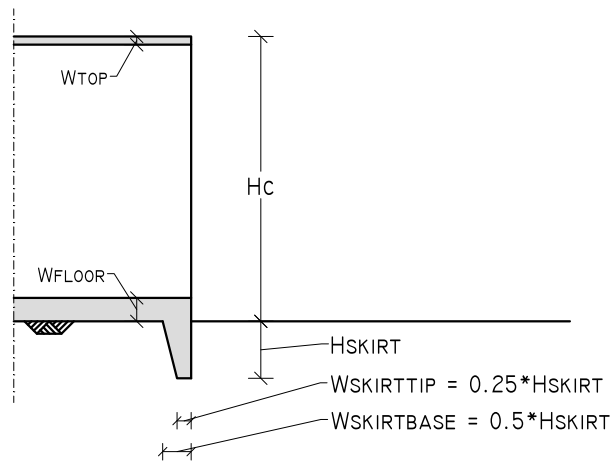


Figure 8.1: Cross-sectional side view of skirt dimensions in relation to caisson floor and top slab (barrier section BB').

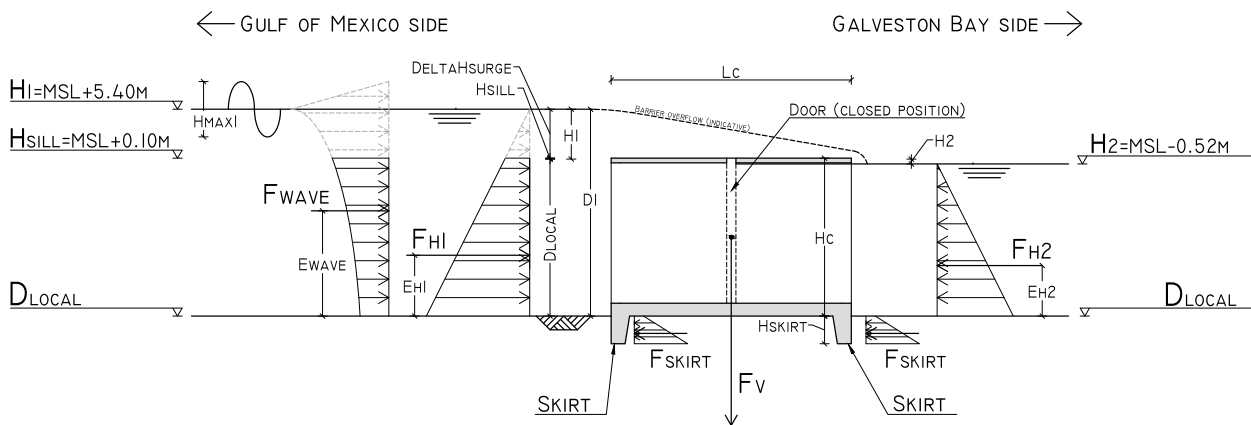


Figure 8.2: Cross-sectional side view of forces due to positive head acting on caissons equipped with skirts. Caisson dimensions not to scale.

Modified dimensions. Now that the soil properties underneath barrier sections AA' and BB' are improved and the caisson skirts are designed the caissons are re-dimensioned. Due to these measures the caissons can be constructed more material efficient. This is attractive to do, but now a new static stability criterion has to be checked. Next to the shear plane between the concrete and subsoil a new possible shear plane can occur between the (replaced) sand layer on which the caissons are founded and the underlying clay layer. For the friction capacity between these layers the weakest soil friction capacity is governing; in this case the clay layer with a friction factor $c_{f,c}$ equal to 0.35. The caissons have to fulfill the following unity check:

$$\frac{c_{f,c} \cdot F_{v,tot,sh}}{F_{H,tot}} \geq 1.0 \quad 8.1$$

In which $F_{v,tot,sh}$ is equal to the sum of the sand layer weight and the vertical forces acting from the caissons on the shear plane. See Figure 8.3.

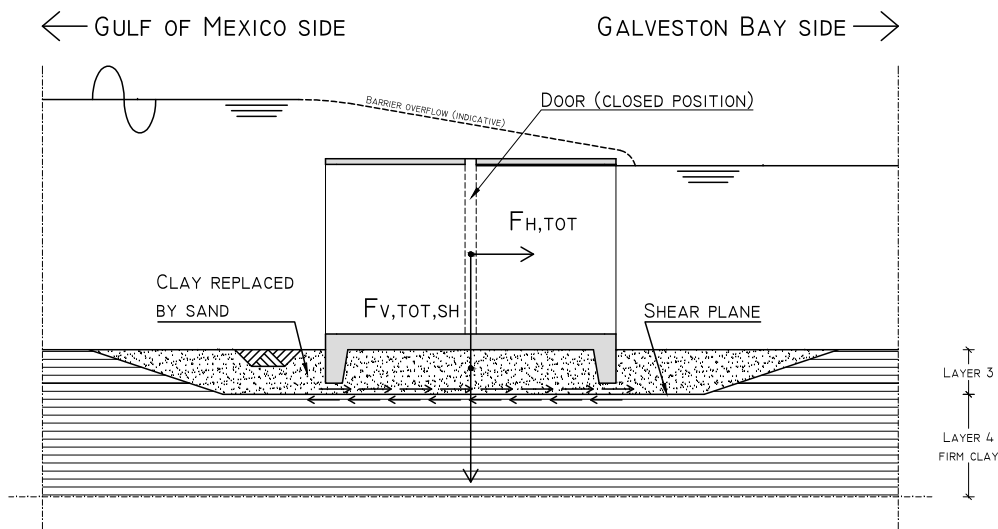


Figure 8.3: Cross-sectional side view of shear plane between replaced sand and clay layer for barrier section BB'. Caisson dimensions not to scale.

The revised caisson dimensions are presented in Table 8.2.

One could expect the caisson skirt heights for caisson sections EE' and GG' to be the same, as these caissons have identical dimensions. However, during transport, the caissons for barrier section GG' have to pass shallower water, namely along barrier section FF' (see Figure 7.3). Due to this fact, the maximum draft for GG' is limited by the depth at section FF'. The smaller skirts subsequently results in longer caissons for section GG'.

The unity checks for the revised caisson dimensions are presented in Table 8.3 (for dimensions in imperial units: refer to Table G.3). For barrier sections AA' and BB' the overturning moment criterion now has become governing instead of the soil shear capacity. This is due to the weak clay layer replacement. For sections CC' - GG' the soil shear capacity is still governing.

Note: in this design step also the door weight of the caissons is included. The dimensions and properties of these doors are not known, their weight is represented by a 0.30 m [1 ft] thick concrete plate, with height and width equal to the internal caisson height and width.

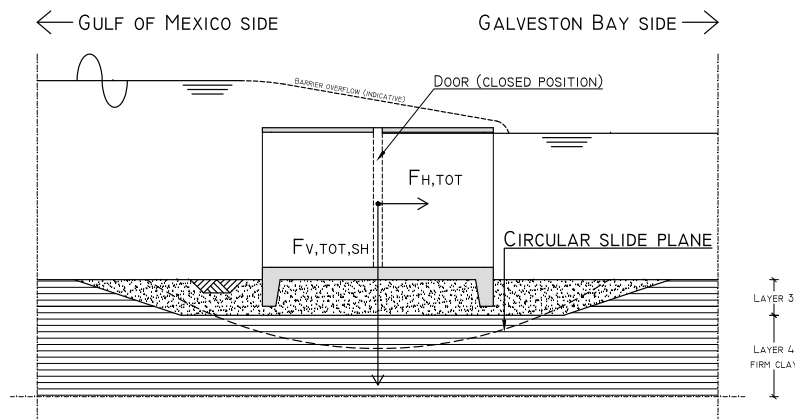
Table 8.2: Revised caisson dimensions in metric (SI) units.

Barrier section (see Fig. 7.3)		AA'	BB'	CC'	DD'	EE'	FF'	GG'
– Local depth d_{local}	[MSL-m]	15	17	10	7.5	5	3.5	5
Geometry								
<u>Caisson dimensions</u>								
– Height H_c	[m]	15.1	17.1	10.1	7.6	5.1	3.6	5.1
– Width W_c	[m]	20.2	26.9	20.2	13.8	13.3	13.1	13.3
– Length, old L_c	[m]	85	85	50	45	40	40	40
– Length, new $L_{c,new}$	[m]	40	41	43	42	38	38	40
<u>Skirt dimensions</u>								
– Skirt height h_{skirt}	[m]	3.02	3.42	2.02	1.52	1.02	0.72	0.41
– Skirt base $w_{skirt,base}$	[m]	1.51	1.71	1.01	0.76	0.51	0.36	0.20
– Skirt tip $w_{skirt,tip}$	[m]	0.76	0.86	0.51	0.38	0.26	0.18	0.10
<u>Wall/slab thickness</u>								
– Floor slab w_f	[m]	1.25	1.40	1.25	1.00	0.90	0.60	0.90
– Top slab w_t	[m]	0.50	0.50	0.50	0.50	0.50	0.50	0.50

Table 8.3: Relevant checks for optimized caisson dimensions.

Barrier section (see Figure 7.3)	AA'	BB'	CC'	DD'	EE'	FF'	GG'
<u>Checks final location</u>							
– Soil tensile stresses	1.09	1.04	1.91	2.40	2.67	3.19	2.93
– Shear capacity concrete - sand	1.32	1.39	1.02	1.07	1.04	1.04	1.03
– Shear capacity sand - clay	1.93	1.50	1.67	2.68	4.38	6.75	4.33
– Overturning moment	1.09	1.04	1.91	2.40	2.67	3.19	2.93
<u>Checks transport</u>							
– Check Draft	1.77	1.80	1.53	1.37	1.21	1.11	1.00

Slip circle. The caissons should also be checked on circular slide surfaces. This calculation is omitted in this thesis, but should certainly be taken into account in further design, especially during soil consolidation. As there is very little information available about soil properties this calculation would have been executed based on very rough assumptions. It is assumed this circular slide surface mechanism is not governing. For further design it is recommended to check this aspect using the software D-Stab, which calculates the stability of the slide circle using several methods (Bishop, Fellenius). A 2D calculation using Plaxis software in which the stability during soil consolidation is checked could also be an option.

**Figure 8.4:** Cross sectional side view of principle of caisson failing on circular slide surface stability. The exact location of the circle is a possible location.

8.2 Foundation design

As concluded in the previous chapter the settlements in the soil underneath the caissons are considerable and variable along the barrier span. One could think of accepting the settlements and stick to the shallow foundation. As stated in the evaluation of Section 7.4 over the course of time the caissons will tilt compared to one another. By monitoring the unequal settlements and excavating some of the material and do local grout injections the tilting of the caissons can be mitigated. In this way it is possible to keep the caissons in horizontal position. However, they will still sink into the clay, which results in a lower retaining height. It can be counteracted by increasing the caisson height beforehand. This 'soil improvement' measure to deal with the settlements is discussed in Section 8.2.1.

The second foundation alternative is also based on improving the soft soil conditions. Contrary to the first one the caisson dimensions stay as they are (no increased height). In order to do so the soil has to be fully consolidated before the caissons are placed in position. It is done through applying an accelerated version of vertical drainage, the so-called vacuum preloading. See Section 8.2.2.

The last and most rigorous option is to construct a hard foundation whereby all of the horizontal and vertical loads will be transferred to the low-lying bearing sand layer at MSL-40m. In this way the clay layers with poor bearing capacities are bypassed. See Section 8.2.3.

In this section these three alternatives are investigated and a preliminary design is drawn. Also their (dis)advantages, feasibility and costs are presented. Next to these three alternatives there are more ways to deal with the poor soil conditions (such as the excavation of all the weak clay layers) but these will not be considered.

8.2.1 Alternative 1: Shallow foundation using vertical drainage with Prefabricated Vertical Drains

The first alternative is based on monitoring and taking action based on the occurring unequal settlements. The idea is not to mitigate the settlement magnitude, but accepting the soil settlements and let the caissons settle horizontally down into the soil. It is made sure the tilting will be counteracted, this can for example be done by local soil adjustments/improvements such as excavation and grout injections. The caisson height should be adjusted proportionally beforehand to maintain the required retaining height.

The soil consolidation process is accelerated to reduce the monitoring and excavation/grouting costs. The longer this monitoring and adjusting has to take place, the more expensive it will be. To accelerate the soil consolidation Prefabricated Vertical Drains (PVDs) (100mm wide and 4 mm thick) are installed before the caissons are placed. These vertical drains decrease the drainage length of the soil layers. The distance the porewater has to travel becomes less and in this way the soil layer squeezes out faster under the dead weight pressure from the caissons. This speeds up the consolidation time. The magnitude of the maximum soil pressure varies between 16 and 50 kN/m² [2.3 – 7.3 psi], see Table E.7. The influence of a water column pushing down is neglected here. For an accurate approximation of accelerated consolidation by means of vertical drainage under water this should be investigated and included. In this consideration the vertical drainage with PVDs is assumed to be as effective as on shore.

Costs. The costs for this vertical drainage depend on the applied grid spacing of the PVDs. A denser grid accelerates the consolidation and thereby decreases the monitoring duration, but requires more PVD material. An optimum between these should be found. From here arises the question: what is the most cost-effective drain grid spacing? This is done using time and cost unit rates for these aspects. In this way the total costs can be expressed in terms of grid spacing. Figure 8.5 shows the relation between vertical drainage costs and grid spacing for the storm surge barrier case.

From Figure 8.5 it appears that the most cost-effective grid spacing s_{opt} is 2.3 m. Calculations in Appendix G.2.1 show that for this grid spacing the total vertical drainage costs are approximately \$142 million. By investing this \$142 million in vertical drainage the soil consolidation is accelerated, but this technique requires higher caissons due to the loss in retaining height as a consequence of their subsidence in the soil. The caisson height increment is equal to the occurring settlement magnitude (stated in Table 7.4, Koppejan method). The increased weight due to heightening the structure is taken into account too. This caisson heightening obviously requires more concrete, and results in higher caisson construction costs. These caisson construction costs are calculated in Appendix G.2.1 and amount approximately \$533 million. The sum of caisson construction and vertical drainage costs is around \$675 million. This concerns direct costs only.

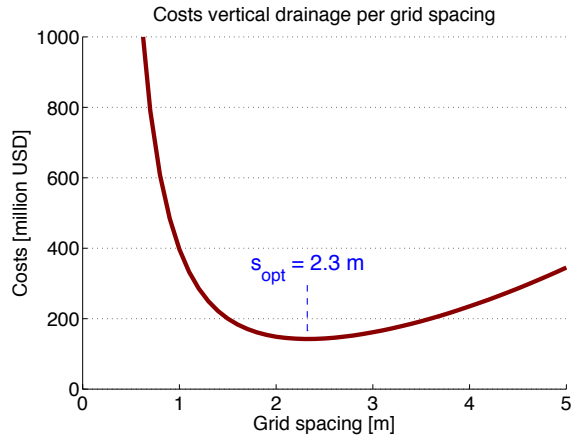


Figure 8.5: Costs vertical drainage expressed in terms of grid spacing.

Acceleration. The consolidation duration using vertical drainage through PVDs and the caisson dead weight has decreased from $t_{99\%} = 18.5$ years to $t_{99\%,acc} = 648$ days⁽¹⁾. This means that after placing the caissons, one should monitor the settlements for 648 days. For impressions of the accelerated settlements in the course of time for barrier section BB', see Figures 8.6 and 8.7.

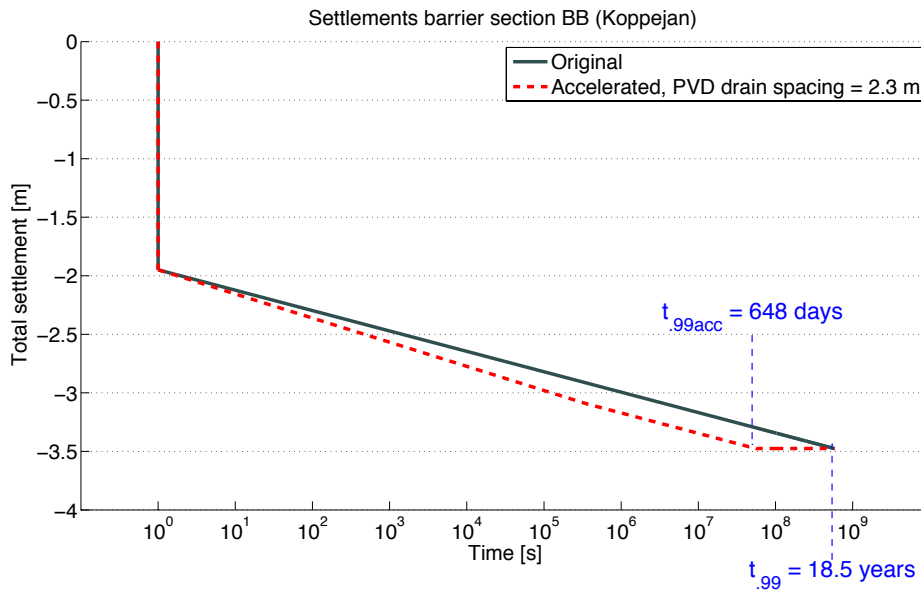


Figure 8.6: Original and accelerated settlements using vertical drainage for barrier section BB' (Koppejan method).

⁽¹⁾ Calculated using Koppejan method

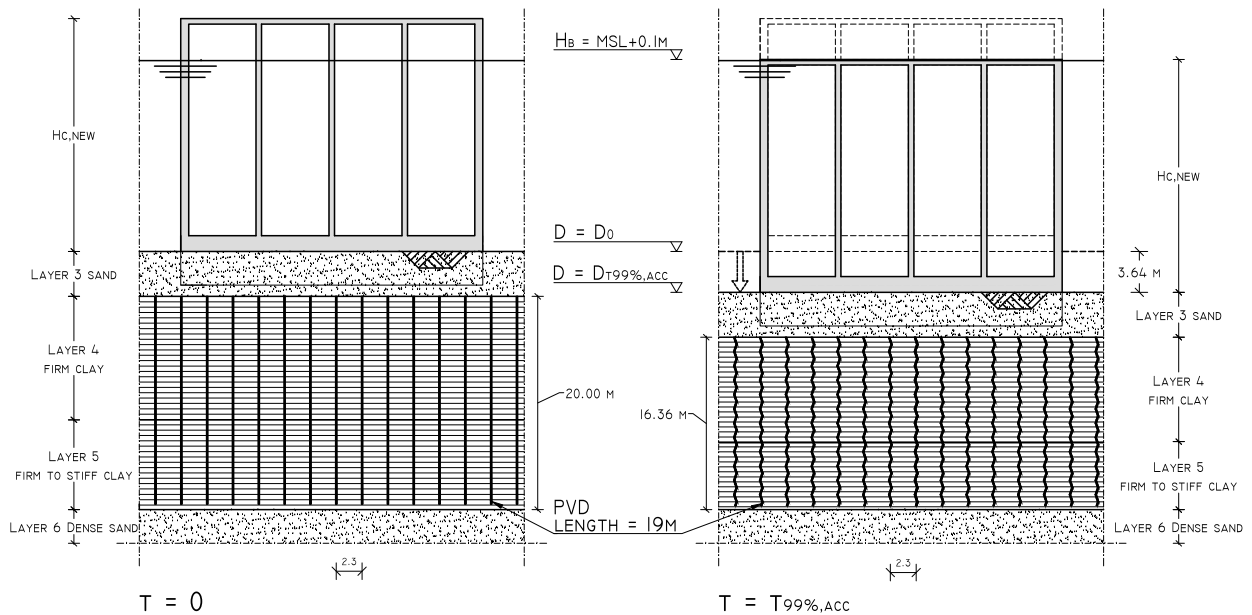


Figure 8.7: Cross-sectional front view of caisson settlement with vertical drains (barrier section BB').

Conclusion vertical drainage. By installing PVDs the soil consolidation is accelerated. It seems like a working alternative. Compared to *not* using these drains the win of this alternative lies in the accelerated soil consolidation time. During the soil consolidation the caissons founded this not yet fully consolidated soil is more vulnerable for soil instabilities, such as sliding along the slide circle. The less time this unconsolidated state of the soil takes, the smaller the risk for such instability. However, the caissons have to be heightened which increases caisson construction costs.

Another disadvantage of this method is the siltation in the caissons. Due to the settlement of the caissons their openings will sink down to a level below the bottom. Sand and other material could slit up inside the caissons. This could affect the functioning of the doors. The floor slab of the caissons could be simply heightened, but it is doubtful whether this is the best option. It could also turn out that this will not be that bad, as the tide induced flow velocities in the caissons will be considerable washing all the material away. One could also place a gravel layer before caisson placement to compensate for the loss in retaining height. This option should be further investigated, as well as the actual occurrence of siltation inside the caissons.

Furthermore the vertical drainage is assumed to be as effective as when applied on land. The influence of a water column pushing down is neglected here. For an accurate approximation of accelerated consolidation by means of vertical drainage under water this should be investigated and included.

8.2.2 Alternative 2: Shallow foundation using vacuum preloading with Capped Prefabricated Vertical Drains

The second alternative is similar to the first one, but instead of using the caisson's dead weight to reach the ultimate soil settlement a preload will be applied in addition to the vertical drainage. On land the easiest way of preloading is by means of a sand or granular embankment. However, in the under water conditions for the storm surge barrier preloading through such an embankment is quite problematic as the material will probably wash away due to the tide-induced water flow between the Galveston Bay and the Gulf of Mexico.

To deal with this issue of under water preloading in tidal zones the vacuum preloading technique could be an alternative. Since its first proposal by Kjellman (1952) the method has evolved into a mature and cost-efficient technique for the treatment of soft clay. It proved to be a successful technique in several land reclamation projects in a number of countries (Chu et al., 2008). The original technique with Prefabricated Vertical Drains (PVDs) for

onshore applications requires placing an air-tightening sheet on the ground surface at first and then sucking our air and water below the sheet by a vacuum pump.

Under water the placement of such a sheet is hard to do. Recently a new technique of applying vacuum pressure to soft clayey subsoil has been developed in which vacuum pressure is combined with Capped Prefabricated Vertical Drains (CPVDs). A CPVD consists of a regular PVD (as used in the vertical drainage alternative) connected with a cap to a drainage hose (Fuji et al., 2002), see Figure 8.8. The drainage hose is connected to a vacuum pump. According to Dam et al. (2006) the suggested vacuum pressure ranges between 50 – 80 kPa [7.3 – 11.6 psi]. Instead of an air/watertight sheet as mentioned above the vacuum preloading with CPVD uses a subsurface soil layer as sealing layer. This method is often applied to reduce the volume of waste at dredging disposal sites. For the preloading for the surge barrier it could be a very convenient method as the difficult installation of a watertight sheet under water is not needed.

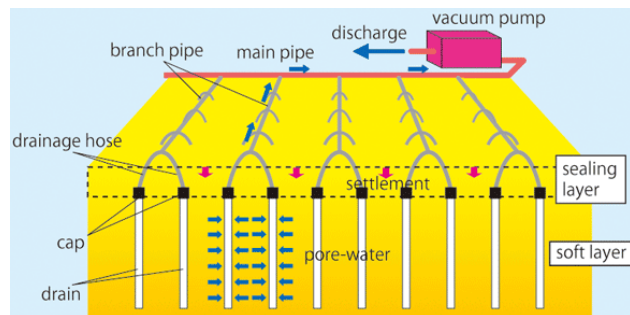


Figure 8.8: Illustration of under water vacuum preloading using CPVDs (Penta Ocean, 2013).

Costs. Just like for the first alternative the drain grid spacing determines the total costs for vacuum preloading with CPVD because drain spacing determines how fast the clay layers will consolidate. Obviously the consolidation duration determines how long the pumps have to work before the clay layers have fully consolidated. But again, the denser the grid, the more vertical drains will be needed, the more CPVD material needed and thus the higher the material costs will be. From here arises again the question what the most cost-effective grid spacing would be. To answer this question, the total costs for vacuum preloading are expressed in terms of grid spacing.

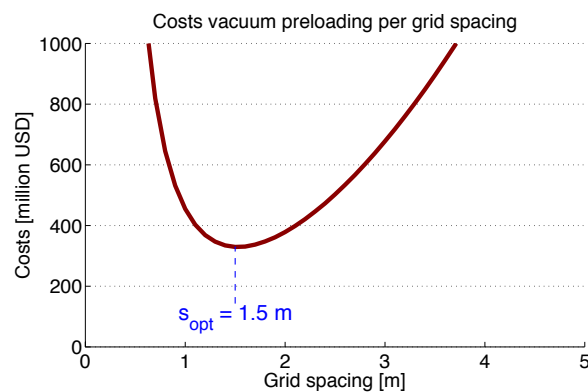


Figure 8.9: Costs vacuum preloading expressed in terms of grid spacing.

From Figure 8.9 it appears that the most cost-effective grid spacing is 1.5 m. Calculations in Appendix G.2.2 show that for this grid spacing the total vacuum preloading costs are approximately \$329 million. By investing \$329 million in vacuum preloading the soil consolidation is accelerated, but calculations in Appendix G.2.2 show that one still has to invest approximately \$471 million in caisson construction costs. This makes the total costs for caisson construction and preloading with CPVDs are \$800 million. This is \$125 million more than for the vertical drainage alternative. It concerns direct costs only.

Acceleration. Next to using the CPVDs the applied pump pressure accelerates the clay consolidation even more. The applied pressure has to be at least equal to the pressure imposed by the caisson weight, or else the caissons would be placed on a non-fully consolidated soil. In that case the caissons would settle further down after placement. As the maximum (caisson weight induced) pressure is at most around 50 kN/m² [7.3 psi] (see Table E.7), the applied vacuum preloading pressure is assumed as 60 kPa. This is equal to a preload of 60 kN/m² [8.7 psi]. The consolidation duration with this method decreases from $t_{99\%} = 18.5$ years to $t_{99\%,acc} = 46$ days⁽²⁾. For impressions of the accelerated settlements in the course of time for barrier section BB', see Figures 8.10 and 8.11.

⁽²⁾ Calculated using Koppejan method

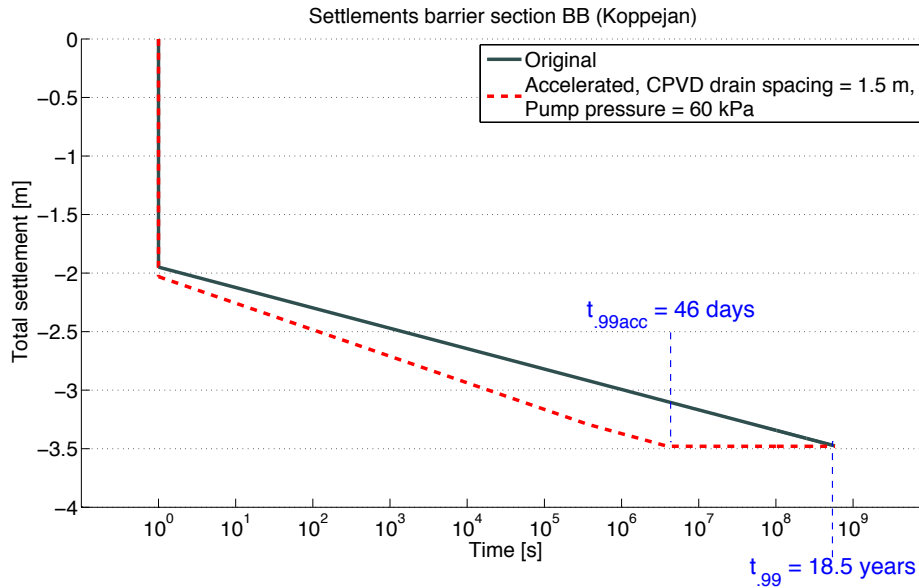


Figure 8.10: Original and accelerated settlements using preloading with CPVD for barrier section BB' (Koppejan method).

Minimum thickness sealing layer. To prevent punctures the sealing layer (indicated in Figure 8.8) should be sufficiently thick. With the known grid spacing, the minimum sealing layer thickness can be determined. According to Chai et al. (2003) this minimum sealing layer thickness $w_{vp,seal}$ is calculated through:

$$w_{vp,seal} = \frac{P_{vac}}{\rho_{sw} \cdot Q_{pump}} \cdot v_{air} \cdot A_d \text{ [m]} \quad 8.2$$

In which P_{vac} is the pump preloading pressure ($= 60 \text{ kN/m}^2$), Q_{pump} is the pump capacity (assumed: $0.1 \text{ m}^3/\text{s}$ per drain), v_{air} the hydraulic conductivity through air ($= 10^{-5} \text{ m/s}$) and A_d is the area of the influence zone by one single drain, which depends on the grid spacing. These parameters are determined according to a calculation example by Chai et al. (2003). The result is a minimum required sealing layer thickness in the order of a few centimeters. This is quite low, local folds and cracks in the clay layer are probably larger than this required sealing layer thickness. Hence for safety reasons a sealing layer thickness of 0.5 m is assumed. See also Figure 8.11.

After the preloading and soil consolidation the weak clay layer replacement will take place. This is done afterwards in order to utilize the sealing capacity of the clay layer (number 3). Subsequently the caissons will be placed.

Conclusion vacuum preloading. Using CPVDs the soil consolidation is accelerated. Again the caissons founded on unconsolidated soil is more vulnerable for instabilities, for example along the slide circle. The shorter this unconsolidated state of the soil takes, the smaller the risk for such instability. Here lies the advantage of vacuum preloading over regular vertical drainage; its most cost-effective consolidation time is a lot faster than regular vertical drainage.

The accelerated consolidation magnitude is presented in Figure 8.11. It seems like a good alternative, but it is a relatively new method that probably needs more development first. Until now it has only proved its feasibility for dredging disposal sites. At these disposal sites it does not really matter when the accelerated settling fails locally; if the soil settles at some point less than anticipated it only means a small loss in disposal volume, which is not such a big deal. For the storm surge barrier it is way more important that the soil settles equally, as an uneven bottom profile directly induces alignment issues. The consequences of the risks involved with this method are very high. It is a method that needs more research before it can be applied as a foundation measure for a storm

surge barriers.

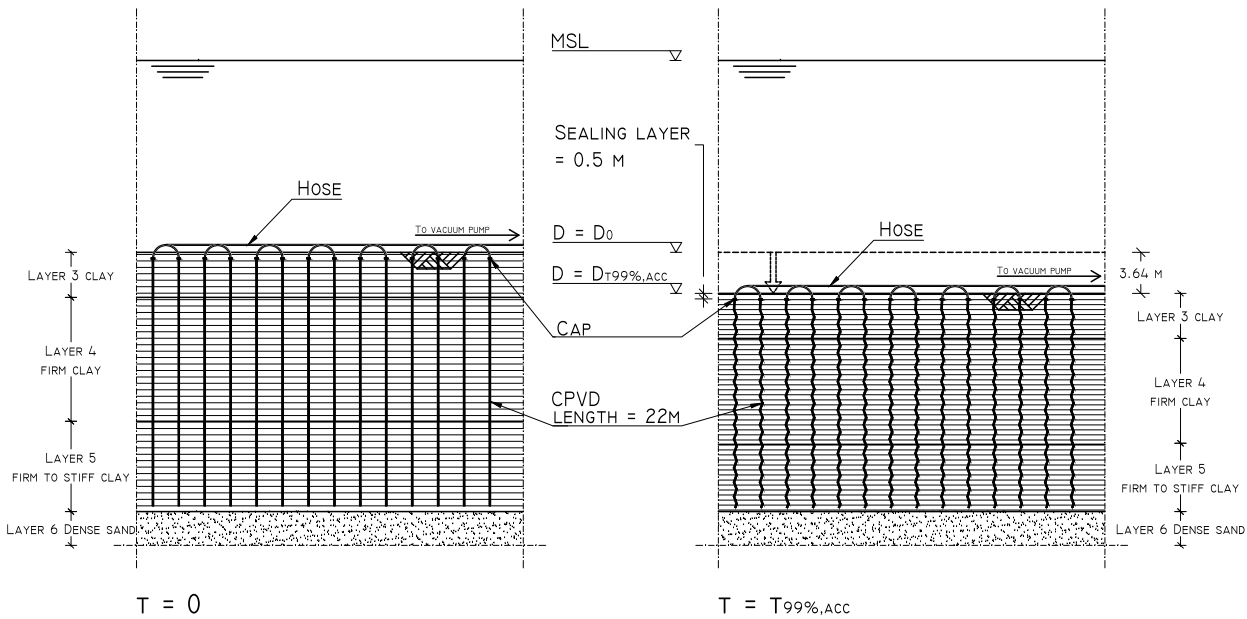


Figure 8.11: Cross-sectional front view of soil settlement using vacuum preloading with CPVDs (barrier section BB').

8.2.3 Alternative 3: Deep foundation with steel tubular piles

The third alternative is a pile foundation underneath the entire caisson barrier span. The foundation piles will transfer all of the horizontal and vertical loads to the bearing soil layer at MSL-40m [131 ft] (no. 6). In this way the weak clay layers are bypassed and the settlements can be reduced to a minimum.

For this pile foundation it first has to be determined which pile type will be applied. Steel tubular piles are an excellent alternative for bearing heavy loads to large depths. Furthermore there is a lot of experience in the installation of steel tubular piles under water, for example in offshore wind farms they are often applied. Main disadvantage of steel tubular piles concerns costs, but in the U.S. steel tubular piles are less costly compared to the Netherlands (W. Broere *TU Delft*, personal communication 22-11-2013) making it a more feasible foundation type for this specific location.

It is decided to construct the steel tubulars closed-ended and fill them with concrete. This makes them less vulnerable for corrosion on the inside and it provides resistance against buckling effects.

Closed end tubular piles have the advantage of a high tip bearing capacity. For determining the number of foundation piles the maximum pile bearing capacity has to be determined. Two criteria play a role in this. The first one is the bearing capacity of the soil and the second is the tubular's structural strength.

The deep foundation is designed with the following assumptions and starting points.

- The steel tubular piles are driven 2 m into the bearing sand layer (no. 6), see Figure 8.12
- The applied pile inclination is equal to $\tan \alpha_t = 1/3$ with respect to the vertical, see Figure 8.12
- The entire calculation is executed in SLS

First the pile bearing capacity is determined using Equation (8.3). Next the required wall thickness is determined, as well as the pile's structural strength. Subsequently the costs for a steel tubular pile foundation are presented as

well as the reduced caisson costs. Finally a pile plan is drafted according to the required number of foundation piles for barrier section BB'.

Pile bearing capacity. The total bearing capacity is:

$$F_{t,max} = F_{t,tip} + F_{t,skin,+} - F_{t,skin,-} - F_{t,dw} \text{ [kN]} \quad 8.3$$

In which $F_{t,tip}$ is the pile tip bearing capacity, $F_{t,skin,+}$ the positive skin friction, $F_{t,skin,-}$ the negative skin friction (down drag) and $F_{t,dw}$ the dead weight of the steel tubular pile. The skin friction between the steel tubular pile and the soil influences the bearing capacity. Positive skin friction increases and negative skin friction decreases the pile bearing capacity. The neutral point indicates the position where skin friction flips from being positive to negative. The location of this neutral point below the surface L_n is 0.95 of the total soft stratum thickness L_s for closed-end piles bearing in sand (Singapore Standard, 2003). See Figure G.7. The depth of this neutral point differs for the different barrier sections as it is dependent on the local depth. The elaborated calculation of the pile bearing capacity is presented in Appendix G.2.3.

Note 1: the contribution of skin friction due to the pulling out of piles is not taken into account. This is the case when negative head acts on the barrier and the tubulars for bearing positive head forces are pulled out. Not taking this contribution into account makes the bearing capacity of all the piles together a conservative estimate, so eventually it will work out on the safe side.

Note 2: in this calculation the theoretical bearing capacity of piles is calculated. Normally the actual bearing capacity will be determined using pile load tests on location.

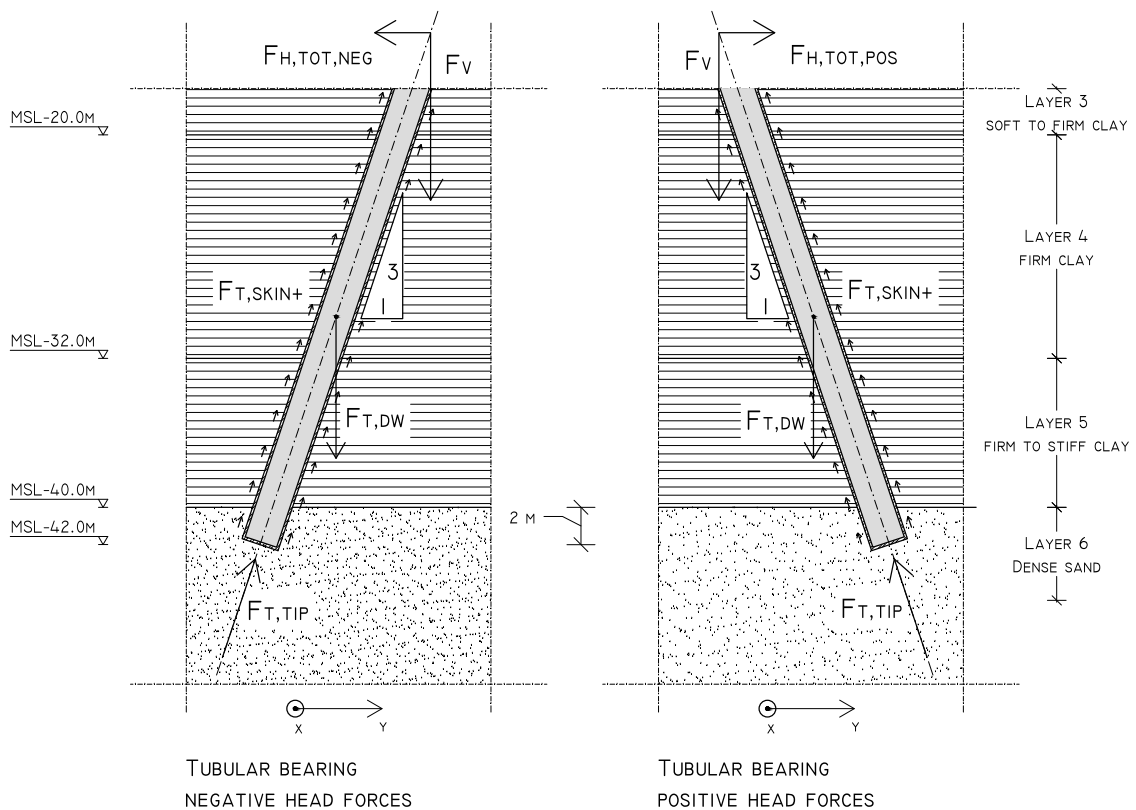


Figure 8.12: Cross-sectional side view of steel tubular piles for bearing forces due to positive and negative head (barrier section BB').

Pile structural strength. The pile wall thickness should be adequate to resist axial and lateral loads as well as the stresses during pile driving. For steel tubular piles that are to be installed by driving where sustained hard driving (≈ 800 blows/meter) is anticipated, the minimum wall thickness used should be no less than (API, 2000):

$$w_{t,min} \geq 6.35 + \frac{\phi_t}{100} \text{ [mm]} \quad 8.4$$

In which ϕ_t is the outer pile diameter. However, this structural requirement will probably not be governing. The aggressive marine environment requires a thicker wall to prevent material degradation due to corrosion. A wall thickness of 75 – 80 mm [2.95 – 3.15 in] should be sufficient to keep this corrosion-induced material degradation to a minimum (W. Broere *TU Delft*, personal communication 11-12-2013).

All of the steel foundation piles must be able to sufficiently transfer the loads down to the bearing layer. If the pile itself is from a structural point of view unable to do so, it needs to be re-dimensioned. The maximum structural strength of the steel piles is given by the steel strength, for standard construction steel S235 this is $\sigma_s = 235 \text{ N/mm}^2$. Quick calculations show that using a wall thickness of 76 mm [3 in] the structural strength of the piles is sufficient in doing so. See also Table G.16.

$$F_{t,steel} = \sigma_s \cdot A_{t,steel} = \sigma_s \cdot \frac{\pi}{4} (\phi_t^2 - (\phi_t - 2 \cdot w_t)^2) \text{ [kN]} \quad 8.5$$

Number of steel tubular piles. Now the number of tubulars per caisson can be calculated. This is done for both the occurring positive and negative head plus wave force, according to Section 7.2. The skirts have become obsolete as all of the horizontal forces will be transferred to the bearing layer through foundation piles, but the steel tubular foundation will still be based on the caissons with the footprint as determined in Table 8.2.

$$n_{t,h,pos} = \frac{F_{h,tot,pos}}{F_{t,max}} \cdot \sqrt{1^2 + (1/\tan \alpha_t)^2} \text{ [-]} \quad 8.6$$

$$n_{t,h,neg} = \frac{F_{h,tot,neg}}{F_{t,max}} \cdot \sqrt{1^2 + (1/\tan \alpha_t)^2} \text{ [-]}$$

In which $n_{t,h,pos}$ and $n_{t,h,neg}$ are the number of required steel tubulars per caisson to bear the horizontal loads due to positive and negative head respectively. $F_{h,tot,pos}$ and $F_{h,tot,neg}$ are the total horizontal forces on the caissons due to wave load and water head (positive and negative respectively, see also Appendix F2.1). The inclination of the piles is expressed as $\tan \alpha_t$ with respect to the vertical, see Figure 8.12.

Now the total number of steel tubulars required to bear the horizontal forces is determined. Maybe these piles are able to bear all of the horizontal forces, but not all of the vertical forces. The vertical bearing capacity per inclined tubular is calculated through:

$$F_{t,v} = \frac{1/\tan \alpha_t}{\sqrt{1 + (\tan \alpha_t)^2}} \cdot F_{t,max} \text{ [kN]} \quad 8.7$$

Subsequently the required number of additional tubulars that only aim on bearing vertical forces is:

$$n_{t,v} = \frac{F_{V,tot} - (n_{t,h,pos} + n_{t,h,neg}) \cdot F_{t,v}}{F_{t,max}} \text{ [-]} \quad 8.8$$

The foundation piles are spread out over the caisson footprint. The piles in x-direction (short edge) are placed right beneath the caisson walls for a better load transfer. The number of piles in x-direction per caisson is therefore equal to the number of compartments. The remaining number of piles required in y-direction (long edge) is spread out over the caisson length.

Costs deep foundation. The costs for the steel tubular pile foundation depend on the applied diameter (with a constant wall thickness). A larger tubular is able to bear a higher load, resulting in less tubulars and relatively less steel, but higher installation costs. Again the optimization question arises: what is the most cost-effective pile diameter? This is done using time and cost unit rates for these aspects. In this way the total costs can be expressed in terms of pile diameter spacing. Figure 8.13 shows the relation between deep foundation costs and grid spacing. The complete calculation procedure is presented in Appendix G.2.3.

The graph in Figure 8.13⁽³⁾ shows the relation between standard sized pile diameters (ranging 406 - 1220 mm [16 - 48 in]) and costs. Larger piles have to be custom made and are therefore presumed to be more expensive. The cost unit rate for custom piles is unknown, but it is expected the deep foundation costs will increase with those custom made tubulars (dashed line in Figure 8.13). Calculations in Appendix G.2.3 and the graph Figure 8.13 show that a pile diameter of 1016 mm [40 in] with wall thickness 76 mm [3 in] is the most cost-effective, standard sized pile diameter.

When applying these pile dimensions a problem for barrier sections AA' and BB' arises. A large number of piles is required when applying this pile diameter, which results in a very dense pile plan. The minimum pile spacing requirement for end-bearing piles (given by Equation (G.24)) is not met. Therefore the foundation piles for these barrier sections will be custom made. It is determined that an enlarged pile diameter for barrier section AA' of 1626 mm [64 in] meets the pile spacing requirement. For barrier section BB' an outer diameter of 2286 mm [90 in] will suffice. In this way a more likely pile plan is possible. For these pile dimensions the total deep foundation costs are estimated at \$356 million, see Appendix G.2.3.

A pile foundation does not need the caissons to be equipped with skirts as the horizontal forces will be fully transferred by the steel tubular piles. This makes the total caisson costs less than for alternative 2: \$467 million. This is calculated in Appendix G.2.3. By investing in a deep foundation the investment costs for caisson construction and a deep foundation amount \$823 million. This concerns direct costs only.

Pile plan. Now the steel tubular pile dimensions are known the number of piles can be determined. They are calculated for each barrier section separately. The results are presented in Table 8.4, more extensive calculations are presented in Appendix G.2.3.

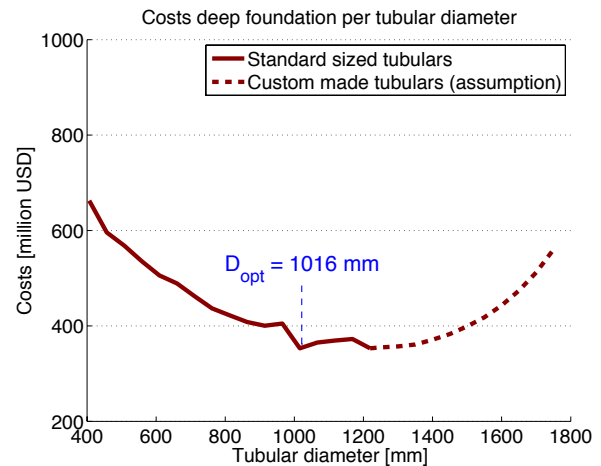


Figure 8.13: Costs steel tubular pile foundation expressed in terms of pile diameter.

⁽³⁾Figure 8.13 shows a kinked graph. This is because a round number of piles is needed, resulting in a non-proportional relation between pile diameter and costs. The graph is further extended by the dashed line for custom made piles. It is expected their unit price is higher and thus their total costs. For a better cost overview these costs should be calculated.

Table 8.4: Required number of steel tubulars.

Barrier section (see Figure 7.3)		AA'	BB'	CC'	DD'	EE'	FF'	GG'
Steel tubular pile geometry								
– Diameter ϕ_t	[mm]	1626	2286	1220	1220	1220	1220	1220
– Wall thickness w_t	[mm]	76	76	76	76	76	76	76
– Bearing capacity $F_{t,max}^{(1)}$	[kN]	6,138	9,822	4,966	6,126	7,480	8,452	7,480
Number of piles per caisson								
– For positive head		15	16	15	6	4	2	4
– For negative head		12	12	12	4	4	2	4
– For additional vertical force		0	0	0	0	0	0	0
Number of piles per barrier section								
– Total		243	112	1377	160	128	116	80

(1) Bearing capacity for piles differs due to the distinct initial effective soil pressures under the barrier sections (e.g. section FF' piles vs section AA' piles). See Table F.6.

The pile plan can be drafted according to the number of required piles as presented in Table 8.4. As calculated in Appendix G.2.3 the steel tubulars are also able to bear the vertical forces, no additional vertical piles are necessary. For barrier section BB' a pile plan is presented in Figure 8.14. The piles will be installed right under the outer and inner walls of the caissons. In order not to mix up piles that aim on bearing forces due to positive and negative head (they are pointed in opposite direction) they are positioned on one side of the caisson, right underneath the caisson walls to minimize the bending moment in the floor slab. For barrier section BB' this is done by placing the negative head piles on the Gulf of Mexico side and the positive head piles on the Galveston Bay side. See cross sectional drawing II-II' in Figure 8.14.

Conclusion deep foundation. Using steel tubular piles filled with concrete all of the horizontal and vertical loads are transferred to the bearing soil layer at MSL-40m. In this way the weak clay layers are bypassed. A cost calculation shows that the optimal pile diameter is 1016 mm [40 in], with wall thickness 76 mm [3 in]. For barrier sections AA' and BB' these pile dimensions do not suffice as the pile spacing requirements are not met. For these sections custom made piles with larger diameter are required; 1626 mm [64 in] and 2032 mm [80 in] (walls 76 mm [3 in]).

Due to this steel tubular foundation high punch loads occur in the bottom slab. Ideally all of the piles will be placed directly underneath a caisson wall, but misalignment of the caissons on the final location may introduce eccentricities in the load transfer from caissons to pile foundation. The resulting moments in the floor slab and caisson walls due to such eccentricities must be examined.

Other than increasing the pile diameter the steel tubular piles for the last mentioned barrier sections could also be founded deeper. In this way a higher tip bearing capacity could be obtained due to the higher effective soil pressure. This option is not investigated here, but could be point of attention in further detailing of the steel tubular pile foundation.

Because the spacing between the piles is quite small at some places (smaller than five times the pile diameter) it is recommended for further research to take pile group effects into account.

Note: in the pile plan (Figure 8.14) a seepage barrier is not indicated as it is not yet designed. Optional seepage barriers will be discussed in Section 8.3, but not for the deep foundation. A possible location of the seepage barrier could be in between the tubulars.

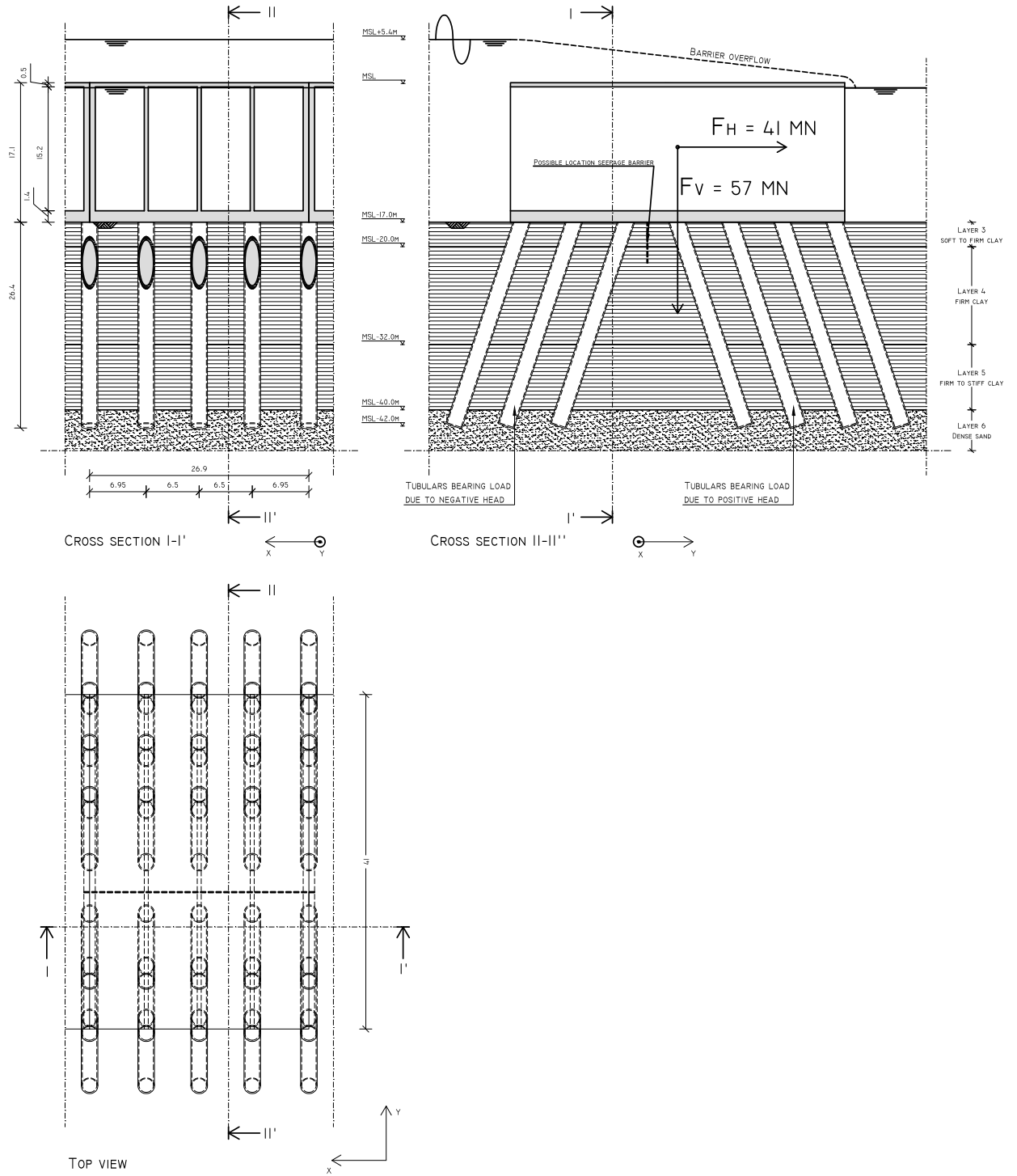


Figure 8.14: Technical drawing of pile plan for barrier section BB'

8.2.4 Alternative 4: Shallow foundation using complete soil replacement

Other than constructing a shallow or deep foundation an alternative could be to replace the weak clay soil layers in their entirety down to a level of MSL-40 m [131 ft] and replace them with sand. In this way the caissons can be shallow founded on a stable sand layer without the necessity of drainage or a deep foundation. See Figure 8.15.

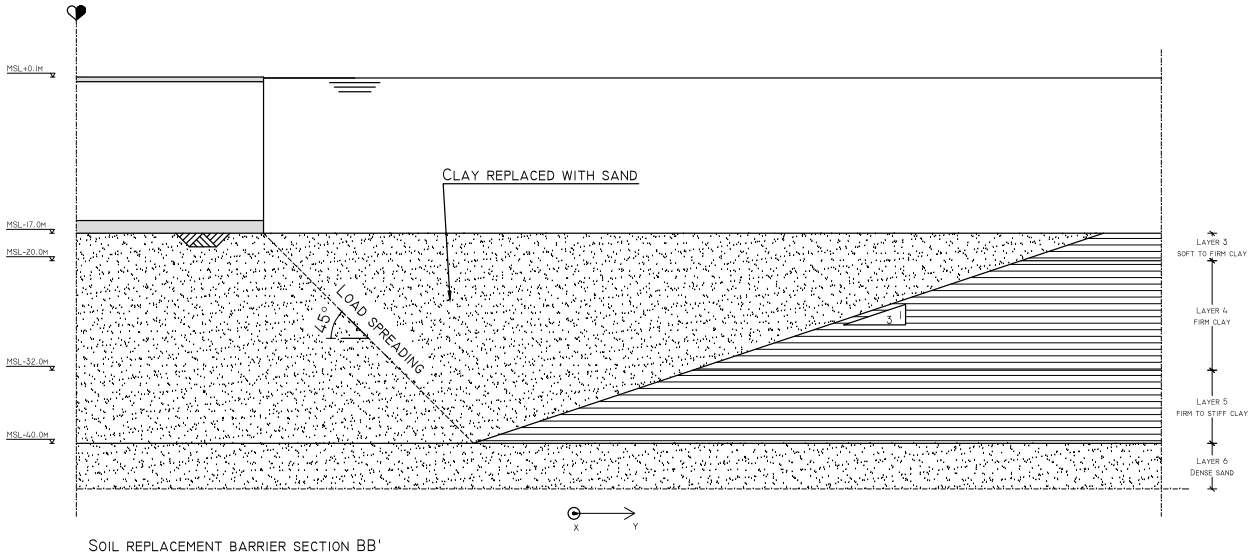


Figure 8.15: Half cross sectional side view of barrier section BB' indicating the clay layers replaced with sand.

Issue in this soil replacement regards the compaction of the sand. Settlements could occur when the caissons are placed on the non-compacted sand. These settlements are not considered here, but it is recommended to investigate them. Other issues regards the washing away of the material during the dredging/dumping process under the tide induced water flow. The profile of the pit that is created by dredging the clay should be monitored to ensure the sand will form a proper foundation for the caissons. Furthermore in the final design stage a bed protection should be installed to prevent the material from washing away.

Costs soil replacement. The costs for this soil replacement are calculated in Appendix G.2.4 using a cost unit rate of 30 \$/m³ (adopted from Braam (2011)). This is quite high, but it concerns all of the costs for dredging the clay material, dump it offshore and fill the pit with sand as well as the mobilization and demobilization costs of the dredging vessels. The costs for a complete soil replacement are estimated at \$355 million. The caisson construction costs are calculated for the regular caisson dimensions as they were determined in Section 8.1 and are equal to the caissons costs for the vacuum preloading alternative: \$471 million.

This makes the total cost estimate for caisson construction and soil replacement \$897 million. It is the most costly foundation alternative.

Conclusion soil replacement. Other than the earlier described foundation alternatives an option could also be to excavate the entire weak clay layer down to a depth of 40 m [131 ft] and replace the clay with sand. It appears that this is very costly. Furthermore issues remain in the soil settlements as dumped sand is not yet compacted and is likely to settle. This settlement will not be as high as the settlement of the clay layers, but it can not be neglected beforehand. Research in the underwater compacting of this sand is recommended.

8.2.5 Assessment foundation alternatives

This assessment treats both the feasibility and costs of the considered foundation alternatives.

Feasibility. Compared to the vacuum preloading alternative vertical drainage has the advantages of being an experienced method but its effectiveness under water is subject to discussion. In this thesis the influence of a water column on the effectiveness of the PVDs is not taken into account. It is assumed this method is as effective as when applied onshore. This should be further investigated and included in the design and assessment. Even though the appliance is tough to do under water it is probably still a more convenient method than vacuum preloading.

The siltation inside the caissons at final location is another point of interest of the vertical drainage method. Due to the soil settling the caisson openings will sink down to a level below the regular bottom profile. It could turn out not that bad because of high tide induced flow velocities, but still sand and other material could easier slit up inside the caissons. This could cause door malfunctioning. One could also place a gravel layer before caisson placement to compensate for the loss in retaining height. Further research in these siltation effects on barrier functioning is recommended.

Applying a steel tubular pile foundation (the third alternative) goes beyond the advantage of a caisson barrier. The advantage of a caisson construction was its ability to spread out of forces over a large footprint to reduce stresses in the subsoil. By constructing a steel tubular pile foundation this whole spreading out of forces has become obsolete, as all of the forces will be transferred down to the bearing sand layer. In other words: a construction other than a caisson could be more feasible when a steel tubular pile foundation is applied. For example a wide-footed T-wall construction with vertical lifting gate can suddenly become a lot more cost-effective than a caisson. Such a T-wall construction requires less concrete, through which the deep foundation (alternative 3) might become more cost-effective than the vertical drainage solution (alternative 1).

Complete soil replacement (alternative 4) deals with soil settling issues and is therefore problematic.

Costs. The total costs for the foundation measure as calculated in this section and for the caisson construction (Appendix G.2) are summarized in Table 8.5.

Table 8.5: Foundation and caisson construction costs per foundation alternative in million US\$.

	Foundation	Caisson construction	Total
1. Vertical drainage with PVD	\$ 142 M	\$ 533 M	\$ 675 M
2. Vacuum preloading with CPVD	\$ 329 M	\$ 471 M	\$ 800 M
3. Steel tubular pile foundation	\$ 356 M	\$ 467 M	\$ 823 M
4. Complete soil replacement	\$ 426 M	\$ 471 M	\$ 897 M

A disadvantage of vertical drainage (first alternative) concerns the higher caisson construction costs, as these have to be heightened beforehand to maintain the required retaining height. The summed costs however, are still less than the summed costs for vacuum preloading (second alternative). This cost calculation shows that vertical drainage is the most cost-effective foundation alternative for a caisson barrier. But there are reasons to speed up this consolidation time and have a look at faster consolidation using vacuum preloading. For example when the soil consolidates, the caissons are more vulnerable for instabilities (e.g. instability along a circular slide circle) in the unconsolidated soil. The probability of occurrence of a severe storm during this consolidation period might become a point of interest. The shorter the consolidation time, the smaller the probability of such a storm and thus the smaller the probability of occurrence of these soil instabilities. This could be a reason for the client to speed up the soil consolidation time. In that case the vacuum preloading (second alternative) comes into the picture, as it has a consolidation time of only 46 days which is a lot shorter than the 648 days for the vertical drainage⁽⁴⁾.

⁽⁴⁾These consolidation durations apply to the most cost-effective grid spacing. The consolidation duration for vertical drainage in fact can be a lot quicker too, but this requires a denser grid and thus again higher costs. For simplicity reasons the only most cost-effective grid spacing is considered.

As stated in the feasibility paragraph above, a construction other than a caisson could be more feasible when a steel tubular pile foundation (alternative 3) is applied. As stated above, a wide-footed T-wall construction with vertical lifting gate could be less costly than a caisson. Such a T-wall construction requires less concrete, through which the deep foundation (alternative 3) might become more cost-effective than vertical drainage (alternative 1). A deep foundation is probably the most cost-effective solution in case a barrier other than a caisson barrier is built.

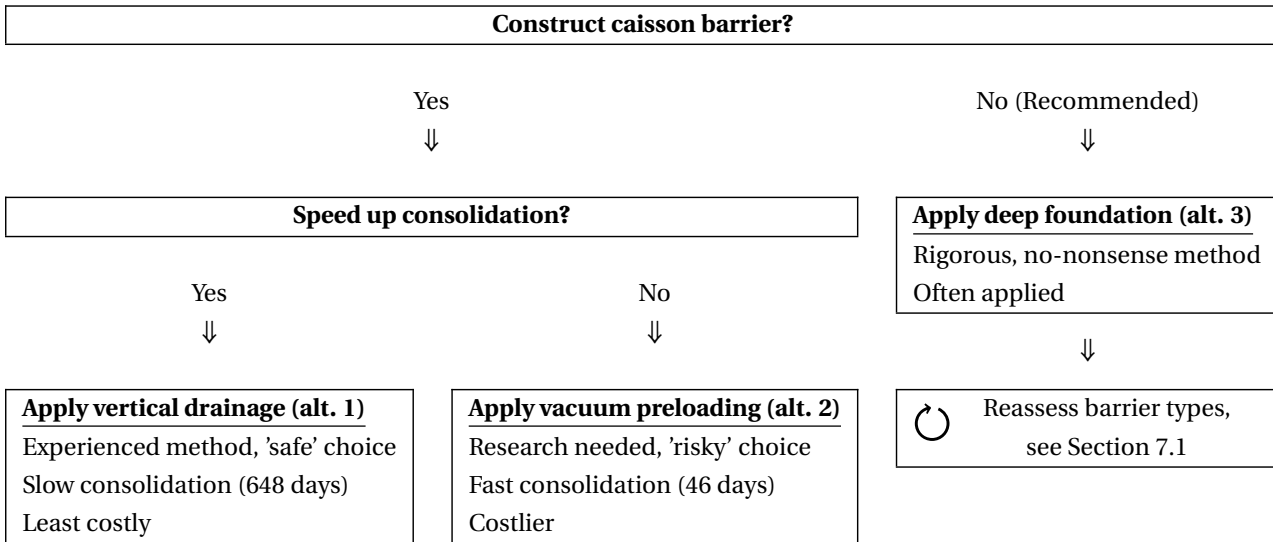
The complete soil replacement (alternative 4) not only deals with soil settling issues but is also the costliest alternative.

Conclusion foundation alternatives assessment and suggested strategy. The conclusion of this foundation alternatives assessment is two-fold. The client first has to decide whether a caisson barrier design is continued. If so, vertical drainage with PVDs is the least costly method, but its consolidation duration is longer than for the vacuum preloading. The latter has a faster consolidation duration, but is a more expensive method and not often applied yet.

If the client does not want to continue with the caisson barrier a more rigorous deep foundation is preferred above soft soil improvement. It is recommended to first investigate the most appropriate barrier type with a deep foundation. The knowledge gained from this foundation alternatives assessment should be included when reassessing barrier types in the environmental barrier design level (previous chapter; Section 7.1).

This conclusion is schematically presented in the flowchart below. Complete soil replacement (alt. 4) is not recommended under any circumstances and therefore omitted in this flowchart.

Table 8.6: Flowchart for selecting barrier construction and barrier foundation type.



The next steps in the design do not only depend on the client's wishes but also on his risk profile. Continuing the caisson barrier design process puts him in the position where it has to be decided to invest in the risk-averse vertical drainage method or the risk-seeking vacuum preloading method. If a no-nonsense, (and also risk-averse) approach of constructing a barrier with a deep foundation is preferred it is recommended to loop back to the environmental barrier design level and reassess other barrier types first on their applicability with a deep foundation. The latter approach is recommended as knowledge gained from the design steps can be implemented. For example a wide-footed T-wall construction with a vertical lifting gate hanging in two large slots founded on steel tubular foundation piles may emerge as an alternative. Such a construction requires less concrete making the steel tubular

pile foundation a less costly alternative than the current least costly method: vertical drainage.

For the remainder of this thesis one of four foundation alternatives has to be chosen or else no seepage measure and construction method can be presented. It is recommended to reassess the barrier types and possibly apply a deep foundation, but the aim of this thesis was to present a complete barrier design in short time. Therefore the report proceeds with a design for a seepage prevention measure and a construction method for a caisson barrier with vacuum preloading soil improvement. Despite the fact that its costs are higher than for vertical drainage the application of this method is further investigated because it has not yet been applied as a soil improvement measure for a shallow founded storm surge barrier. The seepage measure will be designed in the next section and a construction method is presented in the next chapter.

8.3 Seepage prevention measures

Now that it is determined that the design process will be continued for the vacuum preloading method the last design aspect is to deal with water level differences across the caissons structure that can cause groundwater flow underneath the structure. This 'seepage' can occur at the plane between the impermeable structure and a loose grain layer. It is the flow of water through a pipe-like channel that has been created by internal erosion. Seepage occurs predominantly in sand as it has a high hydraulic conductivity. It is assumed that the clay layers underneath Bolivar Roads have such a low hydraulic conductivity that seepage will not occur here. Since the caissons will be placed on sand layers they have to be checked for seepage.

Calculations in Appendix G.3 show that the caisson length is not sufficient for all barrier sections. Along the entire environmental barrier span a seepage barrier should be placed. One could consider the following measures (Vrijling et al., 2011):

1. Use sheet piling as a screen against seepage
2. Install grout columns to make the soil impermeable and cohesive
3. Insert a diagonal protective textile in the ground
4. Insert a filter structure

In this thesis a thorough investigation into all of these measures barriers is omitted. For now the first alternative, a vertical sheet pile penetrating 1 m into the clay layer (layer no. 3, see Figure F.1) is chosen to prevent this seepage. This penetration depth of 1 m is assumed to be sufficient in blocking the seepage. It is recommended to do further research in the required length of this seepage screen. To prevent the caissons from leaning on these sheet piles when the soil settles down, they are placed just next to the caissons on the open coast side. A poorly permeable material is placed between the sheet pile and the caissons to make an as much as possible water tight sealing. The exact procedure of this is presented in the construction method, see Section 9.3.

8.4 Conclusions & recommendations

This third and final design step focusses on dealing with the poor soil conditions. First the revised caisson dimensions were obtained according to increased horizontal force resistance by the application of skirts and the replacement of a few meters of weak soil layer underneath barrier sections AA' and BB'. This resulted in shorter caissons. The skirts are dimensioned in such a way that they look reasonable from a geometrical point of view. They should be able to sufficiently transfer all the forces, but a strength calculation is necessary to conclude whether they are strong enough. Skirt design optimization is not considered in this thesis, for further detailing it is recommended to do so. Furthermore the caissons should also be checked on circular slide surfaces. This calculation is omitted

in this thesis, but should certainly be taken into account in further design. It is assumed this circular slide surface mechanism is not governing. For further design it is recommended to check this aspect using, for example using the software D-Stab or Plaxis.

After determining the optimized caisson dimensions three alternatives for a foundation are drafted. These concern a deep foundation through steel tubular piles and two soft soil improvement measures: vertical drainage and vacuum preloading. These three alternatives are assessed on their feasibility, foundation costs and caisson construction costs. The latter one plays a role as different foundation types require distinct caisson dimensions.

The foundation alternatives assessment provided an important insight: the drafted design criteria in the second design step (environmental barrier design level; Section 7.1), on which the choice for a caisson barrier was based, were unbalanced. There should have been more emphasis on the foundation. This results in a two-fold advise for the client. If the decision is to continue the caisson barrier design it is recommended to apply vertical drainage, as it is less costly than a deep foundation and there is substantial experience with this method. As an alternative, the client is advised to reassess the barrier types on the environmental barrier design level while taking into account that a deep foundation is more appropriate for Bolivar Roads.

As the aim of this thesis was to present a complete barrier design in a short time, the suggested reassessment of barrier types is not further elaborated. Despite the fact that its costs are higher than for vertical drainage the application of this method is further investigated because it has not yet been applied as a soil improvement measure for a shallow founded storm surge barrier. Therefore the seepage measure is designed for the vacuum preloading method. A vertical sheet pile penetrating 1 m [3.3 ft] into the clay layer (layer no. 3) will be applied to prevent seepage under the caisson structures. This penetration depth of 1 m [3.3 ft] is assumed able to sufficiently block the seepage. For further research it is recommended to precisely determine this required seepage screen depth. They are placed just next to the caissons on the open coast side to prevent the caissons from leaning on them. A rubber sealing layer will make a watertight connection between the sheet piles and the caissons. As this is a very vulnerable connection more detailed design in this sealing is recommended.

Furthermore it is useful to think about construction methodology. The barrier design would be incomplete without a description of the construction activities that have to be carried out. This might reveal issues which have not previously been thought. The next chapter will revolve around a construction method for the caisson barrier using vacuum preloading as a foundation measure. Despite its relatively high costs, further investigating the application of this method is preferred as it has not yet been applied before for a large, shallow founded structure like a storm surge barrier.

9 Construction method and costs

As stated in the previous chapter (Section 8.4) the construction method is presented for a shallow founded caisson barrier with vacuum preloading as soil improvement.

The consecutive activities up until the completion of the structure are described in the upcoming sections. This will go along with a cost indication for each activity, for which the numbers are calculated in Appendix H. The approach of this construction method is based on a case study by de Vries et al. (2012). An indication of the total project costs is presented in Section 9.5. Visual impressions of this design process and the barrier on its final location are presented in Section 9.6.

9.1 Construction of dry dock

The construction dock will be located on Pelican Island. This is right next to the deep-drafted Houston Shipping Channel (HSC) to ensure a short transportation time to the final location, see Figure 9.9. The dry dock construction consists of the following activities.

- 1.1 Install vertical drains in a square grid spaced 1 m [3.3 ft] through driving mandrels with PVDs into the ground⁽¹⁾ over a surface of 350 by 450 m [1,150 by 1,475 ft]. The weight of the upper lying soil layers will act as a preloading⁽²⁾ on the construction dock's subsoil of 267 kN/m². After a consolidation time of 1 year⁽³⁾ the soil has settled 4 m [13.1 ft] in depth⁽⁴⁾, down to MSL-19 m [62.3 ft].

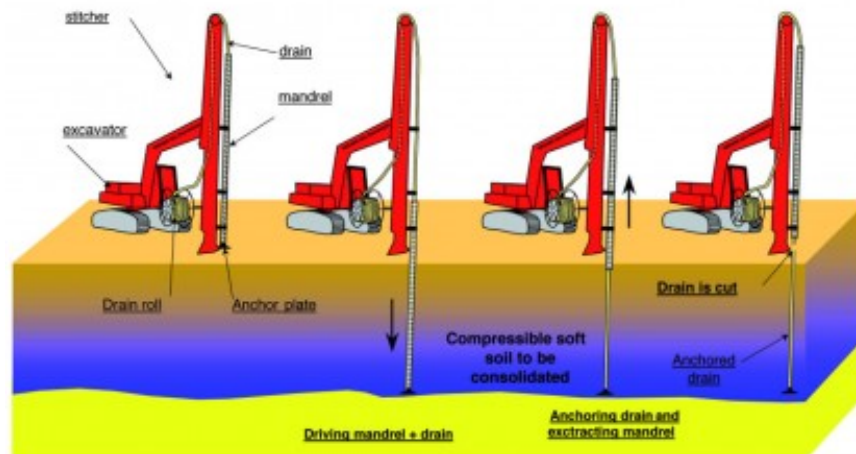


Figure 9.1: Installation of PVDs with mandrels (Vibro Menard, 2013).

- 1.2 Drive sheet piles in a rectangular shape of 350 by 450 m. This ensures a rectangular dock floor footprint of 250 by 350 m [820 by 1,150 ft]. The sheets should be driven 2 m [6.6 ft] into the consolidated clay layer (layer no. 3, see Figure E.1) that starts at a depth of MSL-19 m [62 ft]. In this way the groundwater is prevented from seeping into the building dock. The sheet piles have to be 21 m [69 ft] long.

⁽¹⁾The most optimal spacing of this vertical drainage for the building dock is not designed.

⁽²⁾The building dock will eventually be excavated down to a level of MSL-11.9 m, and the clay layers start at a depth of MSL-15 m (see Figure E.1). The weight of layers 1 and 2 (with densities from Table E.1: $\rho_{s,1} = 13 \text{ kN/m}^2$, $\rho_{s,2} = 19 \text{ kN/m}^2$) will act as the preloading force. The magnitude of this preloading pressure is of $w_{s,1} \cdot \rho_{s,1} + w_{s,2} \cdot \rho_{s,2} = 3 \cdot 13 + 12 \cdot 19 = 267 \text{ kN/m}^2$ [38.7 psi].

⁽³⁾The consolidation time of the clay layers in the building dock is a rough assumption.

⁽⁴⁾The settlement magnitude in the building dock is assumed equal to the maximum settlement that occurs for the final location of barrier section BB'; rounded up to 4 m [13 ft].

- 1.3 Lower the groundwater table in the dock created by the sheet piles down to a level MSL-11.9 m [39.0 ft]. This is the level the construction dock will be excavated to. The preloading pressure of the upper lying layers on the clay layers due to this excavation weight has dropped⁽⁵⁾ from 267 kN/m² to 135 kN/m² [38.7 psi to 19.6 psi].
- 1.4 The dock is excavated down to a level of MSL-11.9 m. This depth ensures enough clearance for the deepest caisson draft (for barrier section BB') to be safely transported out of the dock. See also activity 4.2. The excavated soil is moved to the perimeter to create levees right on top of the sheet piles. These levees have a slope of 1:3 and have a flat crest of 5.0 m [16.4 ft] wide. A gravel lane over the levees allows equipment and workers to enter the dock.
- 1.5 Excavating the dock down to a maximum level of MSL-11.9 m will leave a sand layer of 3.1 m [10.2 ft] to rest on the consolidated clay (see also Figure F.1). This sand layer provides enough stiffness and strength to support the caissons during construction. It is also crucial during the flooding of the dry dock. The sand layer will allow the water to flow easily underneath the structure and build up the required buoyancy force.
- 1.6 Construct lock doors in front of the levee of Pelican Island, through which the caissons will finally float to the HSC. After connecting the dock levee to the door abutments the old levee in front of the lock doors is removed. The construction of these doors will not influence the critical time path of the project, as they can be constructed simultaneously with the caissons.
- 1.7 Dredge a channel of 11.9 m deep between the building dock on Pelican Island and the HSC for ensuring enough draft during the transport of the caissons from building dock to final location. The dredging of this channel will not influence the critical time path, as it can be done parallel to dock construction.

Calculations in Appendix H.1 show that the costs for above described activities are estimated at \$206 million. For an overview image of the dry dock see Figure 9.11.

9.2 Caisson construction

The construction of a single caisson in the dry dock consists of the following activities.

- 2.1 Construct the formwork for the caisson skirts out of plywood. This part will be casted at once, so no repetition of the skirt formwork is possible. The plywood can be placed on top of the consolidated sand layer. The sides will have to be supported with struts to bear the horizontal load of the fluid concrete.
- 2.2 Heighten the bed level of the construction site in order to place the formwork for the floor slab in position.
- 2.3 Construct the formwork for the bottom slab out of plywood. The floor slab has to be casted at once, so no repetition can be achieved here too. At least one of the sides must not be placed yet, to provide easy access to the site for reinforcement benders, see next activity.
- 2.4 Positioning and fixing the reinforcement bars for the bottom slab, as well as the vertical starts of reinforcement for the walls. Special attention is needed with respect to the concrete cover due to the hostile marine environment.
- 2.5 After the concrete mixture is approved the concrete pouring can be started. This has to be done in one shift, to prevent discontinuities in the slab that could be unfavorable with respect to the structure's durability. After two days of hardening, the concrete is stiff enough to allow working on the walls.
- 2.6 As the caisson walls have a height up to 15.2 m [49.9 ft] it is hard to cast the walls at once. The limited drop height of concrete requires multiple casting shifts. Using climbing formwork (see Figure 9.2) the concrete

⁽⁵⁾The drainage accelerated settlement ratio is assumed to be 4 m, see activity 1.1. To maintain the building dock depth the remaining thickness of the sand layer (number two) that still acts on the clay layer is $15 - 11.9 + 4 = 7.1$ m. This induces a preloading pressure of $7.1 \cdot 19 \approx 135$ kN/m².

is casted in shifts of a few meters. Because of the frequent reuse of the climbing formwork plates, they are fabricated from steel instead of plywood. Special attention is needed for the construction of the door slots.

- 2.7 After finishing the walls the vertical lifting structure is constructed. As the focus in this thesis lies in the geotechnical design challenges this is not further elaborated.
- 2.8 Next the prefabricated caisson doors can be placed in position. The exact construction of these doors is also not treated in this thesis.
- 2.9 The caisson top slab is constructed. The top slab can be prefabricated as the connection between the caisson walls and the top slab does not require to be fixed, see moment calculations in Appendix F.2.1. This makes the caissons a little more constructible, as no complicated formwork and concrete pouring of the top slab is necessary. If the adjustable retaining height criterion⁽⁶⁾ is met by constructing a retaining wall one should bear in mind that rebars or another structure should protrude out of the caisson top slab and walls. In this way a wall can easily be connected to the top of the caissons in a later stage.
- 2.10 Bulkheads will be constructed on the short edges of the caissons. It is important the connection between the bulkheads, walls and slabs is watertight, to ensure the buoyancy during transport. The exact design and detailing of these bulkheads is not further discussed in this construction method overview.
- 2.11 After the caissons are finished their pressure acting on the bed of the dry dock⁽⁷⁾ varies between 33 kN/m² (caissons for section FF') and 89 kN/m² (section BB'). This is lower than the governing preloading pressure of 135 kN/m² [19.6 psi] as calculated under activity 1.3, so no additional settlements during construction are expected to occur. The effects of soil swelling after removal of the caissons on the stability of the bed of the construction dock are not considered, but it is recommended to take this into account.

In the third design step (Appendix G.2.2) the construction time and costs for above described activities are estimated at \$471 million. For an overview image of the caissons in the dry dock see Figure 9.11.

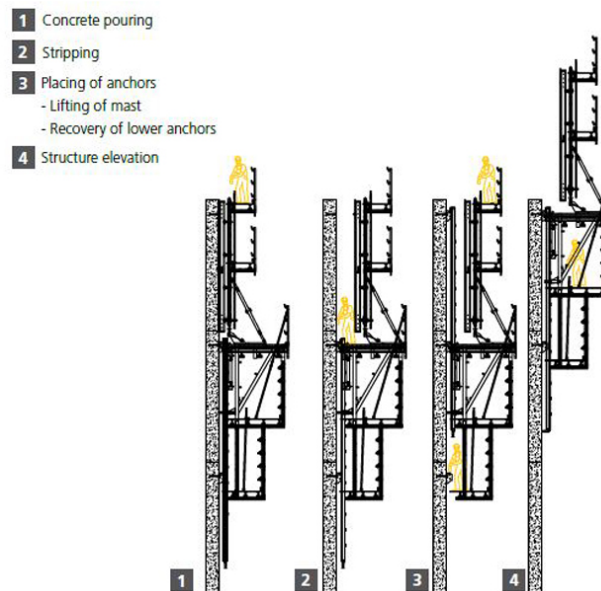


Figure 9.2: Climbing formwork procedure (ULMA Construction, 2013).

⁽⁶⁾To cope with the higher water levels due to SLR.

⁽⁷⁾Calculated by: $\sigma_{c,dry} = \frac{V_{c,con} \cdot \rho_c}{W_c \cdot L_c}$ [kN/m²] in which $\sigma_{c,dry}$ is the caisson weight induced pressure on the bottom of the dry dock, ρ_c the mass density of concrete (25 kN/m²), W_c the caisson width and L_c the caisson length.

9.3 Preparing final location

Parallel to the actual caisson construction the final location has to be prepared. These activities have to be finished before the specific caisson for that location is finished. In this way the preparation of the final location does not influence the critical time path of the project. It is recommended to do this final location preparation outside the hurricane season (which runs from June until November) to avoid severe weather conditions. In this section the installation and operation of the vacuum preloading method (Section 8.2.2) is described.

- 3.1 Drive steel mandrels with PVDs in a square grid spaced 1.5 m [4.9 ft] down to a level of MSL-39.5 m [130 ft] and 0.5 m [1.6 ft] below the bottom surface along the entire barrier span, 10 m [33 ft] outside the caisson perimeter. The latter spacing is to prevent unstable slopes close to the barriers. It is assumed the driving is done from a floating pontoon.
- 3.2 Remove the steel mandrels and connect the CPVDs to the vacuum pumps via hoses.
- 3.3 As the maximum (caisson weight induced) pressure is at most around 50 kN/m² [7.3 psi] (see Table E7), a pump pressure of 60 kPa [8.7 psi] is applied to the CPVDs. After 46 days the clay layers have settled the required 99%.
- 3.4 Remove the hoses. Doing so will relax the pressure on the clay layers which makes them swell again. The bottom profile will come up a little. This effect is neglected here, but should be taken into account. The resulting hole is filled up with sand and has to be flattened.
- 3.5 Position the floating caisson above the final location. Open the valves in the bulkheads to let the water flow in and submerge the caisson slowly. The dividers ensure a gradual distribution of the water in the caissons to maintain the horizontal position during submergence. During placement the caisson's position should be monitored for a precise placement. This step has to take place during calm weather.
- 3.6 During placement the barrier doors should stay a little open until the seepage screen is installed. This is to prevent a water head difference between both sides so no seepage can occur before the seepage screen is installed. After touchdown the bulkheads and dividers are removed.
- 3.7 Install the sheet pile wall on the open coast side of the barrier. This will act as a screen to prevent seepage under the caisson. The door may now be closed. Subsequently place a bed protection on both sides of the caisson to prevent the sand from washing away under the influence of water flow. The exact design of this bed protection is outside the scope of this thesis.

Calculations in Appendix H.1 show that the costs for above described activities are estimated at \$373 million. The cross-sectional side views presented in Figure 9.3 – Figure 9.8 accompany the steps described for barrier section BB' (see Figure 7.3). Units are in meters.

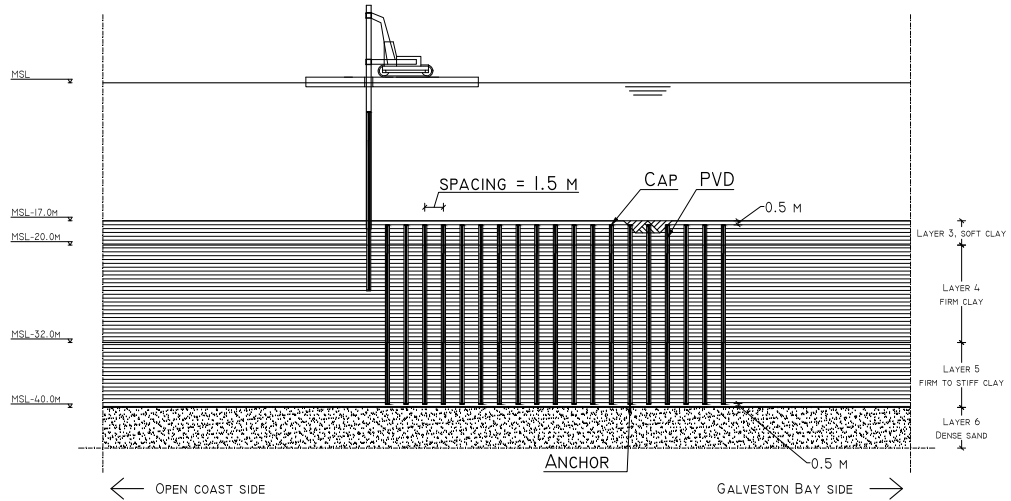


Figure 9.3: Step 3.1 – Install steel mandrels with CPVDs in clay layers.

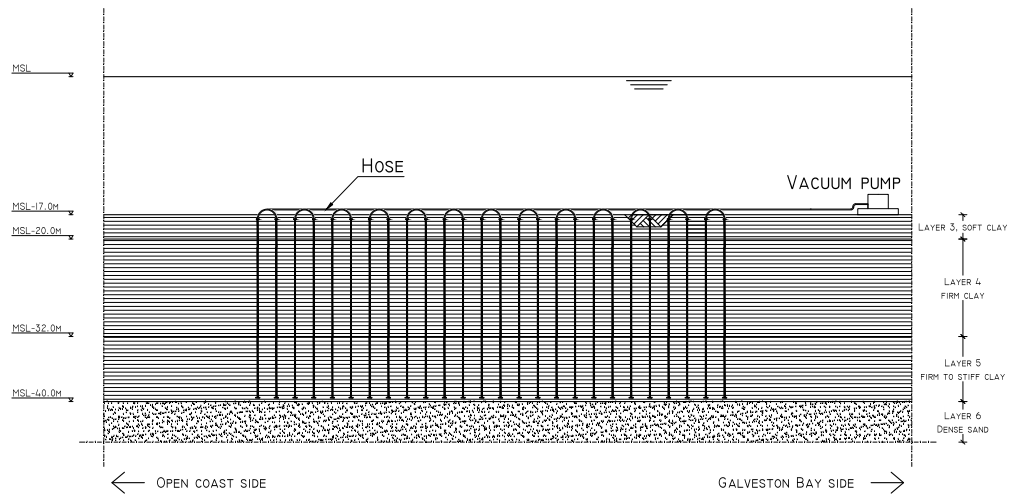


Figure 9.4: Step 3.2 – Remove steel mandrels, connect vacuum pumps to CPVDs via hoses.

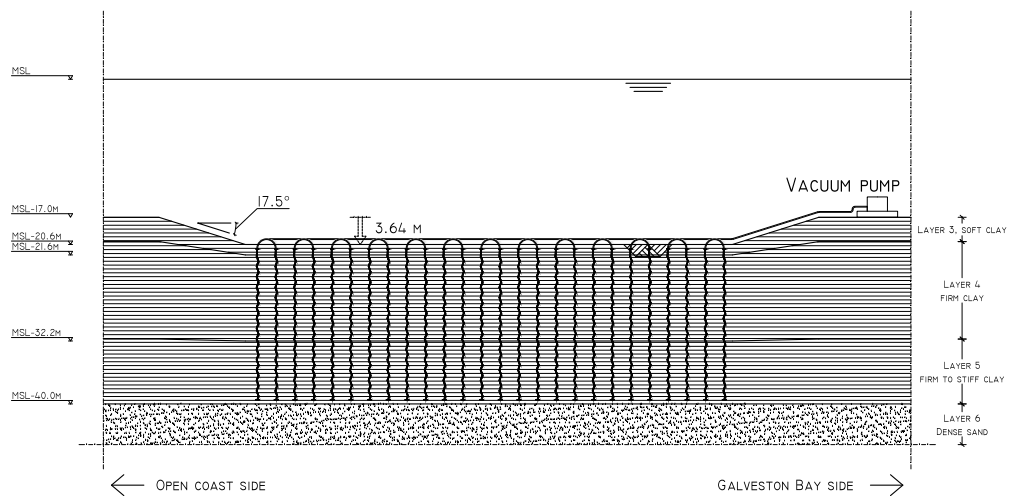


Figure 9.5: Step 3.3 – Pump for 46 days.

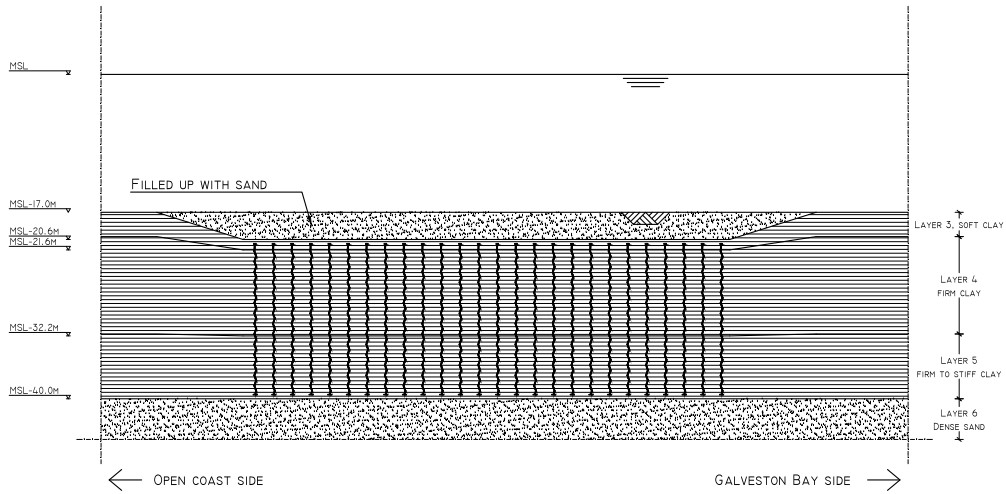


Figure 9.6: Step 3.4 – Remove hoses, fill the resulting hole up with sand.

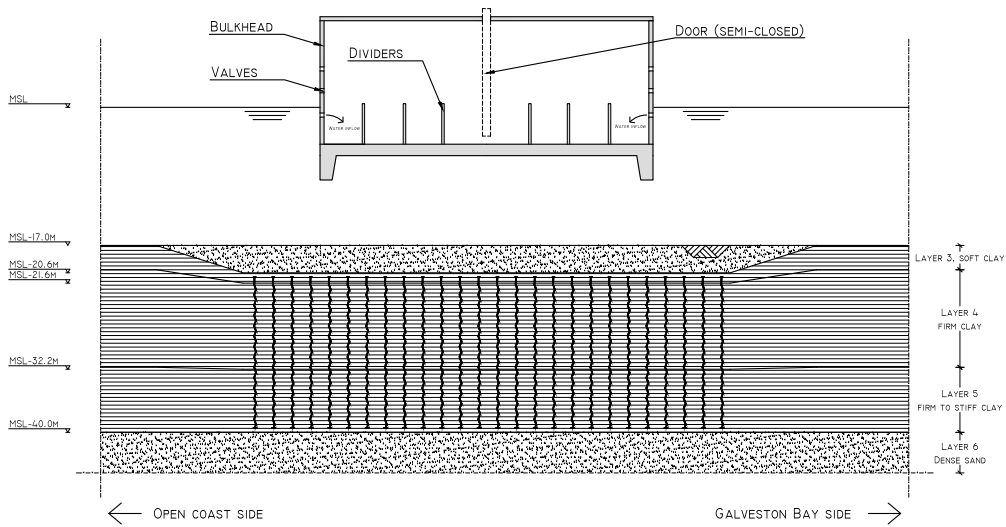


Figure 9.7: Step 3.5 – Monitor the position of the floating caisson during submergence.

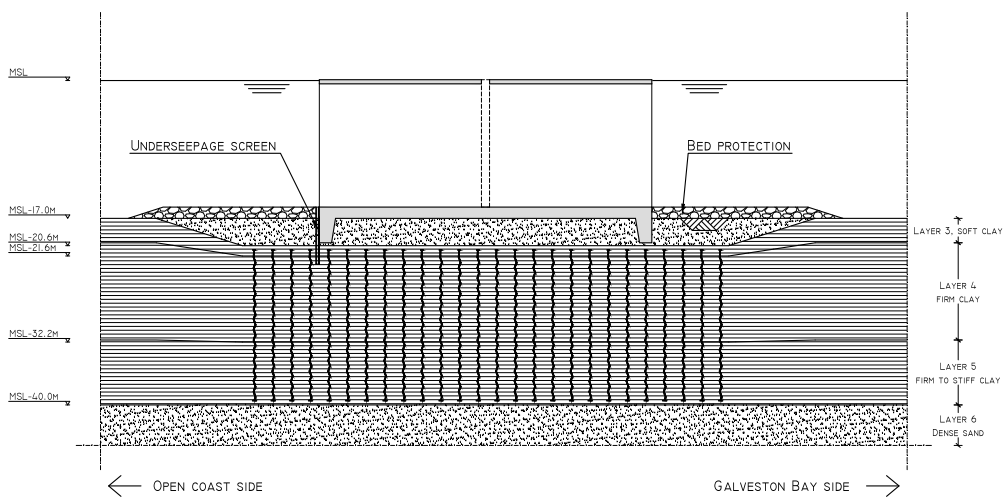


Figure 9.8: Step 3.6 – Place the caisson on the sand bed, install the sheet pile wall on the open coast side and place the bed protection.

9.4 Caisson transport and placement

The caisson transport and placement on the final location consists of the following activities.

- 4.1 After the caissons have been constructed the equipment will be removed from the workplace and the valves in the dry dock's lock doors can be opened. The dock is gradually filled with water and the caissons will start to float due to the buoyant forces. Several aspects have to be monitored during this process. The levees should be checked if they are able to bear the water pressure in the dock. Second the caissons must be secured after the start floating, to prevent collision with other caissons or crashing against the dock levees.
- 4.2 As the water level in the dock is the same as in Bolivar Roads, the lock doors can be opened and the caissons are ready to be towed out, see Figure 9.12. After this is done, the lock doors are closed, the water is drained again and the sand layer is restored. First the smallest caissons will be constructed. If they are all ready, first the bed level is lowered and flattened to create a deeper-drafted construction site. In this way a next shift of caisson construction can take place, meanwhile the finished caissons can be placed on their final location. Time can be saved, as not all caissons have to be finished before towing them out. It also reduced the size of the building dock. This cycle can be done a number of times to save time and costs. The quantification of this optimization however, is outside the scope of this thesis.
- 4.3 Tugboats do the towing of the caissons over the HSC to their final location, see Figure 9.13.
- 4.4 The valves in the bulkheads have to be opened a little to ensure a controlled submergence of the caissons. The tugboats keep monitoring the right position during this submergence process, see Figure 9.14.
- 4.5 After touchdown the sealing layer between the caissons and the seepage sheet pile is placed. Special attention should be given to this sealing layer as it is the key element in preventing the seepage under the caissons. If this layer leaks the whole blocking effect of the sheet pile is at stake.
- 4.6 The following caissons will be positioned next to each other with leaving a space of 0.2 - 0.5 m [0.7 - 1.6 ft] open. This spacing between the caissons serves to prevent collision in case of unequal settlements. The resulting intermediate space between the caissons could be filled up with a gravel layer in order not to create additional flow openings in the barrier. This gravel is captured at the edges of the caissons with nets, to ensure that the material will not wash away.
- 4.7 After the final placement damage to the bed protection is monitored and maintained. Settlements, though not expected, will be monitored and where necessary soil material will be excavated or grout is injected to maintain the horizontal position of the caissons.

Calculations in Appendix H.1 show that the costs for caisson transport and placement are estimated at \$20 million.

9.5 Total project costs

The total investment costs are presented in Table 9.1. The numbers for each activity are calculated in Appendix H.1.

A first, crude cost estimate in the system level design (Section 6.3.2) for the environmental barrier section amounted approximately \$3.8 billion. Probably the reason why this initial cost estimate is two times higher than the amount of \$1.9 billion calculated here is because of a wrong assumption in unit cost rate per cubic meter in Equation (6.1). This was set to \$30,000 for the environmental barrier section. The cost index numbers drafted by van der Toorn (2012) on which this cost unit rate is based is very widespread: the values in this nine-numbered dataset vary between \$20,000 and \$43,000. The reason why the cost estimate came out so high was probably due to the uncertainty in these cost index numbers.

The calculation in this chapter is more accurate than in the system level design as the costs for activities are estimated separately. The number of \$1.9 billion is quite low, this is probably due to the fact that some unit cost rates are roughly estimated, especially installation costs need more substantiation. A thorough, detailed cost estimate is outside the scope of this thesis.

With these facts in mind the total costs for a storm surge barrier in Bolivar Roads (including the navigational barrier) are estimated to range between \$2.7 and \$4.0 billion. This concerns a crude estimate.

Table 9.1: Cost overview environmental barrier. Direct costs calculated in Table 9.1.

<u>Direct costs</u>	
– Dry dock	\$ 206 M
– Caisson construction	\$ 471 M
– Final location	\$ 373 M
– Caisson transport	\$ 20 M
Site overhead costs (5%)	\$ 55 M
Unforeseen (10%)	\$ 116 M
Total direct costs	\$ 1,276 M
<u>Indirect costs</u>	
– One time costs (2%)	\$ 25 M
– Implementation costs (5%)	\$ 64 M
– General costs (5%)	\$ 64 M
– Risk & Profit (10%)	\$ 128 M
Total indirect costs	\$ 280 M
Total construction costs	\$ 1,557 M
Engineering, administration, survey	\$ 150 M
Administration	\$ 45 M
Project unforeseen (10%)	\$ 175 M
Total investment costs	\$ 1,927 M

9.6 Drawings

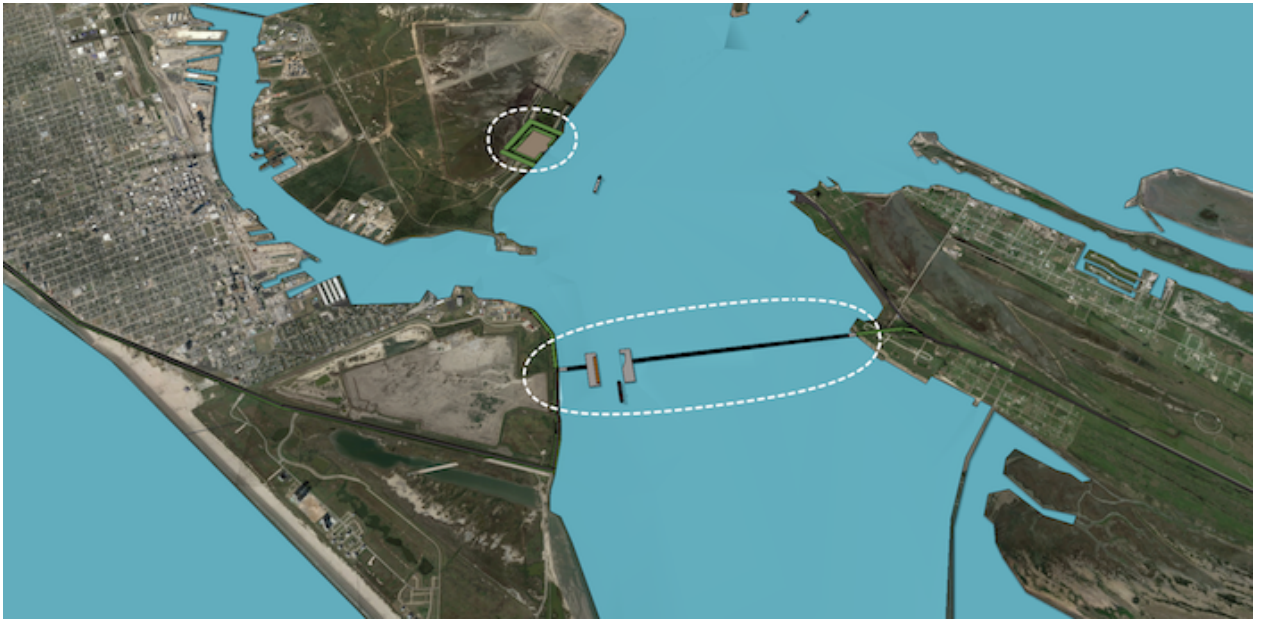


Figure 9.9: Overview barrier in Bolivar Roads and dry dock on Pelican Island. Satellite image: Google Earth (2013).

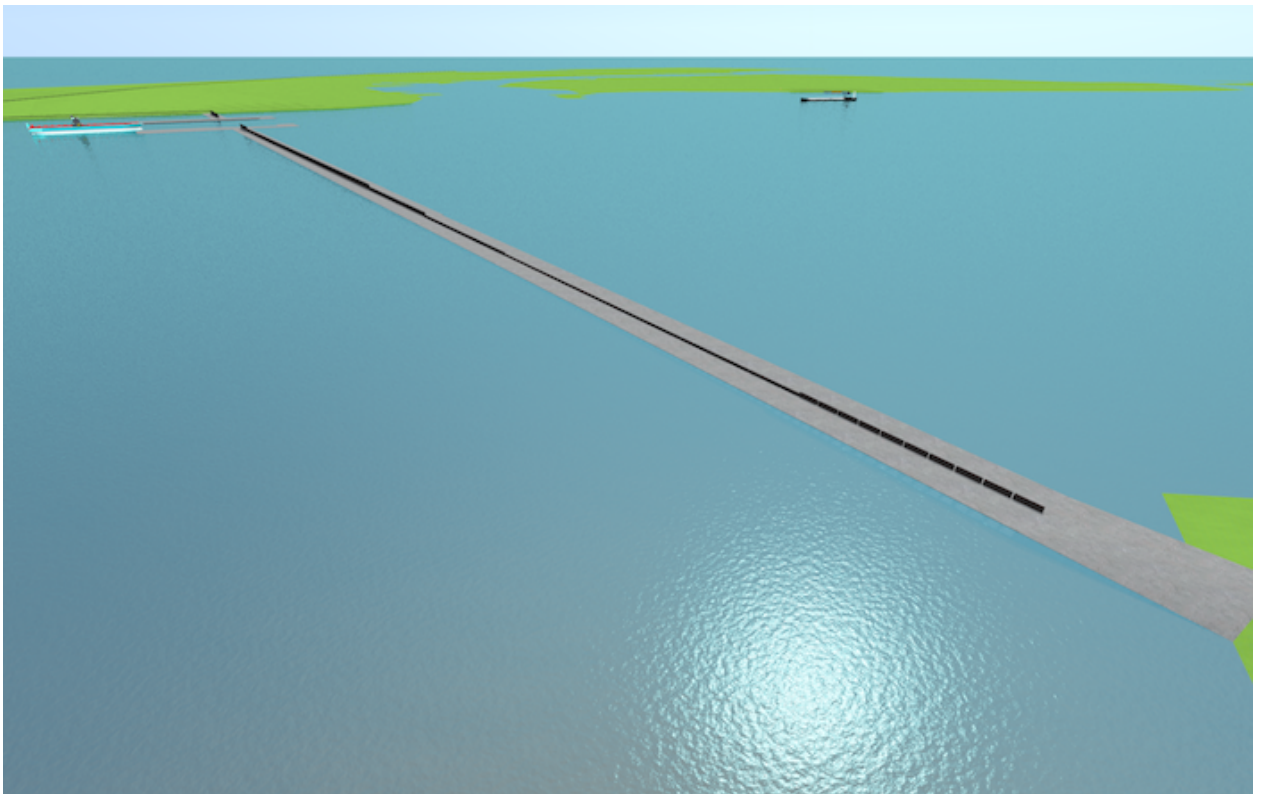


Figure 9.10: Storm surge barrier in opened position. Birds eye view from Bolivar Peninsula.

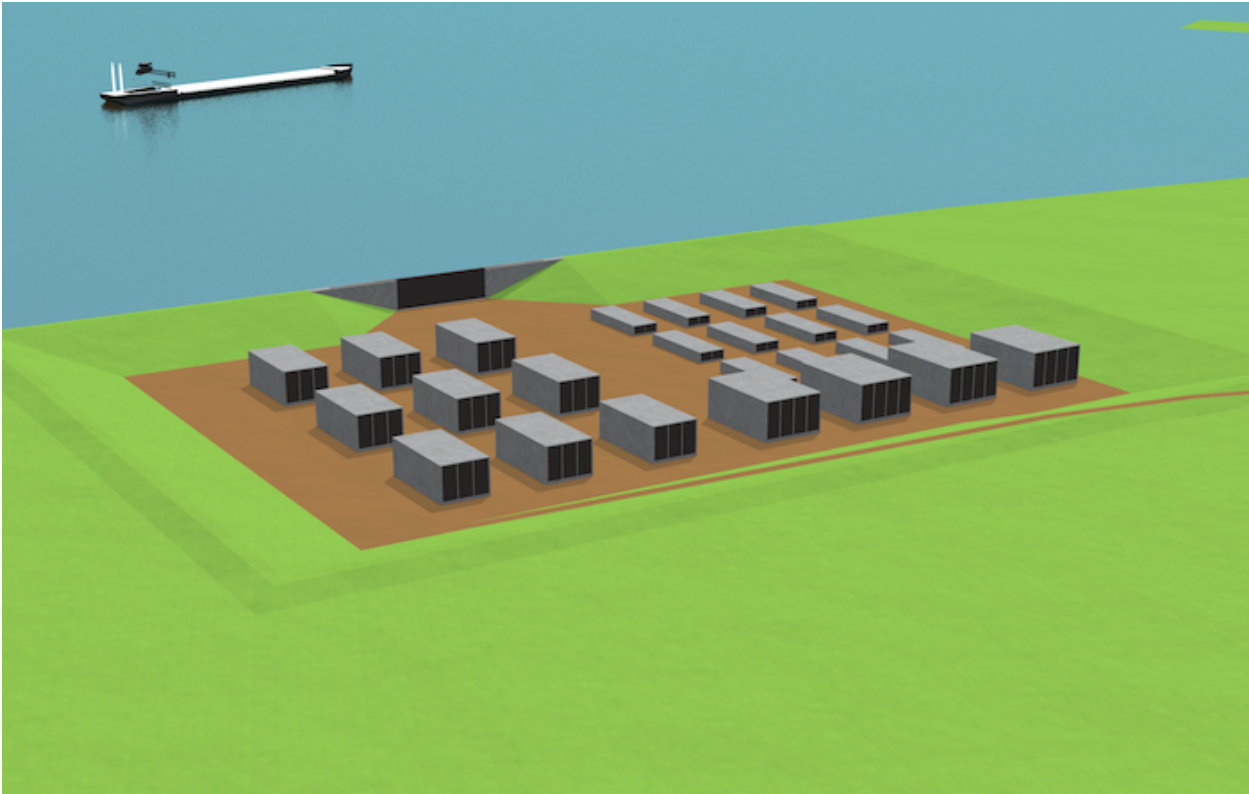


Figure 9.11: Caissons under construction in dry dock on Pelican Island.

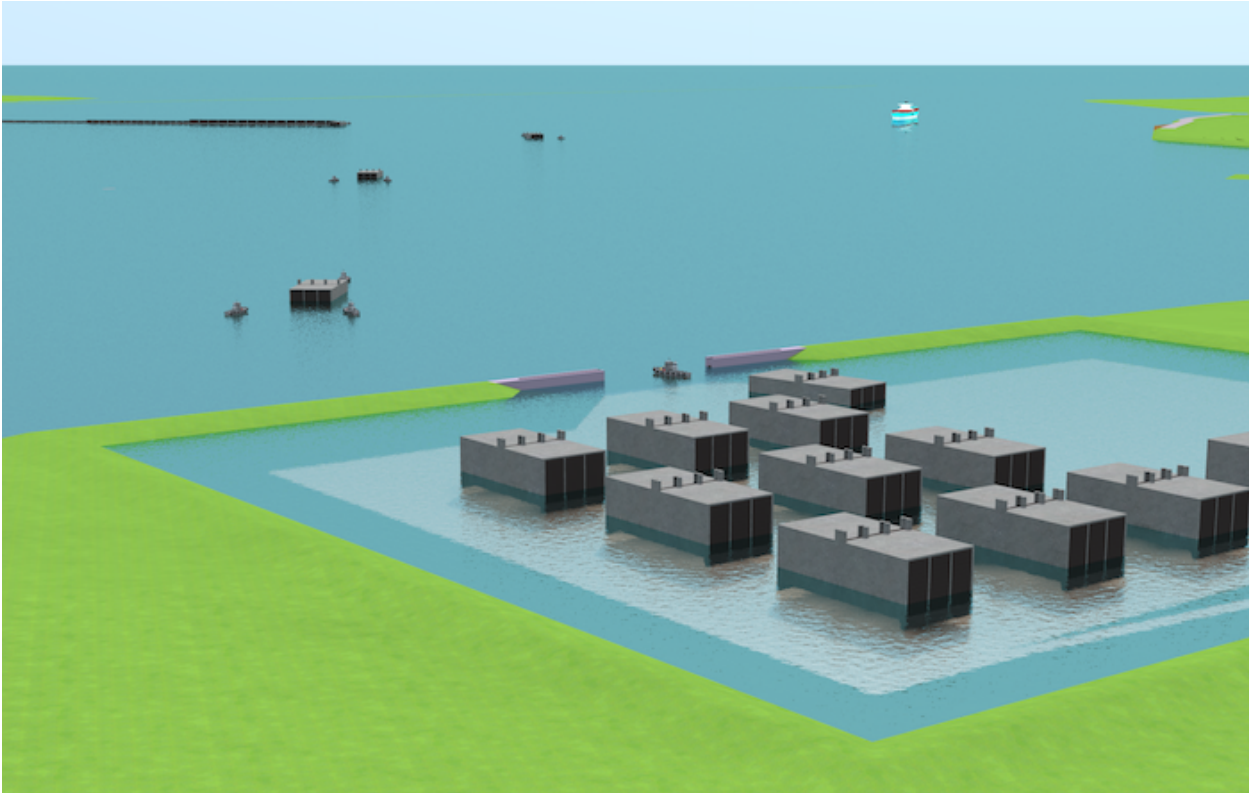


Figure 9.12: Step 4.2 – Towing of caissons out of the dry dock towards the HSC.

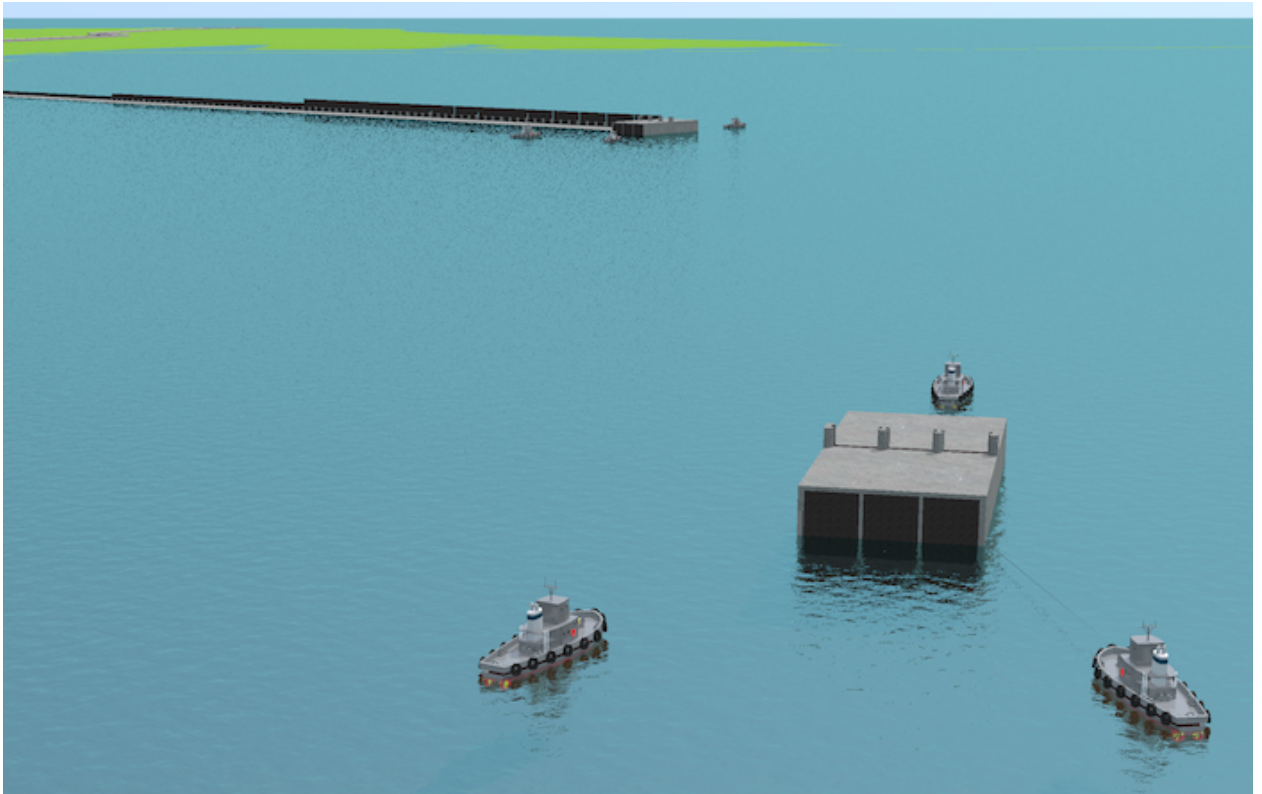


Figure 9.13: Step 4.3 – Towing of caissons over the HSC towards the final location.

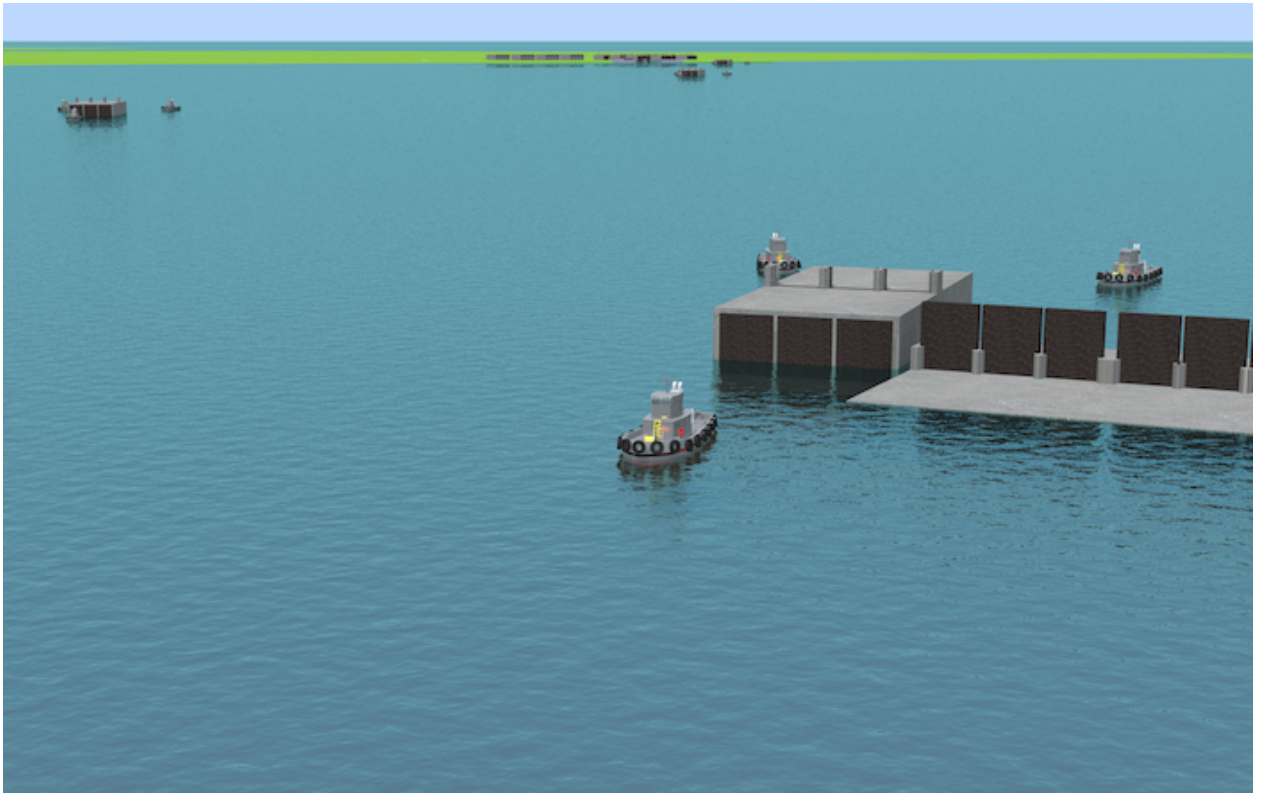


Figure 9.14: Step 4.5 – Placement of caissons at the final location. See also Figures 9.7 and 9.8.

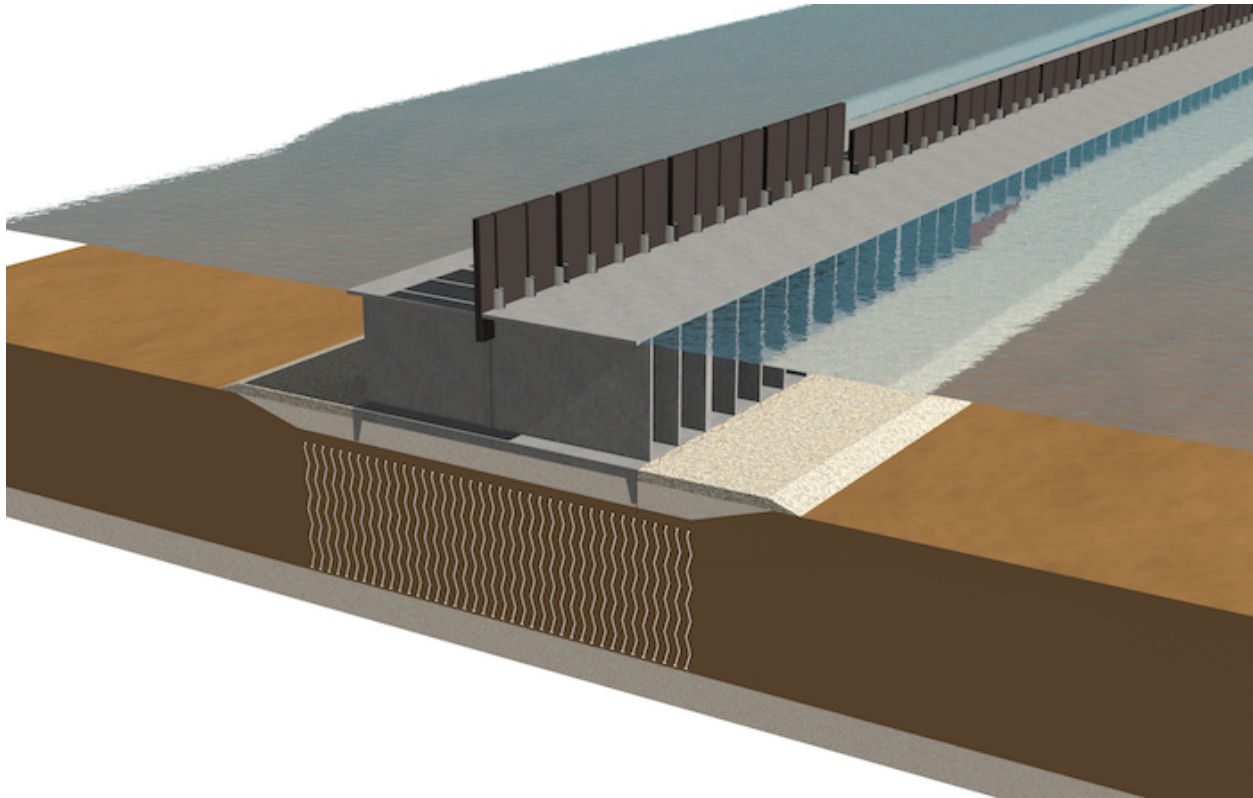


Figure 9.15: Caisson barrier environmental section in opened position with vacuum preloading soil improvement (section BB', see Table 8.2 for dimensions).

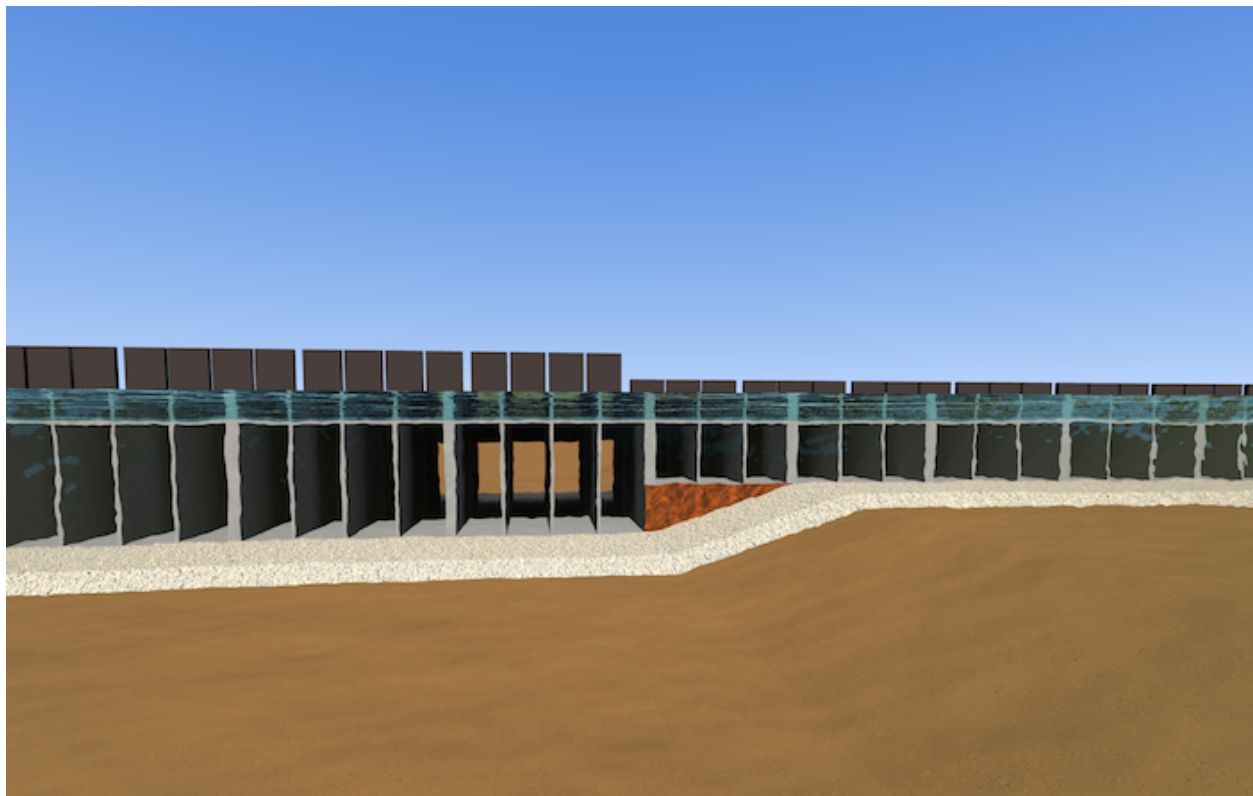


Figure 9.16: Underwater front view of transition between caisson barrier sections BB' and CC'.

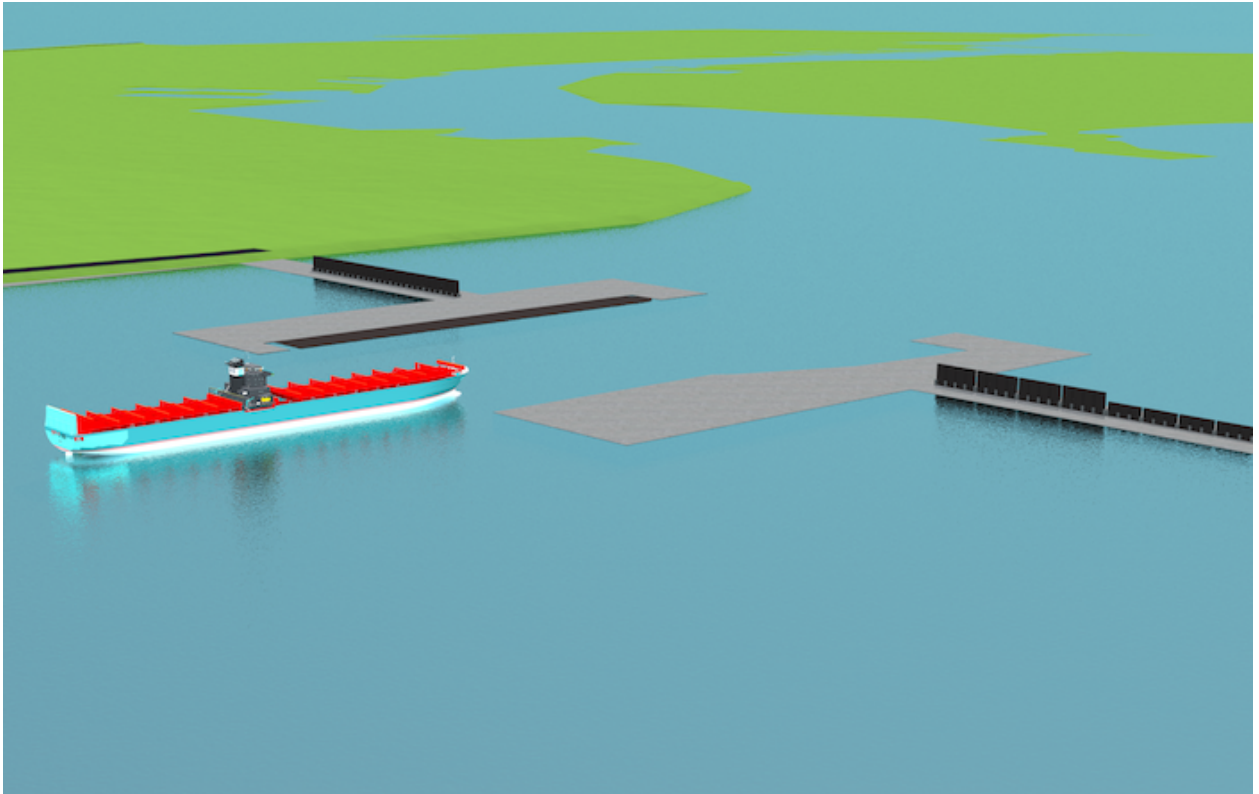


Figure 9.17: Navigational section.

Notes: the navigational barrier is indicated as a barge gate in these drawings. The design of this barrier is not treated in this thesis. In the drawings the caissons are equipped with door slots. The design of these slots is also not treated in this thesis.

9.7 Conclusions & recommendations

In this chapter a construction method is presented for a caisson barrier using the vacuum preloading foundation method. It is given for this vacuum preloading as time is short to do the recommended reassessment of barrier types on the environmental barrier design level. The method shows the consecutive activities up until the completion of the structure, together with a cost estimate. It is possible to construct a technically feasible storm surge barrier in Bolivar Roads which is priced approximately \$1.9 billion. This concerns a crude cost estimate, for a more accurate cost estimate it is recommended to further investigate the cost rates for each activity.

In this construction method the caissons will be constructed in a dry dock on Pelican Island. This does not necessarily have to be the best way of approach; alternatively the caissons can also be constructed in the dry using cofferdams on the final location. These other alternatives are not considered. For an optimal design also the building dock should be the result of an evaluation of different alternatives. This evaluation, in turn, is linked again to the optimal barrier type. The integral character of this interaction between construction dock and barrier type is not considered in this thesis, but could be interesting for further research.

The series of activities that need to be executed regarding the vacuum preloading method are a suggestion. It is not sure whether this is the way to go. For example the driving of steel mandrels from a floating pontoon might not be ideal. More issues can be expected regarding unequal soil consolidation due to uneven pumping. These aspects further emphasize that applying a deep foundation is a better and easier way to go for a storm surge barrier

foundation than vacuum preloading.

10 Final conclusions & recommendations

The main conclusions and recommendations of this thesis are listed in this chapter as well as a reflection on the applied methodology. Refer to the last section of each chapter for more detailed conclusions and recommendations that cover specific parts of the design process.

10.1 Conclusions

The main research question of this thesis is:

What is a technically feasible design for a storm surge barrier in Bolivar Roads Pass?

Using the global-to-detailed design methodology a technically feasible design is presented. First a design framework consisting of requirements and boundary conditions is drafted. The first design step on barrier system level investigates the optimal barrier location and the barrier's required retaining height. Subsequently a preliminary design for the environmental barrier is drafted in design step two. The governing design aspect that came up during this design step, namely the foundation, is detailed in the third and final design step. The most important conclusions while working towards the final barrier design are listed as:

- **The barrier can be constructed as a reduction barrier, it does not have to be fully retaining.** In the first design step a barrier with a continuous retaining height of MSL+0.1 m [3.3 ft] along the entire barrier span appears to sufficiently reduce the surge with a probability of occurrence of $1/10,000 \text{ yr}^{-1}$. With this retaining height along both the navigational and environmental section the barrier is vastly overflowed during storms, but the Bay's retention capacity ensures the flood hazard along the Galveston Bay to remain acceptable.
- **A caisson barrier is the best alternative for environmental section.** In the second design step the caisson alternative fulfills the drafted design criteria for the environmental section best. This caisson barrier decreases the flow area at Bolivar Roads down to 68%, which is more than the minimum required 60%.
- **A shallow foundation with vertical drainage as soil improvement is the best foundation alternative for a caisson barrier.** Problems arise when the caisson barrier as it is designed in design step 2 is placed on its final location: considerable settlements occur due to the barrier weight. The third design step investigates four measures to deal with the poor soil conditions. Despite its debatable effectiveness under water the soil improvement using vertical drainage is preferred. Quicker consolidation is possible through vacuum preloading; the consolidation duration is accelerated to 46 days opposed to 648 days for vertical drainage. This method, however, is costlier and has not yet been applied as a soft soil improvement for a shallow founded storm surge barrier before. Alternatively, it is advised to take a few steps back in the design process and reassess different barrier types knowing the issues around the problematic soil conditions. Applying another barrier type than a caisson barrier with a deep foundation is likely to become more appropriate foundation for Bolivar Roads, see 'Reflection on methodology' below. Complete replacement of the weak clay layers with sand is the least favorable alternative due to its high costs and under water compaction issues.
- **The total costs complete storm surge barrier are estimated at \$2.7–\$4.0 billion.** The report describes the construction method for a caisson barrier with vacuum preloading soil improvement. Despite the fact that its costs are higher than for vertical drainage the application of this method is further investigated because it has not yet been applied as a soil improvement measure for a shallow founded storm surge barrier before. The construction method shows the consecutive activities up until the completion of the structure, together with a cost estimate. For an amount ranging from \$2.7 to \$4.0 billion it is possible to construct a technically feasible storm surge barrier in Bolivar Roads. This includes both the navigational and environmental sections.

In this thesis the goal is to find a cost-effective barrier that sufficiently reduces the surge. The calculated total costs as stated above apply for a barrier with retaining height at MSL+0.1 m [0.3 ft]. However, such a reductive barrier might give a feeling of being unprotected to the people living in the hinterlying area. Under social pressure the decision can be made to construct a barrier with a higher retaining height. For example a crest level at MSL+2.0 m [6.6 ft] results in a barrier that always protrudes above the water surface in regular conditions⁽¹⁾. The estimated total costs for such a barrier are estimated to increase up to \$3.4–\$5.0 billion⁽²⁾.

10.2 Reflection on methodology

As stated above several options were available to deal with the weak soil conditions. The client's risk profile and his preferences determine which foundation alternative is chosen. If the decision would be to continue the caisson barrier design it is recommended to apply vertical drainage as it is the least costly. Alternatively, it is recommended to go back to the barrier type evaluation in design step 2 and reassess different barrier types while taking into account that a deep foundation is likely to be more appropriate for Bolivar Roads. Such a deep foundation however, goes beyond the advantages of the load-spreading character of a caisson barrier because all the loads will be transferred down to a bearing soil layer. Hereby other barrier alternatives than a caisson barrier come into the picture again. For example a wide-footed T-wall construction with a vertical lifting gate hanging in two concrete slots founded on steel tubular pile foundation piles might emerge as one of the alternatives in this reassessment.

This provided an important insight: the drafted design criteria in the second design step (environmental barrier design level; Section 7.1), on which the choice for a caisson barrier was based, were unbalanced. There should have been more emphasis on the foundation. This shows that decisions made in an earlier design stage can change the remainder of the design path drastically. It could even result in completely distinct barrier designs that all satisfy the requirements and boundary conditions. This makes designing a large civil engineering structure such as a storm surge barrier is a highly integrated process in which some design steps need to be carried out over and over again. Even while the outcome of a design step seems plausible, further insight could lead to reconsideration of design steps that were assumed to be finished.

10.3 Recommendations

The recommendations are divided into two categories. The first category discusses design specific recommendations for the storm surge barrier. Subsequently suggested design aspects that are not taken into account in this thesis are listed intending to give a start for further research into the caisson barrier.

10.3.1 Design specific recommendations

Design specific recommendations for the storm surge barrier design are listed below.

- **Geotechnics.** Most important design aspect appeared to concern the problematic soil conditions in Bolivar Roads. Accurate soil information is unavailable. In this thesis information from boring logs on Galveston Island is assumed to be representative for the entire soil stratum along Bolivar Roads. This soil profile generalization introduces uncertainties. More borings and lab test results of multiple locations in Bolivar Roads might give a better insight in the soil behavior under the loads caused by a storm surge barrier along the entire barrier span. Moreover, detailed information about the the location of strong, load-bearing soil layers

⁽¹⁾ the barrier at MSL+0.1 m [3.3 ft] is submerged during each high tide

⁽²⁾ A crude estimate for the cost increase is calculated using the formula by van der Toorn (2012), see Equation (6.1). For this barrier the average construction height increases from 9.5 m [31.2 ft] to 11.5 m [37.7 ft]. The cost increase for this higher retaining height is estimated around 25%.

may provide an optimal, cost-effective barrier alignment that is different from the barrier location presented in this thesis.

- **Hydraulics.**

- The volume of water that flows over a barrier in Bolivar Roads may induce at most a 1.4 m [4.6 ft] rise of the water level inside the Galveston Bay. This calculation is based on assumptions and the wind setup is calculated using a very simplified model. In order to determine an accurate amount of overflow it is strongly recommended to perform a 3D calculation to investigate the surge levels due to wind setup in the Bay. Besides an economical study into the damage to the buildings and industrial facilities is recommended to determine the maximum allowed surge levels in the Bay.
- Hurricane Ike's forerunner surge caused a lot of water flowing in the Galveston Bay before the real storm hit. This very adverse aspect of hurricane surge is hard to express in terms of return period. Therefore in this thesis the adopted course of the design water level is drafted by manually combining extrapolated Hurricane Ike data with an estimated $1/10,000 \text{ yr}^{-1}$ peak surge height. Though this results in a conservative storm surge, further research is recommended in distinct $1/10,000 \text{ yr}^{-1}$ storm characters to obtain more accurate governing surge levels.
- For the barrier a Sea Level Rise of 1.0 m [3.3 ft] for the next 100 years is assumed. This number is based on diverse estimates from different sources. It can be concluded that estimating SLR accurately is hard to do. A rather high uncertainty lies in these SLR estimates, so it is recommended to further investigate future SLR.

- **Environmental.** To maintain sufficient water exchange between the Gulf of Mexico and the Galveston Bay a maximum decrease in inflow area in Bolivar Roads is set. The inflow area at Bolivar Roads may decrease at most to 60% of its original size. As this number determines a lot for the barrier design further research in the effects of a reduction in inflow area in Bolivar Roads is needed.

- **Safety level.** According to Stoeten (2013) the storm surge barrier reaches the highest cost-benefit ratio when designed to protect against surge levels with a probability of occurrence of $1/10,000 \text{ yr}^{-1}$. As this is based on a flood risk assessment with limited accuracy a more thorough cost benefit analysis should be executed in which wind damage and inundation damage are assessed separately.

- **Probabilistic design.** All of the formulas presented in this thesis are deterministic formulas. By identifying probabilistic distributions for design parameters the decisions taken in the design process can be done based on economic considerations resulting in a more cost-effective design. For example using probabilistic parameters the settlement magnitudes of the caisson barrier can be expressed in terms of probability of occurrence. The choice for an expensive, higher quality measure to counteract the settlements can subsequently be based on this likelihood. In this thesis this probabilistic design strategy is omitted, but for a cost-effective design based on economic considerations it is recommended to do so.

10.3.2 Suggested research topics

Suggested research topics for further detailing the caisson barrier design are listed below.

- **Door type.** According to calculations for the total caisson construction costs the doors appear to be a dominant cost item (see Tables G.7, G.10 and G.15). In this design the caisson barriers are equipped with vertical lifting gates, for further research it is recommended to determine the optimal door type by assessing different door alternatives. Examples of applicable door types for the caisson barrier could be:
 - Flap doors, similar to the MOSE project doors (Appendix B.4)
 - 'Vertical butterfly valve door', see Figure 10.1
 - 'Horizontal butterfly valve door', similar to Figure 10.1 but rotating around the horizontal axis
 - Radial doors (Appendix B.2)

- Mitre doors (Appendix B.1)

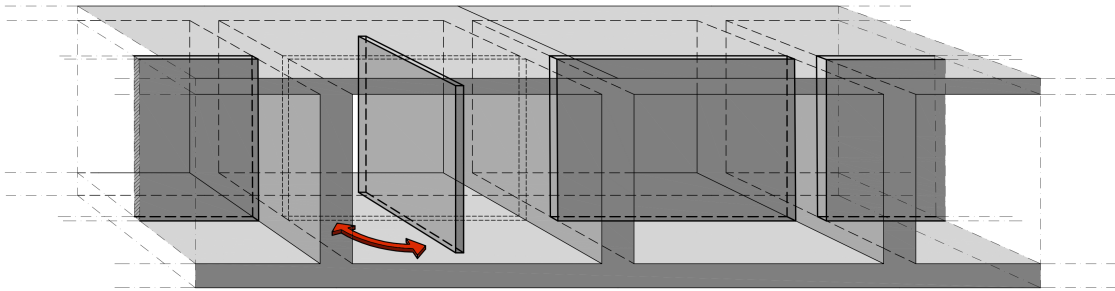


Figure 10.1: Schematic birds eye view of the 'vertical butterfly valve door' for the caisson barrier.

Design considerations in selecting the optimal barrier door could concern the door operability and the slots through which the doors slide in their closing position. Also the maintainability and structural lifetime are important assessment criteria.

- **Adaptability to uncertain Sea Level Rise.** The barrier will initially be designed for a water levels including 1 m [3.3 ft] SLR after a 100 years from now. After that time period it should be possible to increase the retaining height to respond flexibly to uncertain future Sea Level Rise up until a lifetime of 200 years. In case of a caisson barrier this could be done by constructing a vertical concrete wall on top of the caissons that are connected by the existing structure through rebars that protrude out of the caisson structure. An alternative way to increase the caisson barrier's retaining height is to construct a small levee on top of the caissons with a decent bed protection. For further research both these options could be alternatives, but there are probably more ways to do so. It applies to all that one should bear in mind that the foundation needs to be dimensioned beforehand that it is able to transfer the additional forces.
- **Bed protection.** Flow induced scour holes could threaten the stability of the barrier. A complete storm surge barrier design contains an approach for a bed protection to prevent these scour holes and includes a strategy to maintain it.
- **Optimize caisson walls and slabs.** Currently the caissons are just quickly dimensioned using rules of thumb. After the second design step the accuracy of wall and slab strength calculations has not increased. Whilst a detailed design for the foundation is presented the level the caisson dimensions remained the same. For further research it is recommended to check in detail whether the walls and slabs are able to bear the occurring loads, also due to second order effects. A reinforcement plan, with or without prestressing, should be drafted, possibly by using FEM software.

Another aspect named in Section 7.5.1 that could be interesting for further research is the optimization and streamlining of caisson walls. More streamlined caisson walls mean less obstruction of tidal flow between the Gulf of Mexico and the Galveston Bay. Part of the wall design could also include the barrier door slots, as the space for these slots decreases the flow area through the caissons.

- **Failure mechanisms and reliability.** Soil failure mechanisms and to a lesser extent also structural failure are taken into account in the design process. Next to these also human, computer and mechanical failure are aspects that could affect the barrier's reliability. Research in these failure aspects is needed for a complete barrier design.

In the requirements for the barrier was stated that if one or more barrier doors fail to close, the barrier must still sufficiently block the surge. The retaining height of the barrier must be increased to compensate for

such failure. This reliability issue has not been addressed in this thesis, but should be taken into account in further design. The same applies to the reliability of reopening the barrier after a closure regarding water circulation impediment.

- **Maintenance.** During the operational phase the barrier has to be inspected and maintained. Research into the possibility of applying probabilistic management and maintenance; a principle that links failure probability to the way management and maintenance are executed. Investigating in this could reduce operational costs of the barrier.
- **Construction dock.** In the construction method the caissons are constructed in a dry dock on Pelican Island. This does not necessarily have to be the best way of approach; alternatively the caissons can also be constructed in the dry using cofferdams on the final location. These other alternatives are not considered. For an optimal design also the construction dock should be the result of an evaluation of different alternatives. This evaluation, in turn, is linked again to the optimal barrier type. The integral character of this interaction between construction dock and barrier type is not considered in this thesis, but could be interesting for further research.

References

- Abebe, A. and Smith, I. G. N. (1994). Pile Foundation Design: A Student Guide. *School of the Built Environment, Napier University, Edinburgh.*
- Adey, M. (2013). Proposed Ike Dike Project in Galveston, Texas. *Coastal and Ocean Engineering Undergraduate Student Forum, COASTAL-2013. Faculty of Engineering and Applied Science, Memorial University, St. John's, NL, Canada.*
- Aerolin Photo BV (2007). Luchtfoto Maeslantkering bij hoogwater 10 november 2007.
<http://www.knmi.nl/cms/viewimage.jsp?number=60653>, retrieved 31-5-2013.
- API (2000). Recommended Practice for Planning, Designing and Constructing Fixed Offshore Platforms - Working Stress Design: API Recommended Practice 2A-WSD (RP 2A-WSD). *American Petroleum Institute.*
- Bear, J. (1972). Dynamics of fluids in porous media. *Dover Publications.*
- Bedient, P. B. and Penland, C. M. (2013). The SSPEED Center Presentation to TU Delft. Powerpoint Presentation.
- Benitez, M. E. (2009). Dimensions for future lock chambers and 'New Panamax' vessels.
- Berg, R. (2009). Hurricane Ike. *Tropical Cyclone Report.*
- Bing Maps (2013). Bolivar Roads satellite image.
<http://www.bing.com/maps/>, retrieved 21-5-2013.
- Bjerrum, L. (1967). Progressive failure in slopes of overconsolidated plastic clay and clay shales. *Journal of Soil Mechanics & Foundations.*
- Bosboom, J. and Stive, M. J. (2012). Lecture notes CIE4305: Coastal Dynamics I.
- Braam, C. R. (2011). Information for cost comparison and estimate. *Case study CIE4170: fresh water production unit.*
- Brinch Hansen, J. (1970). A revised and extended formula for bearing capacity. *Danish Geotechnical Institute, Copenhagen, (28):5-11.*
- BUG (1990). The Houston Ship Channel: A History.
<http://www.betterbay.org/html/releases/HoustonShipChannelHistory.htm/>, retrieved 17-5-2013.
- Calkins, L. B. (2010). Texas Proposes \$10 billion 'Ike Dike' for Storm-Surge Shield.
<http://www.bloomberg.com/apps/news?pid=newsarchive&sid=am6OBaGxFtws>, retrieved 30-7-2013.
- Casselmann, B. (2009). Planning the 'Ike Dike' defense.
<http://online.wsj.com/article/SB124407051124382899.html>, retrieved 07-5-2013.
- Census (2012). Census estimates show new patterns of growth nationwide.
<http://www.census.gov/newsroom/releases/archives/population/cb12-55.html>, retrieved 03-5-2013.
- Chai, J., Miura, N., Nomura, N., and Yoneya, H. (2003). Vacuum consolidation of soft clayey subsoil using cap-drain. *Proceedings of 18th geosynthetics symposium, vol. 18, Japan Branch. International Geosynthetics Society, pages 231-236.*
- Chu, J., Yan, S., and Indraratna, B. (2008). Vacuum Preloading Techniques - Recent Developments and Applications. *ASCE, pages 586-595.*
- Costa, A. and Appleton, J. (1999). Chloride penetration into concrete in marine environment - Part I: Main parameters affecting chloride penetration. *Materials and Structures, 32:252-259.*
- Cox, C., Davis, J., Hennigan, S., and Robichaux, L. (2013). Bolivar Roads Sector Gates. *Capstone Class Project, Texas A&M University at Galveston, LCSJ Coastal Engineering.*
- Cushman, T. (2009). Scientists Puzzle Over Hurricane Ike's "Forerunner" Wave.
<http://www.jlconline.com/coastal-contractor/scientists-puzzle-over-hurricane-ikes-forerunner.aspx>, retrieved 30-7-2013.
- Dam, L. T., Sandanbata, I., and Kimura, M. (2006). Vacuum Consolidation Method - Worldwide Practice and the Latest Improvement in Japan.
- Davis, Z., Flores, K., Szempruch, P., and Thomas, J. (2010). Design of the Galveston Bay Storm Surge Protection

- Barrier. *Capstone Class Project, Texas A&M University at Galveston.*
- de Boom, L. (2013). Reduction Barrier Western Scheldt. *Masters Thesis; TU Delft.*
- de Kort, R. (2013). Sketches Texas Barrier. *Workshop Texas Barrier TU Delft 20-6-2013.*
- de Rooij, M. R., Polder, R. B., de Vries, J., and Gulikers, J. (2003). Chloride ingress in a marine concrete structure after 20 years in a North Sea environment.
- de Vries, P. A. L., Lavies, H. G., and Moen, J. C. (2012). Fresh water production unit. *Case study CIE4170: fresh water production unit.*
- Dircke, P., Jongeling, T., and Jansen, P. (2009). Global Overview of Navigable Storm Surge Barriers from a Dutch Perspective. *ASCE Met Section Infrastructure Group Seminar 2009.*
- Dircke, P. T. M., Jongeling, T. H. G., and Jansen, P. L. M. (2012). An overview and comparison of navigable storm surge barriers.
- Economic Commission for Europe (1965). Effects of Repetition on Building Operations and Processes on Site, Report of an enquiry undertaken by the Committee on Housing, Building and Planning. *ST/ECE/HOU/14, New York: United Nations.*
- Emanuel, K. and Jagger, T. (2010). On Estimating Hurricane Return Periods. *Journal of Applied Meteorology and Climatology*, 49:837–844.
- Environment Agency (2012). Thames Barrier Project pack. *Environment Agency.*
- Erbisti, P. C. F. (2004). Design of hydraulic gates.
- FindTheData.org (2013). Data Galveston-Port Bolivar Ferry Service.
<http://ferry-service.findthedata.org/1/242/Galveston-TX-Port-Bolivar-TX/>, retrieved 21-5-2013.
- Freudenrich, C. (2013). How Barrier Islands Work.
<http://science.howstuffworks.com/environmental/conservation/issues/barrier-island.htm>, retrieved 19-5-2013.
- FRP & Composite Technology Resource Centre (2012). Definition of fibre reinforced composite.
<http://www.fibre-reinforced-plastic.com/2008/12/definition-of-fibre-reinforced.html>, retrieved 07-5-2013.
- Fuji, A., Tanaka, H., Tsuruya, H., and Shinsha, H. (2002). Field test on vacuum consolidation method by expecting upper clay layer as sealingup material. *Proceedings of the Symposium on Recent Development about Clayey Deposit - From Microstructure to Soft Ground Improvement*, pages 269–274.
- Galveston Bay Status and Trends (2013). Oyster Reefs in Galveston Bay.
<http://galvbaydata.org/Habitat/OysterReefs/tabid/836/Default.aspx/>, retrieved 28-5-2013.
- Galveston.com (2013a). Galveston Island ferry.
<http://www.galveston.com/history/>, retrieved 21-5-2013.
- Galveston.com (2013b). Galveston Island history.
<http://www.galveston.com/history/>, retrieved 02-5-2013.
- Goda, Y. (1985). Random seas and design of maritime structures. *University of Tokyo Press: Tokyo.*
- Google Earth (2013). Bolivar Roads satellite image.
- Groeneveld, R. (2002). Inland Waterways: Ports, Waterways and Inland Navigation. *Lecture Notes CT4330.*
- Haby, M. G., Miget, R. J., and Falconer, L. L. (2009). Hurricane Damage Sustained by the Oyster Industry and the Oyster Reefs Across the Galveston Bay System with Recovery Recommendations. College Station, TX. *TAMU-SG-09-201.: The Texas A&M University System.*
- Handbook of Texas Online (2013). Bolivar Roads.
<http://www.tshaonline.org/handbook/online/articles/rrb08>, retrieved 17-5-2013.
- HGNSAC (2011). Navigating the Houston Ship Channel. *Houston-Galveston Navigation Safety Advisory Committee.*
- Hill, D. (2013). Storm Surge Barriers to Protect New York City: Against the Deluge. *ASCE Publications.*
- Hodgin, B. (2007). Bay Area Houston: Overview. *Bay Area Houston Economic Partnership.*
- Holcombe, T. L., Holcombe, L. H., and Bryant, W. R. (2006). Bathymetry of Bolivar Roads. *Bathymetry of the Northwest Gulf of Mexico Continental Shelf, surveyed 2004-2006.*
- Hussin, J. D. (2006a). The Foundation Engineering Handbook, Edited by Manjriker Gunaratne. Chapter 12: Meth-

- ods of Soft Ground Improvement. *Taylor & Francis Group, LLC*.
- Hussin, J. D. (2006b). The Foundation Engineering Handbook, Edited by Manjriker Gunaratne. Chapter 6: Design of Driven Piles and Pile Groups. *Taylor & Francis Group, LLC*.
- I-Storm (2013). Storm Surge Barriers.
<http://www.i-storm.org/international/storm-surge-barriers/>, retrieved 01-5-2013.
- INC-WG26 (2006). Design of Movable Weirs and Storm Surge Barriers. *PIANC Inland Navigation Commission. Working Group 26 and International Navigation Association*.
- Institute for Business & Home Safety (2009). Hurricane Ike: Nature's Force vs. Structural Strength.
- Jin, J., Jeong, C., Chang, K.-A., Song, Y. K., Irish, J., and Edge, B. (2010a). Site Specific Wave Parameters for Texas Coastal Bridges: Final Report. *Table 8*, page 61.
- Jin, J., Jeong, C., Chang, K.-A., Song, Y. K., Irish, J., and Edge, B. (2010b). Site Specific Wave Parameters for Texas Coastal Bridges: Final Report. *Table 12*, page 67.
- Kennedy, A. B., Gravois, U., Zachry, B. C., Westerink, J. J., Hope, M. E., Dietrich, J. C., Powell, M. D., Cox, A. T., Luettich, R. A., and Dean, R. G. (2011). Origin of the Hurricane Ike forerunner surge. *Geophysical Research Letters*, 38(8).
- Kjellman, W. (1952). Consolidation of clay by mean of atmospheric pressure. *Massachusetts Institute of Technology: Conference on soil stabilization*, 5:32–34.
- Knippels, A. and Pechtold, E. (1992). Project Keersluis Heusdensch Kanaal.
- Kok, L. R. (2013). Feasibility study for FRP in large hydraulic structures. *Masters Thesis; TU Delft*.
- Koppejan, A. W. (1948). A formula combining the Terzaghi load compression relationship and the Buisman secular time effect. *Proc. 2nd Int. Conf. Soil Mech. And Found. Eng.* 3:32–38.
- Labeur, R. J. (2007). Open Channel Flow. *Lecture Notes CT3310*.
- Lane, E. W. (1934). Security from Under-Seepage: Masonry Dams on Earth Foundations.
- Lansen, J. and Kluyver, M. (2006). Cress Definition CIRIA. *Royal Haskoning*.
- Leatherwood, A. (2013a). Galveston Bay.
<http://www.tshaonline.org/handbook/online/articles/rrg01>, retrieved 19-5-2013.
- Leatherwood, A. (2013b). Gulf Intracoastal Waterway.
<http://www.tshaonline.org/handbook/online/articles/rrg04>, retrieved 19-5-2013.
- Lester, J. and Gonzalez, L. (2002). The State of the Bay: A Characterization of the Galveston Bay Ecosystem. *The Galveston Bay Estuary Program*.
- Ligteringen, H. (2009). Lecture Notes CIE4330 and CIE5306: Ports and Terminals. pages 5–20.
- Lin, Z. (2001). Sediment Transport. *Laboratoriet for Hydraulik og Havnebygning Instituttet for Vand, Jord og Miljøteknik*.
- Maritime Journal (2002). Thames Barrier.
http://www.maritimejournal.com/_data/assets/image/0010/155971/mj20020901_21.jpg, retrieved 03-6-2013.
- McClelland Engineers (1985). Reconnaissance Study U.S. Navy Home Port Galveston, Texas. *Report to Navel Facilities Engineering Command, Charleston, South Carolina*.
- Merrell, W. J. (2010a). Hurricane Ike path, Ike Dike and Bolivar Roads.
<http://houstonstrategies.blogspot.nl/2009/06/ws-j-on-ike-dike.html>, retrieved 16-5-2013.
- Merrell, W. J. (2010b). Ike Dike: A coastal barrier protecting the Houston/Galveston region from hurricane storm surge. Powerpoint Presentation.
<http://www.tamug.edu/ikedike/Presentations.html>, retrieved 17-5-2013.
- Merrell, W. J. (2012). Ike Dike: A coastal barrier protecting the Houston/Galveston region from hurricane storm surge. Powerpoint Presentation.
<http://www.tamug.edu/ikedike/Presentations.html>, retrieved 17-5-2013.
- Merrell, W. J., Reynolds, L., Cardenas, A., Gunn, J. R., and Hufton, A. J. (2011). The Ike Dike: a coastal barrier protecting the Houston/Galveston region from Hurricane storm surge. *Macro-engineering Seawater in Unique*

- Environments*, pages 691–716.
- Meyerhof, G. G. (1953). The bearing capacity of foundations under eccentric and inclined loads. *Proc. 3rd Int. Conf. Soil Mech. Zurich*, 1:440–45.
- Ministerie van Infrastructuur en Milieu (2009). Wet op de Waterkering.
http://wetten.overheid.nl/BWBR0007801/geldigheidsdatum_21-12-2009, retrieved 03-6-2013.
- National Geographic (2013). Encyclopedic Entry: Bayou.
http://education.nationalgeographic.com/education/encyclopedia/bayou/?ar_a=1, retrieved 19-5-2013.
- Needham, H. F. and Keim, B. D. (2012). A storm surge database for the US Gulf Coast. *International Journal of Climatology*, 32(14):2108–2123.
- NFEC (1986). Foundations & Earth Structures, Design Manual 7.02. *Naval Facilities Engineering Command*.
- Nienhuis, P. H. et al. (1982). De ecologische consequenties van de Deltawerken.
- NOAA-NGS (2013). National Geodetic Survey (NGS): Frequently Asked Questions.
<http://www.ngs.noaa.gov/faq.shtml#WhatVD29VD88>, retrieved 16-5-2013.
- NOAA-NHC (2012). Storm Surge Overview.
<http://www.nhc.noaa.gov/surge/>, retrieved 01-5-2013.
- NOAA Tides and Currents (2011). Tidal Datums.
http://tidesandcurrents.noaa.gov/datum_options.html, retrieved 12-7-2013.
- NOAA Tides and Currents (2013a). Mean Sea Level Trend Galveston Pleasure Pier.
http://www.tidesandcurrents.noaa.gov/sltrends/sltrends_station.shtml?stnid=8771510, retrieved 30-7-2013.
- NOAA Tides and Currents (2013b). NOAA Tide Predictions.
http://tidesandcurrents.noaa.gov/tide_predictions.shtml?gid=232, retrieved 01-7-2013.
- NOAA/US EPA (2009). US Sea Level Trends, 1900-2000.
<http://www.richardcotman.com/etnobofofin/2009/12/hot-air-cold-air-compressed-air/>, retrieved 30-7-2013.
- NWS Weather Forecast Office (2008a). Hurricane Ike Rainfall.
http://www.srh.noaa.gov/hgx/?n=projects_ike08_rainfall, retrieved 30-7-2013.
- NWS Weather Forecast Office (2008b). Storm Surge Estimates from Damage Surveys.
http://www.srh.noaa.gov/hgx/?n=projects_ike08_storm_surge_overview, retrieved 17-5-2013.
- NWS Weather Forecast Office (2013). Storm Surge Estimates from Damage Surveys.
<http://www.nws.noaa.gov/climate/xmacis.php?wfo=hgx>, retrieved 16-7-2013.
- Pachauri, R. K. (2008). Climate change 2007. synthesis report. contribution of working groups i, ii and iii to the fourth assessment report.
- Penta Ocean (2013). Vacuum consolidation method using cap-attached prefabricated vertical drains.
http://www.penta-ocean.co.jp/english//business/civil/vacuum_drain.html, retrieved 10-12-2013.
- Petitt, B. W. and Winslow, A. G. (1955). Geology and ground water resources of Galveston County, Texas. *Texas Board of Water Engineering Bulletin*, (5502):219.
- Philips, J. D. (2004). A Sediment Budget for Galveston Bay. *Department of Geography, University of Kentucky*.
- PIANC-IAPH (1997). Approach Channels, A Guide for Design. *Report of the joint working group II-30, PIANC-Bulletin*, (95).
- Powell, G. L., Brock, D. A., and Paternostro, C. (2005). Effects of Structures and Practices on the Circulation and Salinity Patterns of Galveston Bay, Texas. *Texas Water Development Board*.
- Prasuhn, A. L. and FitzSimons, N. (2002). ASCE History and Heritage Programs. *Journal of Professional Issues in Engineering Education and Practice*, 129(1):14–20.
- Reed, C. and Sanchez, A. (2010). Representation of Weir in the CMS. *CIRPwiki*.
- Rigo, P., Rodriguez, S., and Marchal, J. L. J. (1996). The Use of Floating Gates for Storm Surge Barriers. *Barrages: Engineering, Design & Environmental Impacts*, page 421.
- Rijkswaterstaat (2010). Basisdocumentatie Maeslantkering 1&2. *Rijkswaterstaat; Ministry of Transport, Public Works and Water Management, the Netherlands*.
- Riley, J. (2006). H-Texas: The City's Greatest Getaway.

- <http://web.archive.org/web/20071004204140/http://www.htexas.com/feature.cfm?Story=592>, retrieved 19-5-2013.
- Rövekamp, N. H. (1998). Storm Surge Barrier Ramspol. *Hollandsche Beton- en Waterbouw, Engineering Department, Gouda, The Netherlands*.
- Ruijs, M. (2011). The effects of the 'Ike Dike' barriers on Galveston Bay. *Masters Thesis; TU Delft, Texas A&M University at Galveston*.
- sakura.ne.jp (2005). Visor Gate.
<http://non-chan2.sakura.ne.jp/Okkiimono/Okkiimon/VisorGate/VisorGate.htm>, retrieved 10-6-2013.
- Schellnhuber, H. J., William, H., Olivia, S., Sophie, A., Dim, C., Katja, F., Maria, M., Otto Ilona, M., Mahé, P., Alexander, R., et al. (2012). Turn down the heat—why a 4 C warmer world must be avoided. *A Report for the World Bank by the Potsdam Institute for Climate Impact Research and Climate Analytics*.
- Schiller, A. R. (2011). The impact of a storm surge on business establishments in the Houston MSA. *Natural Hazards*, 56(1):331–346.
- Schott, T., Landsea, C., Hafele, G., Lorens, J., Taylor, A., Thurm, H., Ward, B., Willes, M., and Zaleski, W. (2012). The Saffir-Simpson Hurricane Wind Scale. *NOAA-NHC*.
- Sehgal, C. K. (1996). Design Guidelines for Spillway Gates. *Journal of Hydraulic Engineering*, 122(3).
- Siman, V. (2012). Picture of Eastern Scheldt Barrier.
<http://www.water-technology.net/projects/7644/images/148754/large/11-image.jpg>, retrieved 31-5-2013.
- Singapore Standard (2003). Code of practice for foundations. *Singapore Standard*, (4).
- Skempton, A. W. (1951). The Bearing Capacity of Clays. *Building Research Congress, 1951*.
- Smaal, A. C. and Nienhuis, P. H. (1992). The Eastern Scheldt (The Netherlands), from an estuary to a tidal bay: a review of responses at the ecosystem level. *Netherlands Journal of Sea Research*, 30:161–173.
- Smith, K. and Ward, R. (1998). Floods: Physical Processes and Human Impacts. *Wiley Chichester*.
- SSPEED Center (2011). SSPEED Center Phase I Report. Learning the Lessons of Hurricane Ike: Preparing for the Next Big One. *SSPEED Center*.
- SSPEED Center (2012). SSPEED Center: Houston Ship Channel Gate.
http://sspeed.rice.edu/sspeed/HSC_Gate.html, retrieved 15-5-2013.
- Stanton, R. (2013). Condemning land to close Rollover Pass. *Houston Chronicle*.
<http://www.houstonchronicle.com/>, retrieved 30-7-2013.
- Stewart, S. W. (2008). U.S. Offshore Extreme Wind Analysis Based on Hurricane Return Probabilities.
- Stoeten, K. J. (2012). Applying best practices from the Delta Works and New Orleans to Galveston Bay.
- Stoeten, K. J. (2013). Hurricane Surge Risk Reduction For Galveston Bay. *Masters Thesis; TU Delft*.
- TAMUG (2010). Ike Dike: A coastal barrier protecting the Houston/Galveston region from hurricane storm surge.
<http://www.tamug.edu/ikedike/>, retrieved 17-5-2013.
- Tappin, R. G. R., Dowling, P. J., and Clark, P. J. (1984). Design and model testing of the Thames Barrier gates. *The Structural Engineer*, 62A(4).
- Taube, M. G. (2008). Prefabricated Vertical Drains - The Squeeze Is On. *Geo-Strata—Geo Institute of ASCE*, 9(2):12–14.
- Tavenas, F., Jean, P., Leblond, P., and Leroueil, S. (1983). The permeability of natural soft clays. Part II: Permeability characteristics. *Canadian Geotechnical Journal*, 20(4):645–660.
- Taylor, L. A., Eakins, B. W., Cargignan, K. S., Warnken, R. R., Sazonova, T., and Schoolcraft, D. C. (2008a). Digital elevation model of Galveston, Texas: Procedures, Data sources and Analysis. *National Geophysical Data Center: Marine Geology and Geophysics Division*.
- Taylor, L. A., Eakins, B. W., Cargignan, K. S., Warnken, R. R., Sazonova, T., and Schoolcraft, D. C. (2008b). Digital elevation model of Galveston, Texas: Procedures, Data sources and Analysis.
<http://www.ngdc.noaa.gov/dem/squareCellGrid/download/403>, retrieved 01-8-2013.
- Terzaghi, K. (1943). Theoretical Soil Mechanics. *Publisher: J. Wiley, New York*.
- TGB (1990). NEN 6740 Geotechnics.

- TGB (2013). Eurocode 2: Design of concrete structures - Part 1-1: General rules and rules for buildings.
- therealgalveston.com (2013). Galveston Seawall under construction.
<http://www.therealgalveston.com/Seawall.html>, retrieved 07-5-2013.
- travelkernel.com (2013). Travel Kernel: Galveston Bay Field.
<http://travelkernel.com/galveston-bay-field/1147>, retrieved 19-5-2013.
- TxSed Mapping Viewer (2013). Texas GLO: TxSed Mapping Viewer.
<http://gisweb.glo.texas.gov/txsed/index.html>, retrieved 21-5-2013.
- ULMA Construction (2013). Image of self climbing formwork.
<http://www.ulmaconstruction.com/imagenes%20de%20productos/atr-encofrado-autotrepante-caract-5-en-amp.jpg>, retrieved 19-12-2013.
- USA Today (2005). Hurricane Alicia, 1983.
<http://usatoday30.usatoday.com/weather/hurricane/history/walicia.htm>, retrieved 07-5-2013.
- USACE (2011). Images of oyster growth on sector gates at Brazos River Floodgates Project, Freeport, TX.
- USACE, Waterborne Commerce Statistics Center (2011). Port Rankings by Cargo Tonnage.
- van der Horst, A. Q. C. (2011). Construction Technology of Civil Engineering Projects. *Lecture Notes CT4170*.
- van der Toorn, A. (2012). Cost index numbers storm surge barriers. *Excel sheet*.
- van der Toorn, A. and de Gijt, J. G. (2012). Lecture notes CT5313: Structures in Hydraulic Engineering.
- van der Ziel, F. (2009). Movable water barrier for the 21st century. *Masters Thesis; TU Delft*.
- Van Noortwijk, J. and Klatter, H. (1999). Optimal inspection decisions for the block mats of the eastern-scheldt barrier. *Reliability Engineering & System Safety*, 65(3):203–211.
- Venice Water Authority (2013). Venice MOSE.
http://www.wunderground.com/hurricane/2008/venice_mose.jpg, retrieved 31-5-2013.
- Verruijt, A. (2001). Grondmechanica.
- Vibro Menard (2013). Illustration of installation Prefabricated Vertical Drains.
<http://www.vibromenard.co.uk/wp-content/uploads/2011/08/Vertical-drains-2-420x243.jpg>, retrieved 19-12-2013.
- Voorendt, M. Z., Molenaar, W. F., and Bezuyen, K. G. (2011). Hydraulic Structures: Caissons. *Lecture Notes CT3330*.
- Vrijling, J. K., Kuijper, H. K. T., van Baars, S., Bezuyen, K. G., Molenaar, W. F., van der Hoog, C., Hofschreuder, B., and Voorendt, M. Z. (2011). Manual Hydraulic Structures. *Lecture Notes CT3330*.
- Wall, J. S. (2008). Rollover Fish Pass.
<http://www.crystalbeach.com/rollover.htm>, retrieved 21-5-2013.
- water-technology.net (2012). Image of MOSE project.
<http://www.water-technology.net/projects/mose-project/>, retrieved 31-5-2013.

List of Figures

1.1	Location of the proposed Ike Dike, Bolivar Roads Pass and Hurricane Ike's path in the Galveston Bay Area (Merrell, 2010a).	1
1.2	Front and top views of the design proposed by Davis et al. (2010). Image based on the design by Arcadis for a Verrezano Narrows Barrier in New York (Dircke et al., 2009).	2
1.3	Aerial view of the theoretical ship channel gate and levee structure at Hartman Bridge (SSPEED Center, 2011).	3
1.4	Location of the HSC Gate in the Galveston Bay. Satellite image: Bing Maps (2013).	3
2.1	The Galveston Bay estuary. Satellite image: Bing Maps (2013).	8
2.2	Satellite views of the three inlets. Satellite images: Bing Maps (2013).	10
2.3	Current Galveston Seawall and shoreline protection.	11
2.4	Aerial view of the modern Seawall (Merrell et al., 2011).	11
2.5	Galveston Seawall and proposed Ike Dike along Galveston Island and Bolivar Peninsula. Satellite image: Bing Maps (2013).	12
2.6	Schematic cross section of the HSC showing its current dimensions. Modified from HGNSAC (2011).	13
2.7	Overview of Bolivar Roads highlighting important aspects. Satellite image: Bing Maps (2013).	15
3.1	Development of the reliability of the Maeslantkering (Rijkswaterstaat, 2010).	19
3.2	Expected scour-hole depth in the Eastern Scheldt block mats, and its 5th and 95th percentile, as a function of time (Van Noortwijk and Klatter, 1999).	20
3.3	Tidal range in the Oosterschelde pre-, during and post-barrier construction at station Yerseke (Smaal and Nienhuis, 1992).	20
4.1	Surge due to wind setup related to increase of water level in the Galveston Bay for an average depth of 3 m.	23
5.1	Depth profile Bolivar Roads along the shortest span between Galveston Island and Bolivar Peninsula. Based on data by Taylor et al. (2008b).	27
5.2	Water levels for a 1/10,000 yr ⁻¹ design storm compared to the water levels during Hurricane Ike. Hurricane Ike data from NOAA Tides and Currents (2013b).	28
5.3	Oyster growth on sector gates at Brazos River Floodgates Project, Freeport, TX (USACE, 2011).	30
6.1	Different alignment alternatives in Bolivar Roads. Satellite image: Bing Maps (2013).	34
6.2	Depth profiles barrier spans. Based on data by Taylor et al. (2008b).	34
6.3	Schematic distribution of navigational and environmental barrier sections (not to scale).	36
6.4	Schematic front view of a barrier with open navigational section and fully retaining environmental section (not to scale).	37
6.5	Bay water levels due to 1/10,000 yr ⁻¹ open coast surge conditions. Current situation compared to applying a storm surge barrier with an open Navigation section.	38
6.6	Schematic front and top view of barriers with a yet to be determined retaining height (not to scale).	38
6.7	Costs for 21 distinct distributions in retaining height that all result in a 1.4 m [4.6 ft] water level rise in the Galveston Bay.	39
6.8	Both sections equally retaining (at MSL+0.1m)	39
7.1	Cross-sectional side view of forces due to positive head (surge from the Gulf of Mexico) acting on caissons. Caisson dimensions not to scale. Units: m. MSL includes 100 year SLR.	44
7.2	Cross-sectional side view of forces due to negative head (backsurge from the Galveston Bay) acting on caissons. Caisson dimensions not to scale. Units: m. MSL includes 100 year SLR.	44
7.3	Cross sectional front view of Bolivar Roads showing the location of barrier sections AA' - GG' for the environmental barrier. The horizontal scale is compressed 40 times with respect to the vertical scale. Units: m.	46
7.4	Cross section of caisson unit without doors in floating condition for barrier section FF'. Units: m.	48
7.5	Cross section of caisson unit without doors in floating condition for barrier section BB'. Units: m.	48
7.6	Preliminary 3-D impressions of caisson barrier alternative.	49
7.7	Total soil settlement under caisson barrier section AA' (largest occurring) for both methods.	51

7.8	Cross section of barrier section BB' showing possible position of caissons after $t_{99\%}=18.5$ years (Koppejan method)	51
7.9	Graphical representation of the influence of design parameters on design aspects.	53
8.1	Cross-sectional side view of skirt dimensions in relation to caisson floor and top slab (barrier section BB')	60
8.2	Cross-sectional side view of forces due to positive head acting on caissons equipped with skirts. Caisson dimensions not to scale.	60
8.3	Cross-sectional side view of shear plane between replaced sand and clay layer for barrier section BB'. Caisson dimensions not to scale.	61
8.4	Cross sectional side view of principle of caisson failing on circular slide surface stability. The exact location of the circle is a possible location.	62
8.5	Costs vertical drainage expressed in terms of grid spacing.	64
8.6	Original and accelerated settlements using vertical drainage for barrier section BB' (Koppejan method).	64
8.7	Cross-sectional front view of caisson settlement with vertical drains (barrier section BB').	65
8.8	Illustration of under water vacuum preloading using CPVDs (Penta Ocean, 2013).	66
8.9	Costs vacuum preloading expressed in terms of grid spacing.	66
8.10	Original and accelerated settlements using preloading with CPVD for barrier section BB' (Koppejan method).	67
8.11	Cross-sectional front view of soil settlement using vacuum preloading with CPVDs (barrier section BB')	68
8.12	Cross-sectional side view of steel tubular piles for bearing forces due to positive and negative head (barrier section BB').	69
8.13	Costs steel tubular pile foundation expressed in terms of pile diameter.	71
8.14	Technical drawing of pile plan for barrier section BB'	73
8.15	Half cross sectional side view of barrier section BB' indicating the clay layers replaced with sand.	74
9.1	Installation of PVDs with mandrels (Vibro Menard, 2013).	79
9.2	Climbing formwork procedure (ULMA Construction, 2013).	81
9.3	Step 3.1 – Install steel mandrels with CPVDs in clay layers.	83
9.4	Step 3.2 – Remove steel mandrels, connect vacuum pumps to CPVDs via hoses.	83
9.5	Step 3.3 – Pump for 46 days.	83
9.6	Step 3.4 – Remove hoses, fill the resulting hole up with sand.	84
9.7	Step 3.5 – Monitor the position of the floating caisson during submergence.	84
9.8	Step 3.6 – Place the caisson on the sand bed, install the sheet pile wall on the open coast side and place the bed protection.	84
9.9	Overview barrier in Bolivar Roads and dry dock on Pelican Island. Satellite image: Google Earth (2013).	87
9.10	Storm surge barrier in opened position. Birds eye view from Bolivar Peninsula.	87
9.11	Caissons under construction in dry dock on Pelican Island.	88
9.12	Step 4.2 – Towing of caissons out of the dry dock towards the HSC.	88
9.13	Step 4.3 – Towing of caissons over the HSC towards the final location.	89
9.14	Step 4.5 – Placement of caissons at the final location. See also Figures 9.7 and 9.8.	89
9.15	Caisson barrier environmental section in opened position with vacuum preloading soil improvement (section BB', see Table 8.2 for dimensions).	90
9.16	Underwater front view of transition between caisson barrier sections BB' and CC'.	90
9.17	Navigational section.	91
10.1	Schematic birds eye view of the 'vertical butterfly valve door' for the caisson barrier.	96
B.1	Cross section of a vertical lifting gate (Sehgal, 1996).	B-4
B.2	Picture of the Eastern Scheldt Barrier (Siman, 2012).	B-4
B.3	Cross section of MOSE project (Venice Water Authority, 2013).	B-5
B.4	Aerial view of the Maeslantbarrier in closed position (Aerolin Photo BV, 2007).	B-6
B.5	Front view of a Visor Gate in Osaka, Japan (sakura.ne.jp, 2005).	B-6
B.6	Basic concept of a vertically rotating segment gate, cross sectional drawings (Tappin et al., 1984).	B-7

B.7	Aerial view of the Thames Barrier with one segment gate in operating position (Maritime Journal, 2002).	B-7
B.8	Cross section of the Balgstuw near Ramspol (Rövekamp, 1998).	B-8
B.9	Illustration of the Parachute barrier principle (Knippels and Pechtold, 1992).	B-9
B.10	Top view of the floating barge gate principle (Rigo et al., 1996).	B-9
B.11	Top view of a reduction barrier in the Western Scheldt (de Boom, 2013).	B-10
B.12	Side view of the 'Mailbox' barrier. Illustration by de Kort (2013).	B-10
B.13	Schematic birds eye view caisson structures with vertical lifting gates.	B-11
C.1	Surge due to wind setup related to increase of water level in the Galveston Bay for an average depth of 3 m.	C-2
D.1	Bathymetry of Galveston Bay, DEM (Taylor et al., 2008a).	D-1
D.2	Bathymetry of Bolivar Roads (Holcombe et al., 2006).	D-2
D.3	U.S. Sea Level Trends 1900-2000 (NOAA/US EPA, 2009).	D-3
D.4	Influence of landfall location on storm surge within semi-enclosed bays (Stoeten, 2013).	D-4
D.5	Wind rose Galveston Pleasure Pier station, 1983 - 2006. Units: m/s. (NOAA Tides and Currents, 2013b).	D-6
D.6	Subsurface soil conditions at the east end of Galveston Island based on borings N-2, N-4 and N-5 (McClelland Engineers, 1985).	D-9
D.7	Locations of the boring logs. The green arrows indicate the cross-sectional view of Figure D.6. Satellite image: Bing Maps (2013).	D-9
E.1	Schematic view of the rigid-column approximation.	E-2
E.2	Bay water levels under a $1/10,000 \text{ yr}^{-1}$ storm. Current situation compared to applying a barrier with full open Navigation section.	E-3
E.3	Schematic side view of a storm surge barrier modeled as a sharp crested weir. In free flow and submerged conditions respectively. Based on Reed and Sanchez (2010).	E-4
E.4	Navigational section fully retaining (MSL+5.4m), environmental section semi-open (MSL-0.1m)	E-5
E.5	Both sections equally retaining (MSL+0.1m)	E-6
E.6	Navigational section semi-open (MSL-11.0m), environmental section fully retaining (MSL+5.4m)	E-6
F.1	Cross-sectional view of Bolivar Roads indicating soil layers under caisson foundations. Dimensions not to scale.	F-2
F.2	Cross-sections of a caisson with three compartments showing the directions of the mass moments of inertia.	F-7
F.3	Cross-sectional side view of forces due to positive head (surge from the Gulf of Mexico) acting on caissons. Caisson dimensions not to scale. Units: m.	F-10
F.4	Cross-sectional side view of forces due to negative head (backsurge from the Galveston Bay) acting on caissons. Units: m.	F-11
F.5	Cross-sectional side view of the bottom part of a caisson structure when placed on its final location. Based on Voorendt et al. (2011).	F-13
F.6	Cross-sectional front view of forces for a floating caisson structure with active shear forces on caisson walls and slabs (not to scale).	F-15
F.7	Cross-sectional front view of a floating caisson structure with active bending moments on walls and slabs (not to scale).	F-16
F.8	Cross-sectional front view of a floating caisson indicating relevant points for evaluating the meta-centric height (not to scale).	F-17
G.1	Cross-sectional side view of forces due to positive head (surge from the Gulf of Mexico) acting on caissons equipped with skirts. Caisson dimensions not to scale.	G-1
G.2	Cross-sectional side view of forces due to negative head (surge from the Galveston Bay) acting on caissons equipped with skirts. Caisson dimensions not to scale.	G-2
G.3	Skirt dimensions for barrier section BB'.	G-3
G.4	Top view of vertical drains and drain spacing	G-5
G.5	Total vertical drainage costs expressed in terms of grid spacing.	G-7
G.6	Total costs vacuum preloading with CPVDs expressed in terms of grid spacing.	G-9
G.7	Position of neutral point in soft soil stratum (Singapore Standard, 2003).	G-12

LIST OF FIGURES

G.8 Total costs deep foundation expressed in terms of pile diameter. G-15
G.9 Half cross sectional side view of barrier section BB' indicating the clay layers replaced with sand. . . . G-17

List of Tables

1.1	Report structure.	5
4.1	Stakeholders involved	25
5.1	Hydraulic boundary conditions	28
5.2	Soil layer classification and strength properties. Modified from McClelland Engineers (1985).	29
6.1	Overflow configurations	36
7.1	Barrier alternatives and their score on different criteria.	41
7.2	Relevant levels and depths.	43
7.3	Caisson dimensions.	47
7.4	Relative deformation under each barrier section.	50
7.5	Relative influence of different design parameters.	56
8.1	Flowchart of decision process involved with selection of foundation type. Adopted from Hussin (2006a).	59
8.2	Revised caisson dimensions in metric (SI) units.	62
8.3	Relevant checks for optimized caisson dimensions.	62
8.4	Required number of steel tubulars.	72
8.5	Foundation and caisson construction costs per foundation alternative in million US\$.	75
8.6	Flowchart for selecting barrier construction and barrier foundation type.	76
9.1	Cost overview environmental barrier. Direct costs calculated in Table 9.1.	86
D.1	Surge and wave heights for different protection levels.	D-5
D.2	Average precipitation for Galveston Scholes International Airport, 1981-2010 (NWS Weather Forecast Office, 2013).	D-5
D.3	Saffir-Simpson Hurricane Wind Scale (Schott et al., 2012; Stewart, 2008)	D-7
E.1	Costs and peak discharge of three overflow configurations.	E-7
F.1	Soil properties per layer.	F-1
F.2	Characteristics of concrete classes (TGB, 2013).	F-3
F.3	Unity checks.	F-19
F.4	Caisson dimensions in metric (SI) units.	F-20
F.5	Caisson dimensions in imperial units.	F-20
F.6	Effective stresses in the middle of the soil layers.	F-21
F.7	Applied stresses due to caisson weight in the middle of the soil layers.	F-22
F.8	Consolidation properties per soil layer for Koppejan method.	F-23
F.9	Relative deformation per soil layer Koppejan method.	F-24
F.10	Consolidation properties per soil layer for Bjerrum method.	F-25
F.11	Relative deformation per soil layer Bjerrum method.	F-25
G.1	Properties of relevant soil layers for skirt resistance per barrier section.	G-2
G.2	Revised caisson dimensions in metric (SI) units.	G-3
G.3	Revised caisson dimensions in imperial units.	G-4
G.4	Unity checks for final caisson dimensions.	G-4
G.5	Time and cost unit rates for vertical drainage with Prefabricated Vertical Drains.	G-6
G.6	Caisson construction time for foundation alternative 1.	G-7
G.7	Caisson construction costs for foundation alternative 1.	G-8
G.8	Time and cost unit rates for vacuum preloading with CPVDs.	G-8
G.9	Caisson construction time for foundation alternative 2.	G-9
G.10	Caisson construction costs for foundation alternative 2.	G-10
G.11	Parameters for bearing layer.	G-12
G.12	Parameters for skin friction.	G-13
G.13	Time and cost unit rates for vacuum preloading with CPVDs.	G-14
G.14	Caisson construction time for foundation alternative 3.	G-15
G.15	Caisson construction costs for foundation alternative 3.	G-16
G.16	Total pile bearing capacities.	G-16

LIST OF TABLES

G.17 Required number of steel tubulars.	G-17
G.18 Replaced soil.	G-18
G.19 Seepage.	G-18
H.1 Costs for building dock.	H-1
H.2 Costs for preparing final location.	H-2
H.3 Costs for caisson transportation.	H-2
H.4 Total costs environmental barrier.	H-3

Appendices

Appendix A presents factors for converting between the imperial and metric (SI) unit systems.

Appendix B gives an overview of different barrier and gate types.

Appendix C presents calculations for the requirements (chapter 4).

Appendix D contains data and calculations for the boundary conditions (chapter 5).

Appendix E presents calculations and an elaborated approach as used when considering the barrier as a system (first design step, chapter 6).

Appendix F presents calculations and an elaborated approach as used for the environmental barrier design step (second design step, chapter 7).

Appendix G presents calculations and an elaborated approach as used in the foundation design (third design step, chapter 8).

Appendix H presents cost calculations for the construction method (chapter 9).

A Conversion factors

In the appendices only metric units are presented. The table below presents factors for converting between the imperial and metric units used in this thesis.

Length			
feet [ft]	x 0.3048	=	meters [m]
inch [in]	x 0.0254	=	meters [m]
inch [in]	x 2.54	=	centimeters [cm]
inch [in]	x 25.4	=	millimeters [mm]
miles [mi]	x 1609.34	=	meters [m]
miles [mi]	x 1.60934	=	kilometers [km]
Area			
square feet [sqft]	x 0.09290	=	square meters [m ²]
square miles [sqmi]	x 2.58999	=	square kilometers [km ²]
Volume			
cubic feet [ft ³]	x 0.02831	=	cubic meters [m ³]
Velocity			
feet per second [ft/s]	x 0.3048	=	meters per second [m/s]
miles per hour [mph]	x 1.60934	=	kilometers per hour [km/h]
miles per hour [mph]	x 0.44704	=	meters per second [m/s]
knots [kt]	x 1.85200	=	kilometers per hour [km/h]
Discharge			
cubic feet per second [ft ³ /s]	x 0.02831	=	cubic meters per second [m ³ /s]
Acceleration			
feet per second squared [ft/s ²]	x 0.3048	=	meters per second squared [m/s ²]
Force			
kilo pounds-force [kips]	x 4.44822	=	kilonewtons [kN]
Density			
pounds per cubic feet [lb/ft ³]	x 0.15713	=	kilonewtons per cubic meter [kN/m ³]
Pressure/stress			
pounds per square inch [psi]	x 0.006894	=	newtons per square millimeter [N/mm ²]
pounds per square inch [psi]	x 6.894	=	kilonewtons per square meter [kN/m ²]
kilo pounds-force per square feet [kips/sqft]	x 0.02088	=	kilonewtons per square meter [kN/m ²]

B Gate and barrier types

This appendix gives an overview of different barriers and gate types that could fit into the specific location of Bolivar Roads. These concern not only the obvious solutions for storm surge barriers like vertical lifting gates or sector gates, but also less obvious solutions like the 'Parachute' and 'Mailbox' barriers. Furthermore the principle of a reduction barrier is briefly discussed.

B.1 Mitre gates



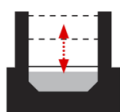
Mitre gates, probably an invention of Leonardo da Vinci (Hill, 2013), were already common in the 16th and 17th century and are very often used in shipping locks in canals. In closed position, mitre gates are double-leaf gates forming an angle pointing upstream. At shipping locks, waves and currents are limited, while the navigation width seldom exceeds 50 m [164 ft]. In such a case, mitre gates are very cost-effective. At locations where more severe conditions are present, mitre gates are less attractive. Also their sensitivity to reversed head makes it unfavorable as gates for a storm surge barrier (Dircke et al., 2012).

B.2 Radial gates



Radial gates, also referred to as Tainter gates (Named after J. B. Tainter, an engineer who invented the Radial or *Tainter* gate in 1886), are the most frequently used movable water control structures as they are applied in many dams. They are a cost-effective, simple and very reliable gate type in many applications. They consist of a skin plate formed into a segment with radius about the pivot. It can be constructed both with tension and compression gate arms. An example of application as a storm surge barrier is in a section of the Thames Barrier, see Appendix B.7.

B.3 Vertical lifting gates



Vertical lifting gates are often preferred over radial gates as they are simpler to construct and install and do not require support girders embedded in piers (Sehgal, 1996). Much experience and documentation is available on construction techniques and on functioning and behavior under flow and wave conditions. Favorable aspects are the large applicable gate span (up to 100 m [300ft]), the option of overflowing and the simplicity of maintenance. They may be undesirable from an aesthetic point of view as the required gate tower protrudes high above the water surface. Vertical lifting gates are usually designed as wheeled gates rather than sliding gates. This is because of the necessity to close under gravity and to reduce the required hoisting forces. In order to minimize flow disruption the seals and skin plate on the vertical lifting gates are provided on the upstream side of the gate slot (Dircke et al., 2012; Sehgal, 1996).

Currently most vertical lifting gates consist of moveable steel doors hung up on concrete support towers. In the future these steel doors might be replaced by FRP based constructions, see Section 3.2.

Eastern Scheldt Barrier. The Eastern Scheldt storm surge barrier is the most famous example of a vertical lifting gate (Figure B.2). It is the largest of the Dutch Delta Works⁽¹⁾ and stretches over 9 km [5.6 mi] between the islands

⁽¹⁾The Delta Works is a series of construction projects in the southwest of the Netherlands to shorten the Dutch coastline and protect the hinterland around the Rhine-Meuse-Scheldt delta against storm surges from the North Sea (Nienhuis et al., 1982). The initiative for the con-

of Schouwen-Duiveland and Noord-Beveland, province of Zeeland, Netherlands. The gates can be closed in case the water level exceeds NAP+3m [9 ft]. In this way the saltwater marine life behind the dam is preserved while the dike ring behind the barrier is protected in case of high surge levels. The design lifetime is 200 years. The Eastern Scheldt barrier was the most difficult to build and most expensive part of the Delta Works. Construction time took a decade, starting in 1976 to be finished in 1986. In 1987 the road over the dam was ready for use, creating a connection between the islands of Schouwen-Duiveland and Noord-Beveland.

Hydraulic cylinders lower the steel gates. In fully lowered position they close off the flow opening between the upper and sill beams. There are 62 flow openings, each with a width of 40 m [131 ft]. The steel gates that are able to close off the flow opening are 42 m [138 ft] wide. The gate height varies between 5.9 m [19.4 ft] and 11.9 m [39.0 ft]. Each of the 65 concrete pillars is between 35 and 38.75 m [115-127 ft] high, depending upon their location in the three main gullies (Dircke et al., 2012).

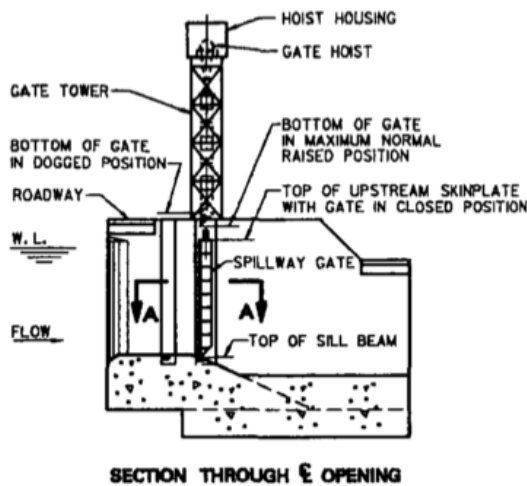


Figure B.1: Cross section of a vertical lifting gate (Sehgal, 1996).

Figure B.2: Picture of the Eastern Scheldt Barrier (Siman, 2012).

B.4 Flap gates



Just like the vertical lifting gates described above the so-called flap gates are also very favorable in terms of maximum gate span, which can be up to 100m [300 ft]. In series they can theoretically form an undisturbed opening of unlimited length since no protruding abutment structures are required.

In contradiction to the vertical lifting gates the flap gates are hidden under the water surface when the gates are not in use. This minimizes the visual hindrance. They are stored in a bottom recess, one side is hinged to the sill, the free end emerges above the water surface in closed position. The invisibility aspect has been the main argument for applying a flap gate in the MOdule Sperimentale Elettromeccanico (MOSE) project. Apart from their aesthetic benefits, flap gates are usually applied when the reservoir level must be accurately maintained or when floating debris and/or ice have to be skimmed (Sehgal, 1996). Downside aspects of the flap gates primarily concern its costs; the height of the flap gates is economically feasible is up to about 4 m [13 ft]. This makes the flap gates an unfavorable alternative for storm surge barriers in deep waterways.

struction of the Delta Works was in response to the widespread damage and number of casualties due to the North Sea Flood of 1953. The ASCE has declared the works to be one of the Seven Wonders of the Modern World (Prasuhn and FitzSimons, 2002).

MOSE project. The MODulo Sperimentale Elettromeccanico (MOSE) project is a system consisting of flap gates serving to protect the famous city of Venice and neighboring areas along the Venice Lagoon against floods from the Adriatic Sea. Over the years the Venice floods have become more intense as a result of the combined effect of sea level rise and land subsidence. The Great Flood of 1966 (which caused massive loss of life and property) and a land subsidence of 28 cm [11 in] over last century, provided momentum and necessity to protect Venice. The construction works started in 2003 and are expected to be fully completed in 2014 (water-technology.net, 2012)

The barrier consist of 78 flap gates installed at the three inlets connecting the Venice Lagoon and the Adriatic Sea which can be closed during high water levels. They are 28 m [92 ft] long, 20 m [65 ft] wide and have been designed to provide protection from tidal levels up to 3 m [10 ft]. When a level of more than 110 cm [3.6 ft] is expected, air is pumped into the metal box structure. The gates will rise up and block the tidal flow, preventing the water from flowing into the lagoon.

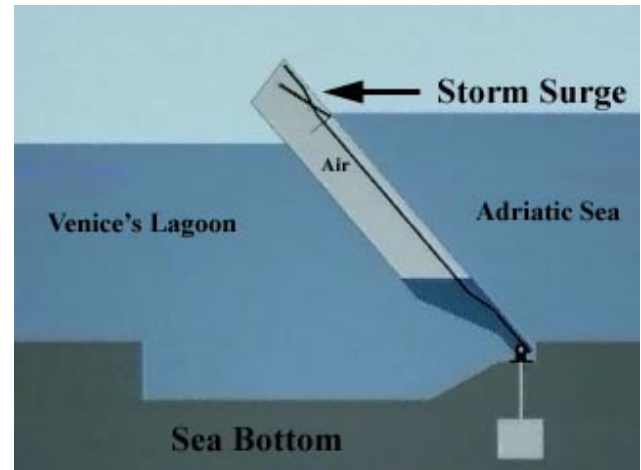
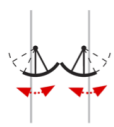


Figure B.3: Cross section of MOSE project (Venice Water Authority, 2013).

B.5 Sector gates



Sector gates can be either floating or non-floating. Major disadvantages of non-floating sector gates include for example the need for deep side chambers in the abutments (where the gates are housed when the gates are not in use), and the risk of malfunctioning when siltation occurs on the sill. Floating sector gates do not have these disadvantages and are therefore preferable, despite of their sensitivity to flow-induced oscillations and dynamic wave loads.

Maeslantbarrier. An example of a floating sector gate is the Maeslantbarrier located in the Nieuwe Waterweg, which is the entrance to the Port of Rotterdam and one of the estuaries of the main rivers (Rhine and Meuse) in the Netherlands. It is the final part of the Delta Works. The barrier was designed to solve the problem of keeping the port open under normal circumstances and allow the outflow of river water. It was preferred over increasing the height of the dike ring in the whole area of 1.2 m [4 ft], as it was considered less intrusive, cheaper and technologically more appealing. The construction of this well-known storm surge barrier started in 1991 and was completed in 1997. The gate closes in case a storm surge of NAP+3 m [10 ft] is expected. These alarming water levels can only be caused by a combination of spring tide and a northwest storm, occurring on average once in every ten years. Until now it had its first successful closure under storm conditions in November 2007. The barrier is built for a design lifetime of 100 years.

The barrier consists of two floating-sector gates, each with a radius of 246 m [807 ft], an arch length of 208 m [682 ft] and a gate height of 22 m [72 ft]. The gate arms are connected to a single ball hinge on the abutments, well above the mean water level. These hinges are constructed on top of concrete gravity caissons filled with sand. Driven by two 'Locomobiles' the gates can be floated into the river and they are moved towards eachother. Immersion takes place within 1.5 hours and the mobilization and filling of the dry docks requires about 1 hour.



Figure B.4: Aerial view of the Maeslantbarrier in closed position (Aerolin Photo BV, 2007).

B.6 Visor gate



The visor gate derives its name from the visors in the helmets worn by Middle Age knights. The leaf is designed as a three-hinged arc, pivoted on horizontal pins. In closed position, the leaf presses continuously against the sill. In open position it allows vessels to pass under the leaf, limiting the allowable air draft. The gate closure is done by gravity while opening of the gate is made by two mechanical hoists with wire ropes placed on concrete structures built on the piers. This type of gate could be applied for large spans (Erbisti, 2004).



Figure B.5: Front view of a Visor Gate in Osaka, Japan (sakura.ne.jp, 2005).

B.7 Vertically rotating gate



One type of vertically rotating gate, the radial gate, has been briefly discussed in Appendix B.2. This section specifically describes another type of vertically rotating gate: the segment gate. It is a segment of a circle which normally lies in a recess in the concrete sill in the bed of the river or estuary. The gate is supported on both sides in hollow steel side disks which rotate in a vertical plane about central pivot bearings mounted on trunnions protruding from the piers. The side disks are partly filled with cast iron to counterbalance the weight of the gate body. Operation of the gate is achieved by the rotation of the end disks through approximately 90° . Further rotating it by an angle of 90° places the gate fully lifted above the water level in maintenance position (Tappin et al., 1984).

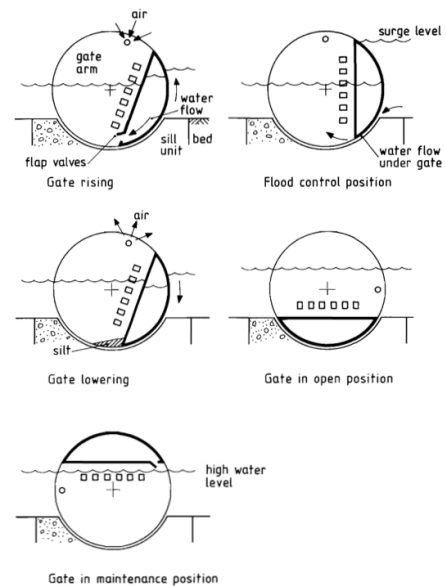


Figure B.6: Basic concept of a vertically rotating segment gate, cross sectional drawings (Tappin et al., 1984).

Thames Barrier. The Thames Barrier, located downstream of central London in the United Kingdom is a vertically rotating segment gate that protects all but the easternmost boroughs of Greater London from being flooded by storm surges originating from the North Sea. The barrier comprises navigable segment gates (four main openings of 61 m [200 ft] and two smaller openings of 31.5 m [103 ft]) and non-navigable radial gates (four openings of 31.5 m [103 ft]) (Dircke et al., 2012). Construction took place between 1974 and 1982.



Figure B.7: Aerial view of the Thames Barrier with one segment gate in operating position (Maritime Journal, 2002).

Next to storm surge conditions the barrier may also be closed under periods of high flow to reduce the risk of fluvial (river) flooding in some areas of west London. As of October 2011, the Thames barrier has been closed

119 times since it became operational. This number increased through time, as two-third of its closures took place since 2000. In the future the Thames barrier will have to close more frequently to prevent overtopping over the upstream flood defenses (Environment Agency, 2012). The Thames Barrier is closed in case the tidal limit at Teddington Weir indicates water levels would exceed 4.87 m [16 ft] in central London. The design surge is taken as the 1/1000 yr⁻¹ event for conditions until the year 2030, this includes an allowance for annual sea level rise of 8 mm/yr [0.31 in/yr] (Environment Agency, 2012).

B.8 Inflatable rubber dam

Inflatable rubber dams are classified as cylindrical, rubber fabrics placed across rivers or estuaries which can be inflated to raise above the water level and protect the area behind it against high water levels. The fabric is fixed to a reinforced concrete sill using clamp plates and anchor bolts. It is inflated by pumping in air, water or both until the design height or required pressure level is reached. Long spans of up to 100m are no exception. Disadvantage of the inflatable dam is its unsuitability for discharge regulation. The inflatable rubber dam is also an unfavorable solution when it comes down to sensitivity to UV-exposure and external damage from floating objects like ships and debris.

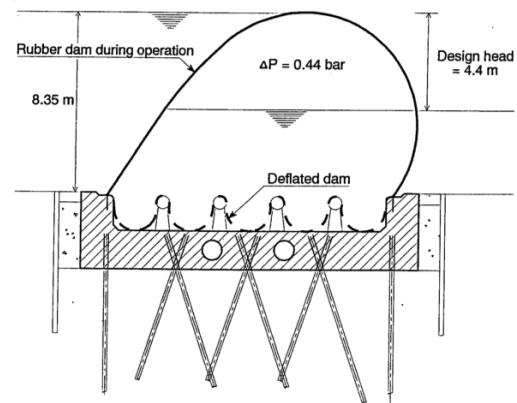


Figure B.8: Cross section of the Balgstuw near Ramspol (Rövekamp, 1998).

Balgstuw Ramspol. The Balgstuw near Ramspol is an inflatable rubber dam serving to protect the western part of the Province of Overijssel in the Netherlands against flooding due to high water at the IJsselmeer and Ketelmeer. When construction completed in 2002 it was the largest inflatable rubber dam of the world (Rövekamp, 1998). It is inflated when the water level reaches the alarm level of 0.5 m [4.9 ft] above NAP⁽²⁾. The protection level of the barrier is to withstand storm conditions occurring 1/10,000 yr⁻¹, corresponding to a design height of 8.35 m [27.4 ft] and head of 4.4 m [14.4 ft]. See Figure B.8. The inflatable rubber dam is a very appropriate solution in situations where the water head switches from side to side, for example driven by tidal movement.

B.9 Parachute barrier

As its name already reveals, a parachute barrier is an open fabric moveable water barrier that unfolds like a parachute in horizontal direction. Where the inflatable rubber dam is classified as *closed fabric*, the parachute dam is an *open fabric* because only one side of the rubber material is constrained. The principle is that it is opened by the water flow and kept open by the hydraulic pressure. This makes its appliance very complex in situations where a reversed head can be present.

Until now, the parachute barrier has not yet been constructed. However, a structural design for a parachute barrier has been made within the context of a Master's thesis carried out by Van der Ziel (2009).

⁽²⁾Normaal Amsterdams Peil: Amsterdam Ordnance Datum. The vertical reference point in use for large parts of Western Europe which was originally established in 1684 for use in the Netherlands.

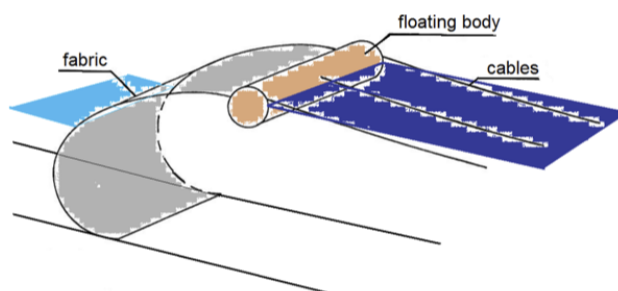


Figure B.9: Illustration of the Parachute barrier principle (Knipfels and Pechtold, 1992).

B.10 Barge gate



A barge gate is stored on one side of a waterway and pivots about a vertical axis to close against abutments on either side of the waterway. In order to reduce hinge and operating forces a barge gate may ideally be buoyant. The gate may optionally have wall openings with valves to keep it permeable during closure. This permeability allows better control over the barrier when rotating it in position. After the gate is positioned and immersed, the valves are closed to make it water retaining. Rigo et al. (1996) investigated the appliance of a 390 m [1280 ft] span floating barge gate in the Nieuwe Waterweg. It was one of the alternatives to the eventually constructed sector gate barrier (Appendix B.5). Maneuverability and feasibility tests were performed and demonstrated the reliability of gate. Up to now, a barge gate with such dimensions is not yet constructed.

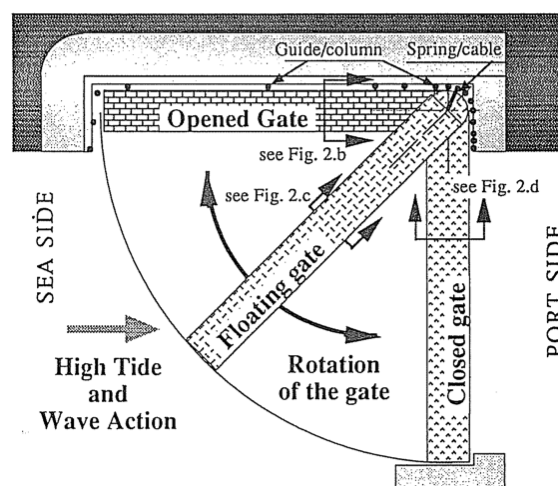


Figure B.10: Top view of the floating barge gate principle (Rigo et al., 1996).

B.11 Reduction barrier

The principle of a reduction barrier is to reduce tidal amplitudes in a river branch, bay or estuary by providing additional resistance near the mouth. The reduction barrier itself can for example be constructed as concrete caissons or rubble mound. Sections which are left open enable navigation and allow water circulation inside the estuary (de Boom, 2013). As slow changes in water level are better able to penetrate the reduction barrier the principle is most effective at fast changing water levels. Storm surges have longer time scales than tidal waves and are therefore more difficult to reduce. For locations with long storm durations (e.g. the North Sea) the reduction barrier is not that effective. For locations with shorter storm durations (e.g. hurricane prone areas like the Galveston Bay) the surges are more effectively damped increasing their applicability.

The main advantages of the reduction barrier are related to the open nature of the barrier. It enables the in and outflow of water and sediments and gives migrating fish free passage. Disadvantages mainly concern the openness. The water levels inside the estuary can still rise. A sufficient retention pond behind the barrier limits this effect, but flooding will still be possible. Besides, the openness entails a feeling of being unprotected against surges. This

can influence the social basis for a reduction barrier. Another downside is the high flow velocity in the openings during storm conditions. This requires a high quality bed protection to ensure the barrier's stability.



Figure B.11: Top view of a reduction barrier in the Western Scheldt (de Boom, 2013).

B.12 Mailbox gate

The 'Mailbox' gate is a new type of gate. It is a heavy concrete flap gate hanging on two yokes. The yokes are founded on inclined foundation piles. In this way, an eventual soft top soil layer with poor bearing capacity is avoided. In normal conditions the flap is positioned horizontally. It can now serve as walkway while currents or tidal movement can flow underneath it. In case of surge the barrier is lowered, hanging in a somewhat diagonal position. It is a leaky system as the barrier is the combination of a top and bottom spillway. High water pressure due to surge or waves pushes the flaps open the gate. Advantage of this concept is its ability to be simply adjustable to the bathymetry.

Up to now there are no examples where this gate is applied. It therefore requires thorough research in occurring internal and external forces.

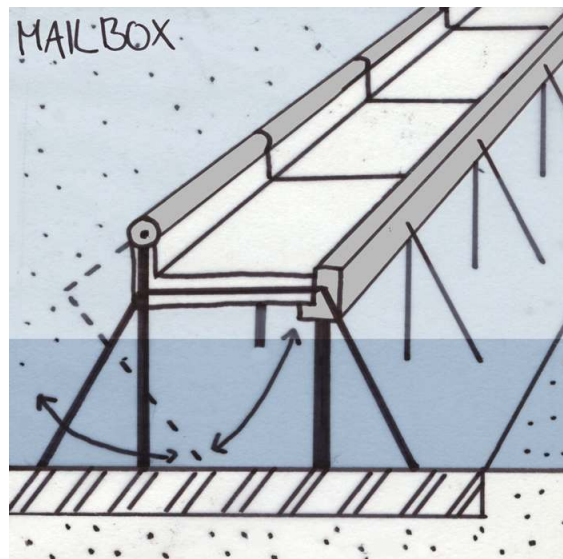


Figure B.12: Side view of the 'Mailbox' barrier. Illustration by de Kort (2013).

B.13 Caisson structure

The caisson structure is in fact a concrete closure dam that is permeable in normal conditions and can be closed during surge events. In the middle of the caissons for example a vertical lifting gate can be constructed. In normal conditions the water is able to flow back and forth. In case a surge event approaches the gate will be lowered, just like a regular vertical lifting gate. The disadvantage it has compared to a vertical lifting gate is that it is unlikely

that that navigation will be possible through this barrier. The advantage it has compared to the vertical lifting gate is it deals better when shallow founded on weak soils. The loads on the structure are spread out over a bigger footprint.

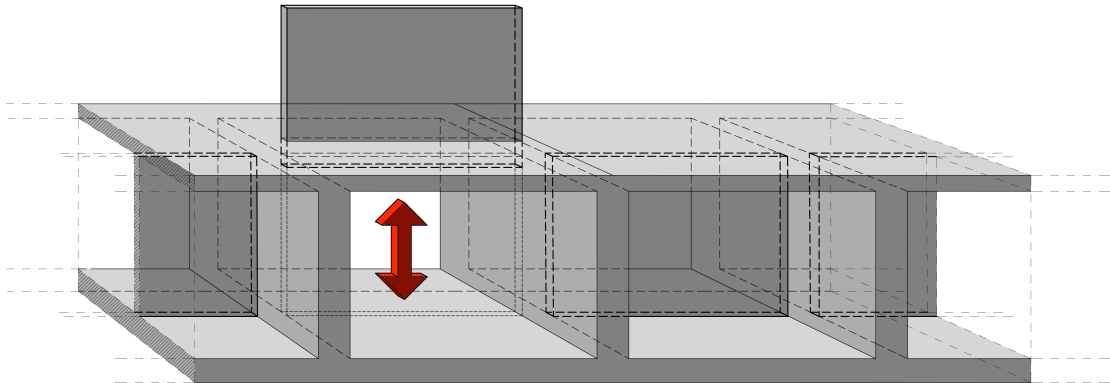


Figure B.13: Schematic birds eye view caisson structures with vertical lifting gates.

C Requirements

This appendix contains calculations for the requirements (chapter 4).

C.1 Overflow

The actual storm surge within the Galveston Bay is dependent on wind setup in the Bay. Wind setup is a function of water depth as can be seen from Equation (C.1). Under Hurricane forcing water flows through Bolivar Roads pass increasing the water level inside the Bay. This increased water level has its influence on the wind setup that results in surge levels along the shoreline of the Bay. The influence of elevated bay levels on wind setup is assessed by simulating surges on a closed basin under hurricane forcing.

Computations by Stoeten (2013) show that the surge levels at the Northern parts of the Bay are governing. By modeling the Galveston Bay as a circular shaped water body with a diameter of 25 km and an average depth of $d_{bay} = 3$ m the wind setup can be calculated. This is done using a formula for wind setup in a closed basin (Lansen and Kluyver, 2006).

$$\Delta h_{setup} = \frac{1}{2} \frac{\rho_{air}}{\rho_{sw}} C_D \frac{U_{10}}{g d_{bay}} L_{fetch} \text{ [m]} \quad \text{C.1}$$

In which:

Δh_{setup}	[m]	Maximum wind setup
ρ_{air}	[kN/m ³]	Mass density of air (= 0.01225 kN/m ³)
ρ_{sw}	[kN/m ³]	Mass density of salt water (= 10.25 kN/m ³)
C_D	[-]	air/water drag coefficient (= 0.0015) ^(I)
U_{10}	[m/s]	Wind velocity at 10 m above MSL (= 62 m/s) ^(II)
g	[m/s ²]	Gravitational constant (= 10)
d_{bay}	[m]	Water depth in bay (= 3 m)
L_{fetch}	[m]	Fetch length (= 25,000 m)

^(I)Default value (Lansen and Kluyver, 2006)

^(II)Wind speed for a Cat. 5 Hurricane (Table D.3) is assumed to be representative for a 1/10,000 yr⁻¹ storm.

Figure C.1 shows the influences of water elevation on surge level for the Northern side of the bay. According to Merrell (*TAMUG*, personal communication 11-9-2013) the maximum allowed surge level at this Northern side of the Bay is 3.4 m [11.0 ft]. As can be seen from the graph a surge of 3.4 m [11 ft] occurs when the water depth in the bay has increased to a level of 1.4 m [4.6 ft]. Higher water level elevations induce a too high surge.

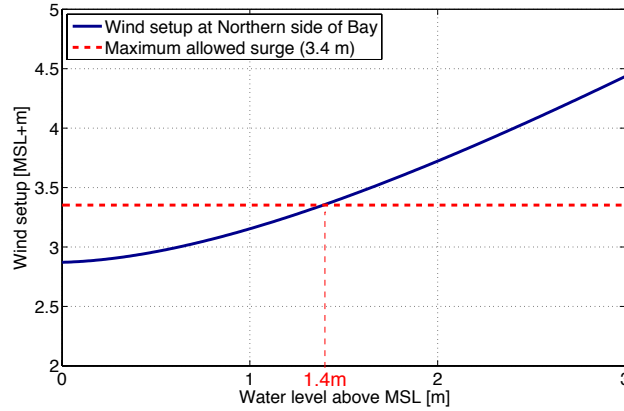


Figure C.1: Surge due to wind setup related to increase of water level in the Galveston Bay for an average depth of 3 m.

This number determines a lot for the eventual required retaining height of the barrier. It is strongly recommended to model a hurricane in a 3-dimensional model to accurately calculate the surge levels in the bay due to different water level elevations. Furthermore also the economical consideration is important; the acceptable damage to the buildings and industrial facilities located in the flood prone areas have to be determined and taken into account to determine the maximum allowed surge levels in the Bay. This is outside the scope of this thesis.

C.2 Nautical requirements

This section presents calculations for the nautical requirements. It concerns the required navigation channel dimensions and the traffic intensity on Bolivar Roads. The calculations support statements made in Section 4.2.

C.2.1 Navigation channel dimensions

The New Panamax tankers dimensions are (Benitez, 2009):

D_s	[m]	Draft of design ship = 15.2 m
W_s	[m]	Width of design ship = 49 m
L_s	[m]	Length of design ship (LOA) = 366 m

Channel depth. The minimum channel depth is determined by the following formula (Ligteringen, 2009):

$$d_{nav} = D_s - \zeta_{tide} + s_{max} + \zeta_m + s_s = 16.95 \text{ [m]} \rightarrow 17.0 \text{ [m]} \quad \text{C.2}$$

In which:

d_{nav}	[m]	Depth of navigation channel
D_s	[m]	Draft of design ship (= 15.2 m)
ζ_{tide}	[m]	Tidal elevation above reference level below which no entrance is allowed (= 0 m)
s_{max}	[m]	Maximum sinkage due to squat and trim (= 0.75 m)
ζ_m	[m]	Vertical motion due to wave response (= 0.5 m)
s_s	[m]	Remaining safety margin or net under keel clearance (= 0.5 m)

Channel width. The minimum width of the channel can be determined using a method developed by the PI-ANC group (Ligteringen, 2009). According to this method, the width of a unidirectional channel should fulfill the following requirement:

$$W_{min} = W_{BM} + \sum W_i + 2 \cdot W_B \text{ [m]} \quad \text{C.3}$$

Wherein:

Width component	Condition	Width implication
Basic width W_{BM}	Good Maneuverability	$1.6W_s$
Additional widths W_i		
– Prevailing cross-winds	25 kts	$0.4W_s$
– Prevailing cross-current	0.4 kts	$0.2W_s$
– Prevailing wave height	<1m	0
– Aids to navigation	VTS	$0.1W_s$
– Seabed characteristics	Soft	$0.1W_s$
– Cargo hazard	High	$1.0W_s$
Bank clearance W_B	Sloping edge	$0.5W_s$
Total		$4.4W_s$

This results in a minimum channel width of $W_{min} = 4.4 \cdot 49 = 215.6 \text{ [m]} \rightarrow 220 \text{ [m]}$.

C.2.2 Traffic intensity

This subsection calculates whether it is possible to let all of the vessels passing through a two-way navigation section in terms of mutual distance.

As stated in Section 4.2.2 the average day would see 55 ocean going vessels and 21 offshore support vessels, so 76 in total. In the future this total number vessels may increase to 100. The daily number of recreational vessels is unknown and is therefore assumed to be around 100 too. Summed up this means that a total 200 vessels would pass Bolivar Roads on an average day for two-way traffic. This means 100 vessels in each direction on average.

For this quick calculation *all* of these vessels are assumed to be New Panamax size and 12hr day of service is applied. This would induce that every $\frac{12 \cdot 3600}{100} = 432$ seconds a vessel will pass Bolivar Roads. Next the distance between to consecutive vessels is calculated through a formula for vessels in inland waterways, according to Groeneveld (2002):

$$\left(\frac{v_{lim}}{\sqrt{g \cdot d_{nav}}} \right) = 0.78 \cdot \left(1 - \frac{A_s}{A_c} \right)^{2.25} \rightarrow v_{lim} = 6.05 \text{ [m/s]} \quad \text{C.4}$$

In which:

v_{lim}	[m/s]	Limit speed of design vessel
d_{nav}	[m]	Depth of navigation channel (= 17 m)
A_s	[m ²]	Wet surface of design vessel (New Panamax: $D_s \cdot W_s = 770 \text{ m}^2$)
A_c	[m ²]	Flow area of channel ($d_{nav} \cdot W_{min} = 3,740 \text{ m}^2$)
L_s	[m]	Length of design ship (LOA) (New Panamax: 366 m)

Assuming that vessels will be sailing at half their limit speed every vessel needs $432 \cdot 0.5 \cdot 6.05 \approx 1300 \text{ m}$ of space. According to Groeneveld (2002) the minimum *mutual* distance (i.e. from the stern of the ship traveling in front and the bow of the ship traveling behind) is $1.45 \cdot L_s$. This means that the total minimum required space for each vessel

is $1.45 \cdot L_s + L_s \approx 900$ m. This is minimum required length is smaller than the available space for each vessel.

So even when all ships passing Bolivar Roads are assumed as New Panamax size and traveling at relatively slow speed, a two-way navigation section in Bolivar Roads will be sufficient. No additional barge lanes will be necessary.

D Boundary Conditions

This appendix contains data and calculations for the boundary conditions (chapter 5).

D.1 Bathymetry maps

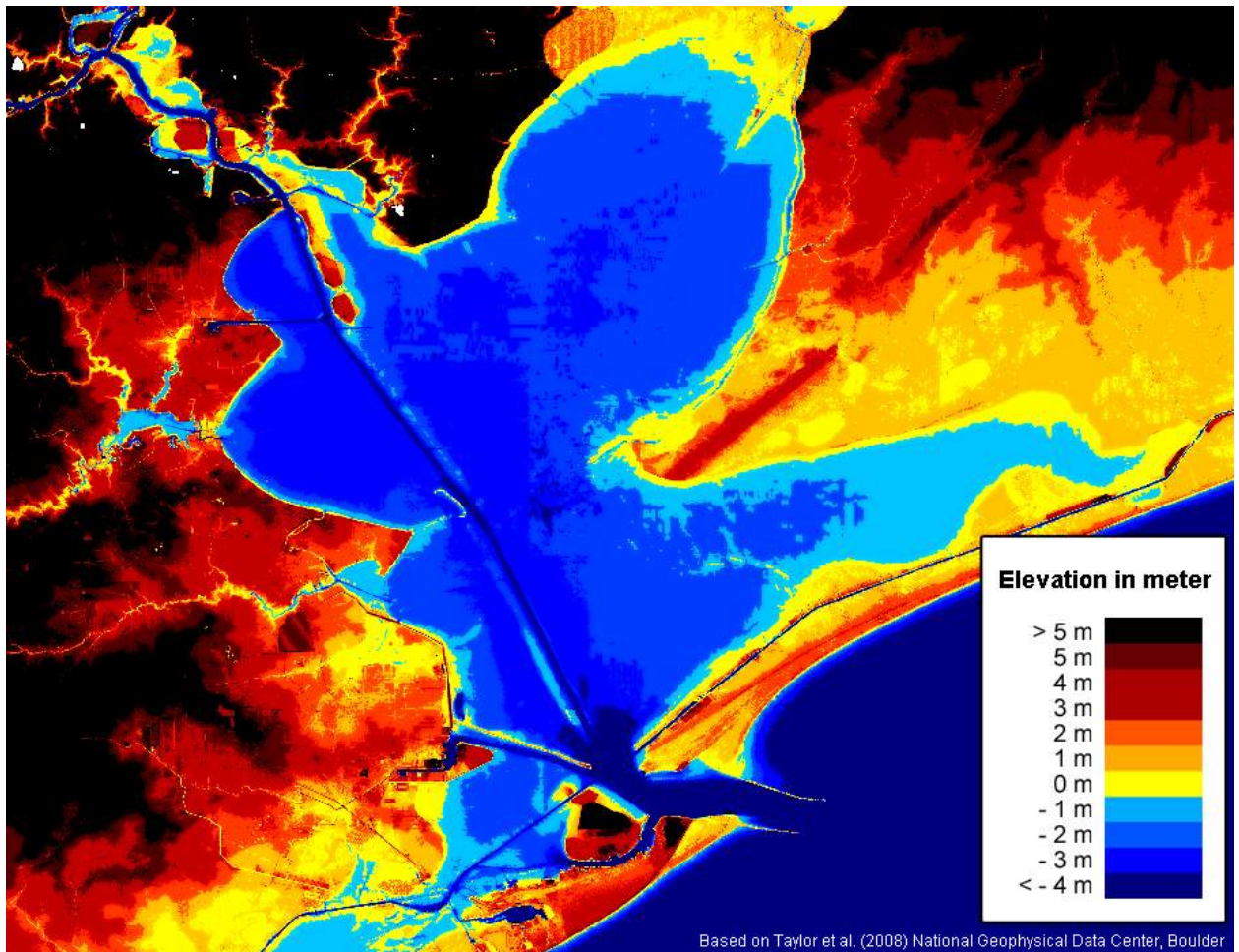


Figure D.1: Bathymetry of Galveston Bay, DEM (Taylor et al., 2008a).

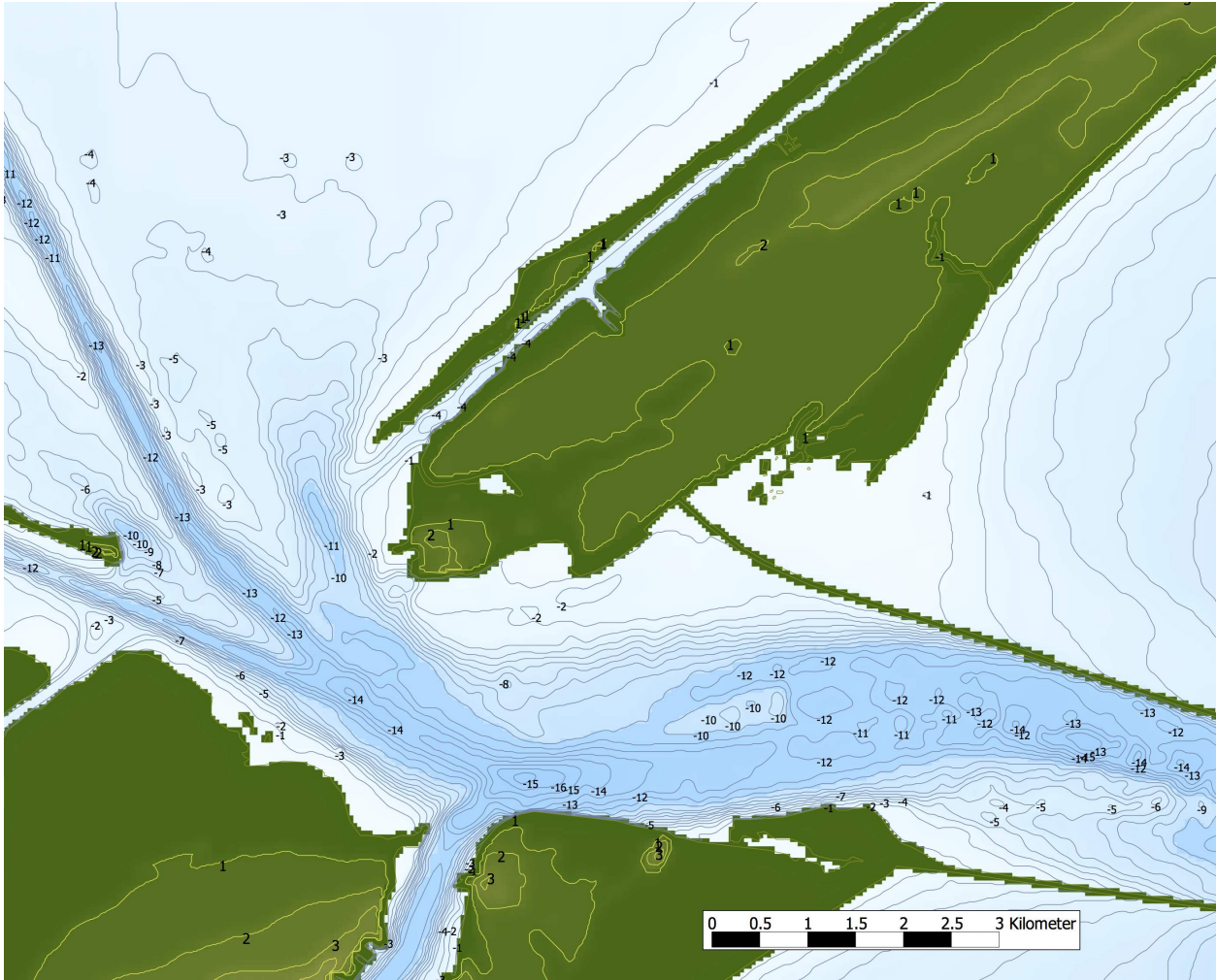


Figure D.2: Bathymetry of Bolivar Roads (Holcombe et al., 2006).

D.2 Hydraulic conditions

The numbers as stated in Table 5.1 (Section 5.2) are established in this section.

D.2.1 Regular hydraulic conditions

Regular hydraulic conditions are always present under normal circumstances, although they may vary when the area is hit by a hurricane. These conditions include tidal conditions, current velocities, SLR and salinity.

Tides. Tidal data is retrieved from NOAA Tides and Currents (2013b). The Galveston Bay experiences semi-diurnal tides. At Bolivar Roads the mean tidal range⁽¹⁾ is 0.35 m [1.16 ft]. Under high declination (2 tides per day) the tidal prism in the entire Galveston Bay system is $2.8 \cdot 10^8 \text{ m}^3$ [$9.9 \cdot 10^9 \text{ ft}^3$]. Under low declination (1 tide per day) the tidal prism is $0.85 \cdot 10^8 \text{ m}^3$ [$3.0 \cdot 10^9 \text{ ft}^3$] (Lester and Gonzalez, 2002).

Currents and discharge. Maximum current velocities in Bolivar Roads are 1.0 m/s [3.3 ft/s]. According to Ruijs (2011) a 40% decrease in inflow area due to the construction of a storm surge barrier results in a current velocity of 1.3 m/s [4.3 ft/s] at Bolivar Roads. This value meets the maximum current velocity for navigation, see Section 4.2.3. The average river discharge through Bolivar Roads Pass is $540 \text{ m}^3/\text{s}$ [$1.9 \cdot 10^4 \text{ ft}^3/\text{s}$], see Section 2.2.1.

Sea Level Rise. For the storm surge barrier the assumption for the relative Sea Level Rise (SLR) during its 100 year lifetime is based on three resources. SLR in the Galveston Bay has occurred due to three reasons: the global SLR, natural compactional subsidence of Gulf Coast sediments and land surface subsidence caused by excessive groundwater withdrawals (Lester and Gonzalez, 2002). The extraction of oil and gas also accelerates land surface subsidence. SLR is a relatively larger threat to Galveston Island than to other coastal areas in the U.S. as it sinks (subsides) at a faster rate, see Figure D.3. NOAA Tides and Currents (2013a) reports a mean SLR of 6.84 mm/yr [0.27 in/yr] based on monthly sea level data from 1957 to 2006. Just based on this historical data it would result in a SLR of 0.68 m [2.24 ft] in 2100.

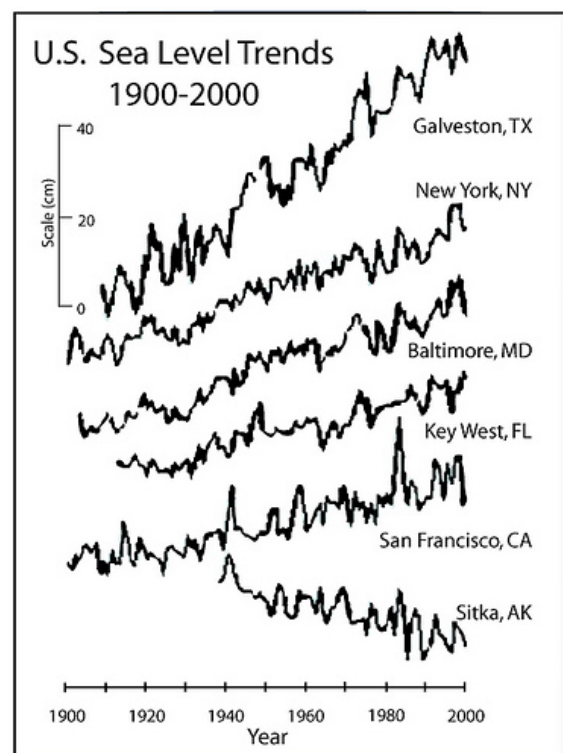


Figure D.3: U.S. Sea Level Trends 1900-2000 (NOAA/US EPA, 2009).

The Intergovernmental Panel on Climate Change (IPCC) releases an extensive study detailing the Earth's climate every six years. The 2007 IPCC report predicts that the upper bound range of global SLR by 2100 will be 0.78 m [2.6 ft] (Pachauri, 2008). However, a more recent study executed by Schellnhuber et al. (2012) indicates there is roughly a 20% likelihood of exceeding 1.0 m [3.3 ft] SLR by 2100 due to accelerated glacial and Antarctic ice melt in recent years. Taking into account the relatively fast land-subsidence of Galveston Island and this prediction by Schellnhuber et al. (2012) the assumed SLR for the storm surge barrier is 1.0 m [3.3 ft].

Salinity. Salinity at Bolivar Roads amounts 25-30 parts per thousand (Lester and Gonzalez, 2002).

⁽¹⁾The mean tidal range is the difference in height between MHW and MLW (NOAA Tides and Currents, 2011).

D.2.2 Hurricane conditions

Hurricanes are tropical storm systems with a low-pressure core surrounded by a spiraling arrangement of thunderstorms. They require a warm ocean, a moist atmosphere and favorable wind pattern. The intensity of a hurricane is based on the SSHWS (see Appendix D.3.3). One hurricane season (which runs between June 1 and November 30) produces 15 hurricanes but only a few make landfall in the United States. The upper Texas shore is affected by a major hurricane about every 15 years (Merrell, 2010b). Between 1900 and 2012 a total of 28 hurricanes made landfall within a 200 km [124 mi] radius of Galveston. The limited availability of historical records makes it very hard to assess the long-term risk of the most intense hurricanes (Emanuel and Jagger, 2010). This, in turn, makes it difficult to determine an accurate relation between surge height and hurricane return period. In this thesis the peak surge height for certain return periods is based on results by Stoeten (2013). They are presented in Appendix D.2.3. Next to the peak surge height other hurricane characteristics that have to be addressed are the presence of forerunners and the circular surge pattern within the Galveston Bay. These are also described in this section.

Forerunners. Far in advance of the landfall of Hurricane Ike a unpredicted water level increase appeared along the Texas coast, referred to as a *forerunners*. The observations of Ike's forerunner surge were similar to descriptions of The Great Storm of 1900. Kennedy et al. (2011) diagnosed Ike's forerunner as being generated by so-called 'Ekman setup' in the continental shelf. The forerunner surge generated a freely propagating continental shelf wave with greater than 1.4 m [4.6 ft] peak elevation that travelled 300 km [186 mi] in advance of the storm track at the time of landfall. The surge began to increase strongly at 24 hours before landfall over much of the region. At Bolivar Peninsula the forerunner surge peaked 12 hours before landfall, reaching an elevation of MSL+3.0 m [MSL+9.8 ft] (Kennedy et al., 2011). The forerunner caused Ike's high water to arrive earlier, stay longer, and cause more damage than was otherwise expected (Cushman, 2009).

As Ike's forerunner contributed to the duration and height of the surge intensity these should also be blocked. Therefore the presence of a forerunner is taken into account in the design surge level, see Section 5.2.

Landfall location. The swirling character of a hurricane induces various loads on dike rings in an basin. Figure D.4 is an schematic illustration of the Galveston Bay simplified as a semi-enclosed bay. It shows the influence of hurricane landfall location on surge height. Hurricanes making landfall West of the bay will force water into the system, increasing the surge. As the hurricane moves onshore, the wind direction shifts from East (stage 1) to South (stage 2) to West (stage 3). If the hurricane makes landfall on the east side of the bay, this circulation pattern will be vice versa (Stoeten, 2013). On the Northern Hemisphere, hurricanes turn counter-clockwise. On south-facing coasts like the Upper Texas Coast, the strongest on-shore winds occur east of the eye. A hurricane track west of the bay therefore generates most severe conditions at Bolivar Roads and inside the bay.

Note: this effect depends heavily on the size of the Hurricane compared to the bay dimensions.

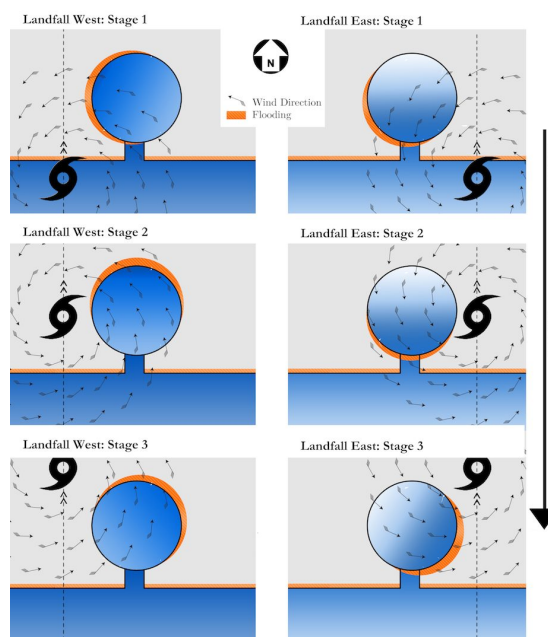


Figure D.4: Influence of landfall location on storm surge within semi-enclosed bays (Stoeten, 2013).

D.2.3 Surge height and waves

The storm surge and wave heights for different return periods are presented in Table D.1. A brief explanation of the acquired data is presented below the table.

Table D.1: Surge and wave heights for different protection levels.

Return period [yr ⁻¹]	$h_{surge}^{(1)}$ [m]	$H_{max}^{(2)}$ [m]	$H_s^{(3)}$ [m]	$T_p^{(4)}$ [s]
1/10	2.9	3.5	2.0	6.5
1/100	3.9	4.3	2.4	6.6
1/1,000	4.8	5.1	2.8	7.8
1/10,000	5.4	5.9	3.3	7.9

(1) Surge height h_{surge} based on computations by Stoeten (2013).

(2) Maximum wave height H_{max} based on near shore Hurricane Ike data near San Luis Pass Bridge (Jin et al., 2010a). This is assumed to be representative for Bolivar Roads.

(3) According to Goda (1985) the near shore maximum wave height H_s is approximately a factor 1.8 smaller than the significant wave height H_{max} .

(4) Peak wave period T_p based on near shore Hurricane Ike data near San Luis Pass Bridge (Jin et al., 2010b). This is assumed to be representative for Bolivar Roads.

D.3 Meteorological conditions

This section presents annual meteorological data and data under hurricane conditions. It also contains the Saffir-Simpson Hurricane Wind Scale (SSHWS) in Appendix D.3.3.

D.3.1 Annual data

Wind data is retrieved from NOAA Tides and Currents (2013b) at the Galveston Pleasure Pier station. From Figure D.5 can be seen that dominant wind directions are south, southeast and north. Annual rainfall in Galveston averages 1104 mm [43.46 in]. From Table D.2 can be concluded that most precipitation falls during the hurricane season which runs from June to November.

Table D.2: Average precipitation for Galveston Scholes International Airport, 1981-2010 (NWS Weather Forecast Office, 2013).

	Jan	Feb	Mar	Apr	May	Jun	Jul	Aug	Sep	Oct	Nov	Dec	Annual
Prec. [mm]	83	50	87	52	55	111	100	103	152	122	105	84	1104
Prec. [in]	3.28	1.95	3.44	2.05	2.18	4.37	3.93	4.07	5.97	4.79	4.13	3.31	43.46

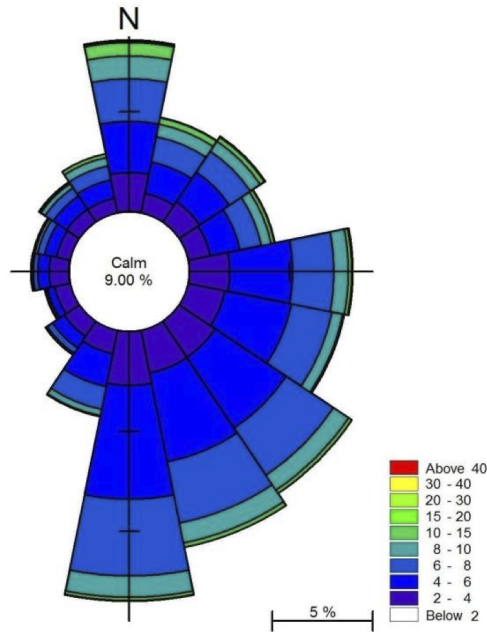


Figure D.5: Wind rose Galveston Pleasure Pier station, 1983 - 2006. Units: m/s. (NOAA Tides and Currents, 2013b).

D.3.2 Hurricane data

Under hurricane conditions wind speeds and precipitation increase firmly compared to annual averages. The maximum wind speed when hurricane Ike made landfall were 176 km/h [95 kt] while maximum wind velocities in hurricanes can exceed speeds of over 240 km/h [130 kt] (Smith and Ward, 1998).

The highest amount of rainfall reported during Hurricane Ike was 480 mm [18.9 in] just north of Houston along Spring Creek (Berg, 2009), which is well over one-third over the annual rainfall in just a few hours. Average rainfall over the Galveston Bay Area over 48 hours during Ike amounts about 200 mm [8 in], resulting in just a slight increase in water level in the Galveston Bay that does not coincide with the peak storm intensity (NWS Weather Forecast Office, 2008a).

D.3.3 Saffir-Simpson Hurricane Wind Scale

The Saffir-Simpson Hurricane Wind Scale (SSHWS) is a 1 to 5 categorization based on a hurricane's intensity at the indicated time developed by wind engineer Herb Saffir and meteorologist Bob Simpson. The scale provides examples of the type of damage and impacts in the United States associated with winds of the indicated intensity.

Table D.3: Saffir-Simpson Hurricane Wind Scale (Schott et al., 2012; Stewart, 2008)

Cat.	Maximum 1-min wind speed	Maximum 10-min wind speed	Types of damage due to hurricane winds
1	74-95 mph 64-82 kt 119-153 km/h 33-42 m/s	66-85 mph 57-74 kt 106-137 km/h 30-38 m/s	Very dangerous winds will produce some damage: Well-constructed frame homes could have damage to roof, shingles, vinyl siding and gutters. Large branches of trees will snap and shallowly rooted trees may be toppled. Extensive damage to power lines and poles likely will result in power outages that could last a few to several days.
2	96-110 mph 83-95 kt 154-177 km/h 43-49 m/s	86-98 mph 75-85 kt 138-158 km/h 38-44 m/s	Extremely dangerous winds will cause extensive damage: Well-constructed frame homes could sustain major roof and siding damage. Many shallowly rooted trees will be snapped or uprooted and block numerous roads. Near-total power loss is expected with outages that could last from several days to weeks.
3	111-129 mph 96-112 kt 178-208 km/h 50-58 m/s	99-115 mph 86-100 kt 159-185 km/h 44-51 m/s	Devastating damage will occur: Well-built framed homes may incur major damage or removal of roof decking and gable ends. Many trees will be snapped or uprooted, blocking numerous roads. Electricity and water will be unavailable for several days to weeks after the storm passes.
4	130-156 mph 113-136 kt 209-251 km/h 58-69 m/s	116-137 mph 101-119 kt 186-220 km/h 52-61 m/s	Catastrophic damage will occur: Well-built framed homes can sustain severe damage with loss of most of the roof structure and/or some exterior walls. Most trees will be snapped or uprooted and power poles downed. Fallen trees and power poles will isolate residential areas. Power outages will last weeks to possibly months. Most of the area will be uninhabitable for weeks or months.
5	>157 mph >137 kt >252 km/h >70 m/s	>138 mph >120 kt >221 km/h >62 m/s	Catastrophic damage will occur: A high percentage of framed homes will be destroyed, with total roof failure and wall collapse. Fallen trees and power poles will isolate residential areas. Power outages will last for weeks to possibly months. Most of the area will be uninhabitable for weeks or months.

D.4 Geotechnical conditions

Drillers' logs of wells provide information about the deeper soil layers in Galveston County (Petitt and Winslow, 1955). It reports the county is underlain by sequences of unconsolidated sands and clays; the so-called Beaumont clay formations. The sediments are mostly of alluvial or deltaic origin.

Both the driller's logs and research into the hydrogeology of gulf coast aquifers report that between 0–150m below MSL [0–500 ft] predominantly clay layers are present. Between 150–215 m below MSL [500–700 ft], a more sandy clay layer is present, the Alta Loma formation, which is part of the Beaumont clay.

D.4.1 Soil information

In order to accurately design the foundation of a storm surge barrier near surface soil information is required. Boring logs that contain very detailed information about the upper soil layers are gathered in the TxSed Sediment

Viewer database (TxSed Mapping Viewer, 2013). Unfortunately, this database only contains accurate soil information for Bolivar Roads to a depth of MSL-13m [43 ft]. As the Houston Shipping Channel (HSC) is already dredged until a depth of approximately MSL-13m [43 ft] this information is mostly irrelevant for the barrier design.

There are two boring logs located northward along the HSC into the Galveston Bay (USACE16872-31 and USACE14872-32) that reach a depth of MSL-19m [64 ft]. Both logs indicate mainly clay and clayey layers. Refer to Figure D.7 for their location.

Information about the soil layers below MSL-19m [43 ft] is only available at the east end of Galveston Island. The reported logs located at the shoreline of the Bolivar Roads Pass are part of a reconnaissance study executed to investigate piling support in the Port of Galveston. This study by McClelland Engineers (1985), contains six sample borings to explore local subsurface conditions that reach a depth of approximately MSL-50m [165 ft]. It gives a good impression of the soil layers in this location, that could be representative for Bolivar Roads Pass. Figure D.6 is an illustration of the generalized subsurface profile based on these borings (see Figure D.7 for the exact locations).

D.4.2 Soil strength

Figure D.6 gives a good impression of the deeper-lying soil layers. As can be seen, a thick stratum of very dense sand is present at a level of approximately MSL-40m [131 ft]. McClelland Engineers (1985) report this soil layer as "an excellent bearing layer for high capacity piles". The test results state that the soil is able to resist a force of 6672 kN [$1.5 \cdot 10^3$ kips] by closed end pipe piles with a diameter of 0.61 m [24 in]. The strength of the cohesive soil layers is summarized in Table 5.2. This information is also adopted from the study performed by McClelland Engineers (1985).

E Barrier system

This appendix presents calculations and an elaborated approach as used in the first design step on barrier system level (chapter 6).

E.1 Overflow distribution

In this section several different divisions of retaining height are calculated. Its results are used in Section 6.3.

E.1.1 Open Navigation section

It is investigated whether applying no barrier for the navigational section is feasible. This is done by the next four-stepped procedure.

1. The navigational section is designed as indicated in Figure 6.4. It consists of a channel with length $L_{channel} = 1000$ m, channel depth $d_{channel} = 17$ m and a width of $B_{channel} = 220$ m, protected by breakwaters on each side. The bottom protection is made of large stones with $D_n = 1.0$ m to increase the bottom roughness. The environmental section is fully retaining.
2. Next the $1/10,000$ yr⁻¹ design storm as defined in Section 5.2 is released on this barrier. This design storm consists of 528 water level data points with a time interval of 5 minutes. The location of these levels is on the open coast, right in front of Bolivar Roads.

For a straight and short channel ($L_{channel} \ll \lambda_{surge}$) with negligible storage ($A_{channel} \ll A_{bay}$) the water level inside the bay may be determined using the so-called 'rigid-column approximation' as presented in Equation (E.1) (Labeur, 2007). This formula is used to calculate water levels in a semi-enclosed basin that is connected to the sea through one narrow channel.

$$h_{bay} = h_{coast} - \left(\frac{1}{2} + c_f \frac{L_{channel}}{R_c} \right) \frac{|Q_c| Q_c}{g A_c^2} \text{ [m]} \quad \text{E.1}$$

In which:

h_{bay}	[m]	Water level inside bay
h_{coast}	[m]	Water level open coast
c_f	[-]	Friction coefficient, see Equation (E.2)
$L_{channel}$	[m]	Channel length (= 1000 m)
Q_c	[m ³ /s]	Discharge through channel
R_c	[m]	Hydraulic radius, see Equation (E.4)
A_c	[m ²]	Flow area of channel

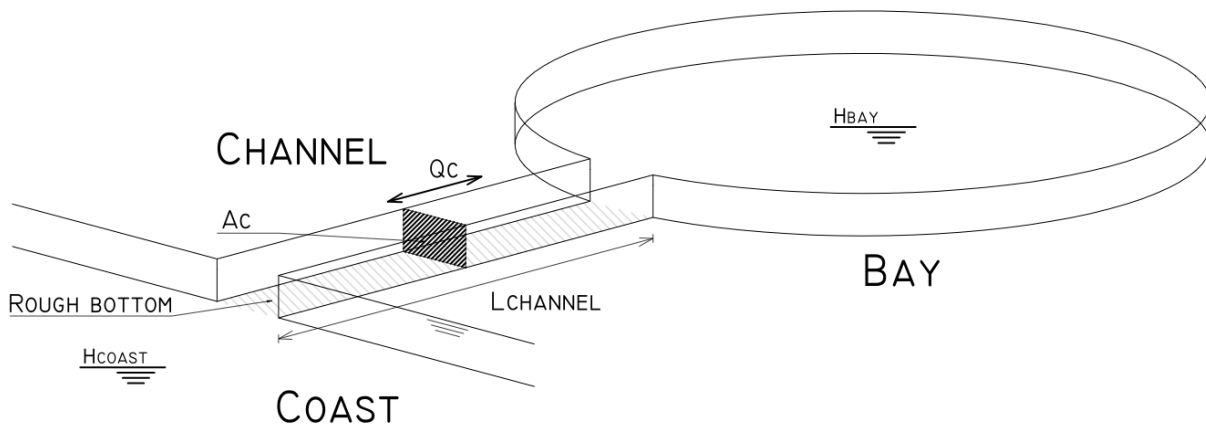


Figure E.1: Schematic view of the rigid-column approximation.

The friction factor c_f is determined using the following formula (Labeur, 2007):

$$c_f = \frac{g}{C^2} [-] \quad \text{E.2}$$

In which c_f is the dimensionless friction coefficient, g the gravitational constant ($= 10 \text{ m/s}^2$) and C the Chézy coefficient in $[\text{m}^{1/2}/\text{s}]$. The latter one is defined by (Lin, 2001):

$$C = 18 \cdot \log \left(\frac{12 \cdot d_{channel}}{H_{ripple}} \right) [\text{m}^{1/2}/\text{s}] \quad \text{E.3}$$

In which:

C	$[\text{m}^{1/2}/\text{s}]$	Chezy coefficient. $C \approx 57$ for the no-barrier situation and ≈ 42 for the barrier with open Navigation section.
$d_{channel}$	$[\text{m}]$	Channel depth
H_{ripple}	$[\text{m}]$	Height of bed ripples. Assumed 0.1 m for Bolivar Roads under regular circumstances and 1 m for Navigation channel with bed protection consisting of stones with diameter $D_{90} = 1.0 \text{ m}$.

The hydraulic radius R_c is determined using:

$$R_c = \frac{A_c}{2 \cdot d_{channel} + B_{channel}} [\text{m}] \quad \text{E.4}$$

In which $d_{channel}$ is the channel depth, $B_{channel}$ the channel width and A_c is the flow area ($= d_{channel} \cdot B_{channel}$).

3. Equation (E.1) contains two unknown variables; h_{bay} and Q_c . In order to solve this system an additional equation is required to compute the water levels inside the bay. It is the balance equation between water inflow at Bolivar Roads and the resulting Bay's water level. It is applied under the assumptions that river inflow is neglected and Bolivar Roads is the only connection to the Gulf of Mexico. The West Bay (see Figure 2.1) does not contribute to the Galveston Bay's retention capacity (Lester and Gonzalez, 2002). It is assumed that water in the West Bay exchanges with the Gulf of Mexico only through the San Luis Pass.

$$h_{bay}(i+1) = h_{bay}(i) + \frac{Q_c(i) \cdot \Delta t}{A_{bay}} \text{ [m]} \quad \text{E.5}$$

In which:

$h_{bay}(i+1)$	[m]	Water level inside bay, at $t = i + 1$
$h_{bay}(i)$	[m]	Water level inside bay, at $t = i$
$Q_c(i)$	[m ³ /s]	Discharge through channel, at $t = i$
Δt	[s]	Timestep between datapoints (= $5 \cdot 60 = 300$ s)
A_{bay}	[m ²]	Surface area of Galveston Bay (= $1339 \cdot 10^6$ m ²) ⁽¹⁾

⁽¹⁾The total area of the Galveston Bay minus the area of the West bay, which does not contribute to the retentional capacity as it receives its water exchange through San Luis Pass (Lester and Gonzalez, 2002).

4. By using Equations (E.1) to (E.5) the water levels inside the bay due to an open navigation section can be calculated. The results for an open Navigation section compared to the current situation⁽¹⁾ is presented in Figure E.2.

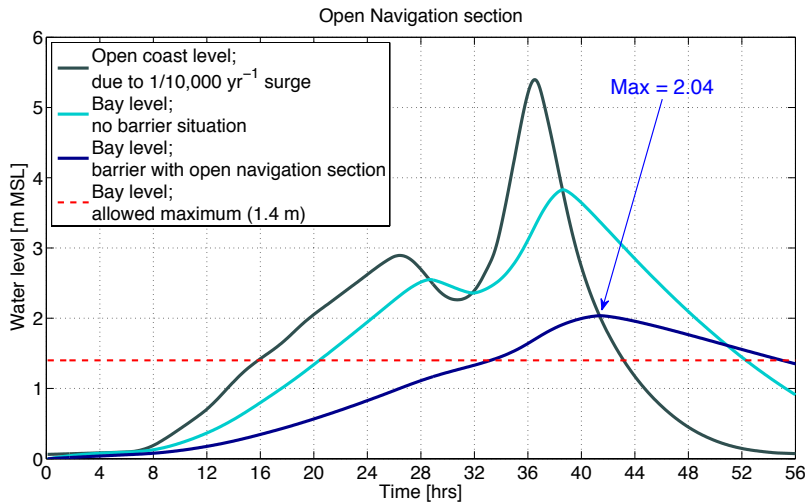


Figure E.2: Bay water levels under a $1/10,000$ yr⁻¹ storm. Current situation compared to applying a barrier with full open Navigation section.

E.1.2 Both sections limited retaining

In this subsection it is investigated what the optimal division between retaining heights of the navigational and environmental sections is. This is done using a similar procedure as for the barrier with open navigational section. This design storm consists of 528 water level data points with a time interval of 5 minutes. The location of these levels is on the open coast, right in front of Bolivar Roads.

⁽¹⁾For the current situation the following parameters are assumed: $C \approx 57$ (see Equation (E.3)), $L_{channel} = 10,000$ m, $B_{channel} = 2,757$ m (see Figure 6.2, and $d_{channel} = 9$ m on average).

1. For the situation where water flows over a barrier the rigid-column approximation in Appendix E.1.1 does not hold anymore. The barrier's retaining character now changed from a rough channel into a weir. Therefore a relation for flow over a (submerged) sharp-crested weir is applied. The formula for flow over such a weir reads (Reed and Sanchez, 2010):

$$Q_w = c_{df} c_w \sqrt{g} B_{weir} (h_{coast} - h_{bay})^{1.5} \text{ [m}^3/\text{s]} \quad \text{E.6}$$

In which:

Q_w	[m ³ /s]	Discharge over weir
c_{df}	[-]	Submergence correction factor, see Equation (E.7)
c_w	[-]	Weir coefficient (= 0.58) ⁽¹⁾
$d_{channel}$	[m]	Channel depth
B_{weir}	[m]	Weir crest length
h_{coast}	[m]	Water level open coast
h_{bay}	[m]	Water level inside bay

⁽¹⁾According to Reed and Sanchez (2010).

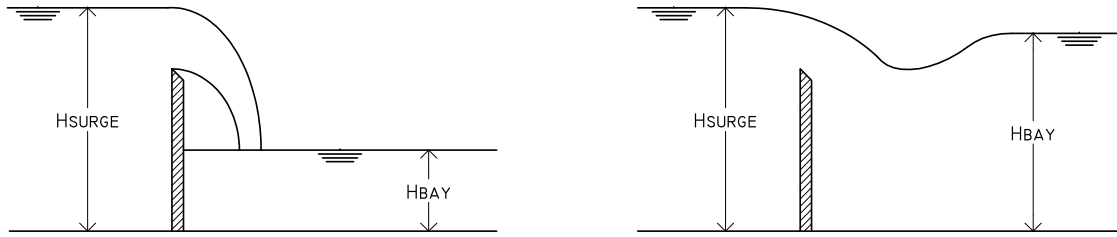


Figure E.3: Schematic side view of a storm surge barrier modeled as a sharp crested weir. In free flow and submerged conditions respectively. Based on Reed and Sanchez (2010).

The weir submergence correction factor c_{df} is determined using (Reed and Sanchez, 2010):

$$c_{df} = 1 - \left(\frac{h_{bay}}{h_{coast}} \right)^{1.5} \text{ [-]} \quad \text{E.7}$$

In which h_{bay} is the water level inside the bay and h_{coast} the water level on the open coast.

2. There are two unknown variables in Equation (E.6): h_{bay} and Q_w . In order to solve this system an additional equation is required to compute the water levels inside the bay, which is similar to Equation (E.5).

$$h_{bay}(i+1) = h_{bay}(i) + \frac{Q_w(i) \cdot \Delta t}{A_{bay}} \text{ [m]} \quad \text{E.8}$$

In which:

$h_{bay}(i+1)$	[m]	Water level inside bay, at $t = i + 1$
$h_{bay}(i)$	[m]	Water level inside bay, at $t = i$
$Q_w(i)$	[m ³ /s]	Discharge over weir, at $t = i$
Δt	[s]	Timestep between datapoints ($= 5 \cdot 60 = 300$ s)
A_{bay}	[m ²]	Surface area of Galveston Bay ($= 1339 \cdot 10^6$ m ²) ⁽¹⁾

⁽¹⁾The total area of the Galveston Bay minus the area of the West bay, which does not contribute to the retentional capacity as it receives its water exchange through San Luis Pass (Lester and Gonzalez, 2002).

3. When using Equations (E.6) to (E.8) the water level inside the bay under hurricane conditions can be calculated. This is done for different distributions of retaining height between the navigational and environmental section. See Figures E.4 to E.6. The distributions are drafted in such a way that the peak water level rise in the bay does not exceed the maximum of 1.4 m [3 ft] as it is defined in Section 4.4.4.

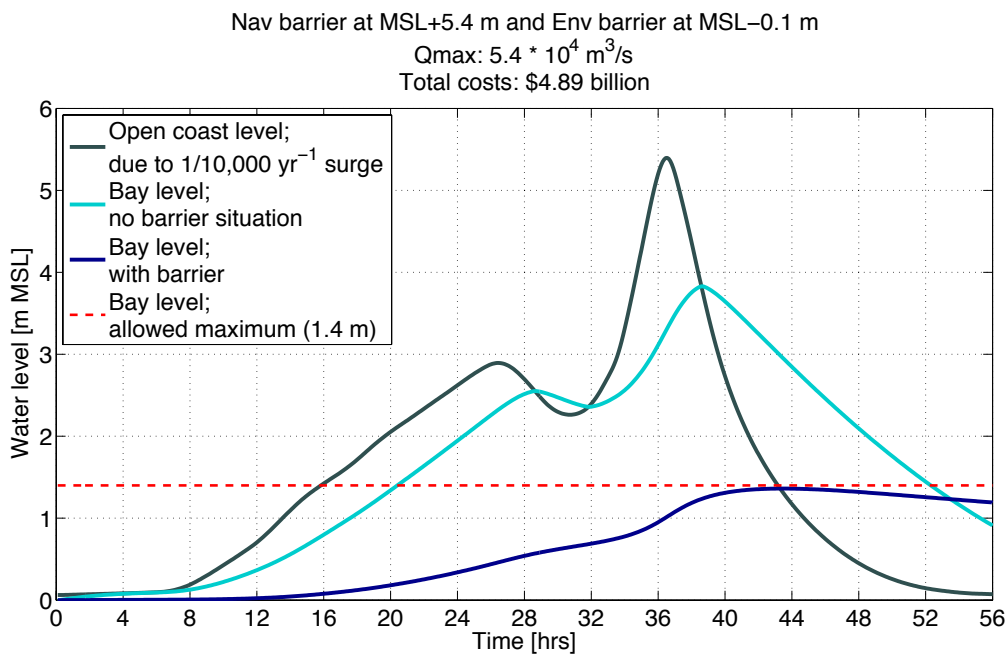


Figure E.4: Navigational section fully retaining (MSL+5.4m), environmental section semi-open (MSL-0.1m)

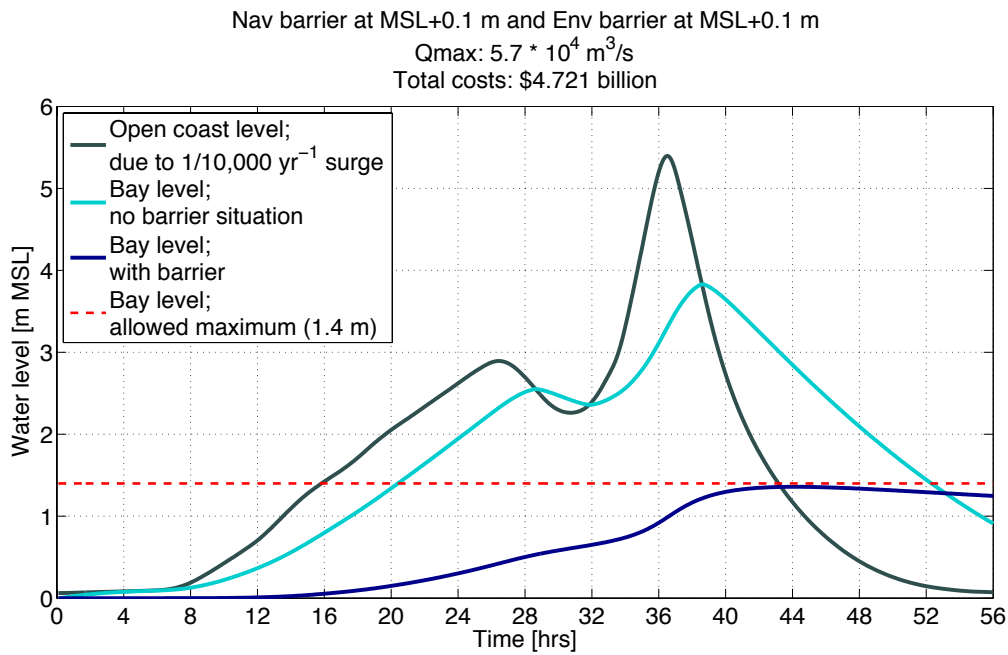


Figure E.5: Both sections equally retaining (MSL+0.1m)

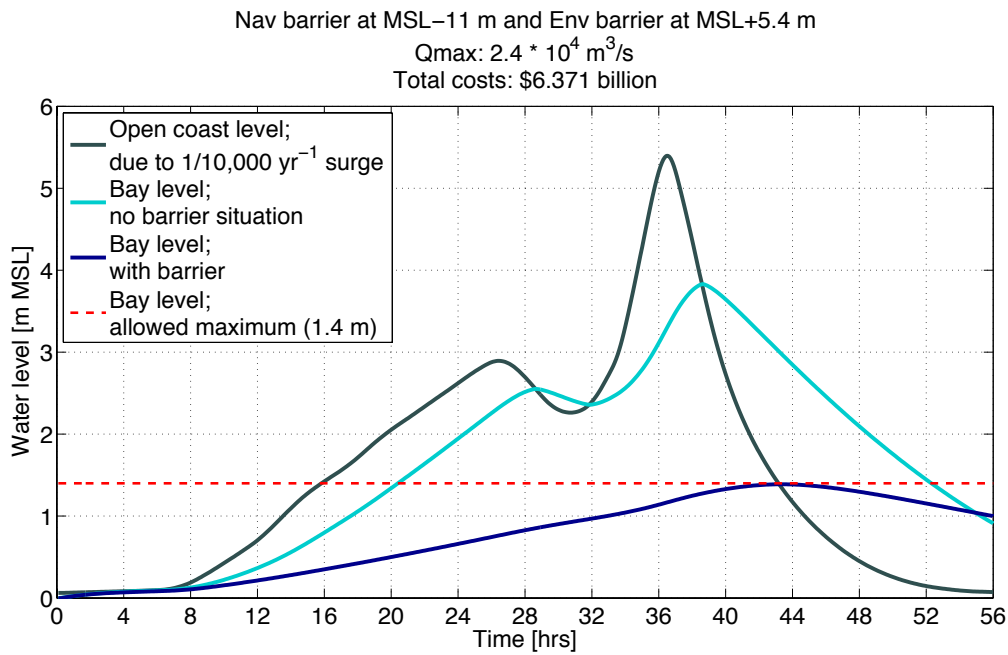


Figure E.6: Navigational section semi-open (MSL-11.0m), environmental section fully retaining (MSL+5.4m)

4. However, the question was to find the most cost-effective division in retaining height for the barrier. An expression for direct construction costs is presented in Equation (6.1), and reads (van der Toorn, 2012):

$$O_b = B_b \cdot \Delta h_b \cdot h_{c,b} \cdot B_b \cdot o_{U,b} \quad \text{E.9}$$

In which:

O_b	[\$]	Total investment costs for the storm surge barrier
Δh_b	[m]	Maximum water level difference over barrier (equal to the maximum surge level h_{surge})
$h_{c,b}$	[m]	Construction height barrier (measured from the channel bottom until the barrier's crest)
B_b	[m]	Barrier span
$o_{U,b}$	[\$/(m \cdot m \cdot m)]	Unit costs barrier

The construction costs of the barrier are influenced by the construction height $h_{c,b}$. As already stated in Section 6.1 the influence of construction height on costs can be minimized by optimizing the division between the construction heights for the navigational and the environmental section, as these have their own unit costs. The unit costs for the navigational section are assumed to be larger, as the large span requires a more complicated and expensive structure. The environmental section does not require a minimum span, so it is likely that the unit costs for this span are somewhat lower. Using unit cost estimations by van der Toorn (2012) the unit costs $o_{U,b}$ are assumed to be 40,000 and 30,000 \$/(m \cdot m \cdot m) for the navigational and environmental section respectively.

5. Using Equation (E.9) the total costs for barriers with varying distributions in constructing height are drafted. Now three configurations with their corresponding construction costs are presented in Table E.1.

Table E.1: Costs and peak discharge of three overflow configurations.

	Barrier height ⁽¹⁾		Construction costs	Peak discharge over barrier
	Nav. section	Env. section		
Config. 1, see Figure E.4	MSL+5.4 m	MSL-0.1 m	\$ 4.9 billion	$5.4 \cdot 10^4 \text{ m}^3/\text{s}$
Config. 2, see Figure E.5	MSL+0.1 m	MSL+0.1 m	\$ 4.7 billion	$5.7 \cdot 10^4 \text{ m}^3/\text{s}$
Config. 3, see Figure E.6	MSL-11.0 m	MSL+5.4 m	\$ 6.3 billion	$2.4 \cdot 10^4 \text{ m}^3/\text{s}$

⁽¹⁾A fully retaining barrier height is assumed to be equal to the maximum surge height = 5.4 m. Wave overtopping is not yet taken into account here.

Note: it is obvious that the most cost-effective configuration in retaining height appears to be an equal height. This is because the water level difference ($h_{coast} - h_{bay}$) goes to the power 3/2, see Equation (E.6). This results in higher costs when constructing barriers of non-equal retaining height. Note 2: in Table E.1 the costs for the different distributions in retaining height are asymmetrical. This is due to the difference in length of the barrier span and the distinct cost unit rates.

6. The plots of the water levels inside the bay under a 1/10,000 yr⁻¹ storm are presented in Figures E.4 to E.6.

F Environmental barrier

This appendix presents calculations and an elaborated approach as used in the second design step on the environmental barrier design level (chapter 7). At this preliminary design stage all calculations are in the Serviceability Limit State (SLS). Only material safety factors are applied yet.

F.1 Design input

This section contains design input for the environmental barrier design level. They are divided in general parameters, soil properties, relevant water levels, concrete properties and wave characteristics.

F.1.1 General parameters

First some general parameters are assumed. The specific weights and gravitational constant are assumed as:

ρ_c	[kN/m ³]	Mass density of concrete (= 25.00 kN/m ³)
ρ_{sw}	[kN/m ³]	Mass density of salt water (= 10.25 kN/m ³)
$\rho_{c,w}$	[kN/m ³]	Mass density of concrete under water (= $\rho_{sw} - \rho_c = 14.75$ kN/m ³)
g	[m/s ²]	Gravitational constant (= 10)

F.1.2 Soil properties

According to data from Section 5.4 the assumed soil properties are presented in Table E.1. A cross section of the soil layers and the position of the caisson foundations is shown in Figure E.1.

Table E.1: Soil properties per layer.

Layer i	Depth [MSL-m]	Class	$\rho_{s,i}^{(1)}$ [kN/m ²]	$\sigma_{su,i}^{(2)}$ [kN/m ²]	$c_f^{(3)}$ [-]
1	0 - 3	Very soft clay	13	12	0.35
2	3 - 15	Loose sand	19 ⁽⁴⁾	24	0.50
3	15 - 20	Soft to firm clay	14	24	0.35
4	20 - 32	Firm clay	15	36	0.35
5	32 - 40	Firm to stiff clay	17	48	0.35
6	Below 40	Very dense sand		20	0.50

(1) Saturated volumetric weight $\rho_{s,i}$ according to TGB (1990).

(2) Undrained shear strength $\sigma_{su,i}$ according to Table 5.2.

(3) Friction factor c_f according to NFEC (1986).

(4) Shear strength loose sand layer assumed to be equal to the underlying clay layer.

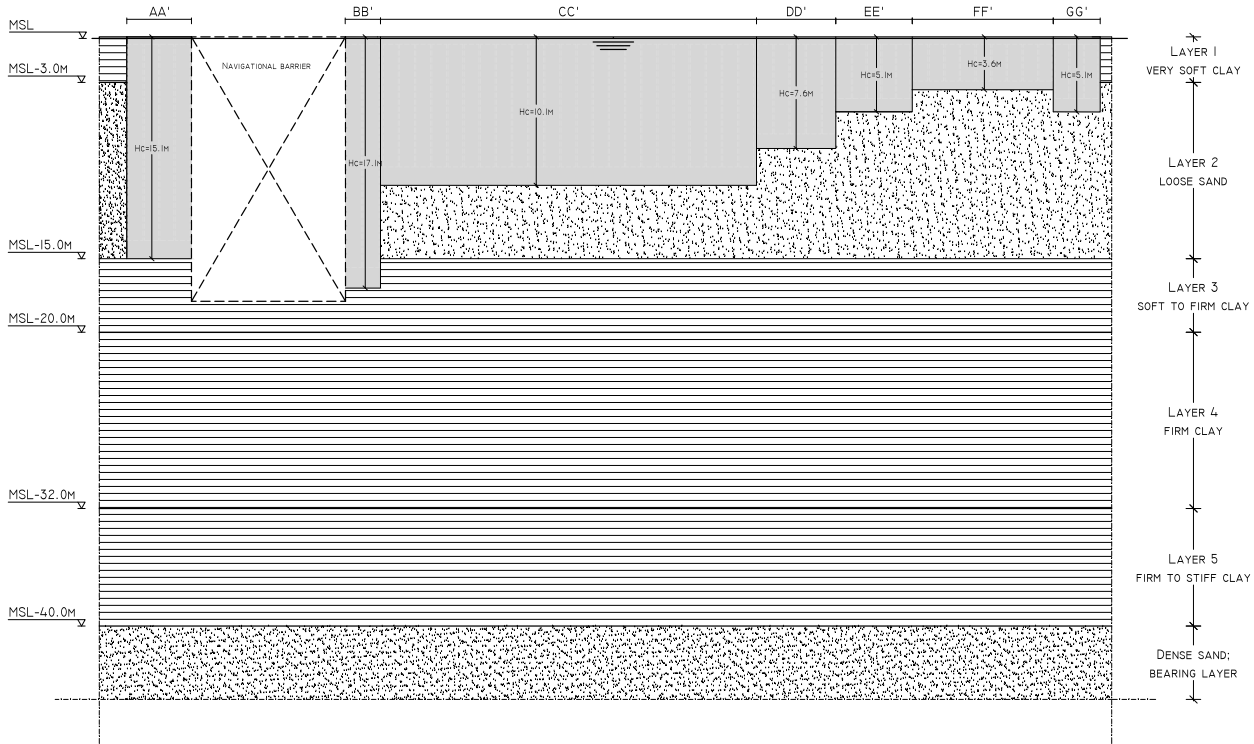


Figure F.1: Cross-sectional view of Bolivar Roads indicating soil layers under caisson foundations. Dimensions not to scale.

F.1.3 Relevant heights, depths and water levels

Relevant depths and water levels are presented below. See also Figures E3 and E4.

h_1	[m]	Maximum surge level ($= h_{surge}$)
h_2	[m]	Corresponding level in the Bay, from Figure 6.8 and section 7.2
d_{local}	[m]	Local water depth at the barrier ⁽¹⁾
h_{sill}	[m]	Crest height of the barrier above MSL ($= 0.1\ m$, see Section 6.4)
d_1	[m]	Water depth during surge on ocean side of barrier ($= d_{local} + h_1$)
Δh_{surge}	[m]	Height of surge above the barrier crest ($= h_1 - h_{sill}$)

⁽¹⁾Varies along the barrier span, see Figure 7.3

F.1.4 Waves

The wave parameters are split up in regular conditions (these values are assumed during construction phase) and storm surge conditions.

Wave heights and periods in regular conditions are assumed using data from (NOAA Tides and Currents, 2013b). Offshore wave height and period in regular circumstances are:

$H_{s,reg}$	[m]	Significant wave height regular circumstances ($= 0.5\ m$)
$T_{p,reg}$	[s]	Peak wave period regular circumstances ($= 4\ s$)

During storm surge the offshore waves have the following height and period:

$H_{max,0}$	[m]	Maximum offshore wave height ($= 3.3\ m$, see Table D.1)
$T_{p,0}$	[s]	Offshore peak wave period ($= 7.9\ s$, see Table D.1)

Offshore wave length and wave number are calculated assuming deep water:

$$\lambda_0 = \frac{g T_{p,0}^2}{2\pi} \quad [\text{m}]$$

$$k_0 = \frac{2\pi}{\lambda_0} \quad [\text{m}^{-1}]$$
E.1

Using the offshore wave length and offshore wave number the wave length near the storm surge barrier can be iteratively calculated. It is dependent on the local water depth, so it varies along the barrier span. The wave number near the barrier depends on the wave length near the barrier, and varies also along the barrier span.

$$\lambda_1 = \lambda_0 \cdot \tanh\left(2\pi \cdot \frac{d_1}{\lambda_1}\right) \quad [\text{m}]$$

$$k_1 = \frac{2\pi}{\lambda_1} \quad [\text{m}^{-1}]$$
E.2

The variable of interest is the wave height near the barrier; $H_{max,1}$. This one is necessary to eventually calculate the horizontal force on the barrier. To calculate the near-barrier wave height the so-called shoaling of waves has to be taken into account, and can be calculated using the next formula (Vrijling et al., 2011). Note: it is assumed that waves attack perpendicular on the barrier, so the influence of refraction can be neglected.

$$H_{max,1} = c_{sh} \cdot H_{max,0} \quad [\text{m}]$$
E.3

With the shoaling coefficient c_{sh} defined as:

$$c_{sh} = \frac{1}{\sqrt{\tanh(k_1 d_1) \cdot \left(1 + \frac{2 \cdot k_1 d_1}{\sinh(2 \cdot k_1 d_1)}\right)}} \quad [-]$$
E.4

Finally for each water depth during the surge d_1 it will be checked whether waves are breaking or not. This is checked by the next rule of thumb (Vrijling et al., 2011). Breaking waves have a different load on the structure.

$$\frac{H_{max,1}}{\lambda_1} \geq \frac{1}{7}$$
E.5

F.1.5 Concrete properties

Concrete properties can be listed in the next table.

Table E.2: Characteristics of concrete classes (TGB, 2013).

Class	f_{ckc} [N/mm ²]	f_{ck} [N/mm ²]	f_{cm} [N/mm ²]	f_{ctm} [N/mm ²]	$f_{ctk,0.05}$ [N/mm ²]	$f_{ctk,0.95}$ [N/mm ²]	E_{cm} [10 ³ N/mm ²]
C12/15	12	15	20	1.6	1.1	2.0	27
C20/25	20	25	28	2.2	1.5	2.9	30
C30/37	30	35	38	2.9	2.0	3.8	33
C35/45	35	45	43	3.2	2.2	4.2	34
C45/55	45	55	53	3.8	2.7	4.9	36
C55/67	55	67	63	4.2	3.0	5.5	38

With:

f_{cke}	[N/mm ²]	Characteristic compressive cylinder strength of concrete at 28 days
f_{ck}	[N/mm ²]	Characteristic compressive cube strength of concrete at 28 days
f_{cm}	[N/mm ²]	Mean value of concrete cylinder compressive strength after 28 days
f_{ctm}	[N/mm ²]	Mean value of axial tensile strength of concrete
$f_{ctk,0.05}$	[N/mm ²]	Characteristic axial tensile strength of concrete, 0.05 fractile
$f_{ctk,0.95}$	[N/mm ²]	Characteristic axial tensile strength of concrete, 0.95 fractile
E_{cm}	[N/mm ²]	Young's modulus of concrete

For the barrier a concrete class B45 is assumed. Using a material factor $\gamma_{c,M} = 1.25$ for concrete the design value for compressive and tensile strength can be computed:

$$f_{cd} = \frac{f_{ck}}{\gamma_{c,M}} = 36 \quad [\text{N/mm}^2]$$

$$f_{ctd} = \frac{f_{ctk,0.05}}{\gamma_{c,M}} = 1.76 \quad [\text{N/mm}^2]$$

F6

F.2 Caisson design

This subsection treats the caisson design. First the caisson dimensions will be defined, next the loads determined and finally the design dimensions of the caisson will be determined.

F.2.1 Definition of caisson geometry

In this section formula for basic dimensions and mass moments of inertia of the caisson structure are presented.

Basic dimensions. The basic dimensions of a caisson (see also Figure F.2) are defined as:

$$\begin{aligned} V_c &= W_c L_c H_c & [\text{m}^3] \\ V_{c,in} &= W_{c,in} L_{c,in} H_{c,in} & [\text{m}^3] \end{aligned} \quad \text{E7}$$

With:

$$\begin{aligned} W_c &= n_x \cdot W_{c,in} + 2 \cdot w_{w,out} + (n_x - 1) \cdot w_{w,in} & [\text{m}] \\ H_c &= d_{local} + h_{sill} & [\text{m}] \\ H_{c,in} &= H_c - w_t - w_f & [\text{m}] \\ L_{c,in} &= L_c - 2w_b & [\text{m}] \end{aligned} \quad \text{E8}$$

In which:

V_c	[m ³]	Volume of caisson
W_c	[m]	Width caisson
L_c	[m]	Length caisson
H_c	[m]	Height caisson
$V_{c,in}$	[m ³]	Volume of compartment
$W_{c,in}$	[m]	Inner width caisson
$L_{c,in}$	[m]	Inner length caisson
$H_{c,in}$	[m]	Inner height caisson
n_x	[-]	Number of compartments in x-direction
w_t	[m]	Thickness top slab
w_f	[m]	Thickness floor slab
$w_{w,out}$	[m]	Thickness outer walls
$w_{w,in}$	[m]	Thickness inner walls
w_b	[m]	Thickness bulkheads ⁽¹⁾

⁽¹⁾ Bulkheads will be placed to prevent the water from flowing in during transport. On the final location they will be removed. For the sake of simplicity the bulkheads are here designed as reinforced concrete plates.

Mass moments of inertia. The mass moments of inertia of the caisson are calculated in two directions; along the short side (x-direction) and long side (y-direction). See Figure F.2 for terminology. Before doing so, the position of the neutral axes in z-direction have to be determined:

$$\begin{aligned} s_{na-x} &= \frac{A_f \cdot s_f + 2 \cdot A_{w,out} \cdot s_{w,out} + (n_x - 1) \cdot A_{w,in} \cdot s_{w,in} + A_t \cdot s_t}{A_{c,con-x}} & [\text{m}] \\ s_{na-y} &= \frac{A_f \cdot s_f + 2 \cdot A_{w,out} \cdot s_{w,out} + A_t \cdot s_t}{A_{c,con-y}} & [\text{m}] \end{aligned} \quad \text{E9}$$

The neutral axes in x-direction are always located in exactly in the middle, as the caissons are symmetric in horizontal direction. Now the mass moments of inertia I_{zz} and I_{xx} can be calculated using the 'Parallel axis theorem' by Jakob Steiner. The bulkheads do not contribute to the mass moment of inertia, their only function is to prevent leakage of the caissons during transport. See Figure F.2 for the directions.

Note: one would expect underbraced part of the last term in Appendix F.2.1 to be a fourth order expression because the Parallel axis theorem tells that the contribution of a mass which is eccentrically mass located with respect to the neutral axis is a fourth order expression. This underbraced part is in fact a fourth order equation too, but the term prior to n_x^4 is in the order of 10^{-14} and is therefore negligible and omitted.

$$I_{zz-x} = 2 \cdot \frac{1}{12} \cdot w_{w,out} \cdot H_{c,in}^3 + (n_x - 1) \frac{1}{12} \cdot w_{w,in} \cdot H_{c,in}^3 + \frac{1}{12} W_c \cdot w_f^3 + \frac{1}{12} W_c \cdot w_t^3 + A_f \cdot (s_{na-x} - 0.5 \cdot w_f)^2 + A_t \cdot (H_c - s_{na-x} - 0.5 \cdot w_t)^2 \quad [\text{m}^4] \quad \text{F10}$$

$$I_{xx-x} = \frac{1}{12} \cdot (w_f + w_t) \cdot W_c^3 + 2 \cdot \frac{1}{12} \cdot H_{c,in} \cdot w_{w,out}^3 + 2 \cdot A_{w,out} \cdot (0.5 \cdot W_c - 0.5 \cdot w_{w,out})^2 + (n_x - 1) \cdot \frac{1}{12} \cdot H_{c,in} \cdot w_{w,in}^3 + \underbrace{\left(\frac{1}{12} \cdot n_x^3 - \frac{1}{4} \cdot n_x^2 + \frac{1}{6} \cdot n_x \right)}_{\text{See note above}} \cdot A_{w,in} \cdot (W_{c,in} + w_{w,in})^2 \quad [\text{m}^4] \quad \text{F11}$$

$$I_{zz-y} = \frac{1}{12} L_c \cdot w_f^3 + \frac{1}{12} L_c \cdot w_t^3 + A_f \cdot (s_{na-x} - 0.5 \cdot w_f)^2 + A_t \cdot (H_c - s_{na-x} - 0.5 \cdot w_t)^2 \quad [\text{m}^4] \quad \text{F12}$$

$$I_{xx-y} = \frac{1}{12} \cdot (w_f + w_t) \cdot L_c^3 \quad [\text{m}^4] \quad \text{F13}$$

In which:

s_{na-x}	[m]	Position of neutral axis in z-direction with respect to the bottom fiber, along the x-direction (short side)
s_{na-y}	[m]	Position of neutral axis in z-direction with respect to the bottom fiber, along the y-direction (long side)
I_{zz-x}	[m ⁴]	Mass moment of inertia in zz-direction along the x-direction (short side)
I_{xx-x}	[m ⁴]	Mass moment of inertia in xx-direction along the x-direction (short side)
I_{zz-y}	[m ⁴]	Mass moment of inertia in zz-direction along the y-direction (long side)
I_{xx-y}	[m ⁴]	Mass moment of inertia in xx-direction along the y-direction (long side)
A_f	[m ²]	Area of floor slab (= $w_f \cdot W_c$)
A_t	[m ²]	Area of top slab (= $w_t \cdot W_c$)
$A_{w,out}$	[m ²]	Area of outer wall (= $w_{w,out} \cdot H_{c,in}$)
$A_{w,in}$	[m ²]	Area of inner wall (= $w_{w,in} \cdot H_{c,in}$)
s_f	[m]	Distance mass center of floor slab and bottom fiber (= $0.5 \cdot w_f$)
s_t	[m]	Distance mass center of top slab and bottom fiber (= $w_f + H_{c,in} + 0.5 \cdot w_t$)
$s_{w,out}$	[m]	Distance mass center of outer wall and bottom fiber (= $w_f + 0.5 \cdot H_{c,in}$)
$s_{w,in}$	[m]	Distance mass center of inner wall and bottom fiber (= $w_f + 0.5 \cdot H_{c,in}$)
$A_{c,con-x}$	[m ²]	Area of concrete in short side cross-section (= $H_c \cdot W_c - H_{c,in} \cdot W_{c,in}$)
$A_{c,con-y}$	[m ²]	Area of concrete in long side cross-section (= $H_c \cdot L_c - H_{c,in} \cdot L_{c,in}$)
n_x	[-]	Number of compartments in x-direction

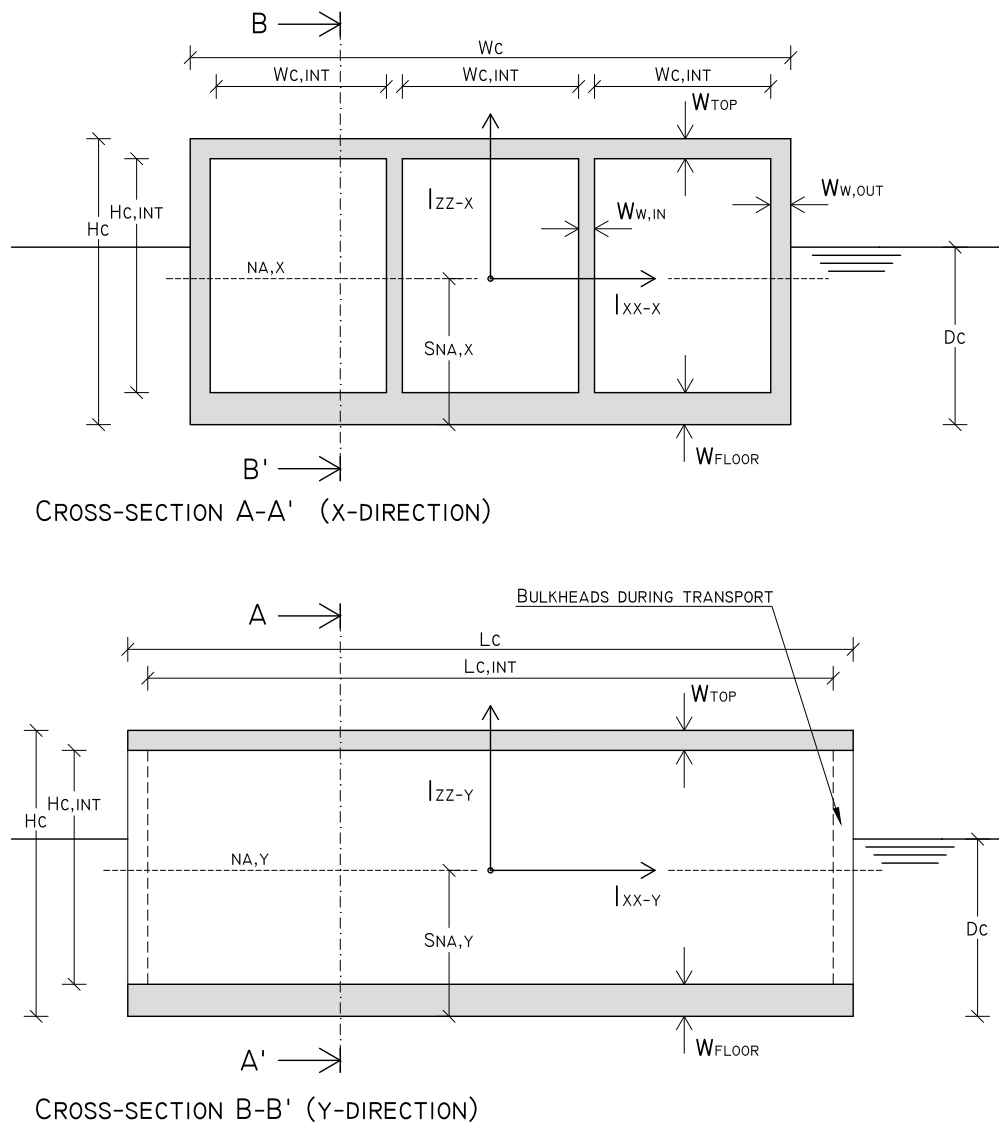


Figure F.2: Cross-sections of a caisson with three compartments showing the directions of the mass moments of inertia.

Vertical loads. The vertical loads are determined initially only by the dead weight of the caissons. An additional vertical load is applied due to the structure that accounts for the additional retaining height after a lifetime of a 100 years. This additional vertical load does therefore only have to be applied on the final location and not during transport and immersion.

- **Dead weight.** For this first design step the total vertical load on the final location equals the dead weight of the caisson in submerged conditions.

$$\begin{aligned}
 F_{V,tot} &= F_{V,dw} = \rho_{c,w} \cdot V_{c,con} && [\text{kN}] \\
 &= \rho_{c,w} \cdot (V_c - n_x \cdot W_{c,in} \cdot L_{c,in} \cdot H_{c,in}) && [\text{kN}]
 \end{aligned}
 \tag{F.14}$$

Note: right after construction the top 1.1 m of the caissons will protrude above the water level because SLR has not occurred yet. Also for this top part of the caissons a concrete mass density in submerged conditions will be assumed instead of the 'dry' concrete mass density. This results in an underestimation of vertical forces on the soil but will eventually work out on the safe side. This is because (as one will see later on) the shear stress

between the caisson and the soil will be governing and those shear stresses are lower with larger vertical forces. So assuming a little too low vertical force because of assuming the concrete being submerged will eventually work out on the safe side.

- **Additional weight.** Additional weight will be taken into account when the required additional retaining height for 200 year SLR is determined. The way this is done (e.g. a wall or a levee on top of the caissons) will be determined in a later design stage, and so is the resulting additional vertical load.

Horizontal loads. The horizontal loads are determined by the hydrostatic pressure and the wave loading. Friction between the water flow and the top of the caisson is assumed to be of a negligible magnitude compared to the wave loading and hydrostatic pressure.

- **Hydrostatic pressure.** The highest hydrostatic pressure occurs when the surge level is at its maximum; $h_1 = \text{MSL} + 5.40$ m [17.7 ft]. The corresponding water level inside the bay is then $h_2 = \text{MSL} - 0.52$ m [MSL - 1.71 ft]. This number includes a water level decrease due to wind set down right behind the barrier of 1.5 m (see Section 7.2). To obtain the maximum horizontal load, the case of a caisson barrier in closed position is taken. The water can only flow over the barrier, see Figures E3 and E4.

The resultant force is calculated through:

$$F_h = F_{h1} - F_{h2} \quad [\text{kN}] \quad \text{E15}$$

$$= 0.5 \cdot \rho_{sw} \cdot W_c \cdot \left((h_1 + H_c)^2 - h_1^2 - (h_2 + H_c)^2 \right) \quad [\text{kN}]$$

In which:

F_h	[kN]	Horizontal load on caisson due to hydrostatic pressure
F_{h1}	[kN]	Horizontal load surge side
F_{h2}	[kN]	Horizontal load Bay side
h_1	[m]	Maximum surge level
h_2	[m]	Corresponding level in the Bay
H_c	[m]	Height caisson (= $d_{local} + h_{sill}$)

- **Wave load.** The wave loading on the structure is calculated using the linear wave theory for non-breaking waves. The general expression for the total force on the caisson structure can then be calculated using (Vrijling et al., 2011):

$$F_{wave} = W \cdot \int_{-d}^0 \rho \cdot g \cdot H_i \frac{\cosh(k \cdot (d + z))}{\cosh(k \cdot d)} dz + W_c \cdot \int_0^{H_i} \left(1 - \frac{z}{H_i} \right) dz \quad [\text{kN}] \quad \text{E16}$$

However, the highest wave action takes place during the storm surge level. As one can see in Figures E3 and E4 the caisson structure will be completely submerged. Therefore the upper part of the wave load does not interact with the caisson, see Figures E3 and E4. The equation reduces to:

$$F_{wave} = W_c \rho_{sw} H_{max,1} \int_{-d_1}^{-\Delta h_{surge}} \frac{\cosh(k_1 \cdot (d_1 + z))}{\cosh(k_1 \cdot d_1)} dz \quad [\text{kN}] \quad \text{E17}$$

- **Total horizontal load.** The total load is the resulting horizontal load due to hydrostatic pressure plus the wave load. For the negative head (backsurge from the Galveston Bay) the wave load is taken equal to the regular wave loading from the Gulf of Mexico, which probably is an overestimation.

$$F_{H,tot} = F_h + F_{wave} \quad [\text{kN}] \quad \text{E18}$$

Moments. The acting moment on the caisson is only due to horizontal loading, as the hinge is assumed to be positioned along the vertical neutral axis, at the interface between the caisson and the soil (see Figures E3 and E4). It is calculated by multiplying the resultant horizontal forces by their eccentricity to the hinge. Clockwise directed moments are positive.

$$M_{tot} = F_{h1} \cdot e_1 - F_{h2} \cdot e_2 + F_{wave} \cdot e_{wave} \text{ [kNm]} \quad \text{E.19}$$

The eccentricity of the wave loading e_{wave} , measured from the surge level, is still unknown. It can be found by solving the following formula for e_{wave} . The formula is adopted from Equation (E.17).

$$W_c \rho_{sw} H_{max,1} \int_{-d_1}^{-e_{wave}} \frac{\cosh(k_1 \cdot (d_1 + z))}{\cosh(k_1 \cdot d_1)} dz = W_c \rho_{sw} H_{max,1} \int_{-e_{wave}}^{-\Delta h_{surge}} \frac{\cosh(k_1 \cdot (d_1 + z))}{\cosh(k_1 \cdot d_1)} dz \quad \text{E.20}$$

Rewrite and evaluate:

$$\int_{-d_1}^{-e_{wave}} \cosh(k_1 \cdot (d_1 + z)) dz = \int_{-e_{wave}}^{-\Delta h_{surge}} \cosh(k_1 \cdot (d_1 + z)) dz \quad \text{E.21}$$

$$2 \cdot \sinh(k_1 \cdot (d_1 - e_{wave})) = \sinh(k_1 \cdot (d_1 - \Delta h_{surge})) \quad \text{E.22}$$

$$\rightarrow e_{wave} = \frac{\sinh^{-1}(0.5 \cdot \sinh((d_1 - \Delta h_{surge}) \cdot k_1)) - d_1 \cdot k_1}{k_1} \text{ [m]} \quad \text{E.23}$$

Overview of loads. Figures E3 and E4 shows the vertical and horizontal loads that act on a caisson structure. Note: MSL includes a 100-year SLR of 1 m [3.3 ft].

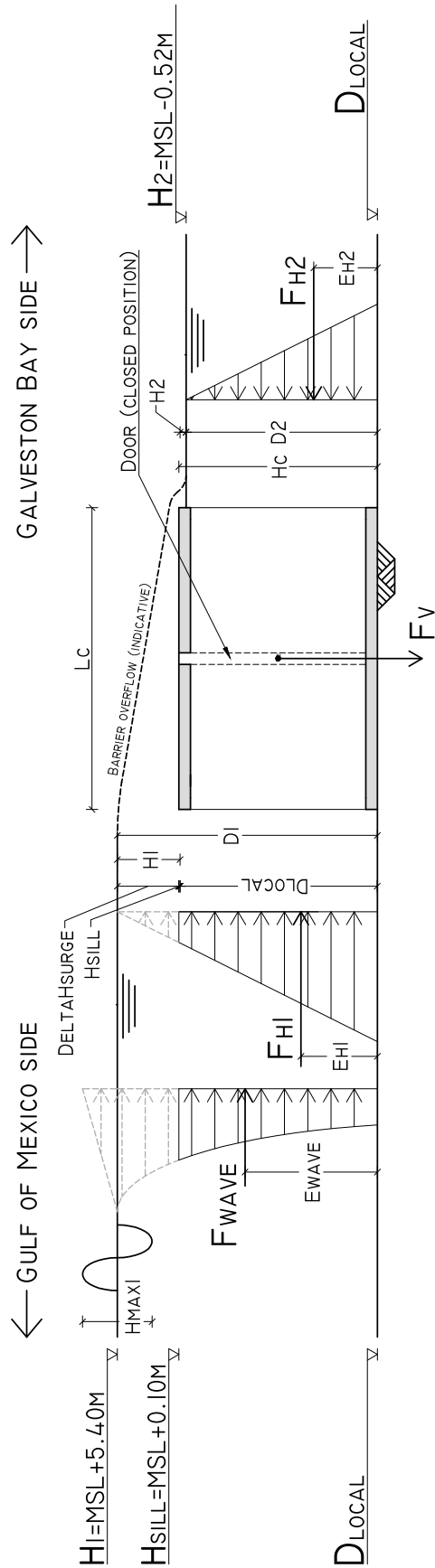


Figure F3: Cross-sectional side view of forces due to positive head (surge from the Gulf of Mexico) acting on caissons. Caisson dimensions not to scale. Units: m.

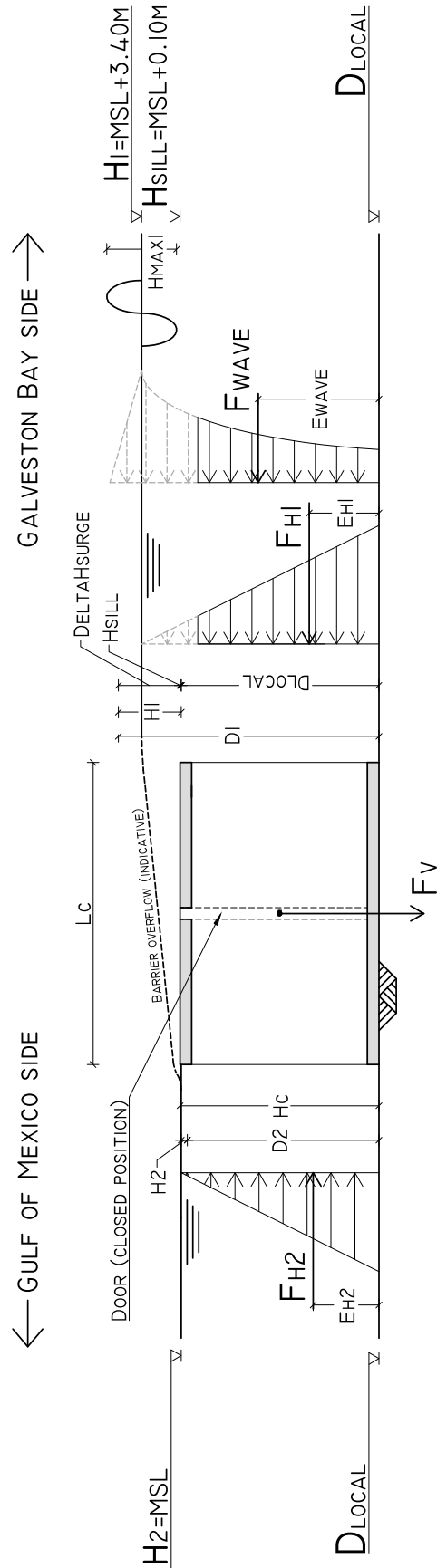


Figure F.4: Cross-sectional side view of forces due to negative head (back-surge from the Galveston Bay) acting on caissons. Units: m.

F.2.2 Design checks

The dimensions of the caissons are determined by iteratively adjusting their dimensions until they fulfill all of the strength and stability checks described in this paragraph. These concern checks for the stability at final placement and strength and stability checks during transport. All of these checks are presented in the form of a unity check. To meet the requirements, all unity checks have to be larger than one. See Table F.3.

Checks on stability at final placement. At final placement, the caisson has to be checked on five strength and stability requirements regarding the soil it is founded on.

- Check on vertical bearing capacity. First it is checked whether the soil is able to withstand the vertical loading due to the caissons on the subsoil. For saturated clay soils the bearing capacity for shallow foundations (see Appendix G.2.3 for the complete formula) simplifies to:

$$\frac{\sigma_{R,vb}}{\sigma_{E,vb}} \geq 1.0$$

$$N_c \cdot \sigma_{s,u,2} / \left(\frac{F_{V,tot}}{W_c L_c} + \frac{M_{tot}}{1/6 \cdot W_c \cdot L_c^2} \right) \geq 1.0 \quad \text{F24}$$

In which:

$\sigma_{R,vb}$	[kN/m ²]	Soil bearing capacity ^(I)
$\sigma_{E,vb}$	[kN/m ²]	Effective vertical stress on soil
N_c	[-]	Bearing capacity factor for cohesion = 5.14 ^(II)
$\sigma_{s,u,2}$	[kN/m ²]	Undrained shear stress between 3 and 20 m below MSL ^(III)
$F_{V,tot}$	[kN]	Total vertical load
M_{tot}	[kNm]	Sum of moments on caisson
W_c	[m]	Width caisson
L_c	[m]	Length caisson

^(I)According to the equation for strip foundations by Terzaghi (1943).

^(II)According to Skempton (1951).

^(III)From data presented in Table 5.2.

- Check on occurring soil tensile stresses. Tensile stresses in the subsoil may not occur. These occur if the following unity check (which is derived from the equation for the vertical bearing capacity) does not hold:

$$\left(\frac{F_{V,tot}}{W_c L_c} \right) / \left(\frac{M_{tot}}{1/6 \cdot W_c \cdot L_c^2} \right) \geq 1.0 \quad \text{F25}$$

- Check on inclined loading. Next to the regular vertical bearing capacity the shallow foundation of the caisson has to be checked on its ability to bear the inclined resultant of horizontal and vertical loads. It is determined using the next formula (Meyerhof, 1953):

$$\frac{\sigma_{R,vbi}}{\sigma_{E,vbi}} \geq 1.0$$

$$N_{ci} \cdot \sigma_{s,u,2} / \left(\frac{\sqrt{F_{V,tot}^2 + F_{H,tot}^2}}{W_c \cdot L_c} \right) \geq 1.0 \quad \text{F26}$$

In which:

α_{res}	[°]	Angle of resultant force with respect to vertical, = $\arctan (F_{H,tot}/F_{V,tot})$
$\sigma_{R,vbi}$	[kN/m ²]	Soil bearing capacity under inclined loading
$\sigma_{E,vbi}$	[kN/m ²]	Effective stress on soil due to inclined loading
N_{ci}	[-]	Bearing capacity factor for cohesion under inclined loading = 4.2 ⁽¹⁾

⁽¹⁾Determined using α_{res} and empirical relation according to Meyerhof (1953).

- **Check on overturning moment.** The action line of the resulting force due to horizontal and vertical loading should intersect the core of the structure (Voorendt et al., 2011), see Figure E5. The core of the structure is defined as the area extending to $1/6 \cdot L_c$ on both sides of the gravity centre line.

It should be checked that:

$$\frac{F_{V,tot} \cdot \frac{1}{6} L_c}{M_{tot}} \geq 1.0 \quad \text{E27}$$

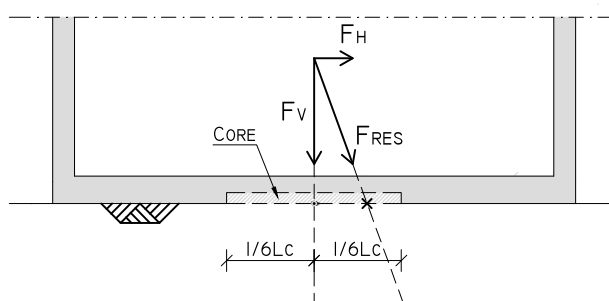


Figure E5: Cross-sectional side view of the bottom part of a caisson structure when placed on its final location. Based on Voorendt et al. (2011).

- **Check on soil shear stress.** In storm surge conditions the caissons will be an almost completely submerged construction. This results in lower gravity forces with respect to the horizontal load and thus a lower shear capacity. It should be checked that:

$$\frac{F_{V,tot} \cdot c_f}{F_{H,tot}} \geq 1.0 \quad \text{E28}$$

Where the friction factor $c_f = 0.35$ and 0.50 for clay and sand layers respectively (NFEC, 1986), see also Table F1.

Checks during transport. During the transport to the final location the caisson's draft D_c is an important parameter. It is determined as follows:

$$D_c = \frac{F_{buoy}}{L_c W_c \rho_{sw}} \text{ [m]} \quad \text{E29}$$

In which:

D_c	[m]	Draft of caisson
F_{buoy}	[m]	Buoyant force (= $F_{V,tot}$)
L_c	[m]	Length caisson
W_c	[m]	Width caisson
ρ_{sw}	[kN/m ³]	Mass density of salt water

High shear stresses and moments occur during the floating phase because of high water pressures outside, while there is no pressure working inside-out in the empty caisson. Therefore the outer walls, bulkheads and the top and floor slabs have to be checked on their shear strength and moment capacity. The inner walls are not treated, as they do not face any water head.

- **Check on shear strength.** The calculation for the bulkheads is the same as for the outer walls. Critical shear stresses appear to occur close to the lower corners of the caisson, see Figure E6. For a first estimate, a cross-section in the middle is considered. The influence of the bulkheads on the wall strength and vice versa is neglected. This will work out on the safe side because in reality the bulkheads take over part of the horizontal forces on the walls, and vice versa (Voorendt et al., 2011).

$$\begin{aligned}
 F_{sh,w,out} &= \frac{1}{2} D_c^2 \rho_{sw} && \text{[kN]} \\
 F_{sh,f} &= \frac{1}{2} \rho_c w_t W_c + w_{w,out} H_c \rho_c && \text{[kN]} \\
 F_{sh,t} &= \frac{1}{2} \rho_c w_t W_c && \text{[kN]}
 \end{aligned} \quad \text{E30}$$

The shear stress criterion reads (TGB, 2013):

$$\begin{aligned}
 \frac{\tau_{max}}{\tau_{sh}} &\geq 1.0 \\
 \frac{0.4 \cdot f_{ctm}}{\frac{3}{2} \frac{F_{sh}}{w}} &\geq 1.0
 \end{aligned} \quad \text{E31}$$

In which:

τ_{max}	[N/mm ² /m']	Maximum allowed shear stress per running meter
τ_{sh}	[N/mm ² /m']	Occurring shear stress per running meter
f_{ctm}	[N/mm ²]	Mean value of axial tensile strength of concrete, see Appendix E1.5
F_{sh}	[kN/m']	Occurring shear force
w	[m]	Thickness of wall or slab

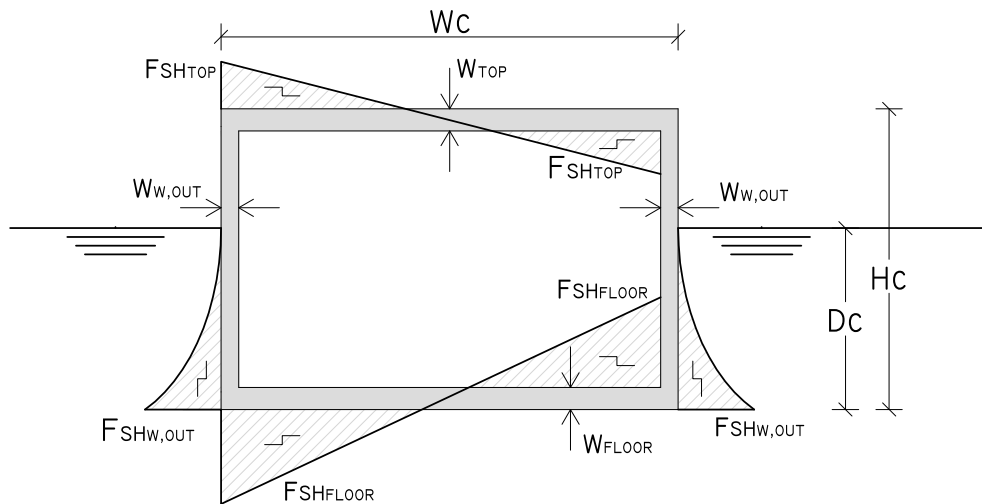


Figure E6: Cross-sectional front view of forces for a floating caisson structure with active shear forces on caisson walls and slabs (not to scale).

- Check on moment capacity. The calculation for the bulkheads is again the same as for the outer walls. Critical moments appear to occur in the corners of the caisson and in the middle of the top and floor slab. See Figure E7. Again a cross-section in the middle is considered, neglecting the influence of the bulkheads on the wall strength (and vice versa).

$$\begin{aligned}
 M_{w,out} &= F_{sh,w,out} \cdot (D_c - 0.5 \cdot w_f) & [\text{kNm/m}'] \\
 M_{f,center} &= \frac{1}{8} \cdot (D_c \cdot \rho_{sw} - w_f \cdot \rho_c) \cdot W_c^2 & [\text{kNm/m}'] \\
 M_{f,max} &= \max(M_{f,wall}, M_{f,center}) & [\text{kNm/m}'] \\
 M_{top} &= \frac{1}{8} \cdot w_t \cdot \rho_c \cdot W_c^2 & [\text{kNm/m}']
 \end{aligned}
 \tag{E32}$$

In which:

$M_{w,out}$	[kNm/m']	Moment on outer walls
$M_{f,center}$	[kNm/m']	Moment at the center of the floor slab
$M_{f,max}$	[kNm/m']	Maximum occurring moment on floor slab
$M_{f,wall}$	[kNm/m']	Moment on floor slab near walls (= $M_{w,out}$)
M_{top}	[kNm/m']	Maximum occurring moment on top slab

With these maximum moments the required wall thickness can be estimated. The unity check on moment capacity is expressed terms of wall and slab thickness. In order to do so, first an economic reinforcement percentage has to be chosen, say 1%. Using the formulas described by TGB (2013) the unity check for moments in walls and slabs:

$$\begin{aligned}
 \frac{w}{w_{req}} &\geq 1.0 \\
 \frac{w}{\sqrt{\frac{M_{bend}}{150 \cdot f_{cd}}}} &\geq 1.0
 \end{aligned}
 \tag{E33}$$

In which:

w	[m]	Thickness of wall or slab
w_{req}	[m]	Required thickness due to bending moment
M_{bend}	[kNm/m]	Occurring bending moment per running meter
f_{cd}	[N/mm ²]	Design value for concrete compressive strength, see Appendix E1.5

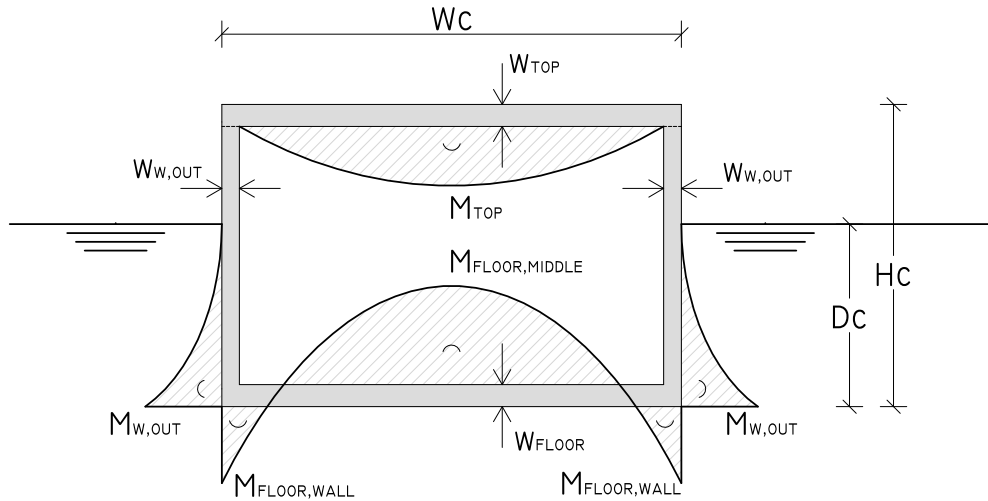


Figure E.7: Cross-sectional front view of a floating caisson structure with active bending moments on walls and slabs (not to scale).

- Check on static stability. To avoid instability of the caisson its metacentric height should be more than 0.5 m. Before the metacentric height can be calculated some parameters have to be defined:

$$\begin{aligned}
 I_{xx, floor} &= \frac{1}{12} L_c W_c^3 \quad [\text{m}^4] \\
 I_{yy, floor} &= \frac{1}{12} W_c L_c^3 \quad [\text{m}^4] \\
 V_{disp} &= L_c W_c D_c \quad [\text{m}^3]
 \end{aligned}
 \tag{E34}$$

In which $I_{xx, floor}$ and $I_{yy, floor}$ is the mass moment of inertia of the floor surface in x-direction and y-direction respectively and V_{disp} the volume of displaced fluids. Now the center of buoyant forces, the center of displaced fluids and the center of gravity can be determined. They are measured with respect to the bottom of the caisson, see Figure E.8.

$$\begin{aligned}
 s_{CB} &= 0.5 \cdot D_c \quad [\text{m}] \\
 s_{DF} &= \frac{\min(I_{xx, floor}, I_{yy, floor})}{V_{disp}} \quad [\text{m}] \\
 s_{CG} &= \frac{0.5 \cdot H_c \cdot V_c - n_x V_{c, in} \cdot (0.5 \cdot H_{c, in} + w_f)}{V_c - n_x V_{c, in}} \quad [\text{m}]
 \end{aligned}
 \tag{E35}$$

In which:

s_{CB}	[m]	Distance between center of buoyancy and bottom of caisson
s_{DF}	[m]	Distance between point of metacentric height and center of buoyancy
s_{CG}	[m]	Distance between center of gravity and bottom of caisson
$V_{c,in}$	[m]	Volume of compartment

Now the metacentric height (see Figure E8) can be calculated, it has to be larger than 0.5 (Voorendt et al., 2011):

$$s_{MH} = s_{CB} + s_{DF} - s_{CG} \quad [\text{m}]$$

$$\frac{s_{MH}}{0.5} \geq 1.0 \quad \text{E.36}$$

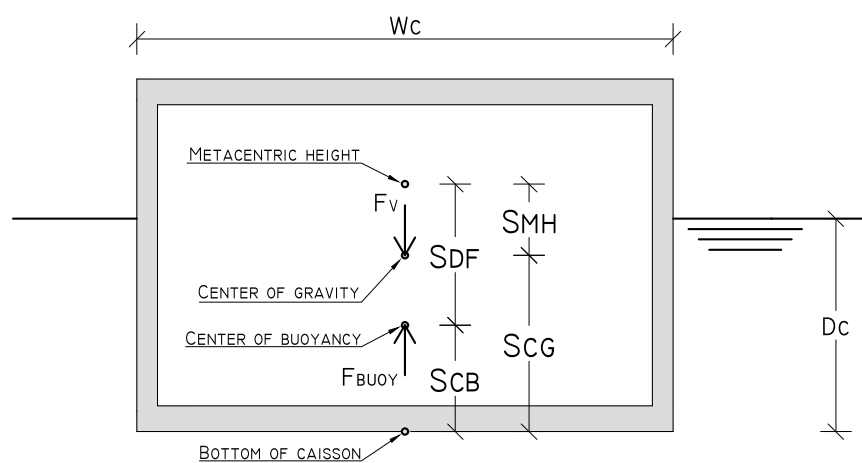


Figure E8: Cross-sectional front view of a floating caisson indicating relevant points for evaluating the metacentric height (not to scale).

- Check on dynamic stability – sway. If the dimensions of a floating element are too small compared to the length of the waves or swell, the element will start swaying on the waves. In practice the, the caisson must fulfill the following rule of thumb (Voorendt et al., 2011):

$$\frac{2\pi \cdot W_c}{g T_{p,reg}^2} \geq 1.0$$

$$\frac{2\pi \cdot L_c}{g T_{p,reg}^2} \geq 1.0 \quad \text{E.37}$$

In which:

$T_{p,reg}$	[s]	Peak wave period regular circumstances (= 4.0 s) ⁽¹⁾
W_c	[m]	Width caisson
L_c	[m]	Length caisson

⁽¹⁾According to wave data by NOAA Tides and Currents (2013b).

Especially in the direction of the short end (W_c) the caisson is likely fail on this condition. This can be easily solved by linking caissons together during transport to decrease the effects due to swaying. Therefore this check is not considered as a governing condition.

- Check on dynamic stability – natural oscillation. Worse than swaying on the waves or swell is the movement

of a caisson if the period of the water movement comes close to the natural oscillation period (eigenperiod) of the caisson. In order to prevent this one must ensure that the natural oscillation period is significantly larger than that of the waves or swell. It is assumed that the eigenperiod has to be at least three times larger than that of the waves or swell. First the polar inertia radii for both the short and long side have to be determined:

$$s_{p-x} = \sqrt{\frac{I_{zz-x} + I_{xx-x}}{A_{c,con-x}}} \text{ [m]} \quad \text{E38}$$

$$s_{p-y} = \sqrt{\frac{I_{zz-y} + I_{xx-y}}{A_{c,con-y}}} \text{ [m]} \quad \text{E39}$$

In which:

s_{p-x}	[m]	Polar moment of inertia radius along the short side
s_{p-y}	[m]	Polar moment of inertia radius along the long side
I_{zz-x}	[m ⁴]	Mass moment of inertia in zz-direction along the x-direction (short side), see Appendix F2.1
I_{xx-x}	[m ⁴]	Mass moment of inertia in xx-direction along the x-direction (short side), see Appendix F2.1
I_{zz-y}	[m ⁴]	Mass moment of inertia in zz-direction along the y-direction (long side), see Appendix F2.1
I_{xx-y}	[m ⁴]	Mass moment of inertia in xx-direction along the y-direction (long side), see Appendix F2.1
$A_{c,con-x}$	[m ²]	Area of concrete in short side cross-section
$A_{c,con-y}$	[m ²]	Area of concrete in long side cross-section

Ignoring the hydrodynamic mass and damping the eigenperiod of the floating caissons for the short and long sides respectively are (Voorendt et al., 2011):

$$T_{0-x} = \frac{2\pi \cdot s_{p-x}}{\sqrt{H_{s,reg} \cdot g}} \text{ [s]} \quad \text{E40}$$

$$T_{0-y} = \frac{2\pi \cdot s_{p-y}}{\sqrt{H_{s,reg} \cdot g}} \text{ [s]}$$

Where $H_{s,reg}$ the significant wave height in regular circumstances.

It was assumed that the eigenperiod has to be at least three times larger than that of the waves or swell, so the checks on natural oscillation now read:

$$\frac{T_{0-x}}{3 \cdot T_{p,reg}} \geq 1.0 \quad \text{E41}$$

$$\frac{T_{0-y}}{3 \cdot T_{p,reg}} \geq 1.0$$

Where $T_{p,reg}$ is the peak wave period in regular circumstances.

E.2.3 Caisson dimensions and design checks

Table E.3 presents all of the the results on the unity checks. The resulting caisson dimensions are presented in Table E.4. Caisson barrier section locations (AA' - GG') are indicated in Figure 7.3.

Table E.3: Unity checks.

Barrier section (see Figure 7.3)	AA'	BB'	CC'	DD'	EE'	FF'	GG'
– Breaking waves?	No	No	No	No	No	No	No
Checks final location							
– Vertical Bearing capacity ⁽¹⁾	2.25	2.03	2.43	2.82	3.77	5.29	3.77
– Soil tensile stresses	4.64	4.21	2.50	2.68	2.90	3.49	2.90
– Inclined loading ⁽¹⁾	2.02	1.83	2.31	2.68	3.48	4.70	3.48
– Shear capacity soil ⁽²⁾	1.03	1.02	1.02	1.03	1.01	1.04	1.01
– Overturning moment	4.64	4.21	2.50	2.68	2.90	3.49	2.90
Checks transport							
<u>Wall and slab strength</u>							
– Shear stress floor slab	1.73	1.76	2.33	2.26	3.04	2.54	3.04
– Shear stress top slab	3.13	3.13	3.13	3.13	3.13	3.13	3.13
– Shear stress walls	2.97	2.44	4.27	5.72	6.91	10.00	6.91
– Moment capacity floor	4.36	4.21	5.81	5.74	7.79	8.01	7.79
– Moment capacity top	4.90	4.90	4.90	4.90	4.90	4.90	4.90
– Moment capacity walls	2.44	2.11	3.25	4.02	4.33	5.34	4.33
<u>Floating static stability</u>							
– Metacentric height	2.88	10.23	9.95	3.40	7.15	12.76	7.15
<u>Floating dynamic stability</u>							
– Sway x-direction ⁽³⁾	0.56	0.74	0.56	0.38	0.37	0.36	0.37
– Sway y-direction	2.34	2.34	1.37	1.24	1.10	1.10	1.10
– Natural oscillation x-direction	2.32	2.81	2.00	1.43	1.23	1.13	1.23
– Natural oscillation y-direction	10.07	8.71	5.02	5.12	4.75	4.88	4.75

- (1) As accurate information about the bearing capacity of the second layer (sand layer between 3 and 15 m below MSL) is unavailable the strength properties of this layer are taken equal to those of the clay layer that lies underneath it (see Table 5.2).
- (2) A sand layer is present between 3 and 15 meter below MSL (see Table 5.2), the caissons founded on this sand layer (CC' - GG') experience higher friction force, making it able to better resist the horizontal forces than the caissons founded on the lower lying clay layer (AA' and BB'). Therefore the caisson length for caissons along cross sections AA' and BB' are relatively longer.
- (3) All caissons fail on their unity check for sway in x-direction. This can be solved by linking caissons together during transport to decrease the effects due to swaying. As this is easily doable this check is not considered as a governing condition.

Table F4: Caisson dimensions in metric (SI) units.

Barrier section (see Fig. 7.3)		AA'	BB'	CC'	DD'	EE'	FF'	GG'
– Local depth d_{local}	[MSL-m]	15	17	10	7.5	5	3.5	5
Geometry								
<u>Caisson dimensions</u>								
– Height H_c	[m]	15.1	17.1	10.1	7.6	5.1	3.6	5.1
– Width W_c	[m]	20.2	26.9	20.2	13.8	13.3	13.1	13.3
– Length L_c	[m]	85	85	50	45	40	40	40
– Draft D_c	[m]	4.64	5.13	3.87	3.35	2.57	1.91	2.57
– No. compartments n_x	[-]	3	4	3	2	2	2	2
<u>Wall/slab thickness</u>								
– Floor slab w_f	[m]	1.25	1.40	1.25	1.00	0.90	0.60	0.90
– Top slab w_t	[m]	0.50	0.50	0.50	0.50	0.50	0.50	0.50
– Outer wall $w_{w,out}$	[m]	0.70	0.70	0.70	0.70	0.50	0.40	0.50
– Inner wall $w_{w,in}$	[m]	0.40	0.50	0.40	0.40	0.30	0.30	0.30
– Bulkheads w_b	[m]	0.30	0.30	0.30	0.30	0.30	0.30	0.30
Section dimensions								
Number of caissons	[-]	9	4	51	16	16	29	10
Width per section	[m]	181.8	107.6	1030.2	220.8	212.8	379.9	133
Total volume of concrete	[m ³]	49511	32364	136986	22810	14995	19906	9372
Effective flow area	[m ²]	2066	1402	7115	1056	595	661	372

Table F5: Caisson dimensions in imperial units.

Barrier section (see Fig. 7.3)		AA'	BB'	CC'	DD'	EE'	FF'	GG'
– Local depth d_{local}	[MSL-ft]	49.2	55.8	32.8	24.6	16.4	11.5	16.4
Geometry								
<u>Caisson dimensions</u>								
– Height H_c	[ft]	49.5	56.1	33.1	24.9	16.7	11.8	16.7
– Width W_c	[ft]	66.3	88.3	66.3	45.3	43.6	43.0	43.6
– Length L_c	[ft]	278.9	278.9	164.0	147.6	131.2	131.2	131.2
– Draft D_c	[ft]	15.2	16.8	12.7	11.0	8.4	6.3	8.4
– No. compartments n_x	[-]	3	4	3	2	2	2	2
<u>Wall/slab thickness</u>								
– Floor slab w_f	[ft]	4.10	4.59	4.10	3.28	2.95	1.97	2.95
– Top slab w_t	[ft]	1.64	1.64	1.64	1.64	1.64	1.64	1.64
– Outer wall $w_{w,out}$	[ft]	2.30	2.30	2.30	2.30	1.64	1.31	1.64
– Inner wall $w_{w,in}$	[ft]	1.31	1.64	1.31	1.31	0.98	0.98	0.98
– Bulkheads w_b	[ft]	0.98	0.98	0.98	0.98	0.98	0.98	0.98
Section dimensions								
Number of caissons	[-]	9	4	51	16	16	29	10
Width per section	[ft]	596	353	3380	724	698	1246	436
Effective flow area	[10 ³ ft ³]	22234	15087	76582	11367	6407	7117	4004

F.3 Settlements calculation

The total settlement due to the weight of the caisson barrier is calculated by summing the deformation of all the soil layers.

$$\Delta h_{tot} = \sum_{i=1}^5 \Delta h_i \text{ [m]} \quad \text{F.42}$$

The deformation per soil layer i can be calculated in two ways: the Koppejan method and the Bjerrum method. For both methods the settlements are calculated. Both methods are based on the local effective stresses, these are defined first.

F.3.1 Effective soil stress

For each layer under each barrier section the effective soil stress is determined, see Table F.6. It is calculated using the next set of formulas:

$$\begin{aligned} \sigma'_{vi,1} &= 0.5 \cdot (\rho_{s,1} - \rho_{sw}) \cdot w_{s,1} & [\text{kN/m}^2] \\ \sigma'_{vi,2} &= 0.5 \cdot (\rho_{s,2} - \rho_{sw}) \cdot w_{s,2} + (\rho_{s,1} - \rho_{sw}) \cdot w_{s,1} & [\text{kN/m}^2] \\ \sigma'_{vi,3} &= 0.5 \cdot (\rho_{s,3} - \rho_{sw}) \cdot w_{s,3} + \sum_{i=1}^2 (\rho_{s,i} - \rho_{sw}) \cdot w_{s,i} & [\text{kN/m}^2] \\ \sigma'_{vi,4} &= 0.5 \cdot (\rho_{s,4} - \rho_{sw}) \cdot w_{s,4} + \sum_{i=1}^3 (\rho_{s,i} - \rho_{sw}) \cdot w_{s,i} & [\text{kN/m}^2] \\ \sigma'_{vi,5} &= 0.5 \cdot (\rho_{s,5} - \rho_{sw}) \cdot w_{s,5} + \sum_{i=1}^4 (\rho_{s,i} - \rho_{sw}) \cdot w_{s,i} & [\text{kN/m}^2] \end{aligned} \quad \text{F.43}$$

In which the soil layer thickness $w_{s,2}$ is zero for barrier sections AA' and BB and equal to the bottom of layer 2 minus the local depth for barrier sections CC' - GG'. The saturated volumetric weight is expressed as $\rho_{s,i}$, values for are 13, 19, 14, 15 and 17 kN/m³ for layers 1-5 respectively, see Table F.1. The volumetric weight of water $\rho_{sw} = 10.25$ kN/m³. The locations of the layers is presented in Table F.1 and fig. F.1.

Table F.6: Effective stresses in the middle of the soil layers.

Barrier section (see Fig. 7.3)		AA'	BB'	CC'	DD'	EE'	FF'	GG'
Foundation depth	[MSL-m]	15	17	10	7.5	5	3.5	5
Effective stress $\sigma'_{vi,i}$								
Layer 1 $\sigma'_{vi,1}$	[kN/m ²]	0	0	0	0	0	0	0
Layer 2 $\sigma'_{vi,2}$	[kN/m ²]	0	0	21.9	32.8	43.8	50.3	43.8
Layer 3 $\sigma'_{vi,3}$	[kN/m ²]	9.4	5.6	53.1	75.0	96.9	110.0	96.9
Layer 4 $\sigma'_{vi,4}$	[kN/m ²]	47.3	39.8	91.0	112.9	134.8	147.9	134.8
Layer 5 $\sigma'_{vi,5}$	[kN/m ²]	102.8	95.3	146.5	168.4	190.3	203.4	190.3

F.3.2 Applied stress due to caisson weight

The effective applied stress $\Delta\sigma'_{vi}$ under each barrier section per soil layer is determined, see Table F.7. It is assumed the loads will spread out in the soil under an angle of 45°, in the length direction (y-direction) only. The stresses are calculated using the following formula:

$$\Delta\sigma'_{vi} = \frac{F_{V,tot}}{W_c \cdot (L_c + 2 \cdot (d_{s,i} - d_{local}) \cdot 0.5)} \quad \text{F.44}$$

In which W_c is the caisson width, L_c the caisson length, $F_{v,tot}$ the total vertical load due to the caisson weight acting on the subsoil at the local depth d_{local} and $d_{s,i}$ the depth of the bottom of soil layer i . The locations of the layers is presented in Table F.1 and fig. F.1.

Table F.7: Applied stresses due to caisson weight in the middle of the soil layers.

Barrier section (see Fig. 7.3)		AA'	BB'	CC'	DD'	EE'	FF'	GG'
Foundation depth	[MSL-m]	15	17	10	7.5	5	3.5	5
Applied stress $\Delta\sigma'_{v,i}$								
Layer 1 $\Delta\sigma'_{v,1}$	[kN/m ²]	0	0	0	0	0	0	0
Layer 2 $\Delta\sigma'_{v,2}$	[kN/m ²]	0	0	36.4	30.0	21.8	15.8	21.8
Layer 3 $\Delta\sigma'_{v,3}$	[kN/m ²]	44.3	50.3	31.5	25.0	17.4	12.5	17.4
Layer 4 $\Delta\sigma'_{v,4}$	[kN/m ²]	36.1	41.7	25.7	20.4	14.2	10.2	14.2
Layer 5 $\Delta\sigma'_{v,5}$	[kN/m ²]	29.7	34.0	21.1	16.7	11.7	8.4	11.7

F.3.3 Koppejan method

The deformation per soil layer i according to Koppejan (1948):

$$\Delta h_i = w_{s,i} \cdot \left(\frac{c_C}{c'_p} + \frac{1}{c'_s} \log_{10}(t_{99\%}) \right) \cdot \ln \left(\frac{\sigma'_{vi,i} + \Delta\sigma'_{v,i}}{\sigma'_{vi,i}} \right) \quad [\text{m}] \quad \text{F45}$$

In which:

Δh_i	[m]	Settlement of concerning soil layer
$w_{s,i}$	[m]	Thickness soil layer
c_C	[-]	Degree of consolidation
c'_p	[-]	Primary compression coefficient
c'_s	[-]	Secondary compression coefficient
$t_{99\%}$	[s]	Duration of one-dimensional consolidation, see Equation (F46)
$\sigma'_{vi,i}$	[kN/m ²]	Initial vertical effective stress, according to Table F6
$\Delta\sigma'_{v,i}$	[kN/m ²]	Additional vertical effective stress due to loading, according to Table F7

The degree of consolidation $c_C^{(1)}$ indicates how much water pressure has already dissipated. For the caisson barrier the complete consolidation is of interest, inducing a degree of consolidation c_C of 1 (Vrijling et al., 2011). This is the case when the pressure has adjusted 99%. This consolidation duration $t_{99\%}$ is calculated through:

$$t_{99\%} \approx \frac{1.78 \cdot w_{s,i}^2}{c_v} \quad [\text{s}] \quad \text{F46}$$

It is assumed the vertical consolidation occurs in one direction only. The vertical consolidation constant c_v depends on the vertical permeability $\nu_v^{(2)}$, the mass density of salt water ρ_{sw} and a coefficient for vertical compressibility. As the latter one is inversely proportional to the Young's modulus E_{soil} the vertical consolidation constant is given by:

$$c_v = \frac{\nu_v \cdot E_{soil}}{\rho_{sw}} \quad [\text{m}^2/\text{s}] \quad \text{F47}$$

The required values for all of the soil parameters are presented in Table F.8.

⁽¹⁾ Commonly referred to as U .

⁽²⁾ Commonly referred to as k .

Table F.8: Consolidation properties per soil layer for Koppejan method.

Layer <i>i</i>	Depth [MSL-m]	Class	$\sigma_{su,i}^{(1)}$ [kN/m ²]	c'_p ⁽²⁾ [-]	c'_s ⁽²⁾ [-]	ν_v ⁽³⁾ [m/s]	$E_{soil}^{(4)}$ [kN/m ²]	$t_{99\%}$ [days]	c_v [m ² /s]
1	0 - 3	Very soft clay	12	7	30	10 ⁻⁷	500	38	4.9 · 10 ⁻⁶
2	3 - 15	Loose sand	⁽⁵⁾	200	⁽⁵⁾	10 ⁻²	25000	⁽⁶⁾	24
3	15 - 20	Soft to firm clay	24	7	80	10 ⁻⁷	1000	53	9.8 · 10 ⁻⁶
4	20 - 32	Firm clay	36	10	110	10 ⁻⁸	1500	2027	1.5 · 10 ⁻⁶
5	32 - 40	Firm to stiff clay	48	15	160	10 ⁻⁹	2000	6757	2.0 · 10 ⁻⁷
6	Below 40	Very dense sand ⁽⁷⁾							

- (1) Undrained shear strength according to Table 5.2.
- (2) Primary and secondary compression coefficients according to TGB (1990).
- (3) Vertical permeability according to Bear (1972).
- (4) Young's modulus according to TGB (1990).
- (5) Does not apply for non-cohesive layers.
- (6) Consolidation sand layer occurs immediately.
- (7) No deformations assumed to occur in bearing sand layer.

It appears that the consolidation duration of the 5th layer is the longest. It will take 6,757 days (18.5 years) before this layer is fully consolidated. This governing settlement time $t_{99\%}$ is used to calculate the total settlements.

Using Equation (F.45) to Equation (F.47) and Table F.8 the deformation per soil layer can now be calculated. The total settlement due to the weight of the caissons is calculated under the assumption that negligible deformation occurs in the dense sand layer (layer no. 6 in Table F.8). The stability criterion for unequally distributed settlement is expressed in terms of rotation. The maximum rotation of the caissons due to settlement θ_s is calculated by dividing the total settlement by the width or length of the caisson for the x and y-direction respectively.

$$\theta_{s,x} = \frac{\Delta h_{tot}}{W_c} \quad [-]$$

$$\theta_{s,y} = \frac{\Delta h_{tot}}{L_c} \quad [-]$$

F.48

The results of the settlement calculations and the caisson rotation per barrier section are presented in Table F.9.

Table F.9: Relative deformation per soil layer Koppejan method.

Barrier section (see Figure 7.3)		AA'	BB'	CC'	DD'	EE'	FF'	GG'		
Foundation depth d_{local}		15	17	10	7.5	5	3.5	5		
Relative settlement per layer										
Layer i	Depth [MSL-m]									
1	0 - 3	[m]	(1)	(1)	(1)	(1)	(1)	(1)		
2	3 - 15	Primary ⁽²⁾	[m]	(3)	(3)	0.024	0.024	0.019	0.015	0.019
3	15 - 20	Primary	[m]	1.251	0.985	0.321	0.194	0.109	0.070	0.109
		Secondary	[m]	0.959	0.756	0.246	0.149	0.084	0.054	0.084
4	20 - 32	Primary	[m]	0.702	0.881	0.280	0.183	0.108	0.072	0.108
		Secondary	[m]	0.559	0.702	0.223	0.146	0.086	0.057	0.086
5	32 - 40	Primary	[m]	0.143	0.171	0.066	0.045	0.028	0.019	0.028
		Secondary	[m]	0.118	0.141	0.054	0.037	0.023	0.016	0.023
Total primary settlement		[m]	2.096	2.037	0.691	0.446	0.264	0.176	0.264	
Total secondary settlement		[m]	1.636	1.599	0.524	0.332	0.193	0.127	0.193	
Total settlement Δh_{tot}		[m]	3.732	3.636	1.215	0.778	0.457	0.302	0.457	
Rotation due to unequal settlement										
x-direction (short edge W_c)		[-]	0.18	0.14	0.06	0.06	0.03	0.02	0.03	
y-direction (long edge L_c)		[-]	0.04	0.04	0.02	0.02	0.01	0.01	0.01	

- (1) None of the caissons will be founded on the first soil layer so deformations do not apply here.
 (2) Only primary settlements occur in sand layers.
 (3) Caissons in sections AA' and BB' are founded below the second soil layer so deformations do not apply in the second layer.

F.3.4 Bjerrum method

The deformation per soil layer i according to Bjerrum (1967):

$$\Delta h_i = w_{s,i} \cdot \left(\frac{1}{1 + e_{0,i}} \cdot c_c \cdot \log_{10} \left(\frac{\sigma'_{vi,i} + \Delta\sigma'_{vi}}{\sigma'_{vi,i}} \right) + c_\alpha \cdot \log_{10}(t_{99\%}) \right) \text{ [m]} \quad \text{F.49}$$

In which:

Δh_i	[m]	Settlement of concerning soil layer
$w_{s,i}$	[m]	Thickness soil layer
$e_{0,i}$	[-]	Initial void ratio layer i , see Equation (F.50)
c_c	[-]	Primary settlement coefficient
c_α	[-]	Secondary settlement coefficient
$t_{99\%}$	[s]	Duration of one-dimensional consolidation, see Equation (F.46)
$\sigma'_{vi,i}$	[kN/m ²]	Initial vertical effective stress, according to Table F.6
$\Delta\sigma'_{vi}$	[kN/m ²]	Additional vertical effective stress due to loading ⁽¹⁾

⁽¹⁾Equal to the stress due to the vertical force exerted by the caisson $\sigma_{E,vb}$ directly beneath the caisson (see Appendix F.2.2). Below the caissons the stress spreads out under an angle of 45° (Vrijling et al., 2011) in y-direction only.

The initial void ratio $e_{0,i}$ for fully saturated soil is calculated through:

$$e_{0,i} = \frac{\rho_{s,spec} - \rho_{s,i}}{\rho_{s,i} - \rho_{sw}} \text{ [-]} \quad \text{F.50}$$

In which $\rho_{s,spec}$ is the specific density of the soil layer (assumed: 26 kN/m³ both for sand and clay), $\rho_{s,i}$ the mass density of soil layer i and ρ_{sw} the mass density of water.

For the caisson barrier the complete consolidation is of interest, this is the case when the pressure has adjusted 99%. This consolidation duration $t_{99\%}$ is equal to the calculation procedure for the Koppejan method (Equations (F.46) and (F.47)).

The required values for all of the soil parameters for the Bjerrum method are presented in Table F.10.

Table F.10: Consolidation properties per soil layer for Bjerrum method.

Layer i	Depth [MSL-m]	Class	$\sigma_{su,i}^{(1)}$ [kN/m ²]	$c_c^{(2)}$ [-]	$c_\alpha^{(2)}$ [-]	$v_v^{(3)}$ [m/s]	$e_{0,i}^{(4)}$ [-]	$t_{99\%}^{(5)}$ [days]
1	0 - 3	Very soft clay	12	1.690	0.015	10^{-7}	4.73	38
2	3 - 15	Loose sand	⁽⁶⁾	0.021	0	10^{-2}	0.80	⁽⁷⁾
3	15 - 20	Soft to firm clay	24	1.357	0.013	10^{-7}	3.20	53
4	20 - 32	Firm clay	36	0.759	0.009	10^{-8}	2.32	2027
5	32 - 40	Firm to stiff clay	48	0.362	0.006	10^{-9}	1.33	6757
6	Below 40	Very dense sand ⁽⁸⁾						

- (1) Undrained shear strength according to Table 5.2.
- (2) Primary and secondary compression coefficients according to TGB (1990).
- (3) Vertical permeability according to Bear (1972).
- (4) Initial void ratio from Equation (F.50).
- (5) Equal to values in Table F.8.
- (6) Does not apply for non-cohesive layers.
- (7) Consolidation sand layer occurs immediately.
- (8) No deformations assumed to occur in bearing sand layer.

Using Equation (F.49), Equation (F.46), Equation (F.47) and Table F.10 the deformation per soil layer can be calculated. The total settlement due to the weight of the caissons is calculated under the assumption that no deformation occurs in the dense sand layer (layer no. 6 in Table F.10). The stability criterion for unequally distributed settlement is expressed in terms of rotation and is presented in Appendix F.3.3. The results of the settlement calculations and the caisson rotation per barrier section are presented in Table F.11.

Table F.11: Relative deformation per soil layer Bjerrum method.

Barrier section (see Figure 7.3)		AA'	BB'	CC'	DD'	EE'	FF'	GG'
Foundation depth d_{local}		15	17	10	7.5	5	3.5	5
Relative settlement per layer								
Layer i	Depth [MSL-m]							
1	0 - 3	[m]	⁽¹⁾	⁽¹⁾	⁽¹⁾	⁽¹⁾	⁽¹⁾	⁽¹⁾
2	3 - 15	Primary ⁽²⁾	[m]	⁽³⁾	⁽³⁾	0.024	0.024	0.020
3	15 - 20	Primary	[m]	1.229	1.613	0.316	0.191	0.107
		Secondary	[m]	0.570	0.570	0.570	0.570	0.570
4	20 - 32	Primary	[m]	0.698	0.876	0.278	0.182	0.107
		Secondary	[m]	0.947	0.947	0.947	0.947	0.947
5	32 - 40	Primary	[m]	0.145	0.173	0.066	0.046	0.028
		Secondary	[m]	0.421	0.421	0.421	0.421	0.421
Total primary settlement		[m]	2.071	2.662	0.685	0.443	0.262	0.262
Total secondary settlement		[m]	1.937	1.937	1.937	1.937	1.937	1.937
Total settlement Δh_{tot}		[m]	4.008	4.599	2.622	2.380	2.200	2.200
Rotation due to unequal settlement								
x-direction (short edge W_c)		[-]	0.20	0.17	0.13	0.17	0.17	0.16
y-direction (long edge L_c)		[-]	0.05	0.05	0.05	0.05	0.05	0.05

- (1) None of the caissons will be founded on the first soil layer so deformations do not apply here.
- (2) Only primary settlements occur in sand layers.
- (3) Caissons in sections AA' and BB' are founded below the second soil layer so deformations do not apply in the second layer.

G Foundation aspects

This appendix presents calculations and an elaborated approach as used in the third design step (foundation aspects, chapter 8).

G.1 Modified caisson dimensions

In this section the final caisson dimensions are determined using the appliance of skirts and the replacement of weak soil layers.

G.1.1 Weak soil layer replacement.

As stated in Table F.1 the shear stress coefficient of clay is lower (0.35) than that of sand (0.50). Especially for layer no. 3 underneath barrier sections AA' and BB' (see Figure F.1) it could be beneficial to replace the clay by sand. A dredging vessel has to show up anyway to flatten the seabed it is assumed this does not result in very high additional costs. By doing so, a big win can be gained for the caisson length for sections AA' and BB'. They won't need to be as long as they were before.

G.1.2 Caisson skirts

Through constructing skirts on either sides of the caissons the horizontal force resistance of the caissons can be increased. Caisson skirts will penetrate into the ground and provide additional resistance against horizontal forces due to passive soil pressure. See Figure 8.2.

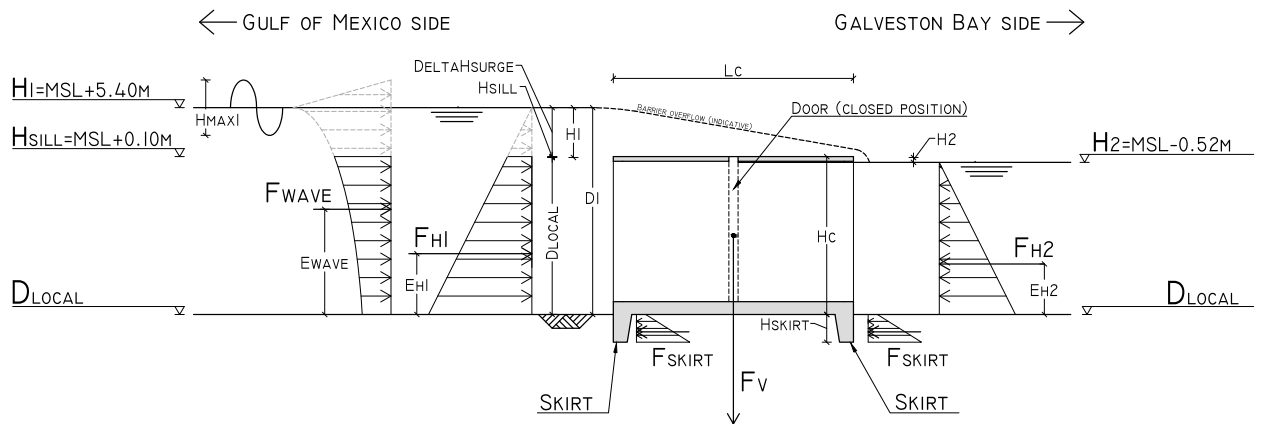


Figure G.1: Cross-sectional side view of forces due to positive head (surge from the Gulf of Mexico) acting on caissons equipped with skirts. Caisson dimensions not to scale.

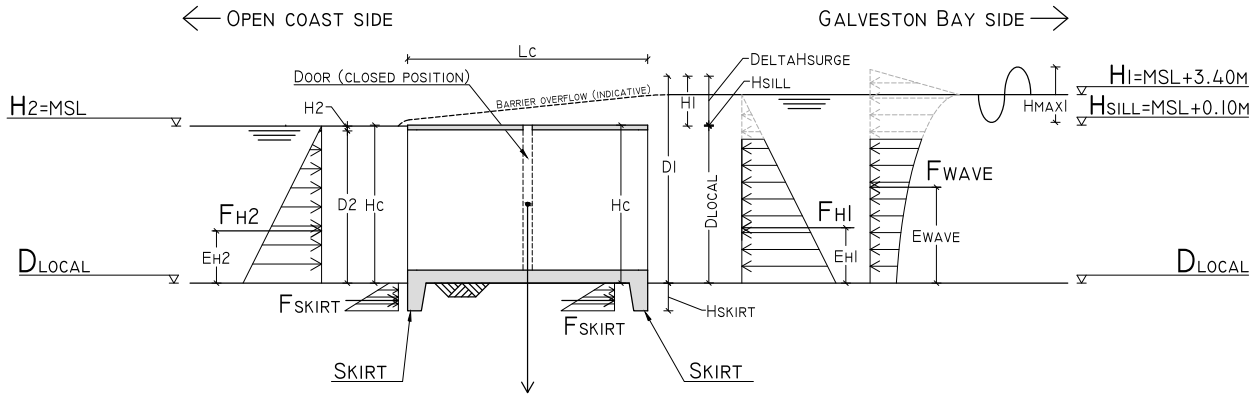


Figure G.2: Cross-sectional side view of forces due to negative head (surge from the Galveston Bay) acting on caissons equipped with skirts. Caisson dimensions not to scale.

Table G.1: Properties of relevant soil layers for skirt resistance per barrier section.

Layer i	Depth [MSL-m]	Sections	Class	$\rho_{s,i}$ [kN/m ³]	φ_i [°]	$K_{p,i}$ [-]
2	3 - 15	CC' - GG'	Loose sand	19	30	3.00
3	15 - 20	AA' - BB'	Loose sand	19	30	3.00

Using an expression for passive soil pressure (Verruijt, 2001) the additional horizontal force per skirt F_{skirt} is calculated.

$$F_{skirt} = W_c \cdot \left(\frac{1}{2} K_{p,i} (\rho_{s,i} - \rho_{sw}) h_{skirt}^2 + 2 \cdot \sigma_{su,i} h_{skirt} \sqrt{K_{p,i}} \right) \text{ [kN]} \quad \text{G.1}$$

In which:

F_{skirt}	[kN]	Passive horizontal force exerted by soil on caisson skirt
W_c	[m]	Width caisson
$K_{p,i}$	[-]	Passive soil pressure coefficient
$\rho_{s,i}$	[kN/m ³]	Mass density soil layer (saturated)
ρ_{sw}	[kN/m ³]	Mass density of salt water
h_{skirt}	[m]	Skirt height with respect to bottom caisson
$\sigma_{su,i}$	[kN/m ²]	Undrained shear stress of clay soil layer

The passive soil pressure coefficient is calculated using the angle of internal friction φ_i (Verruijt, 2001). The additional horizontal force capacity will contribute to optimized caisson dimensions. These revised dimensions are presented in the next paragraph.

$$K_{p,i} = \frac{1 + \sin \varphi_i}{1 - \sin \varphi_i} \text{ [-]} \quad \text{G.2}$$

The skirt height is limited by the local water depth. The design check for the caisson draft reads:

$$\frac{d_{local}}{D_c + s_s} \geq 1.0 \quad \text{G.3}$$

Where D_c is the caisson draft, which includes the skirt height, and a safety clearance s_s ($= 0.5$ m). In case the caisson draft is not governing, the skirt height is at most 20% of the total caisson height. Values of $0.5 \cdot h_{skirt}$ and $0.25 \cdot h_{skirt}$ for the skirt base and tip respectively results in reasonable skirt dimensions from a geometrical point of view and should be able to sufficiently transfer the forces. The dimensions for the caisson skirts for the largest caissons (section BB') are shown in Figure 8.1. Relevant input for Equation (G.1) per barrier section is presented in Table G.1.

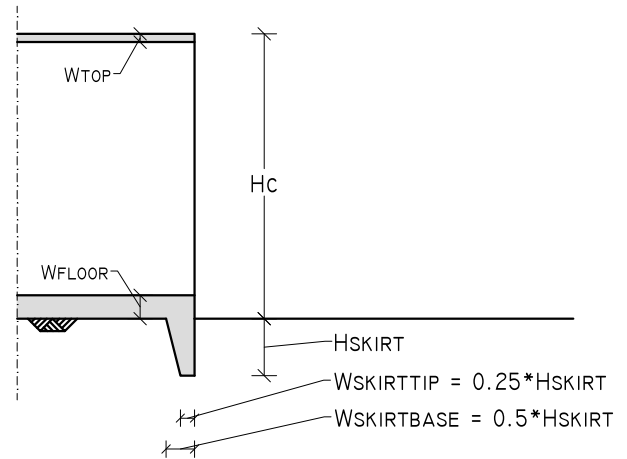


Figure G.3: Skirt dimensions for barrier section BB'.

G.1.3 Revised caisson dimensions

The revised caisson dimensions are presented in Table G.2. The unity checks for the revised caisson dimensions are presented in Table G.4. It appears that after the weak soil layer replacement at barrier sections AA' and BB' the overturning moment criterion now have become governing instead of the soil shear capacity. For sections CC' - GG' the latter is still governing.

Table G.2: Revised caisson dimensions in metric (SI) units.

Barrier section (see Fig. 7.3)		AA'	BB'	CC'	DD'	EE'	FF'	GG'
– Local depth d_{local}	[MSL-m]	15	17	10	7.5	5	3.5	5
Geometry								
<u>Caisson dimensions</u>								
– Height H_c	[m]	15.1	17.1	10.1	7.6	5.1	3.6	5.1
– Width W_c	[m]	20.2	26.9	20.2	13.8	13.3	13.1	13.3
– Length, old L_c	[m]	85	85	50	45	40	40	40
– Length, new $L_{c,new}$	[m]	40	41	43	42	38	38	40
– Draft, old D_c	[m]	4.97	5.52	4.01	3.44	2.63	1.94	2.60
– Draft, new $D_{c,new}$	[m]	7.99	8.94	6.03	4.96	3.65	2.66	3.00
– No. compartments n_x	[-]	3	4	3	2	2	2	2
<u>Wall/slab thickness</u>								
– Floor slab w_f	[m]	1.25	1.40	1.25	1.00	0.90	0.60	0.90
– Top slab w_t	[m]	0.50	0.50	0.50	0.50	0.50	0.50	0.50
– Outer wall $w_{w,out}$	[m]	0.70	0.70	0.70	0.70	0.50	0.40	0.50
– Inner wall $w_{w,in}$	[m]	0.40	0.50	0.40	0.40	0.30	0.30	0.30
– Bulkheads w_b	[m]	0.30	0.30	0.30	0.30	0.30	0.30	0.30
<u>Skirt dimensions</u>								
– Skirt height h_{skirt}	[m]	3.02	3.42	2.02	1.52	1.02	0.72	0.41
– Skirt base $w_{skirt,base}$	[m]	1.51	1.71	1.01	0.76	0.51	0.36	0.20
– Skirt tip $w_{skirt,tip}$	[m]	0.76	0.86	0.51	0.38	0.26	0.18	0.10

Table G.3: Revised caisson dimensions in imperial units.

Barrier section (see Fig. 7.3)		AA'	BB'	CC'	DD'	EE'	FF'	GG'
– Local depth d_{local}	[MSL-m]	15	17	10	7.5	5	3.5	5
Geometry								
<u>Caisson dimensions</u>								
– Height H_c	[ft]	49.54	56.10	33.14	24.93	16.73	11.81	16.73
– Width W_c	[ft]	66.27	88.25	66.27	45.28	43.64	42.98	43.64
– Length, old L_c	[ft]	279	279	164	148	131	125	131
– Length, new $L_{c,new}$	[ft]	131	135	141	138	125	125	131
– Draft, old D_c	[ft]	16.32	18.10	13.16	11.28	8.61	6.38	8.52
– Draft, new $D_{c,new}$	[ft]	26.23	29.32	19.78	16.27	11.96	8.74	9.86
– No. compartments n_x	[-]	3	4	3	2	2	2	2
<u>Wall/slab thickness</u>								
– Floor slab w_f	[ft]	4.10	4.59	4.10	3.28	2.95	1.97	2.95
– Top slab w_t	[ft]	1.64	1.64	1.64	1.64	1.64	1.64	1.64
– Outer wall $w_{w,out}$	[ft]	2.30	2.30	2.30	2.30	1.64	1.31	1.64
– Inner wall $w_{w,in}$	[ft]	1.31	1.64	1.31	1.31	0.98	0.98	0.98
– Bulkheads w_b	[ft]	0.98	0.98	0.98	0.98	0.98	0.98	0.98
<u>Skirt dimensions</u>								
– Skirt height h_{skirt}	[ft]	9.91	11.22	6.63	4.99	3.35	2.36	1.34
– Skirt base $w_{skirt,base}$	[ft]	4.95	5.61	3.31	2.49	1.67	1.18	0.67
– Skirt tip $w_{skirt,base}$	[ft]	2.48	2.81	1.66	1.25	0.84	0.59	0.33

Table G.4: Unity checks for final caisson dimensions.

Barrier section (see Figure 7.3)	AA'	BB'	CC'	DD'	EE'	FF'	GG'
– Breaking waves?	No						
Checks final location							
– Vertical Bearing capacity	1.41	1.28	2.18	2.67	3.63	5.12	3.74
– Soil tensile stresses	1.09	1.04	1.91	2.40	2.67	3.19	2.93
– Inclined loading	1.88	1.70	2.24	2.63	3.43	4.64	3.46
– Shear capacity soil	1.32	1.39	1.02	1.07	1.04	1.04	1.03
– Overturning moment	1.09	1.04	1.91	2.40	2.67	3.19	2.93
Checks transport							
<u>Wall and slab strength</u>							
– Shear stress floor slab	1.73	1.76	2.33	2.26	3.04	2.54	3.04
– Shear stress top slab	3.13	3.13	3.13	3.13	3.13	3.13	3.13
– Shear stress walls	2.59	2.11	3.99	5.42	6.64	9.70	6.79
– Moment capacity floor	3.91	3.75	5.50	5.51	7.55	7.82	7.68
– Moment capacity top	4.90	4.90	4.90	4.90	4.90	4.90	4.90
– Moment capacity walls	2.19	1.88	3.08	3.85	4.19	5.21	4.27
<u>Floating static stability</u>							
– Metacentric height	2.23	8.96	9.48	3.24	6.97	12.56	7.07
– Check Draft	1.77	1.80	1.53	1.37	1.21	1.11	1.00
<u>Floating dynamic stability</u>							
– Sway x-direction ⁽¹⁾	0.56	0.74	0.56	0.38	0.37	0.36	0.37
– Sway y-direction	1.10	1.13	1.18	1.15	1.04	1.04	1.10
– Nat. oscillation x-direction	2.32	2.81	2.00	1.43	1.23	1.13	1.23
– Nat. oscillation y-direction	3.61	3.28	4.06	4.63	4.41	4.53	4.75

G.2 Foundation design

In this section the elaboration of the optimized costs for the three foundation alternatives are presented, as well as their corresponding caisson construction costs.

G.2.1 Alternative 1: Soil improvement using vertical drainage with PVDs

In this subsection the total costs for vertical drainage with PVDs the construction costs for the higher caissons are determined.

Costs vertical drainage. To determine the total costs for vertical drainage first the optimum vertical grid spacing is determined. This is done using the following procure. First the consolidation duration is redefined for vertical drainage, next number of required drains and finally the pumping volume and total costs.

1. Consolidation duration using PVD. In the formula by Bjerrum (1967) (see Equation (F.49) the soil layer thickness determines the distance the water has to 'travel' before dissipating from the soil layer. By installing vertical drains this distance can be significantly reduced, and becomes the governing drainage distance. See Figure G.4. Equation (F.46) can be written in terms of drain distance for an equidistant grid:

$$t_{99\%} \approx \frac{1.78 \cdot D_d^2}{c_{h,soil}} \text{ [s]} \quad \text{G.4}$$

In which $t_{99\%}$ is the drained consolidation duration, c_v the horizontal consolidation coefficient which equal to $1.1 \cdot c_v$ (Tavenas et al., 1983) and D_d the equivalent drain distance. The equivalent drain distance D_d is equal to $\approx 1.13 \cdot s_{d,xy}$ for a square grid (Labeur, 2007). See Figure G.4.

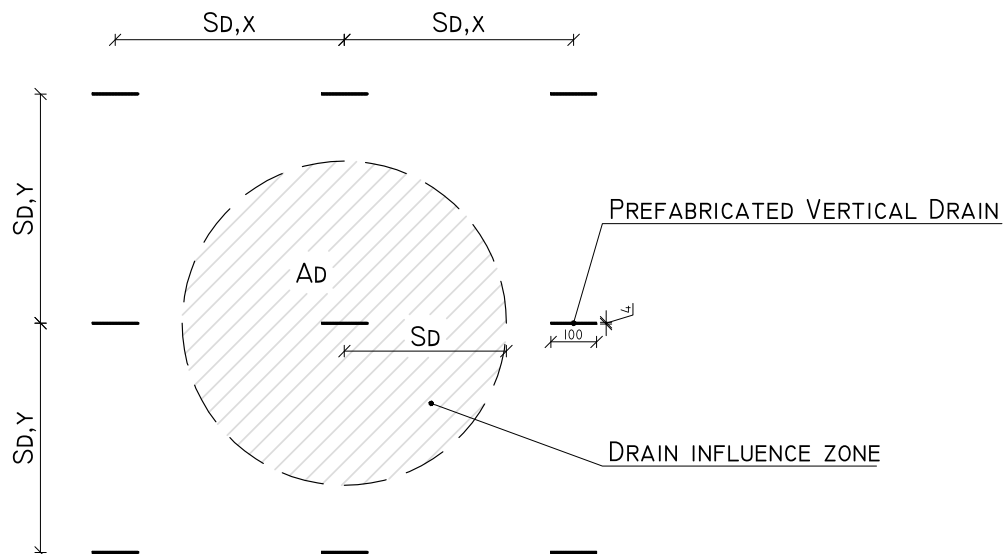


Figure G.4: Top view of vertical drains and drain spacing

2. Number of PVDs. The total number of CPVDs that have to be purchased depend on the density of the grid. The denser the grid, the more drains will be needed to cover the whole storm surge barrier's footprint. The total area that has to be drained per barrier section is:

$$A_{d,tot} = B_{section} \cdot (L_c + 2 \cdot L_{add}) \text{ [m}^2\text{]} \quad \text{G.5}$$

In which $A_{d,tot}$ is the total drainage area per barrier section, L_c the caisson length and L_{add} the additional drainage spacing outward the caisson perimeter. For the additional drainage spacing a value of 25 m is

assumed to be sufficient in preventing unstable slopes near the structure.

The area of the drain influence zone A_d (indicated in Figure G.4) also depends on the drain grid spacing. The larger the drain influence zone, the longer the consolidation time will be.

$$A_d = \frac{\pi}{4} s_{d,xy}^2 \text{ [m}^2\text{]} \tag{G.6}$$

Now that the influence zone per drain and the total area that has to be drained are known, the total number of drains can be calculated.

$$n_d = \frac{A_{d,tot}}{A_d} \text{ [-]} \tag{G.7}$$

The total required length of the drains $L_{PVD,tot}$ is calculated through multiplying the number of individual drains by the thicknesses of the clay layers (no. 3, 4 and 5). Multiplying this number by the drain width and thickness ($W_d = 100 \text{ mm}$ and $w_d = 4 \text{ mm}$ for standard CPVDs) the total volume of material is obtained.

3. Pumping volume. The total volume of water depends on the area of the influence zone of a single drain A_d and the total required length of the drains $L_{PVD,tot}$ and the total duration $t_{99\%}$ for which the drainage has to take place.
4. Costs. As stated above the total costs for drainage depend on both the drainage duration and the material costs. The productivity and unit cost rates are presented in Table G.5.

Table G.5: Time and cost unit rates for vertical drainage with Prefabricated Vertical Drains.

	Time unit rate	Costs unit rate
Installation	1000 [m/day/unit] ⁽¹⁾	250,000 [\$/unit/day] ⁽²⁾
Equipment	20 [units]	
Material		2.00 [\$/m ²] ⁽³⁾
Pumping		0.01 [\$/m ³ /day] ⁽⁴⁾
Settlement monitoring and adjustment		50,000 [\$/day] ⁽⁵⁾

- (1) Rough assumption, should be further investigated
- (2) Adopted and modified from dredging vessel costs unit cost rate according to Braam (2011). Mobilization and demobilization costs are included.
- (3) Adopted from Taube (2008)
- (4) Assumed to 10% of regular dewatering unit cost rates (Braam, 2011)
- (5) For excavating and grouting, rough estimate

Using the unit cost rates the total costs for vertical drainage with PVDs per grid spacing can be determined. The results are presented in Figure G.5.

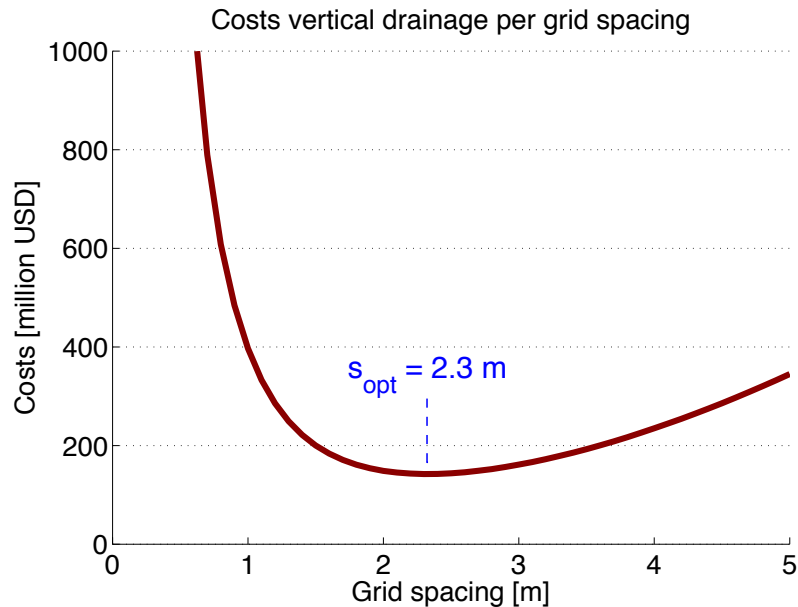


Figure G.5: Total vertical drainage costs expressed in terms of grid spacing.

From Figure G.5 it appears that the most cost-effective grid spacing is 2.3 m. For this grid spacing the total vertical drainage costs are estimated at \$142 million.

Caisson construction costs alternative 1. The caissons have to be heightened proportionally to the settlement magnitude to maintain retaining height. The total construction time (man hour) and costs (\$) are presented in Tables G.6 and G.7.

Table G.6: Caisson construction time for foundation alternative 1.

	Quantity	Time unit rate ⁽¹⁾	Construction time
Concrete			
– Slabs	147,190 [m ³]	0.1 [mhr/m ³]	14,719 mhr
– Walls	85,785 [m ³]	0.2 [mhr/m ³]	17,157 mhr
– Skirts	6,053 [m ³]	0.1 [mhr/m ³]	605 mhr
– Bulks	5,084 [m ³]	0.2 [mhr/m ³]	1,017 mhr
Formwork	508,058 [m ²]	0.5 [mhr/m ²]	254,029 mhr
Rebars	18,644 [ton]	10 [mhr/ton]	186,442 mhr
Doors	16,947 [m ²]	20 [mhr/m ²]	338,939 mhr
Technical installation	135 [caissons]	40 [mhr/caisson]	5,400 mhr
Total			818,308 mhr

(1) Cost and time unit rates adapted from Braam (2011)

Table G.7: Caisson construction costs for foundation alternative 1.

	Quantity	Costs unit rate ⁽¹⁾	Construction costs
Concrete			
– Slabs	147,190 [m ³]	200 [\$/m ³]	\$ 29,437,954.00
– Walls	85,785 [m ³]	200 [\$/m ³]	\$ 17,157,050.00
– Skirts	6,053 [m ³]	200 [\$/m ³]	\$ 1,210,662.05
– Bulks	5,084 [m ³]	200 [\$/m ³]	\$ 1,016,816.40
Formwork			
– Plywood	150,193 [m ²]	40 [\$/m ²]	\$ 6,007,712.58
– Preparation	508,058 [m ²]	80 [\$/m ²]	\$ 40,644,606.70
Rebars	18,644 [ton]	2,000 [\$/ton]	\$ 37,288,419.52
Doors	16,947 [m ²]	20,000 [\$/m ²]	\$ 338,938,800.00
Technical installation ⁽¹⁾	135 [caissons]	150,000 [\$/caisson]	\$ 20,250,000.00
Labor	818,308 [mhr]	50 [\$/mhr]	\$ 40,915,393.19
Total			\$ 532,867,414.44

G.2.2 Alternative 2: Soil improvement using vacuum preloading with CPVDs

In this subsection the total costs for vacuum preloading with CPVDs and the construction costs for the caissons are calculated.

Costs vacuum preloading. To determine the total costs for vacuum preloading first the optimum grid spacing is determined. This is done using the following procure as for alternative 1, but now the time and cost unit rates are different.

Table G.8: Time and cost unit rates for vacuum preloading with CPVDs.

	Time unit rate	Cost unit rate
Installation	1000 [m/day/unit] ⁽¹⁾	250,000 [\$/unit/day] ⁽²⁾
Equipment	20 [units]	
Material		2.50 [\$/m ²] ⁽³⁾
Pumping		0.1 [\$/m ³ /day] ⁽⁴⁾

(1) Rough assumption, should be further investigated

(2) Adopted and modified from dredging vessel costs unit cost rate according to Braam (2011). Mobilization and demobilization costs are included.

(3) Adopted from Taube (2008)

(4) Pumping costs assumed to be equal to regular dewatering unit cost rates as used by Braam (2011)

Using the unit cost rates the total costs for vacuum preloading per grid spacing can be determined. The results are presented in Figure G.6.

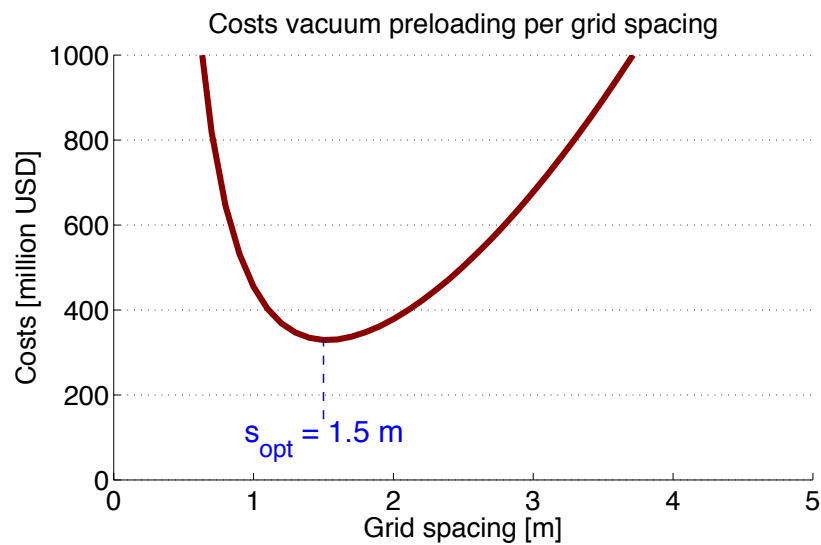


Figure G.6: Total costs vacuum preloading with CPVDs expressed in terms of grid spacing.

From Figure G.6 it appears that the most cost-effective grid spacing is 1.5 m. For this grid spacing the total vacuum preloading costs are estimated at \$329 million.

Caisson construction costs alternative 2. The caisson construction costs have to be calculated for the regular caisson dimensions as they were determined in Section 8.1. The total construction time (man hour) and costs (current U.S.\$) are presented in Tables G.9 and G.10.

Table G.9: Caisson construction time for foundation alternative 2.

	Quantity	Time unit rate ⁽¹⁾	Construction time
Concrete			
– Slabs	147,190 [m ³]	0.1 [mhr/m ³]	14,719 mhr
– Walls	73,345 [m ³]	0.2 [mhr/m ³]	14,669 mhr
– Skirts	6,053 [m ³]	0.1 [mhr/m ³]	605 mhr
– Bults	4,345 [m ³]	0.2 [mhr/m ³]	869 mhr
Formwork	486,477 [m ²]	0.5 [mhr/m ²]	234,239 mhr
Rebars	17,674 [ton]	10 [mhr/ton]	176,739 mhr
Doors	14,483 [m ²]	20 [mhr/m ²]	289,656 mhr
Technical installation	135 [caissons]	40 [mhr/caisson]	5,400 mhr
Total			736,896 mhr

(1) Cost and time unit rates adapted from Braam (2011)

Table G.10: Caisson construction costs for foundation alternative 2.

	Quantity	Costs unit rate ⁽¹⁾	Construction costs
Concrete			
– Slabs	147,190 [m ³]	200 [\$/m ³]	\$ 29,437,954.00
– Walls	73,345 [m ³]	200 [\$/m ³]	\$ 14,699,054.00
– Skirts	6,053 [m ³]	200 [\$/m ³]	\$ 1,210,662.05
– Bulks	4,345 [m ³]	200 [\$/m ³]	\$ 868,968.00
Formwork			
– Plywood	136,249 [m ²]	40 [\$/m ²]	\$ 5,449,970.66
– Preparation	468,477 [m ²]	80 [\$/m ²]	\$ 37,478,185.74
Rebars	17,674 [ton]	2,000 [\$/ton]	\$ 35,347,782.64
Doors	14,483 [m ²]	20,000 [\$/m ²]	\$ 289,656,000.00
Technical installation ⁽¹⁾	135 [caissons]	150,000 [\$/caisson]	\$ 20,250,000.00
Labor	736,896 [mhr]	50 [\$/mhr]	\$ 36,844,795.20
Total			\$ 471,213,372.29

G.2.3 Alternative 3: Deep foundation

For the calculations regarding the deep foundation the following assumptions have been made:

- The steel tubular piles are driven 2 m into the bearing sand layer (no. 6).
- The applied pile inclination is equal to $\tan \alpha_t = 1/3$ with respect to the vertical.
- The entire calculation is executed in SLS

First the pile tip bearing capacity is determined. Next the required wall thickness is determined, as well as a design check for the pile's structural strength. Next the costs for a steel tubular pile foundation are presented as well as the reduced caisson costs.

Pile bearing capacity. The total bearing capacity is a function of the pile diameter.

$$F_{t,max} = F_{t,tip} + F_{t,skin,+} - F_{t,skin,-} - F_{t,dw} \text{ [kN]} \quad \text{G.8}$$

In which $F_{t,tip}$ is the pile tip bearing capacity, $F_{t,skin,+}$ the positive skin friction, $F_{t,skin,-}$ the negative skin friction (down drag) and $F_{t,dw}$ the dead weight of the steel tubular pile.

Note: as the steel tubular piles will be closed-ended and founded on a sand layer the negative skin friction can be neglected (Singapore Standard, 2003).

Pile tip bearing capacity The pile tip bearing capacity is calculated through:

$$F_{t,tip} = A_t \cdot P_{t,tip} \text{ [kN]} \quad \text{G.9}$$

In which $A_t = \frac{\pi}{4} \phi_t^2$ and $P_{t,tip}$ can be determined analogously to the bearing capacity of a shallow foundation, for which the maximum soil bearing pressure is given by Brinch Hansen (1970):

$$P_{t,tip} = \sigma_{su,i} \cdot N_c \cdot s_c \cdot i_c + \sigma'_{vi,i} \cdot N_q \cdot s_q \cdot i_q + 0.5 \cdot B_{eff} \cdot \rho'_\gamma \cdot N_\gamma \cdot s_\gamma \cdot i_\gamma \text{ [kN/m}^2\text{]} \quad \text{G.10}$$

In which:

$P_{t,tip}$	[kN/m ²]	Maximum soil pressure under pile tip
$\sigma_{su,i}$	[kN/m ²]	Undrained shear stress of clay soil layer
$\sigma'_{vi,i}$	[kN/m ²]	Initial vertical effective stress
ρ'_γ	[kN/m ³]	Effective volumetric weight of the soil below construction depth
B_{eff}	[m]	Width of effective foundation area
N_c	[-]	Bearing capacity factor for cohesion
N_q	[-]	Bearing capacity factor for surcharge including soil coverage
N_γ	[-]	Bearing capacity factor of soil below the foundation
s_c	[-]	Shape factor for cohesion
s_q	[-]	Shape factor for surcharge including soil coverage
s_γ	[-]	Shape factor of soil below the foundation
i_c	[-]	Inclination factor for cohesion
i_q	[-]	Inclination factor for surcharge including soil coverage
i_γ	[-]	Inclination factor of soil below the foundation

The bearing capacity (N_c , N_q , N_γ), shape (s_c , s_q , s_γ) and inclination (i_c , i_q , i_γ) factors for undrained soil conditions are given by:

$$\begin{aligned}
 N_c &= (N_q - 1) \cot \varphi_i & N_q &= \frac{1 + \sin \varphi_i}{1 - \sin \varphi_i} \cdot e^{\pi \tan \varphi_i} & N_\gamma &= 2 \cdot (N_q - 1) \tan \varphi_i \\
 s_c &= 1 + 0.2 \cdot \frac{B_{eff}}{L_{eff}} & s_q &= 1 + \frac{B_{eff}}{L_{eff}} \cdot \sin \varphi_i & s_\gamma &= 1 - 0.3 \cdot \frac{B_{eff}}{L_{eff}} \\
 i_c &= 0.5 \left(1 + \sqrt{1 - \frac{F_{H,tot}}{A_{eff} \cdot \sigma_{su,i}}} \right) & i_q &= 1 - \frac{F_{H,tot}}{F_{V,tot} + A_{eff} \cdot \sigma_{su,i} \cot \varphi_i} & i_\gamma &= i_q
 \end{aligned} \tag{G.11}$$

In which:

φ_i	[°]	Angle of internal friction soil layer
B_{eff}	[m]	Width of effective foundation area
L_{eff}	[m]	Length of effective foundation area
A_{eff}	[m]	Area of effective foundation area
$\sigma_{su,i}$	[kN/m ²]	Undrained shear stress of clay soil layer
$F_{H,tot}$	[kN]	Total horizontal load
$F_{V,tot}$	[kN]	Total vertical load

For circular steel tubular piles:

$$\begin{aligned}
 B_{eff} &= L_{eff} & [m] \\
 A_{eff} &= \frac{\pi}{4} \phi_t^2 & [m^2]
 \end{aligned} \tag{G.12}$$

For steel tubular pile foundations the capacity of the soil below the foundation is negligible compared to the surcharge including soil coverage (Vrijling et al., 2011). Combined with the fact that the steel tubular piles are founded on a non-cohesive sand layer Appendix G.2.3 reduces to:

$$P_{t,tip} = \sigma'_{vi,i} \cdot N_q \cdot s_q \cdot i_q \text{ [kN/m}^2\text{]} \tag{G.13}$$

Using Appendix G.2.3 and substitution in Appendices G.2.3 and G.2.3 gives the capacity for one steel tubular pile.

$$F_{t,tip} = \frac{\pi}{4} \phi_i^2 \cdot \sigma'_{vi,6} \cdot N_q \cdot s_q \cdot i_q \quad [\text{kN}]$$

$$= \frac{\pi}{4} \phi_i^2 \cdot \sigma'_{vi,6} \cdot \frac{1 + \sin \varphi_6}{1 - \sin \varphi_6} \cdot e^{\pi \tan \varphi_6} \cdot (1 + \sin \varphi_6) \cdot \left(1 - \frac{F_{H,tot}}{F_{V,tot}}\right) \quad [\text{kN}] \quad \text{G.14}$$

In which φ_6 is the angle of internal friction for the bearing sand layer (assumed: 35°). The occurring vertical and horizontal loads ($F_{V,tot}$, $F_{H,tot}$) are calculated analogously as described in Appendix F.2.1, but now for caissons without skirts. The vertical stress at the pile tip (penetrating 2 m into the bearing sand layer) for each barrier section is presented in Table G.11. This table is in addition to Table F.6.

Table G.11: Parameters for bearing layer.

Barrier section (see Fig. 7.3)		AA'	BB'	CC'	DD'	EE'	FF'	GG'
Effective stress $\sigma'_{vi,6}$	[kN/m ²]	149.3	141.8	193.0	214.9	236.8	249.9	236.8
Angle internal friction φ_6	[°]	35	35	35	35	35	35	35
Max. horizontal load $F_{H,tot}$	[kN]	27,596	40,934	19,337	10,217	6,824	4,528	6,824
Max. vertical load $F_{V,tot}$	[kN]	38,539	56,566	31,916	18,853	13,922	10,191	13,922

Using Appendix G.2.3 and table G.11 the final tip bearing force per steel tubular pile per barrier section can be expressed in terms of pile diameter. The most economic pile diameter will be determined later on, first the skin friction force is also expressed in terms of pile diameter.

Skin friction. The skin friction between the steel tubular pile and the soil influences the bearing capacity. Two types of skin friction have to be taken into account: positive skin friction and negative skin friction. Positive skin friction increases and negative skin friction decreases the pile bearing capacity. The plane division between where the skin friction flips from positive to negative is the neutral point. The location of the neutral point below the surface L_n is 0.95 of the total soft stratum thickness L_s for closed-end piles bearing in sand (Singapore Standard, 2003). The depth of this neutral point differs for the different barrier sections as it is dependent on the local depth. See Figure G.7.

The total wall skin friction is calculated by (Hussin, 2006b).

$$F_{t,skin,+} = \pi \cdot \phi_t \cdot w_{s,i} \cdot P_{t,skin} \quad [\text{kN}] \quad \text{G.15}$$

In which ϕ_t is the steel tubular pile diameter and $w_{s,i}$ the soil layer thickness for which the skin friction is calculated. The skin friction pressure $P_{t,skin}$ for cohesive (alpha-method) and non-cohesive soils is calculated using (API, 2000):

$$P_{skin,c} = \alpha_s \cdot \sigma_{su,i} \quad [\text{kN/m}^2]$$

$$P_{skin,s} = K_n \cdot \sigma'_{vi,i} \cdot \tan\left(\frac{2}{3}\varphi_i\right) \quad [\text{kN/m}^2] \quad \text{G.16}$$

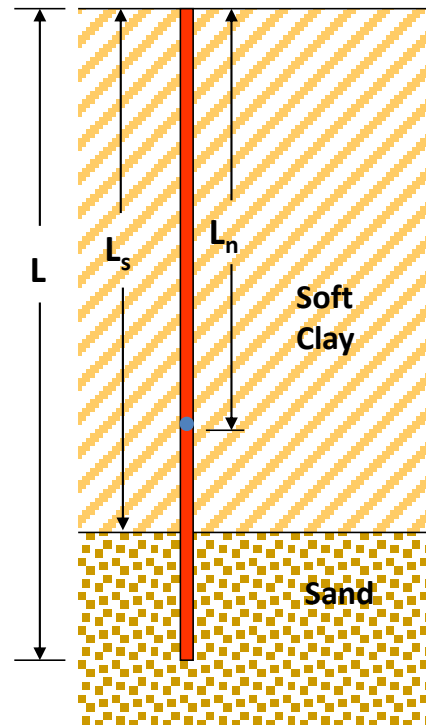


Figure G.7: Position of neutral point in soft soil stratum (Singapore Standard, 2003).

In which α_s is the adhesion factor, $\sigma_{su,i}$ the undrained shear strength of the clay layer, K_n the coefficient of neutral soil pressure (see Equation (G.18)), $\sigma'_{vi,i}$ the vertical effective stress in the middle of soil layer i and φ_i the angle of internal friction for soil layer i (17.5° for clay, 30° for sand layer 2 and 35° for sand layer 6).

The adhesion factor $\alpha_{s,i}$ can be computed by the equations (API, 2000):

$$\alpha_{s,i} = 0.5 \cdot \left(\frac{\sigma_{su,i}}{\sigma'_{vi,i}} \right)^{-0.5} \quad [-] \quad \text{for} \quad \frac{\sigma_{su,i}}{\sigma'_{vi,i}} \leq 1.0$$

$$\alpha_{s,i} = 0.5 \cdot \left(\frac{\sigma_{su,i}}{\sigma'_{vi,i}} \right)^{-0.25} \quad [-] \quad \text{for} \quad \frac{\sigma_{su,i}}{\sigma'_{vi,i}} \geq 1.0$$
G.17

According to Hussin (2006b) the coefficient of neutral soil pressure K_n for driven piles is given by:

$$K_n = 1.4 \cdot (1 - \sin \varphi_i) \quad [-]$$
G.18

The relevant variables are summarized in Table G.12. They are split up in relevant parameters for cohesive and non-cohesive layers.

Table G.12: Parameters for skin friction.

Skin friction factors		AA'	BB'	CC'	DD'	EE'	FF'	GG'
Layer 1: α_s values	[-]	0	0	0	0	0	0	0
Layer 2: $K_n \cdot \tan\left(\frac{2}{3}\varphi_i\right)$ values	[-]	0.25	0.25	0.25	0.25	0.25	0.25	0.25
Layer 3: α_s values	[-]	0.40	0.35	0.74	0.88	1.00	1.07	1.00
Layer 4: α_s values	[-]	0.57	0.53	0.79	0.89	0.97	1.01	0.97
Layer 5: α_s values	[-]	0.73	0.70	0.87	0.94	1.00	1.03	1.00
Layer 6: $K_n \cdot \tan\left(\frac{2}{3}\varphi_i\right)$ values	[-]	0.26	0.26	0.26	0.26	0.26	0.26	0.26

Pile dead weight. The tubulars are filled with concrete to prevent corrosion on the steel tubular inside and to resist buckling effects. This gives additional weight. The force due to pile weight is calculated through:

$$F_{t,dw} = L_t \left(\rho_{s,w} \cdot \frac{\pi}{4} (\phi_t^2 - (\phi_t - 2 \cdot w_t)^2) + \rho_{c,w} \cdot \frac{\pi}{4} (\phi_t - 2 \cdot w_t)^2 \right) \quad [\text{kN}]$$
G.19

In which:

$F_{t,dw}$	[kN]	Dead weight steel tubular pile
L_t	[m]	Length of inclined steel tubular pile, see Equation (G.20)
$\rho_{s,w}$	[kN/m ³]	Mass density of construction steel under water
ϕ_t	[m]	Diameter foundation pile
w_t	[m]	Wall thickness steel tubular pile
$\rho_{c,w}$	[kN/m ³]	Mass density of concrete under water

The total length of the inclined steel tubular piles in terms of inclination angle:

$$L_t = \frac{\sqrt{1 + (1/\tan \alpha_t)^2}}{1/\tan \alpha_t} \cdot (d_t - d_{local}) \quad [\text{m}]$$
G.20

In which $\tan \alpha_t$ is the inclination of the steel tubulars with respect to the vertical and d_t is the foundation depth of the steel tubulars (= MSL-42 m). The local water depth d_{local} varies along the barrier span.

Total bearing capacity. As stated in Equation (G.8) the total steel tubular pile bearing capacity is the sum of the bearing capacity of the tip and skin friction subtracted by the pile's dead weight. Forces during pile driving are

assumed to be not governing and therefore not taken into account.

Number of steel tubular piles. Now the number of tubulars per caisson can be calculated. This is done for both the occurring positive and negative head plus wave force, according to Section 7.2. As all of the horizontal forces will be transferred to the bearing layer through foundation piles the skirts have become unnecessary. However, the pile foundation will still be based on the caissons with the footprint as determined in Table 8.2.

$$\begin{aligned} n_{t,h,pos} &= \frac{F_{h,tot,pos}}{F_{t,max}} \cdot \sqrt{1 + (1/\tan \alpha_t)^2} \quad [-] \\ n_{t,h,neg} &= \frac{F_{h,tot,neg}}{F_{t,max}} \cdot \sqrt{1 + (1/\tan \alpha_t)^2} \quad [-] \end{aligned} \quad \text{G.21}$$

In which $n_{t,h,pos}$ and $n_{t,h,neg}$ are the number of required steel tubulars per caisson to bear the horizontal loads due to positive and negative head respectively. $F_{h,tot,pos}$ and $F_{h,tot,neg}$ are the total horizontal forces on the caissons due to wave load and water head (positive and negative respectively, see also Appendix F.2.1). The inclination of the piles is expressed as $\tan \alpha_t$ with respect to the vertical.

Now the total number of steel tubulars required to bear the horizontal forces is determined. Maybe these piles are able to bear all of the horizontal forces, but not all of the vertical forces. The vertical bearing capacity per inclined tubular is calculated through:

$$F_{t,v} = \frac{1/\tan \alpha_t}{\sqrt{1 + (\tan \alpha_t)^2}} \cdot F_{t,max} \quad [-] \quad \text{G.22}$$

Subsequently the required number of additional piles that only aim on bearing vertical forces is:

$$n_{t,v} = \frac{F_{v,tot} - (n_{t,h,pos} + n_{t,h,neg}) \cdot F_{t,v}}{F_{t,max}} \quad [-] \quad \text{G.23}$$

Costs deep foundation. To determine the total costs for a deep foundation first the optimum pile diameter is determined. This is done using the following procure as for alternatives 1 and 2, but with different time and cost unit rates.

Table G.13: Time and cost unit rates for vacuum preloading with CPVDs.

	Time unit rate	Cost unit rate
Pile driving	20 [m/hr] ⁽¹⁾	30,000 [\$/hr] ⁽¹⁾
Concrete pouring ⁽²⁾		400 [\$/m ³] ⁽¹⁾
Material, steel		1500 [\$/ton] ⁽¹⁾

(1) Productivity and unit cost rates adapted from Braam (2011)

(2) Concrete pouring includes concrete material costs

Using the unit cost rates the total costs for a deep foundation per pile diameter can be determined. The results are presented in Figure G.8.

A pile diameter of 1016 mm [40 in] with wall thickness 76 mm [3 in] is the most cost-effective, standard sized pile diameter. When applying these pile dimensions a problem for barrier sections AA' and BB' arises. A large number of piles is required when applying this pile diameter, resulting in a very dense pile plan. The minimum pile spacing requirement for end-bearing piles (given by Equation (G.24)) is not met. Therefore the foundation piles for these barrier sections will be custom made. It is determined that an enlarged pile diameter for barrier section AA' of 1626 mm [64 in] meets the pile spacing requirement. For barrier section BB' an outer diameter of 2286 mm [90 in] will suffice. In this way a more likely pile plan is possible. For this pile diameter the total deep foundation costs are

estimated at \$353 million.

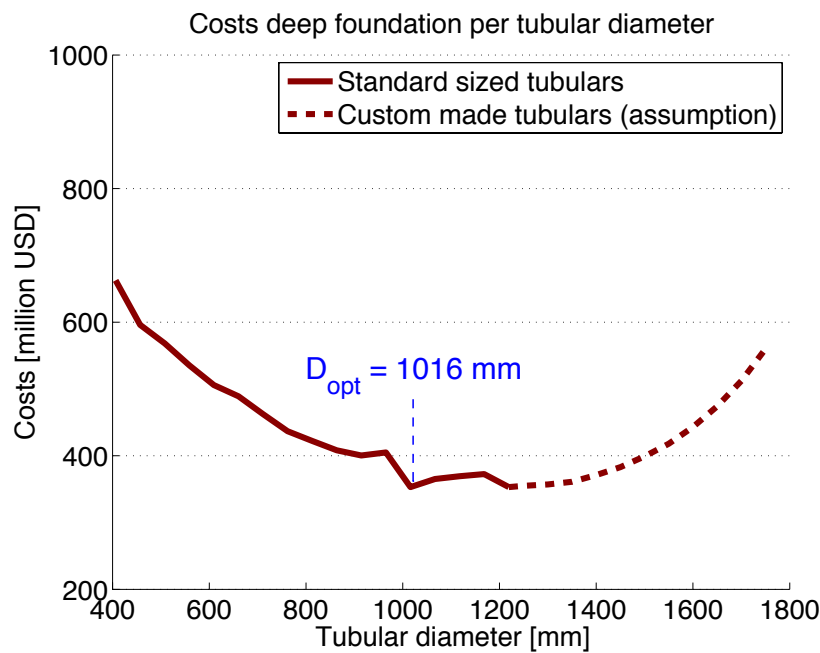


Figure G.8: Total costs deep foundation expressed in terms of pile diameter.

The graph in Figure G.8⁽¹⁾ shows the relation between standard sized pile diameters (ranging 406 - 1220 mm [16 - 48 in]) and costs. Larger piles have to be custom made and are therefore presumed to be more expensive. The cost unit rate for custom piles is unknown, but it is expected the deep foundation costs will increase with those custom made tubulars (dashed line in Figure G.8).

Caisson construction costs alternative 3. The caisson construction costs have to be calculated for the regular caisson dimensions as they were determined in Section 8.1, but without caisson skirts. They have become unnecessary as the horizontal loads will be fully carried by the foundation piles. The total construction time (man hour) and costs (current U.S.\$) are presented in Tables G.14 and G.15.

Table G.14: Caisson construction time for foundation alternative 3.

	Quantity	Time unit rate ⁽¹⁾	Construction time
Concrete			
– Slabs	147,190 [m ³]	0.1 [mhr/m ³]	14,719 mhr
– Walls	73,345 [m ³]	0.2 [mhr/m ³]	14,669 mhr
– Skirts	0 [m ³]	0.1 [mhr/m ³]	0 mhr
– Bults	4,345 [m ³]	0.2 [mhr/m ³]	869 mhr
Formwork	465,245 [m ²]	0.5 [mhr/m ²]	234,239 mhr
Rebars	17,202 [ton]	10 [mhr/ton]	172,017 mhr
Doors	14,483 [m ²]	20 [mhr/m ²]	289,656 mhr
Technical installation	135 [caissons]	40 [mhr/caisson]	5,400 mhr
Total			725,453 mhr

(1) Unit rates adapted from Braam (2011)

⁽¹⁾Figure G.8 shows a kinked graph. This is because a round number of piles is needed, resulting in a non-proportional relation between pile diameter and costs. The graph is further extended by the dashed line for custom made piles. It is expected their unit price is higher and thus their total costs. For a better cost overview these costs should be calculated.

Table G.15: Caisson construction costs for foundation alternative 3.

	Quantity	Cost unit rate ⁽¹⁾	Construction costs
Concrete			
– Slabs	147,190 [m ³]	200 [\$/m ³]	\$ 29,437,954.00
– Walls	73,345 [m ³]	200 [\$/m ³]	\$ 14,699,054.00
– Skirts	0 [m ³]	200 [\$/m ³]	\$ –
– Bulks	4,345 [m ³]	200 [\$/m ³]	\$ 868,968.00
Formwork			
– Plywood	132,838 [m ²]	40 [\$/m ²]	\$ 5,313,518.72
– Preparation	465,245 [m ²]	80 [\$/m ²]	\$ 36,499,592.16
Rebars	17,202 [ton]	2,000 [\$/ton]	\$ 36,403,466.24
Doors	14,483 [m ²]	20,000 [\$/m ²]	\$ 289,656,000.00
Technical installation ⁽¹⁾	135 [caissons]	150,000 [\$/caisson]	\$ 20,250,000.00
Labor	725,453 [mhr]	50 [\$/mhr]	\$ 36,272,639.06
Total			\$ 467,371,192.18

(1) Unit rates adapted from Braam (2011)

Total bearing capacity. As stated in Equation (G.8) the total steel tubular pile bearing capacity is the sum of the bearing capacity of the tip and skin friction subtracted by the pile's dead weight. Forces during pile driving are assumed to be not governing and therefore not taken into account here.

Table G.16: Total pile bearing capacities.

Barrier section (see Fig. 7.3)		AA'	BB'	CC'	DD'	EE'	FF'	GG'
– Local depth	[MSL-m]	15	17	10	7.5	5	3.5	5
– Foundation depth	[MSL-m]	42	42	42	42	42	42	42
Pile bearing capacities								
Tip $F_{t,tip}$ ⁽¹⁾	[kN]	4611	6656	3231	4181	5127	5898	5127
Positive skin friction $F_{t,skin,+}$ ⁽²⁾	[kN]	3110	3997	2657	3027	3417	3662	3417
Negative skin friction $F_{t,skin,-}$ ⁽²⁾	[kN]	224	279	201	233	267	288	267
Dead weight $F_{t,dw}$	[kN]	1358	1898	721	759	797	820	797
Total	[kN]	6138	9822	4966	6126	7480	8452	7480
Structural strength ⁽³⁾	[kN]	87184	110023	52868	52868	52868	52868	52868

(1) Tip bearing capacity varies a lot mainly due to the highly different effective soil stress at the foundation depth. See Table G.11.

(2) Shaft skin friction bearing capacity varies a lot mainly due to the variable composition of the soil layers across the entire barrier span.

(3) Structural strength is equal for all steel tubular piles for an equal pile diameter.

Pile plan. Now that the steel tubular pile dimensions have been determined the number of piles can be determined. They are calculated for each barrier section separately. Using the 'regular' pile dimensions (ranging up to 1220 mm [48 in] in diameter) a problem arises for barrier sections AA' and BB'. The minimum required pile spacing requirement is not met. The pile plan becomes too dense along the y-direction (long edge) of the caissons.

The prescribed center to center distance $s_{t,min}$ between two closed-end bearing piles (Abebe and Smith, 1994) should be:

$$s_{t,min} \geq 2.5 \cdot \phi_t + 0.02 \cdot L_t \text{ [m]} \quad \text{G.24}$$

In which ϕ_t is the pile outer diameter and L_t the pile length. The final steel tubular pile dimensions are presented in Table G.17.

Table G.17: Required number of steel tubulars.

Barrier section (see Figure 7.3)		AA'	BB'	CC'	DD'	EE'	FF'	GG'
Steel tubular pile geometry								
– Diameter ϕ_t	[mm]	1626	2286	1220	1220	1220	1220	1220
– Wall thickness w_t	[mm]	76	76	76	76	76	76	76
– Length L_t	[m]	28.5	26.4	33.7	36.4	39.0	40.6	39.0
– Bearing capacity $F_{t,max}$	[kN]	6138	9822	4966	6126	7480	8452	7480
Per caisson								
– Piles for positive head		15	16	15	6	4	2	4
– Piles for negative head		12	12	12	4	4	2	4
– Piles for add. vertical force		0	0	0	0	0	0	0
Per barrier section								
– Number of piles		243	112	1377	160	128	116	80
– Total running meter steel tubular	[m]	6915.9	2951.5	46447.5	5818.6	4992.2	4707.6	3120.1
– Total steel mass	[ton]	20013	12178	81505	10210	8760	8261	5475
– Total concrete volume	[m ³]	11795	10552	27207	3408	2924	2757	1828

G.2.4 Alternative 4: Complete soil replacement

In this subsection the total costs for complete soil replacement are calculated.

To determine the total volume of replaced soil first the required footprint at the bottom of the replaced soil has to be determined (at the bottom of layer 5). It is assumed the loads under the caissons will spread out under an angle of 45° in the soil. This means at a depth of bottom layer 5 for each barrier section the footprint will stretch at least until the total soil layer thickness outside the caisson perimeter. See Figure G.9.

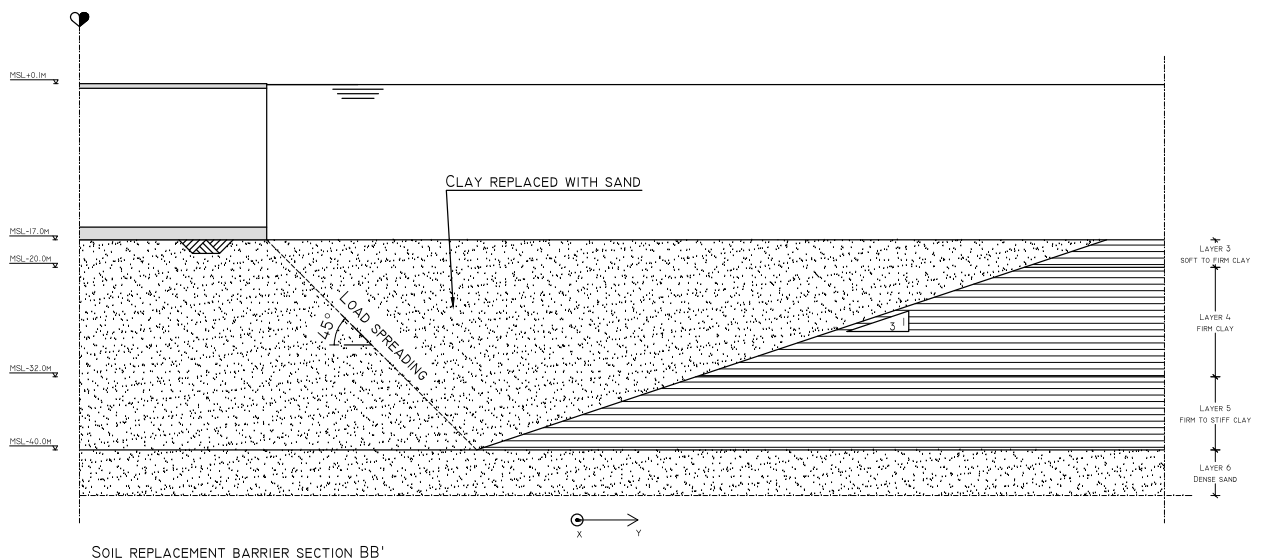


Figure G.9: Half cross sectional side view of barrier section BB' indicating the clay layers replaced with sand.

Using the angle of internal friction of clay $\varphi_{clay}=17.5^\circ \rightarrow \tan 17.5 \approx 1/3$ the total volume of replaced soil can be calculated. A cost unit rate of 30 \$/m³ is assumed⁽²⁾ This is quite high, but it concerns all of the costs for dredging the clay material, dump it offshore and fill the pit with sand as well as the mobilization and demobilization costs of the dredging vessels. The total soil replacement costs per barrier section are presented in Table G.18.

⁽²⁾ adopted from Braam (2011).

Table G.18: Replaced soil.

Barrier section (see Figure 7.3)		AA'	BB'	CC'	DD'	EE'	FF'	GG'
Volume of replaced soil	[10 ⁶ m ³]	0.75	0.39	5.96	1.47	1.59	3.06	1.00
Costs	[\$]	\$ 21 M	\$ 12 M	\$ 179 M	\$ 44 M	\$ 48 M	\$ 92 M	\$ 30 M

The total costs for this soil replacement are estimated at \$426 million. The caisson construction costs have to be calculated for the regular caisson dimensions as they were determined in Section 8.1. These are equal to the caissons costs for the vacuum preloading alternative: \$471 million. The total cost estimate for caisson construction and this foundation alternative are estimated at \$897 million.

G.3 Seepage screen design

The method by Lane (1934) is favorite for estimating if seepage will occur under water retaining structures.

$$\sum L_v + \sum L_h \geq \gamma_{\text{piping}} \cdot c_L \cdot \Delta h_b \tag{G.25}$$

In which:

L_v	[m]	Vertical seepage distance
L_h	[m]	Horizontal seepage distance
γ_{piping}	[-]	Safety factor piping (= 1.5)
c_L	[-]	Lane's seepage constant (= 7.0 for fine sand (Lane, 1934))

Rewrite Equation (G.25) gives the unity check for seepage:

$$\frac{\sum L_v + \sum L_h}{\gamma_{\text{piping}} \cdot c_L \cdot \Delta h_b} \geq 1.0 \tag{G.26}$$

Table G.19 shows that all of the caissons do not meet this unity check. For all of them a seepage barrier should be placed to prevent structural deterioration of the caissons.

Table G.19: Seepage.

Barrier section (see Figure 7.3)		AA'	BB'	CC'	DD'	EE'	FF'	GG'
Horizontal seepage distance $L_h^{(1)}$	[m]	40	41	43	42	38	38	40
Vertical seepage distance $L_v^{(2)}$	[m]	6.04	6.84	4.04	3.04	2.04	1.44	0.82
Check seepage	[-]	0.74	0.77	0.76	0.72	0.64	0.63	0.66

- (1) Equal to the caisson length, see Table G.2.
- (2) Equal to twice the skirt height, see Table G.2.

H Construction method and costs

In this appendix the cost numbers used in Section 9 are calculated.

H.1 Costs per activity

Construction of dry dock. See table below for the cost specification of the dry dock.

Table H.1: Costs for building dock.

	Quantity	Cost unit rate ⁽¹⁾	Construction costs
Sheet piles ⁽²⁾	3,026 [ton]	2,500 [\$/ton]	9,547,500.00
Excavation Channel	1,296,148 [m ³]	10 [\$/m ³]	\$ 12,691,480.00
– Dredging	505,720 [m ³]	10 [\$/m ³]	\$ 5,057,200.00
– Mob/demob ⁽³⁾	1 [vessel]	700,000 [\$/vessel]	\$ 700,000.00
Vertical drainage			
– PVD material	324,352 [m ²]	2 [\$/m ²] ⁽⁴⁾	\$ 648,704.00
– Installation	3,243,520 [m]	4 [\$/m] ⁽⁴⁾	\$ 12,974,080.00
Dewatering			
– Dewatering	981,548 [m ³]	0.15 [\$/m ³]	\$ 153,121,488.00
– Installation	129,741 [m ²]	7.5 [\$/m ²]	\$ 1,297,410.00
Lock doors	1200 [m ²] ⁽⁵⁾	10,000 [\$/m ²]	\$ 12,000,000.00
Total			\$ 206,325,362.00

(1) Cost unit rates adapted from Braam (2011).

(2) The required perimeter of the dry dock, used for the required quantity of sheet piles, is calculated as follows. The sheet piles have to prevent water flowing into the drydock, and therefore need to penetrate into the consolidated clay layer that starts at a depth of MSL-19 m. Assuming the average elevation of Pelican Island is 2 m, the sheet piles should have a total length of 21 m.

(3) Mob/demob indicates mobilization and demobilization costs.

(4) PVD material and installation costs modified from numbers in Table G.5.

(5) Lock door dimensions: $\approx 12 \cdot 100$ [m²].

Caisson construction. The costs for caisson construction are elaborated in the third design step, see Table G.7 for specification.

Preparing final location. The costs for preparing the final location including the foundation measure is presented in Table H.2.

Table H.2: Costs for preparing final location.

	Quantity	Cost unit rate ⁽¹⁾	Costs
Weak soil layer replacement underneath AA' and BB'			
– Dredging clay layer	66,135 [m ³]	10 [\$/m ³]	\$ 671,030.00
– Dump sand	66,135 [m ³]	10 [\$/m ³]	\$ 671,030.00
Flattening seabed	113,305 [m ²]	5 [\$/m ²]	\$ 566,525.00
Mob/demob	1 [vessel]	700,000 [\$/vessel]	\$ 700,000
Bed protection ⁽²⁾	546,318 [m ²]	50 [\$/m ²]	\$ 40,973,850.00
Vacuum preloading ⁽³⁾			\$ 329,373,391.00
Total			\$ 372,955,826.00

(1) Cost unit rates adapted from Braam (2011).

(2) The bed protection is assumed to be necessary until 200 m outside of the caisson perimeter.

(3) From Appendix G.2.1.

Caisson transport and placement. The transport of the caissons from the building dock to the final location is highly dependent on the total transport duration. See Table H.3.

Table H.3: Costs for caisson transportation.

	Quantity	Cost unit rate ⁽¹⁾	Costs
Transport from building dock to final location			
– Towing	540 [hr]	20,000 [\$/hr]	\$ 10,800,000.00
– Mob/demob ⁽²⁾	30 [tugboats]	300,000 [\$/tugboat]	\$ 9,000,000.00
– Caisson submerging	135 [caissons]	150,000 [\$/caisson]	\$ 675,000.00
Total			\$ 20,475,000.00

(1) Cost unit rates rough assumptions.

(2) Mob/demob indicates mobilization and demobilization costs.

H.2 Total costs

Summarizing the costs outlined in the previous section gives total direct construction costs of \$1,276 million. The indirect costs and total project costs are specific in Table H.4.

Table H.4: Total costs environmental barrier.

<u>Direct costs</u>	
– Dry dock	\$ 206 M
– Caisson construction	\$ 471 M
– Final location	\$ 373 M
– Caisson transport	\$ 20 M
Site overhead costs (5%)	\$ 55 M
Unforeseen (10%)	\$ 116 M
Total direct costs	\$ 1,276 M
<u>Indirect costs</u>	
– One time costs (2%)	\$ 25 M
– Implementation costs (5%)	\$ 64 M
– General costs (5%)	\$ 64 M
– Risk & Profit (10%)	\$ 128 M
Total indirect costs	\$ 280 M
Total construction costs	\$ 1,557 M
Engineering, administration, survey	\$ 150 M
Administration	\$ 45 M
Project unforeseen (10%)	\$ 175 M
Total investment costs	\$ 1,927 M

